

VILNIUS UNIVERSITY
CENTER FOR PHYSICAL SCIENCES AND TECHNOLOGY

Edita
VERNICKAITĖ

Electrochemical properties of iron group metals alloys with high W/Mo content

DOCTORAL DISSERTATION

Natural Sciences,
Chemistry N 003

VILNIUS 2019

This dissertation was written between 2014 and 2018 at Vilnius University, Faculty of Chemistry and Geosciences. The research was funded by the EU Research and Innovation funding programme FP7 (Grant No. 05-104-7540), EU Framework Programme Horizon 2020 (Grant No. 778357) and Research Council of Lithuania (Grant No. MIP-14197, No. of scholarships DOK-17420, DOK-17106, P-DAP-18-516, P-DAP-18-269).

Academic supervisor:

Prof. dr. Henrikas Cesiulis (Vilnius University, Natural Sciences, chemistry – N 003).

Academic consultant:

Assoc. prof. dr. Natalia Tsyntsaru (Vilnius University, Natural Sciences, chemistry – N 003).

This doctoral dissertation will be defended in a public meeting of the Dissertation Defence Panel:

Chairman – **Prof. (HP) dr. Stasys Tautkus** (Vilnius University, Natural Sciences, chemistry – N 003)

Members:

Dr. Asta Grigucevičienė (Center for Physical Sciences and Technology, Natural Sciences, chemistry – N 003),

Dr. Vidas Pakštas (Center for Physical Sciences and Technology, Natural Sciences, chemistry – N 003),

Dr. Vilma Ratautaitė (Center for Physical Sciences and Technology, Natural Sciences, chemistry – N 003),

Prof. (HP) dr. Vida Vičkačkaitė (Vilnius University, Natural Sciences, chemistry – N 003).

The dissertation shall be defended at a public meeting of the Dissertation Defence Panel at 2 p.m. on 6 September 2019 at the Inorganic Chemistry Auditorium (141) at the Faculty of Chemistry and Geosciences of Vilnius University. Address: Naugarduko str. 24, LT-03225, Vilnius, Lithuania, tel. (8 5) 219 3108; e-mail: info@chgf.vu.lt

The text of this dissertation can be accessed at the Library of Vilnius University and at the Library of FTMC, as well as on the website of Vilnius University: www.vu.lt/lt/naujienos/ivykiu-kalendorius

VILNIAUS UNIVERSITETAS
FIZINIŲ IR TECHNOLOGIJOS MOKSLŲ CENTRAS

Edita
VERNICKAITĖ

Elektrocheminės didelį W/Mo kiekį turinčių geležies grupės metalų lydinių savybės

DAKTARO DISERTACIJA

Gamtos mokslai,
Chemija N 003

VILNIUS 2019

Disertacija rengta 2014 – 2018 metais Vilniaus universiteto Chemijos ir geomokslų fakultete.

Mokslinius tyrimus rėmė ES 7-oji mokslinių tyrimų programa (projekto Nr. 05-104-7540), ES bendroji mokslinių tyrimų ir inovacijų programa „Horizontas 2020“ (projekto Nr. 778357) ir Lietuvos mokslo taryba (projekto Nr. MIP-14197, stipendijų Nr. DOK-17420, DOK-17106, P-DAP-18-516, P-DAP-18-269).

Mokslinis vadovas:

Prof. dr. Henrikas Cesiulis (Vilniaus universitetas, gamtos mokslai, chemija – N 003).

Mokslinė konsultantė:

Dr. Natalia Tsyntsaru (Vilniaus universitetas, gamtos mokslai, chemija – N 003).

Gynimo taryba:

Pirmininkas – **Prof. (HP) dr. Stasys Tautkus** (Vilniaus universitetas, gamtos mokslai, chemija – N 003).

Nariai:

Dr. Asta Grigucevičienė (Fizinių ir technologijos mokslų centras, gamtos mokslai, chemija – N 003),

Dr. Vidas Pakštas (Fizinių ir technologijos mokslų centras, gamtos mokslai, chemija – N 003),

Dr. Vilma Ratautaitė (Fizinių ir technologijos mokslų centras, gamtos mokslai, chemija – N 003),

Prof. (HP) dr. Vida Vičkačkaitė (Vilniaus universitetas, gamtos mokslai, chemija – N 003).

Disertacija ginama viešame Gynimo tarybos posėdyje 2019 m. rugsėjo mėn. 6 d. 14:00 val. Vilniaus universiteto Chemijos ir geomokslų fakulteto Neorganinės chemijos auditorijoje (141). Adresas: Naugarduko g. 24, LT-03225, Vilnius, Lietuva, tel. (8 5) 219 3108; el. paštas: info@chgf.vu.lt

Disertaciją galima peržiūrėti Vilniaus universiteto ir FTMC Chemijos instituto bibliotekose ir VU interneto svetainėje adresu: <https://www.vu.lt/naujienos/ivykiu-kalendorius>.

ABSTRACT

Innovative multifunctional materials enhance overall operational device performance by incorporating a number of tailorable properties, e.g. thermal, mechanical, electrical, catalytic, etc., into a single material. Such multifunctionality allows reducing the energy consumption, and cost of the processes, while simplifying implementation and improving performance and durability of devices. It is widely described that the electrodeposited iron group metal (Co, Ni, Fe) alloys with W/Mo are characterized by the promising physical properties, e.g. hardness, ductility, strength, etc. However, some discrepancies related to their electrochemical properties (catalysis towards hydrogen evolution, methanol oxidation, corrosion behaviour) even with the same chemical composition reported from author to author can be found.

This confirms the sensitivity of the characteristics to the provided conditions of electrolysis that influence not only chemical but also phase composition, which in turn, influence the electrochemical properties as a whole. In this context, for the first time a comprehensive analysis of electrochemical behaviour, i.e. alkaline hydrogen evolution reaction (HER), methanol oxidation and corrosion behaviour in acidic media, of iron group metals alloys with a wide range of W/Mo content in composition and the distinct structures is presented in this work.

The W-containing coatings having 2-30 at.% of W were electrodeposited by varying electroplating conditions, i.e. current density, potential, temperature, pH. Since the activity towards HER is expected with the higher refractory metal content in composition, Mo-rich alloys (~ 50 at.%) were prepared by performing electrolysis from the acetate-based electrolyte. Different techniques such as Scanning Electron Microscopy (SEM), Energy Dispersive Spectroscopy (EDS), Transmission Electron Microscopy (TEM), X-ray Diffraction (XRD), Linear and Cyclic Voltammetry (CV), Electrochemical Impedance Spectroscopy (EIS) were used to characterize the composition, morphology, structure and the electrochemical properties of the coatings.

It was found that the alloys with a high content of refractory metals (≥ 22 at.% W for Ni-W and Co-W; ≥ 17 at.% W for Fe-W and ~ 50 at.% Mo) are characterized by ultra-nanocrystalline structure with a crystallite size decreasing from ~ 40 nm (for pure iron group metals) up to 2-6 nm. The latter coatings are composed of two phases: tungsten/molybdenum solution in iron group metal and corresponding intermetallic compounds. Apparently, a significant amount of the refractory metal and ultra-nanocrystalline

structure of the alloys predetermines improved electro-catalytic properties towards HER as well as the corrosion resistance in an acidic solution.

Apparently, the higher catalytic activity of the ultra-nanocrystalline alloys is attributed to the formation of stable intermetallic phases which ensures optimal metals distribution over the surface and produces larger active sites for the HER. A significant improvement of catalytic activity leading to the distinct reduction of the overpotential and the enhancement of the apparent exchange current density (ECD) was noticed with increasing the temperature of alkaline solution. The apparent ECD values at 65°C reduced in the following order: (in at.%): Co-52Mo > Ni-54Mo > Fe-54Mo > Ni-29W > Co-33W > Fe-30W. The highest apparent ECD obtained for Co-52at.% Mo electrode reached 46.2 mA cm⁻² and is much higher than that for obtained for Pt under the same experimental conditions (11.5 mA cm⁻²). Notable, the nanostructurization by electrochemical formation of alloys nanowires (NWs) into porous templates enables enhanced HER, e.g. the apparent ECD increases on Co-5at.%W electrode increases from 0.02 mA cm⁻² (coating) to 3.7 mA cm⁻² (NWs).

Also it was determined that the highest corrosion resistance in sulfuric acid solution is characteristic for the Co-W alloy with 24 at.% of W in which the phase transition from W solid solution in Co to Co₃W intermetallide occurs. The Co₃W phase enhances good corrosion resistance in H₂SO₄ medium and leads to the positive catalytic effect towards methanol oxidation reaction. The anodic peak current density of methanol oxidation reaches 12.3 mA·cm⁻², whereas this value for Pt under the same laboratory conditions was 2.4 mA·cm⁻².

Moreover, the addition of the third element into binary iron group metal alloys with W allowed improving the corrosion resistance of the coating in the acidic media and in such way to broaden the range of their possible applications in engineering fields (j_{corr} of the proposed Co-Cu-W alloy decreases from $1.9 \cdot 10^{-4}$ to $6.9 \cdot 10^{-6}$ A cm⁻²) as well as in food industry machining (j_{corr} of proposed Fe-W-P alloy decreases from $4.3 \cdot 10^{-5}$ to $1.8 \cdot 10^{-5}$ A cm⁻²). One more effective modification method for expanding the usage of iron group metals alloys is the formation of their nanowire composites with Au nanoparticles that open the new frontiers for bio-functionalization capabilities that may lead to the development of the nanowire-based sensors for biological and medical applications.

Keywords: electrodeposition, iron group metals alloys, tungsten, molybdenum, citrate electrolyte, catalytic properties, corrosion resistance, hydrogen evolution reaction, methanol oxidation reaction.

LIST OF PUBLICATIONS

This thesis is based on the articles included in the Web of Science database:

- I. **E. Vernickaite**, N. Tsyntaru, K. Sobczak, H. Cesiulis, Electrodeposited tungsten-rich Ni-W, Co-W and Fe-W cathodes for efficient hydrogen evolution in alkaline medium, *Electrochimica Acta* 31 (2019) 597-606. doi: [10.1016/j.electacta.2019.06.087](https://doi.org/10.1016/j.electacta.2019.06.087).
- II. **E. Vernickaite**, O. Bersirova, H. Cesiulis, N. Tsyntaru, Design of Highly Active Electrodes for Hydrogen Evolution Reaction Based on Mo-Rich Alloys Electrodeposited from Ammonium Acetate Bath, *Coatings* 9(2) (2019) 85. doi: <https://doi.org/10.3390/coatings9020085>.
- III. **E. Vernickaite**, N. Tsyntaru, H. Cesiulis, Electrodeposited Co-W alloys and their prospects as effective anode for methanol oxidation in acidic media, *Surface & Coatings Technology* 307 (2016) 1322–1328. doi: <https://doi.org/10.1016/j.surfcoat.2016.07.049>.
- IV. **E. Vernickaite**, N. Tsyntaru, H. Cesiulis Electrodeposition and Corrosion Behavior of Nanostructured Cobalt Tungsten Alloy Coatings, *Transactions of the IMF*, 94 (6) (2016) 313-321. doi: <https://doi.org/10.1080/00202967.2016.1220071>.
- V. **E. Vernickaite**, N. Tsyntaru, H. Cesiulis, Electrochemical co-deposition of tungsten with cobalt and copper: peculiarities of binary and ternary alloys coatings formation, *Surface & Coatings Technology*, 307 (2016) 1341–1349. doi: [10.1016/j.surfcoat.2016.07.02](https://doi.org/10.1016/j.surfcoat.2016.07.02).
- VI. **E. Vernickaite**, Z. Antar, A. Nicolenco, R. Kreivaitis, N. Tsyntaru, H. Cesiulis, Tribological and corrosion properties of iron-based alloys, *Proceedings of BALTRIB'2015* edited by prof. J. Padgurskas, 162-169. doi: [10.15544/baltrib.2015.29](https://doi.org/10.15544/baltrib.2015.29).
- VII. **E. Vernickaite**, U. Bubniene, H. Cesiulis, A. Ramanavicius, E. J. Podlaha, A Hybrid approach to W alloy and Au nanoparticles, *Journal of The Electrochemical Society*, 163(7) (2016) D344-D348. doi: [10.1149/2.1401607jes](https://doi.org/10.1149/2.1401607jes).

Publication which is not included in the Web of Science database:

- VIII. **E. Vernickaite**, H. Cesiulis, N. Tsyntaru, Evaluation of corrosion and tribological behavior of electrodeposited tungsten alloys, *Proceedings of BALTRIB'2017* edited by prof. J. Padgurskas, 207-214. doi: <https://doi.org/10.15544/baltrib.2017.36>.

AUTHOR'S CONTRIBUTION TO THE ARTICLES

- I. The author designed the conditions for electrodeposition of W alloys with Co, Ni and Fe having various composition. Investigated their morphological and structural peculiarities and evaluated the catalytic activity of the prepared electrodes towards alkaline hydrogen evolution reaction (HER). In cooperation with the co-authors presented the results in the publication.
- II. The author electrodeposited Mo-based alloy coatings with Co, Ni, Fe and analysed the influence of electrolyte composition and current density on their chemical composition, morphology and microstructure. Investigated the electrocatalytic HER performance in an alkaline solution. Prepared the manuscript with support from the co-authors.
- III. The author electrodeposited Co-W alloys having various W contents and microstructure, investigated their catalytic activity for methanol oxidation reaction in acidic medium. Evaluated the effect of thermal treatment on catalytic activity. Summarized the results and in cooperation with the co-authors prepared the manuscript.
- IV. The author designed the conditions for electrodeposition of Co-W alloys with the various W contents. Performed instrumental analysis for determination of morphology and structure of the prepared coatings. Applied linear voltammetry and electrochemical impedance spectroscopy (EIS) techniques for the investigation of corrosion properties in acidic medium. Summarized the results and in cooperation with the co-authors prepared the publication.
- V. The author performed the electrodeposition of ternary Co-Cu-W alloys. Investigated the chemical composition and structural transformations of the prepared alloys as a function of deposition potential and temperature of the bath. Compared the results with those obtained for binary Cu-W and Co-W alloys. In cooperation with the co-authors presented the results in the publication.
- VI. The author performed the electrodeposition of W-rich (~ 30 at.%) Fe-W and Fe-W-P alloys; determined their structural peculiarities. In cooperation with the co-authors evaluated mechanical, tribological and anticorrosion properties of the prepared alloys. Based on the discussions with the co-authors prepared the paper as conference proceeding.

- VII. The author fabricated Co-W alloy nanowires (NWs) by electrodeposition technique into nanoporous polycarbonate membranes. In cooperation with other co-authors fabricated a novel nanocomposite that consists of Co-W NWs matrix and Au nanoparticles. Together with the co-authors prepared the publication.
- VIII. The author presented a comparative study of anticorrosion and wear behaviour of electrodeposited tungsten alloys with Co, Ni, Fe presented in the literature so far. Notable, the proceeding is not uploaded to Web of Science platform, thereby it cannot be formally included in the compendium of required number of articles. However it highlights the main issues related to systematic evaluation of the corrosion and tribological properties of iron group metals alloys with W reported by other researchers and thus, serves to a better understanding of the motivation of this thesis.

LIST OF SYMBOLS AND ABBREVIATIONS

AAO	anodic aluminum oxide
CCE	cathodic current efficiency
C_{dl}	capacitance
CPE	constant phase element
CV	cyclic voltammetry
d	crystallite size
DMFC	direct methanol fuel cell
E_a	activation energy
ECD	exchange current density
E_{corr}	corrosion potential
EDS	energy-dispersive X-ray spectroscopy
EIS	electrochemical impedance spectroscopy
F	Faraday's constant
HER	hydrogen evolution reaction
ICT	information and communications technology
j_0	exchange current density
j_{corr}	corrosion current density
LSV	linear sweep voltammetry
MEMS/NEMS	micro/nano electromechanical system
MOR	methanol oxidation reaction
NW	nanowire
OCP	open circuit potential
R_a	average roughness
R_{ct}	charge transfer resistance
R_s	solution resistance
SEM	scanning electron microscopy
TEM	transmission electron microscopy
TSV	through-silicon via
x_i	weight fraction of species i
X_i	atomic fraction of species i
XRD	X-ray diffraction
α	charge transfer coefficient
η	overpotential
Θ	position of the XRD peak
λ	wavelength

TABLE OF CONTENTS

INTRODUCTION	12
1. LITERATURE OVERVIEW	16
1.1 Advantages of electrodeposition technique	16
1.2 Induced deposition of iron group metals alloys with W/Mo	18
1.3 Structure of iron group metals alloys with W/Mo	20
1.4 Properties of electrodeposited iron group metals alloys with W/Mo ...	22
1.4.1 <i>Physical properties</i>	23
1.4.2 <i>Corrosion resistance</i>	25
1.4.3 <i>Catalytic performance for methanol oxidation reaction</i>	28
1.4.4 <i>Electrocatalytic efficiency in the hydrogen evolution reaction</i>	29
1.5 Summary.....	32
2. EXPERIMENTAL	34
2.1 Formulation of electrolytes vs properties investigated	35
2.2 Electrodeposition procedure	37
2.3 Characterization of alloys	38
2.4 Electrochemical analysis methods	38
2.5 Summary.....	38
3. RESULTS AND DISCUSSIONS	39
3.1 Interdependencies between composition, structure and morphology ...	39
3.2 Electrochemical properties	45
3.2.1 <i>Hydrogen evolution reaction (HER)</i>	45
3.2.2 <i>Methanol oxidation (MOR)</i>	47
3.2.3 <i>Corrosion properties in H₂SO₄</i>	51
3.3 Modification of binary alloys	54
3.3.1 <i>Addition of the third metal</i>	54
3.3.2 <i>Addition of phosphorus</i>	57
3.3.3 <i>Nanostructures</i>	60
4. CONCLUSIONS	65
5. SANTRAUKA	66
6. REFERENCES	75
7. CURRICULUM VITAE	89
Copies of published articles.....	91

INTRODUCTION

Electrodeposition is a well-known conventional surface modification method, which is used to improve the decorative and functional surface characteristics of a wide variety of materials. During the last few decades, electrodeposition has gained importance as an accepted versatile technique for the preparation of nanoscale materials, offering control over their structure, composition and properties, and thus, facilitates the preparation of novel materials with enhanced properties that cannot be obtained by other techniques [1]. This target may be especially assured, when electrodeposition of alloys of iron group metals (Co, Ni, Fe) with W/Mo are realized.

Apparently, the different physical and electrochemical properties of these alloys make them useful for specific purposes, i.e. some of them can be used for their mechanical properties, others for their magnetic properties, others for their high thermal resistance and so on. However, for many applications the combination of competing functional properties is often desired in one material. Thus, the synergism of improved tribological and corrosion properties along with increased thermal stability of nanostructured coatings are expected to protect surfaces of articles and tools exposed simultaneously to elevated temperatures, corrosive media and various types of wear. The combination of high hardness and good electric and/or catalytic properties could be applied in stretchable circuitries and energy devices that are able to perform sophisticated functions and keep the desirable electrode shape under external stimuli of bending, stretching, compressing, and twisting without sacrificing performance and reliability of the device. In other words, the design of multifunctional nanostructured alloys could open the next technology frontiers by providing the desired material solutions to complex technological problems.

In this context, nanocrystalline iron group metals alloys with W/Mo deserve a special note, since they present a tremendous potential as decorative coatings and due to the highly tuneable mechanical, tribological and thermal properties that can be modified in accordance with the technological requirements only by changing their chemical composition. More specifically, the nanohardness of “amorphous-like” W/Mo-rich alloys (with ≥ 23 at.% of refractory metal) with iron group metals reach 10 GPa at 20 mN. Such hardness is comparable to the hardness of electrodeposited chromium at the same load [2]. Also, these alloys have a superior wear resistance than those of steel substrate under dry and lubricating conditions [3], and can achieve a tensile strength up to 2333 MPa as well as high

ductility and complete bending to 180° without fracture [4,5]. Furthermore, a remarkable thermal stability up to 800°C has been determined [6]. Because of these above-mentioned physical properties, iron group metals alloys with the high W/Mo content are considered as suitable target materials for development of multifunctional technologies. However, since they have been widely investigated owing to their mechanical, tribological and thermal properties, the works on the corrosion behaviour and electrocatalytic performance are rather scarce, while the published results so far cannot be systematically generalized due to the fact that most of the investigated alloys are prepared under different electrodeposition conditions and by using various electrolytes that strongly influence their composition and structure and therefore, functional features.

Thus, the aim of present work is to perform the systematic studies of interdependences between the electrodeposition conditions of the iron group metals alloys with W/Mo and their electrochemical properties: a catalytic activity towards hydrogen evolution and methanol oxidation reactions and corrosion behaviour are targeted, in order to unlock a great potential for their application, especially in multifunctional energy conversion devices. Following an attempt to bring an industrial application of the prepared alloys one step closer, the knowledge gained from the results of their electrodeposited coatings has been used to the successful implementation of template-assisted electrodeposition of Co-W nanowires. Furthermore, a novel concept for fabrication of the hybrid nanocomposite, composed of Au nanoparticles and a Co-W matrix has been presented here.

With the aim of giving a consistent overview, in this work alloys' coatings were electrochemically deposited from citrate-based electrolytes that have been used in the previous studies by N. Tsyntaru et al. and H. Cesiulis et al. and that allow to synthesize alloys with the refractory metal content ranging from 2 up to 36 at.% in a controlled way [6,7]. The inherent advantage of this strategy is environmental compatibility due to the fact that the process includes both the treatment of effluents and waste and the development of functional materials with less harmful effects, often denoted as process-integrated environmental protection.

The goal of the study:

To perform a comprehensive investigation on the electrodeposition of iron group metals alloys with W/Mo with variable morphology, composition and crystallite size (nanocrystalline vs. ultra-nanocrystalline) and correlate the observed features with the catalytic activity towards alkaline HER and MOR and corrosion behaviour in acidic media.

Objectives:

1. To design the electrodeposition conditions (pH, current density/potential, temperature, bath composition) for preparation of W/Mo alloys with Co, Ni, Fe having various W content in their composition, and to determine the relationships between W/Mo content and morphological and structural peculiarities.
2. To establish the interdependences between the composition, surface morphology of iron group metals alloys with W/Mo and the electro-catalytic activity towards the HER in alkaline medium.
3. To optimize electrodeposition conditions for Co-W alloys fabrication in order to promote the methanol electro-oxidation reaction in an acidic solution.
4. To investigate the corrosion properties of Co-W alloys in acidic medium as a function of both the content of W and microstructure.
5. To present the possibility of the controlled electrodeposition of Co-W nanowires into nanoporous polycarbonate template and modification with Au nanoparticles in order to fabricate novel nanowire-nanoparticle complex structure.

Statements to be defended:

1. The composition and structure of iron group metals alloys with W/Mo resulting from the electrodeposition are the key parameters to obtain materials possessing targeted electrochemical properties (HER, MOR, corrosion).
2. The heterostructured catalysts fabricated by alloying of the iron group metal and W/Mo, including with the addition of Cu or P, provide improved electrochemical properties (HER, MOR, corrosion), compared to the single iron group metal catalysts.
3. Nanofabrication is a method to expand the applicability of fabricated alloys, which as nanowires of Co-W alloy arrays possess higher catalytic

activity towards HER or can be modified with Au as a novel nanocomposite for promising sensing application.

Organization of the text:

The content of this thesis is organized into different chapters:

Chapter 1: an introduction that sets out the main goal and objectives of the thesis.

Chapter 2: the theoretical concepts related to the electrodeposition of iron group metals (Co, Ni, Fe) alloys with W/Mo and the overview of their functional properties quoting the results reported in the literature with the special emphasis laying on the electrocatalytic (HER, MOR) and anticorrosion behaviour.

Chapter 3: the electrodeposition set-up and experimental conditions used for the fabrication of Co, Ni or Fe alloys with W/Mo that have been investigated in this work; various techniques for compositional, morphological and structural characterization of the prepared samples and the assessment of their catalytic activity and corrosion resistance.

Chapter 4: the obtained results and discussion based on a compliance of the articles that are provided at the end of this work.

Chapter 5: the summary of the results obtained from experiments.

1. LITERATURE OVERVIEW

Elaboration and further development of modern devices/technologies is based on a profound understanding of the mechanism of targeted materials formation, as well as on the interdependences between their structure and functional properties. Furthermore, only a full mapping of functional properties allows to intuit the optimal design principles. Namely, often materials are expected to possess a combination of different properties (e.g. high hardness, wear and corrosion resistance, enhanced catalytic activity, etc.) in order to be able to fit in the demanding world of advanced technologies. One of the methods to manufacture such materials with multi-functional characteristics is electrodeposition. Accordingly, in this chapter the fundamentals of electrodeposition of iron group metals (Co, Ni, Fe) alloys with tungsten, as targeted materials, and their mechanical, tribological and electrochemical properties reported in scientific literature are introduced; including the key advantages of the electrodeposition technique that are presented below.

1.1 Advantages of electrodeposition technique

In general, nanocrystalline iron group metals (Co, Ni, Fe) alloys with W/Mo can be prepared by several techniques, such as spark plasma sintering [8,9], magnetron sputtering [10], hydrothermal treatment [11], mechanical alloying [12–14], electroless deposition [15,16] and electrochemical deposition [17]. However, the metallurgical methods are not attractive due to the easy oxidation at the crystallization step and high melting temperature of alloying metals, e.g. 1495°C for Co [18] and 3422°C for W [19]. Consequently, the metallurgical fabrication of refractory metal-based alloys is very expensive due to the high energy consumption. Thus, among all available alternatives, a water based electrodeposition process is considered as simpler, cheaper and more environmentally friendly method, than those requiring sophisticated apparatus, volatile and corrosive chemicals and extra energy that must be incurred to keep the system in a liquid state [20].

The electrodeposition technique involves deposition of metal or alloy coatings over a conducting surface by means of electrolysis from a well-formulated electrolyte [21]. Several components, including concentration of metal ions in the plating bath, temperature of the electrolyte, current density/potential, etc., can be adjusted in order to affect the outcome. Electroplating is a common metal finishing process with several industrial functions, ranging from the purely decorative to the application of protective coatings [22]. Notable, that the coatings of metal or alloys can be plated on a

substrate surface of any shape and no post-processing is required [23]. In addition, it is possible to use large tanks as electrolytic cells, and therefore, large-area deposits with reproducible properties that are required for a widespread use of nanocrystalline materials for technological applications can be produced. The process can be carried out at low temperatures ($< 100^{\circ}\text{C}$), under atmospheric pressure, and the overpotential for the film growth can be controlled very precisely ($< 1\text{ mV}$) and quickly ($\sim \text{ns}$) [21]. Besides, using the cathode surface as a template, various desired nanostructures or morphologies can be synthesized for specific applications. For instance, micro/nanostructures in the silicon vias (TSV) [24,25] and highly ordered porous anodic aluminum oxide (AAO) templates [26,27] have been reported. From the practical point of view, the fabrication of the micro/nanostructures as components in microelectromechanical systems (MEMS) and interconnect vias has attracted much attention due to the potential application in an information and communication technologies (ICT), chemical engineering [28], micromachines [29] and robotics [30,31], environmental engineering [32], and medical technology [33].

As is evident, the electrodeposition offers several important advantages compared to other plating technologies (Fig. 1).

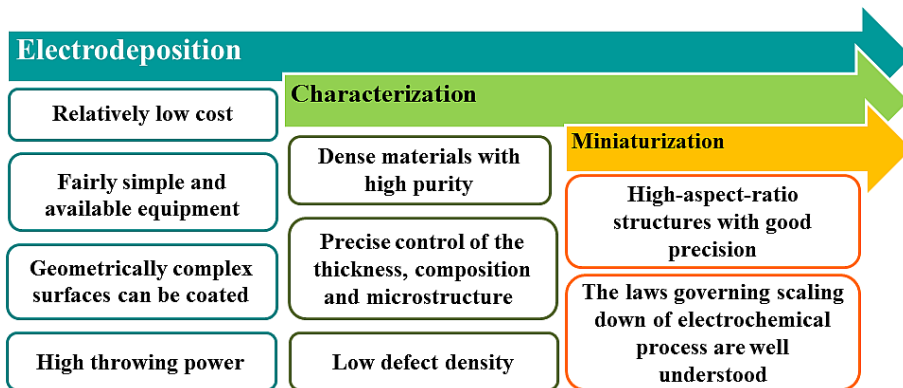


Fig. 1. Schematic representation of the advantages of electrodeposition technique. Ipvav. Elektronusodinimo technikos privalumai.

Importantly, this method allows to control and predict the composition and structure of the alloys as a function of electrolyte chemistry and deposition conditions. At the same time, it is possible to modify continuously the structure of alloys being grown, with the possibility to correspondingly tune their functional properties. Following all these arguments in the present work a cost-effective and high throughput electrodeposition technique has been

applied to produce a wide range of Co, Ni or Fe alloy coatings with W/Mo as targeted materials for possible multifunctional application.

1.2 Induced deposition of iron group metals alloys with W/Mo

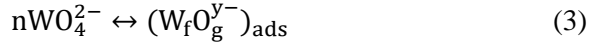
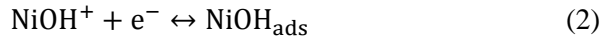
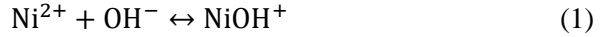
It is known that metallic tungsten cannot be separately electrodeposited from aqueous solutions of any soluble salt of this element due to the formation of an oxide layer on the cathode during electrodeposition. This oxide film is characterized by a very low overvoltage for hydrogen evolution and thus, the applied cathodic current practically is used for more favourable HER instead of W (VI) ions reduction. On the other hand, as it was indicated above, metallic tungsten can be successfully co-deposited in the presence of iron group metal ions (Ni(II), Co(II), Fe(II)) [34]. Initially, it was proposed that since the rate of hydrogen evolution on tungsten is very high, its rate on the Ni-W alloy is considerably lower, so deposition of binary alloy, contrary to tungsten alone, can be sustained. However, this hypothesis was discredited by the experimental proofs showing that tungsten deposition did not occur on mercury, even though the rate of hydrogen evolution on this metal is very low [35]. Consequently, comprehensive studies in order to explain this extraordinary behaviour were conducted by a number of researchers later on. Some different models are summarized to explain the co-deposition mechanism depending on the chosen iron group metal and plating bath composition in [36,37]. Here, it is important to mention that similar induced co-deposition mechanism is observed if W is replaced by Mo and each of the latter can be coupled with the host metals, notably Ni, Co and Fe, forming a corresponding binary alloys [38].

Within a timeline outlining the key theories of induced co-deposition can be seen that an extensive review in this field was published by Brenner [34] in 1963. This review introduced the concept that aqueous solutions of tungstate with an iron group metal are generally unstable and precipitated out unless a suitable salt of a hydroxyl organic acid is also present to reduce the quantity of free iron group metal ions in the solution. However, the attempts to deeply understand the mechanism were lacking. The first induced co-deposition mechanism of Ni-W alloy was reported by Holt and Vaaler [39] who proposed that alternative layers of W and Ni are deposited: the iron-group metal reduces firstly and the solid metal layer acts as a catalyst for tungsten reduction. However, the difficulties of this explanation arise from the fact that later on the XRD studies showed the formation of a solid solution of W in Ni, which is not consistent with the layered structure.

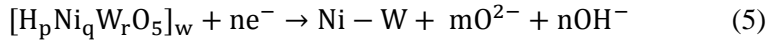
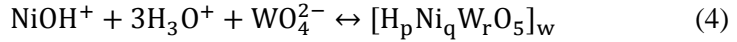
The authors in [40,41] declare that the soluble complexes in the electrolyte, e.g. $[(M)(WO_4)(H)(Cit)]^{2-}$, $[M(WO_4)_2(H_2)(Cit)]^{3-}$ and $[M(HWO_4)(HCit)]^{2-}$,

where M is the iron group metals, are addressed as the major responsible precursors for electrodeposition of W/Mo based alloys. Based on UV/visible absorption spectroscopy analysis the formation of [Co–gluc–WO₄²⁻] species in Co–W–gluconate bath has been suggested in [42]. Later on the existence of the heteropolynuclear Co–W citrate complex during electrodeposition process has been confirmed by gel chromatography analysis method [43].

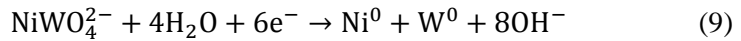
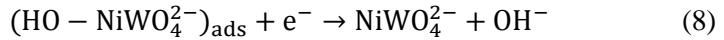
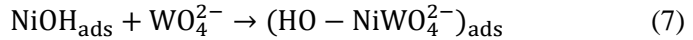
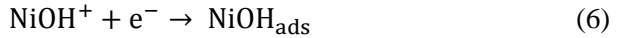
However, the complexing species model does not explain the variety in dependencies of refractory metal content in the alloys dependently on the electrodeposition conditions. Thus, the adsorption model has been proposed as an alternate interpretation of the induced co-deposition of iron group metals with W/Mo. For instance in [44] was shown that the formation of hydroxyl species aids the adsorption of tungstate species:



A heteropolytungstate film [H_pNi_qW_rO_s]_w is formed giving the following overall deposition process:



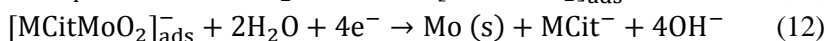
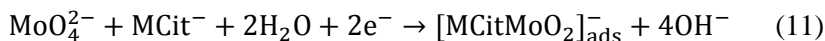
The mechanism of the tungsten reduction to metal through the stage of nickel ions, Ni (II), reduction to intermediate particle NiOH_{ads} was also suggested in [45]:



Agreeably to the abovementioned theories based on hydroxo-species formation was demonstrated that the electrodeposition of Co occurs via the formation of CoOH⁺ intermediates [46].

In course of alloys electrodeposition hydrogen evolution occurs as a side reaction. Thus, many researchers were focused to determine the role of the hydrogen on induced co-deposition phenomenon. It was suggested that hydrogen is adsorbed onto the co-deposited iron-group metal and that the inducing element is reduced at these sites [47]. This approach came from the

observation that the higher content of W/Mo in the deposit facilitates the hydrogen evolution reaction. However, it is also possible to find the contrary observations that rise doubts about the role of hydrogen. For instance, Podlaha and Landolt proposed an approach [48,49] in which the induced co-deposition of W/Mo occurs without the need for the adsorbed hydrogen via the catalysis reaction, assuming that the catalyst consists of a mixed adsorbed W/Mo(IV), iron group metal M(II) and citrate intermediate:



The intermediates suggested by Podlaha and Landolt was further proved by in situ surface Raman spectroscopy in [50,51]. Important to highlight that the Podlaha–Landolt model does not exclude the importance of the side reaction and confirms that the adsorbed intermediates of hydrogen can also compete with the mixed-metal intermediates, indirectly influencing the reaction rate.

However, despite the extremely high amount of alternative theories, a consensus how iron group metals alloys with tungsten/molybdenum are co-deposited and the nature of the inducing species has not yet been completely elucidated. Nevertheless, the mentioned aspect does not suppress the practical interest in these materials and since 1990s many investigations have been devoted to the electrodeposition of iron group metals alloys with tungsten/molybdenum. Apparently, they are of extreme interest in both academic and industrial fields due to their ability to extend the range of available properties beyond those of pure iron group metals.

1.3 Structure of iron group metals alloys with W/Mo

Most of the physical properties of solids are structurally sensitive. Therefore, from the perspective of the industrial use of new materials, it is extremely important to study their structure and stability as well as the correlation of structure and properties of the material. In this context, the purpose of the following subchapter is briefly to introduce the current state of research of the structure evolution in iron group metals alloys with W. Analogous interdependencies can be applied for Mo alloys with iron group metals (unless otherwise stated).

The introduction of W into alloys with iron group metals (< 12-14 at.%) leads to the transformation of their crystallographic texture: from nanocrystalline one which is typical to pure electrodeposited Co, Ni and Fe, to their dominant (111) texture for Co-W [52] and Ni-W [53–56,56], and

(110) – for Fe-W [2,52] alloys. A shift of W-based alloys peaks toward lower angles, in comparison with pure iron group metals is usually observed. Besides, it was shown that the iron group metal lattice increases with an increase in tungsten percentage in accordance with Vegard's law which implies that the lattice parameter of a metallic solid solution changes linearly with composition between the parameter of the solvent and that of the solute [57,58]. These observations imply the formation of W solid solution in face centred cubic (fcc) nickel [55,59–66], W solid solution in body centred cubic (bcc) iron [67] and W solid solution in hexagonal close packed (hcp) cobalt [68,69]. However, some controversial results are documented. For instance, for the W content of 10 at.%, a mixture of Co_3W and Co_7W_6 , and no traces for pure Co phase are seen in Co-W alloy system [70]. Meantime in [71] the qualitative phase analysis revealed that peaks in the diffractograms of Ni-W alloy coatings having 10-14 at.% of W correspond to the intermetallic Ni_{17}W_3 phase which was also confirmed by the calculation of tungsten content in alloys composition by using Vegard's law. In [56] was specified that the diffractograms of Ni-W coatings show the characteristic peaks corresponding to crystalline Ni_{17}W_3 phase along with a crystalline tungsten rich Ni-W phase, when the electrodeposition is performed at cathodic current density higher than 20 mA cm^{-2} . Apparently, the prevailing phase depends on the tungsten content based on the applied process parameters.

As the amount of W in alloys composition exceeds the solubility limit of iron group metal (15-20 at. %) a widening of the diffraction peaks appears indicating that the crystallite size of the electrodeposited W-based alloys decreases [4,61,72,73]. However, due to the overlapped XRD peaks it is rather difficult to elucidate which phases have been formed. For example, in Co-W alloy case two possible hcp phases, namely cobalt–tungsten solid solution in the hcp Co phase or the intermetallic Co_3W phase, can be deposited [7]. Meanwhile in [74] was reported that Ni-W alloys with a W content of around 20 at.% consist of three different phases: solid solution of W in Ni matrix, intermetallic compound Ni_4W and another solid solution of Ni in W. The latter phase has been described also in [73], but at lower W content (11-15 at.%). At the higher tungsten percentages (> 22-25 at.%, depending on the electrodeposition conditions) the formation of thermodynamically stable intermetallic compounds – NiW [61] or Ni_4W [5], Co_3W [75,76] and Fe_2W [67] – have been reported for corresponding tungsten alloy systems. Those types of electrodeposited alloys are usually of “amorphous-like” structure, hard and characterized by smooth morphology [4]. During the transformation of W-based alloys from crystalline to “amorphous-like” structure the crystallite size is reduced from

approximately 60 nm up to 3 nm [52,59,77]. Based on 3D surface analysis given in [52] the mean roughness (R_a) of “amorphous-like” structure coatings varied in the range of 200-500 nm. The cross sectional images showed that the structures of electrodeposited “amorphous-like” alloys of tungsten with the iron-group metals are fibrous and the nanofibers grow perpendicularly to the support surface [78]. At the same time, it is well known that amorphous state is metastable due to the large fraction of mass concentrated at grain boundaries with an excess free energy stored at these grain boundaries. Consequently, the annealing of “amorphous-like” alloys will firstly lower their energy by relaxation toward a more stable state microstructure through the so-called recrystallization process [6]. The transition of “amorphous-like” phase to the partially crystalline or fully crystalline state, as well as the correlation of structure and properties of W alloys with iron group metals is presented in the following subchapters of this thesis.

1.4 Properties of electrodeposited iron group metals alloys with W/Mo

In general, iron group metals alloys with W/Mo are characterized by superior mechanical, tribological, electrical, corrosion and catalytic properties. Certainly, a combination of such properties makes them suitable for versatile purposes: e.g. as environmentally friendly substitutes for hard chrome plating; substrates for high temperature superconductors; barrier layers or capping layers in micro/nano electro mechanical systems (MEMS/NEMS); catalysts for hydrogen evolution from alkaline solutions, etc. Meanwhile, the combination of properties in one alloy could make it suitable for the use in the applications in which different loading conditions must be sustained. The Fig. 2 illustrates various properties for a material to become multifunctional. Certainly, other issues, including processing requirements (e.g. sustainability, expenses) should be considered as well. This type of material design gives an exigent task to integrate different functions (especially if those seem to exclude each other) into the base material to achieve overall improved system performance.

In this context, the knowledge of individual material functions by itself is the first step to predict multifunctional materials suitability in an application setting. Accordingly, the thermal, mechanical, tribological, corrosion and catalytic properties of iron group metal alloys with W/Mo are overviewed in the following subchapters.

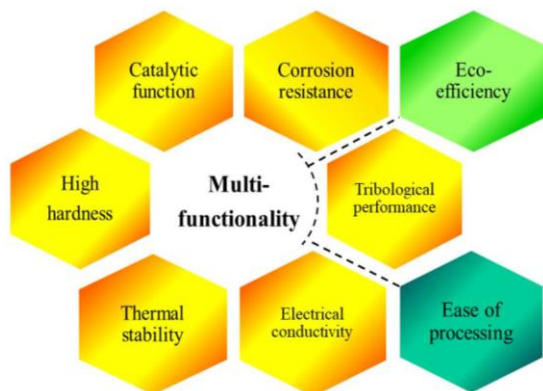


Fig. 2. Schematic illustration of various properties of multifunctionality [36].
2 pav. Daugiafunkcinių medžiagų savybių įvairovė [36].

A combination of these characteristics has been chosen for the strategy of fabrication of the active and stable catalysts for HER/MOR that would be resistant to attrition, corrosive environment, elevated operating temperature and degradation during start-up/shutdown cycling.

1.4.1 Physical properties

The physical properties of the alloys, such as hardness, tribological behaviour and thermal stability are connected with the refractory metal content, i.e. tungsten or molybdenum, in the coatings, and therefore, to the structural characteristics. It is known that W/Mo can enhance the hardness of the binary alloys due to the solid solution strengthening or grain refining strengthening effects [79]. It has been shown that the solid solution strengthening effect of W/Mo is about an order of magnitude smaller than the contribution of a grain size [80]. The so-called Hall–Petch mechanism predicts that as the grain size decreases, the hardness values increases [81]. However, it was demonstrated, that this mechanism is not applicable for very small grain sizes. The most common explanation is that below the critical grain size, the nanocrystalline materials cannot support the grain-boundary dislocations anymore [82]. Hence, the deformation mechanism transforms from dislocation movement (up to critical size) in the Hall-Petch regime to grain boundary sliding (below critical grain size) in the inverse Hall-Petch regime [82]. In previous studies was shown that the hardness of Co-W alloys increases up to $\sim 917 \text{ HV}_{20}$ with increasing the tungsten content from 8 to 25 at.% which is linked to a decrease in the grain size from 36 up to 5 nm, respectively. Below this critical value the inverse Hall-Petch relation is observed for Co-W alloys, i.e. the hardness decreases with the further grain

size reduction [7]. For Fe-W alloys the critical grain size of about 4 nm, i.e. when the tungsten content in Fe-W deposit increases up to 26 at.%. The hardness in this case reaches a maximum value of 1020 HV₉₈₀ [2]. In Ni-W alloy system, the classical Hall-Petch relationship mostly has been found to break down already at the grain sizes of about 10 nm [80,83].

According to the literature, the maximum hardness values for Ni-W deposits reported in the literature under the same conditions are usually lower (in the range of 734±70 HV at 10 mN [80] and 621±63 at 196 mN [4]) than for Co-W and Fe-W alloys. Thus, not surprisingly, in [84] was reported that the wear rate of fcc structure nickel-based coatings is more than an order of magnitude higher than cobalt-based coatings with hcp structure having similar grain size and hardness. However, in the case of Fe-W coatings a substantial decrease of wear resistance was reported resulting from the oxidation of the surface [67,85]. As a result, the fretting of hard Fe-W alloys at dry friction is accompanied by tribo-oxidation during which iron oxides are accumulated towards the edges of the wear track. This leads to revealing of a new surface and propagation of the oxidation that increases general wear loss. Taking into account an extremely high hardness of Fe-W coatings that has been mentioned above can be concluded that the wear resistance does not solely depend on the hardness of the coating. By and large, wear resistance requires a balance of low friction, low affinity with the contacting material and ductility in addition to the hardness of the coating [86].

Notable, the considerable increase in hardness has been observed for the annealed iron group metals alloys with W/Mo [87–90]. Apparently, the heat treatment of the coatings results in partial crystallization, and this correspondingly causes the strengthening effect of the iron metal matrix containing the dissolved tungsten/molybdenum [87]. The annealing also yields reduced internal stresses of the deposit that are related to the HER occurring simultaneously with iron group metals alloys co-deposition with tungsten/molybdenum. Thus, due to the thermal treatment the hardness of these alloy coatings significantly increases [4,87]. Regarding the investigation of the annealed samples the exceptional thermal stability of nanocrystalline Co-W [6], Ni-W [62,91] and Fe-W [92] alloys has been noticed between 400-600°C. Meanwhile, the “amorphous-like” structure of W-based alloys is reported to be much more thermal resistant. For instance, the amorphous structure of Fe-W deposits with 23-30 at.% W does not change up to 800°C [2]. This temperature is slightly higher than those reported for “amorphous-like” Co-35at.%W [6] and Ni-21at.%W [57] alloys that are characterized by the re-crystallization temperature above 600°C. Above the characteristic re-crystallization temperature the metallic

compounds precipitated by annealing correspond to the stable phases expected from equilibrium phase diagram of the binary Ni-W [93], Co-W [94] and Fe-W [95] alloy systems.

1.4.2 Corrosion resistance

Usually the corrosion behaviour of the prepared metallic alloy coatings is investigated mainly by means of electrochemical techniques, such as open circuit potential (OCP), linear sweep voltammetry (LSV) and electrochemical impedance spectroscopy (EIS). Among a number of corrosion parameters, the values of corrosion current density, j_{corr} , and corrosion potential, E_{corr} , are often used to compare corrosion behaviour of electrodeposited coatings. Notwithstanding, the corrosion potential values usually do not show any evident dependence on the composition of an alloy and varies independently from the corrosion rate. This is under the assumption that potential values are driven by the rates of cathodic reaction (hydrogen evolution) and anodic reaction (electrolytic dissolution or passivity of the metal) of the corresponding system. These values are strongly affected by the corrosive media, chemical composition of material and its surface state. Thus, the further investigation of the corrosion behaviour of iron group metals with tungsten is mainly based on the comparison of j_{corr} determined from LSV analysis results that is commonly presented in the literature.

Several factors are contributed to the corrosion resistance of tungsten-based alloys, including W content, grain size, and crystallographic texture, and these parameters vary together in the set of experiments. In this context the porosity, cracks, smoothness and thickness of the deposits should be evaluated impartially to ensure that the obtained data corresponds particularly to the tested alloys and the substrate below has no influence on the results. But in some papers related to W alloys electrodeposition, the discussion about the coatings morphology or structure is suppressed. Thus, the accuracy of the summarized anti-corrosive characteristics can be only speculated. Interestingly, sometimes the results are presented as more attractive than those determined for electrolytic chromium or metallurgical steel [96]. For example, in [97] it was concluded that the anticorrosive protection ability of Co-7at.%W alloy coating can be 6–14 times better than mild steel and that the corrosion resistance varies in the range of 170–375 $\text{k}\Omega \text{ cm}^{-2}$ depending on the tested acid (the corrosion resistance decreases in the following order: 1 M HCl > 1 M H_2SO_4 > 1 M HClO_4). Furthermore, when the corrosion is discussed, it is important to think of a combination of

both material and environment as well. A maximum corrosion resistance among various tested medium has been observed in the neutral NaCl solutions (Fig. 3a). Meanwhile j_{corr} values of the nanocrystalline W alloys having 5–22 at.% of W in acidic 3.5 wt.% NaCl solution (pH 3) have been found to be much higher than those in neutral and alkaline 3.5 wt.% NaCl solution (pH 10) (Fig. 3b), for comparison, for Ni-22at.%W the $j_{corr} = 40 \mu\text{A cm}^{-2}$ at pH 3 and $j_{corr} = 4.9 \mu\text{A cm}^{-2}$ for the same alloy at pH 10 [98]. Furthermore, it was concluded that in the alkaline saline environment the corrosion rate of nanocrystalline iron group metals alloys with W generally increases with the reduction of the grain size, suggesting that the increase in grain boundary volume is the dominating factor controlling j_{corr} under this condition. Meanwhile in the acidic saline environment the corrosion resistance of such coatings increases with the reduction of the grain size, implying that the higher W content is associated with the formation of more stable surface oxide film preventing the alloys dissolution under this regime.

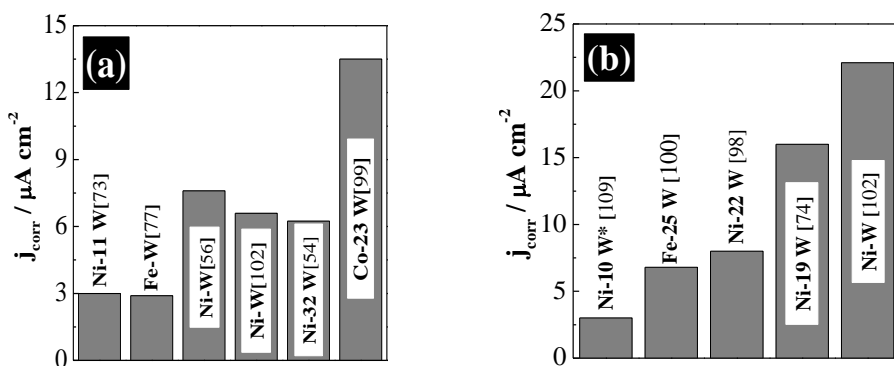


Fig. 3. j_{corr} values in neutral (a) and acidic (b) NaCl media of electrodeposited iron group metals alloys with W (in at.%) published in the literature.

3 pav. Literatūroje pateikiamos elektrochemiškai nusodintų skirtingos sudėties geležies grupės metalų lydinių su W j_{corr} vertės neutraliame (a) ir rūgštiniame (b) NaCl tirpale.

Notable, that in neutral Na_2SO_4 solution the corrosion resistance of iron group metals alloys with W is comparable to that found in neutral chloride containing media and is very close to that of the electrolytic chromium coating (Fig. 4) [99]. While using a mixture of sulphates and chlorides an increase in corrosion current has been noticed [100]. The lower corrosion resistance in sulphate-chloride media might be related to the stronger effect on the dissolution rate of tungsten alloys in the presence of oxidizing agents.

Describing the effect of the composition of the W-based alloys on their corrosion behaviour, it can be underlined the following aspects. Firstly, it is difficult to find some data showing clear relation between corrosion rate and W content, thus indicating that the corrosion resistance of W alloys is more related to the preparation conditions than to alloys composition [73,101]. Meanwhile in some other papers it is claimed that the higher W content in alloys composition initially increases the corrosion resistance and then after a particular percentage which corresponds to the limiting crystallite size the corrosion resistance decreases owing to the increase in volume of the intercrystalline region of the triple junction [102].

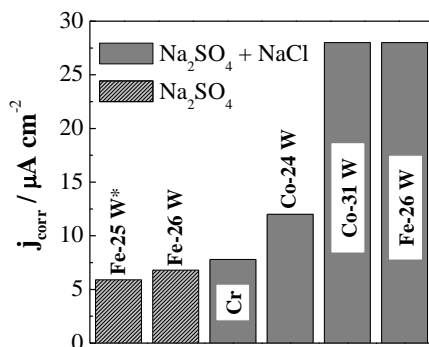


Fig. 4. j_{corr} values of the electrodeposited iron group metals alloys with W in neutral media [72].* - results from [100].

4 pav. Elektrochemiškai nusodintų skirtingos sudėties geležies grupės metalų lydinių su W j_{corr} vertės neutraliuose tirpaluose [72].* - rezultatai, pateikiami [100].

Thus, the higher intercrystalline surface fraction (defect density) provides the higher number of active surface sites for corrosion reactions. For instance, in [59,66] the lowest corrosion rate has been found for the Ni-W alloy with 5-7 at.% W that consists of ~ 20 nm grains and is characterised by a single nanocrystalline phase with fcc structure. Since many authors summarized that the corrosion of tungsten alloys occurs via preferential dissolution of iron group metal [71,79,103], it is believed that after the elution of iron group metal from a single phase solid solution lattice, an evenly structured W-rich film which inhibits further corrosion forms on the surface. This film plays a key role for protection in aggressive media since it was proved that homogeneous surface phase composition leads to the better corrosion resistance [71,104]. Contrary, other authors reported that nanocrystalline Ni-W alloy comprising the highest amount of W (the smallest crystallite size, respectively) demonstrates the best anti-corrosion properties [72,74]. In this case the explanation is based on the observation

that W accumulates on the alloys surface and suppresses the anodic dissolution. In other words, the nanocrystalline material is characterized by much higher diffusivity due to the presence of large amounts of grain boundaries, which promotes the formation of a protective oxide passive film, so that nanocrystallinity of an alloy may improve corrosion resistance as compared with its conventional polycrystalline counterpart. In [105] has been shown that in non-complexing solutions, pH is the major factor controlling passivation of the W-based alloys, i.e. a passive layer is formed rapidly in acidic and alkaline media, meanwhile in neutral solutions passivation does not occur. In the latter case iron group metal is dissolved quantitatively, and the remaining tungsten forms an amorphous layer; e.g. the corrosion resistance of the “amorphous-like” Fe-W deposit in 3 wt.% NaCl solution at 30°C was described as very poor, i.e. with the potential moving toward positive side, the deposit rapidly dissolved [96]. A contradictory information was only found for Ni-W alloy coatings, when in [103] was declared that the formation of a passive corrosion film on Ni-W sample in 5 wt.% NaCl not only stabilizes the corrosion reaction, but also provides the lubrication in tribocorrosion process.

It is widely accepted that both iron group metal and tungsten undergo passivation state forming mixed oxyhydroxides corrosion resistant film on the top of alloys surface [106], e.g. the layer of Ni(OH)₂, NiO, NiOOH and WO₃ for Ni-W system [103,107]. As it was mentioned above, such passive film inhibits the corrosion process and reduces the rate of oxidation reaction. In [108] was specified that refractory metal oxides remain at the passive film/metal interface, while iron group metal oxide/hydroxide segregates to the outer layer of the passive film. Furthermore, XPS analysis revealed that, the passive film growth was enhanced by the presence of higher amounts (> 20 at.%) of refractory metal in the alloy with Ni in the neutral solution. Contrary, in the acidic medium the higher W incorporation enhanced the anodic dissolution and had an unfavourable effect on the stability of the passive film [109].

1.4.3 Catalytic performance for methanol oxidation reaction

In the view of the rapid growth of population in the world and the depletion of non-renewable fossil fuel, the search for new nonconventional electrical energy has become a subject of importance in recent years. Direct methanol fuel cells (DMFCs), which are based on methanol decomposition process have the potential use as an alternative power sources due to their high power density, low operating temperature, substantial efficiency, and

environmentally friendly characteristics [12]. Despite these advantages, high overpotentials for the methanol oxidation reaction prevent the use of DMFCs in practical applications. This is due to the presence of partial oxidation intermediates such as $-\text{CH}_3\text{O}$, $-\text{CH}_2\text{O}$, $-\text{CHO}$, and $-\text{CO}$, which adsorb strongly on the surface of the catalysts resulting in their deactivation. As a result, the development and characterization of the better poison-tolerant and less expensive catalyst with great stability for the methanol oxidation reaction is of tremendous interest to this technology. As it was summarized above, relatively cheap and simple electrodeposition technique offers a possibility to prepare W/Mo-based alloy electrodes with a wide range of compositions. The catalytic surface activity of these alloys depends on the pH of the working medium, composition, structure (crystalline/amorphous) and the phases present in the alloy. In [106,110] was demonstrated that the anodic current density peak, a measure of methanol oxidation reaction rate, in H_2SO_4 medium is considerably higher by using the electrochemically prepared W alloys with iron-group metals in comparison with iron-group metals itself. In addition, the same tendency was reported for W-based coatings in alkaline solution and this was attributed to the larger surface roughness achieved by alloying process [106,111]. Notable, that information about catalytic activity towards methanol oxidation so far is available only for Co-W [112], Fe-W [110] and Fe-Mo [111] alloy electrodes. In general, it was concluded that the catalytic activity increases with increasing the content of refractory metal in composition [111,112]. Also, it was indicated that the heat treatment enables to increase the catalytic activity of W(Mo)-based alloy electrodes [111,122]. This may be related to the change in nature of the surface of the deposit, i.e. improved crystalline structure with the formation of the new phases, e.g. heat-treated Fe-Mo samples along with FeMo phases found before annealing show the existence of new oxide phases, namely H_2MoO_5 and FeMoO_4 [111]. In this context, clarifying the structure-performance correlation of the methanol oxidation reaction catalysts is crucial for the rational catalyst's design.

1.4.4 Electrocatalytic efficiency in the hydrogen evolution reaction

Continuing the topic about the development of the new environmentally benign energy systems combined with low cost economy, hydrogen might be concerned also as a good candidate to meet such requirements since it is considered as a clean energy carrier and can be easily used along with oxygen from the air in the hydrogen fuel cell to generate electricity through an electrochemical process. In regard with the ecological issues, it is

important that hydrogen can be easily collected during the electrolysis of water, which is recognized as an abundant and renewable hydrogen source. Moreover, hydrogen production via water splitting is safe technology possessing reasonable efficiencies [113]. Consequently, the hydrogen evolution reaction (HER) in both acidic and alkaline media is one of the most investigated reactions in the field of electrochemistry. However, an application of acidic electrolysis for hydrogen production purposes remains limited by a high cost of the required catalysts and proton exchange membranes that are used in the electrolyser system. On the other hand, compared to acidic media, HER in alkaline solution generally requires higher overpotentials and is associated with lower efficiency and larger energy consumption. Notwithstanding, alkaline medium based catalysts are considered as more attractive alternative over the acidic catalysis [114]. Hence, water electrolysis industry is mainly focusing on improving the efficiency of HER in the basic environment by the proper selection of electrode materials.

The mechanism for electrolytic hydrogen evolution on W alloys is usually discussed in terms of various physical and/or electronic parameters and usually is compared to that of Mo alloys. The theory of alloying effect of transition metal-based alloys has been discussed in [115] is based on the Engel–Brewer valence-bond theory. It has been postulated that the intermetallic combination of transition elements having partially or half-filled d-orbital (e.g. Mo, W) with transition metals having internally paired d-electrons (e.g. Ni, Co, etc.), results in a significant change in their bonding strength, and, consequently, increased intermetallic stability, whose the catalytic activity has maximum when the d-orbitals are almost filled. Indeed, the experimental results showed that the electrocatalytic activity of investigated W/Mo alloys for the HER depends on the refractory metal content in composition. However, the most effective composition of the deposits varies from author to author. The electronic structure calculations demonstrated that d-band vacancy of Ni in Ni–Mo and Ni–W alloys decreases with addition of Mo or W and becomes nearly 0 at about 11 at.% Mo and 8 at.% W. Moreover the optimal catalytic activity for the HER on the Ni–W alloy containing 10 at.% W coincides with an increase in the density of states at Fermi level of the 3d Ni band [10]. The increased electron density around Ni-sites influences proton discharge at the Ni–W surface and Ni sites serve as a hydrogen source for the neighbouring W sites. Tungsten sites in Ni–W alloys act as the “traps” for hydrogen where the ion/atom recombination and molecular hydrogen desorption is promoted more efficiently. While in [116] has been shown that in order to obtain more

active electrodeposited Ni-alloy catalyst for the HER, the concentration of Mo should not exceed 15 at.% and for W – 19 at.%. Thus, it is noteworthy that the “threshold” values can be influenced by the electrodeposition conditions.

Commonly, the ability of a given metal to catalyse the HER is measured by the exchange current density, j_0 , i.e. the rate of hydrogen evolution per surface area. It is known, that the higher the j_0 , the lower overvoltage must be applied in order to create a significant current flow. Hence, the electrocatalysts are expected to manifest exchange current densities equivalent or analogous to j_0 of polycrystalline platinum ($\sim 10^{-3}$ A cm⁻² in alkaline electrolytes) which is considered as the most effective HER catalyst so far.

Table 1. Comparison of literature data for the HER exchange current densities (j_0 in mA cm⁻²) of electrodeposited W(Mo)-based alloy electrodes.

1 lentelė. Literatūroje pateikiamų vandenilio mainų srovės tankio verčių (j_0 , mA cm⁻²), nustatytų elektrochemiškai nusodintų skirtingos sudėties geležies grupės metalų su W/Mo lydiniams, palyginimas.

Coating	W/Mo, at. %	Corrosive solution, M	Temperature, °C	j_0 , mA cm ⁻²	Reference
Co-W	18.9	1.0 KOH	65	$1.1 \cdot 10^{-2}$	[117]
Co-W	27.3	1 NaOH		$1.13 \cdot 10^{-2}$	[118]
Co-W	22.6	7 KOH	25	$1.2 \cdot 10^{-3}$	[119]
Ni-W	18.1			$6.5 \cdot 10^{-3}$	
Ni-Mo	-	7 KOH	80	55.24	[120]
	25	2 NaOH	30	$3.1 \cdot 10^{-2}$	[121]
	26	8.25 NaOH	85	44.4	[122]
	-	6 KOH	80	18.62	[123]
	23.8	7 KOH	25	2.8	[124]
	29.8	1 NaOH	30	11.1	[125]
	27.5	1 KOH	25	$3.18 \cdot 10^{-3}$	[126]
	7.5	6 KOH	70	7.3	[127]
	20.8	11 NaOH	80	42.4	[128]
NiMo-modified Ni foam	2.5	0.1 NaOH	25	$4.1 \cdot 10^{-2}$	[129]
Ni + Mo composite	44	5 KOH		1.0	[130]
Ni-Mo-rGO	30.8	1 KOH		$4.31 \cdot 10^{-3}$	[131]
Ni-Mo Co-Mo	10.4 20.8	7 KOH		$2.6 \cdot 10^{-2}$; $2.3 \cdot 10^{-2}$	[119]
Co-Mo	40.9	1 NaOH	25	1.5	[132]
	32	0.5 NaOH	60	$6.9 \cdot 10^{-3}$	[133]
	25	1 NaOH	25	0.13	[134]
	19	1 KOH		0.36	[135]
Fe-Mo	59.3	1 NaOH		$2.4 \cdot 10^{-3}$	[136]

Based on investigations carried out by different authors can be concluded that molybdenum-based alloys are more active in the HER in alkaline medium than tungsten-based alloys. Moreover, in comparison of Ni-Mo, Ni-W, Co-Mo and Co-W coatings, it was found that those containing cobalt in composition show higher catalytic activity than nickel containing alloys. Though, there is also some information suggesting that Ni-based coatings have better catalytic activity for HER compared to cobalt containing deposits [119,137]. At the first glance, these controversial results could be attributed to the different alloys preparation techniques, which are capable to yield uneven composition, morphology and structure of the prepared samples and thus, directly influence the catalytic properties of the samples. On the other hand, the clear tendency of catalytic behaviour cannot be easily defined for alloy cathodes fabricated even by using the same electrodeposition technique (see Table 1).

One of the possible reasons is that the authors in electrocatalytic papers scarcely discuss the surface state and characteristics and in such way prevents any reliable comparison of achieved catalytic effects. In order to do so all samples should be brought on the same roughness factor that enables to calculate the intrinsic current densities and compare the achieved catalytic effects.

1.5 Summary

In previous subchapters, attempts have been made to collect and present concise information regarding different characteristics of nanocrystalline iron group metals (Co, Ni, Fe) alloys with tungsten/molybdenum. This is crucial in order to point up the broad trends in the worthy application of tungsten-based alloys in different industries. It could be generalized that the high temperature resistance and premium mechanical properties of tungsten-based alloys are most attractive for countless targeted engineering applications some of which are presented in Fig. 5.

For instance, as it was indicated above, electrodeposited Fe-W alloy coatings suppress elevated temperatures and considering their high hardness could be utilized at some processes, which require a higher temperature. However, Fe-W coatings usually are characterized by low corrosion resistance, thus their application for corrosion protection becomes restricted. Contrary, electrodeposited Ni-W alloys are characterized by improved anti-corrosive behaviour though slightly lower hardness and thermal stability in comparison with Fe-W coatings. What is more, electrodeposited Ni-W alloys were found to be suitable for electrocatalytic films formation for hydrogen evolution through water electrolysis.

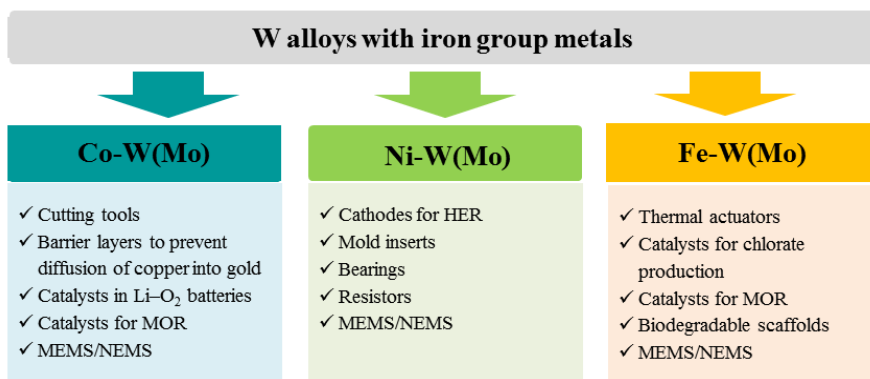


Fig. 5. Various applications of W alloys with iron group metals.

5 pav. Geležies grupės metalų lydinių su W/Mo pritaikymo galimybės.

Meantime, the characteristics described in previous subchapters for Co-W alloys allow proposing these coatings as corrosion resistant ones possessing favourable tribological properties as well as high hardness close to chrome coatings, thus being suitable as an alternative for ones. Furthermore, they can also be considered as promising candidates for the development of advanced and inexpensive electrocatalysts to replace platinum-based materials for the production of hydrogen from alkaline solutions. However, in order to enhance the utilization of these alloys as effective multifunctional catalysts having superior mechanical properties, corrosion resistance combined with good thermal stability, it is necessary to perform consistent studies of their functional properties. In addition to the previous studies made by our group on comprehensive examination of mechanical, thermal and tribological behaviour of W alloys, this study is devoted to the deeper understanding of corrosive and catalytic behaviour in HER and MOR of nanocrystalline W/Mo alloys, in order to supplement the full mapping of the properties and suggest the optimal composition of the sample having coupled functionalities.

2. EXPERIMENTAL

In this chapter some general information is presented on the electrochemical synthesis of iron group metal alloys coatings and nanowires procedures used in this study. The citrate and acetate electrolytes were investigated earlier have been applied for the electrodeposition. The main target of given research was focused on the modification of the above mentioned electrolytes and deposition conditions in order to prepare samples with various content of W or Mo in the alloys. Furthermore, the fundamentals of the techniques applicable to the analysis of the compositional, morphological, structural and functional properties, i.e. corrosion and catalytic behaviour, of the prepared coatings are overviewed as well. It should be pointed out that the detailed info on particular research activities and operating conditions can be found in the appended articles. The overview on the research carried out under this thesis is presented in Fig. 6. The details on the electrolytes used for coatings fabrication are summarized in Table 2.

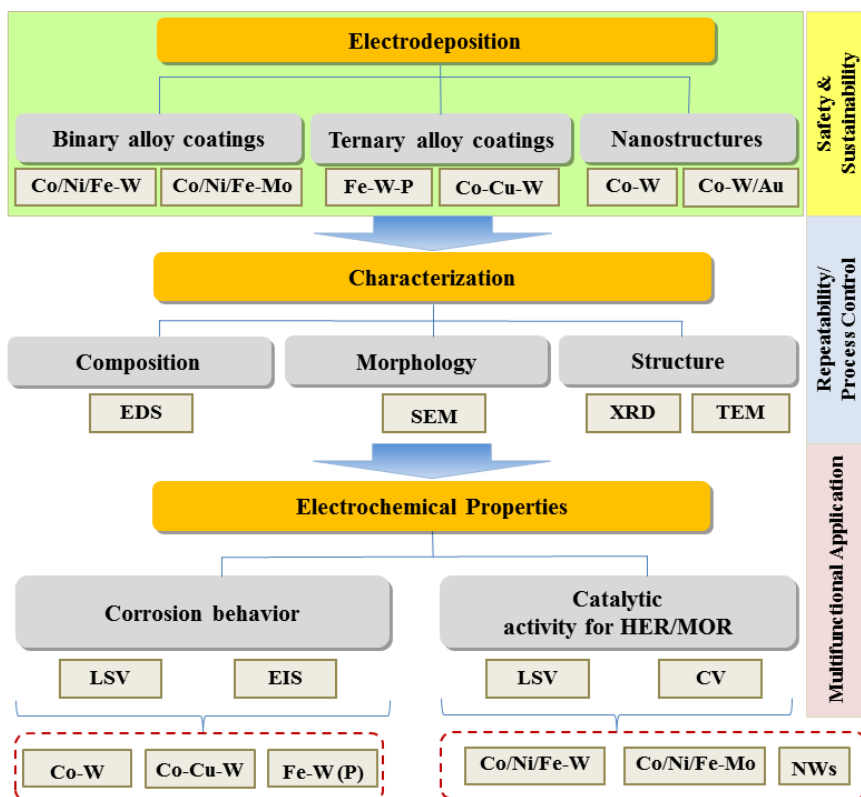


Fig. 6. Schematic diagram of experimental methodology.

6 pav. Bendra geležies grupės metalų lydinių su W/Mo tyrimų metodologija.

Table 2. Chemical composition of the electrolytes. Indexes next to the alloys indicate the references to the corresponding articles.

2 lentelė. Elektrolitų cheminė sudėtis. Indeksai šalia lydinių reiškia nuorodas į atitinkamus straipsnius.

Coating Reagent	Co ^{I,IV}	Ni ^I	Fe ^I	Co-W ^{IV}	Fe-W ^I	Ni-W ^I	Cu-W ^V	Co-Cu-W ^V	Fe-W-p ^{VI}	Co-Mo ^{II}	Fe-Mo ^{II}	Ni-Mo ^{II}	Co-W NW ₅ ^{VII}
CoSO ₄	■							■					
FeSO ₄			■		■				■				
NiSO ₄		■				■							
CuSO ₄							■						
C ₆ H ₈ O ₇	■	■	■	■	■	■	■	■	■				
Na ₃ C ₆ H ₅ O ₇	■	■	■	■	■	■	■	■	■				■
H ₃ BO ₃									■				
Na ₂ WO ₄									■				■
H ₂ NaO ₂ P													
C ₄ H ₁₀ O ₂									(+)				
Rokafenol									(+)				
C ₂ H ₅ NO ₂													■
(NH ₄) ₂ MoO ₄										■	■	■	
CH ₃ CO ₂ NH ₄													
CH ₃ CO ₂ K													

2.1 Formulation of electrolytes vs properties investigated

One of the grand challenges in modern electrochemistry is to develop alternative technologies to produce metals/alloys in a cleaner, safer, and environmentally benign manner [138]. Reaching this goal a citrate-based *plating solution* for electrodeposition of iron group metals alloys with W has been developed [139]. Non-volatile citrate electrolytes are attractive for a long term electrolysis at elevated temperatures [6]. Moreover, a proposed citrate bath allows lowering of the grain size of electrodeposits below 100 nm, so is of great interest for electrodeposition for macro-sized surfaces as well as for the electroforming of micro-/nano- technical devices [6].

The Co-W coatings have been already investigated earlier by Tsytsaru et al. [7,140,141], where has been shown that these coatings have promising potential as multifunctional materials. Therefore, in this research the Co-W coatings have been selected as a main case for investigation, in order to deepen the knowledge on interdependencies between deposition parameters and design of new functional electrodes having high advanced electrochemical properties. Only by changing the pH from acidic to alkaline values, it was possible to control and tune the tungsten content and this was realized even more accurately than in previous research [7,142]. This tuning

ability can be attributed to the ionic equilibrium in the electrolyte, which shifts in the direction of formation of monotungstates that are reduced much more efficiently than polytungstates, which are formed in an acid medium [36]. As a result, the pH increment from 5 to 8 leads to an increase of the W content in the deposits with iron group metals from 2 at.% up to 36 at.%. In order to reveal the influence of iron group metal nature on the electrochemical properties, along with Co-W coatings, Ni-W and Fe-W alloys were electrodeposited as well. For such purpose, the citrate electrolyte was modified by replacing CoSO_4 component with NiSO_4 or FeSO_4 , respectively. The specific electroplating conditions for the electrodeposition of Co-W, Ni-W and Fe-W coatings are provided in *Articles I, III, IV, VI*.

It is known that the substitution of W by Mo significantly increases the concentration of refractory metal in iron group metal alloy's composition [143,144]. Based on the reports [145–147] certifying that the catalytic activity for hydrogen evolution is qualitatively proportional to the refractory metal content in the alloy, in this work Mo-rich electrodes were synthesized from ammonium acetate bath which was adapted from Morley et al. [148]. Notable, such water deficient aqueous electrolyte with high concentration of acetate was proposed for the electrodeposition of the metallic molybdenum layer. In order to determine the influence of iron group metal nature on the catalytic activity of targeted coatings (Co-, Ni- and Fe- Mo-rich alloys) the electrochemical conditions were tuned in such a way to ensure deposition of alloys having the similar content of Mo. The electrodeposition process in detail is described in *Article II*.

Generally, the insufficient corrosion resistance of W alloys is one of the main obstacles preventing their widespread usage in electrocatalysis. Copper introducing as a third component into binary iron group metals alloys with W may assist in improving the corrosion resistance of the coating and in such way to expand the range of its possible applications. For this purpose to the initial solution used for Co-W alloys electrodeposition the appropriate amount of CuSO_4 salt was introduced in order to form ternary Co-Cu-W alloys. Furthermore, special attention was paid to the electrodeposition of Cu-W coatings since it was reported that such system cannot be electrodeposited [149]. The outcomes of this study are described in *Article V*.

Furthermore, it was shown that the addition of phosphorus to iron group metals alloys is also quite effective way to enhance the corrosion resistance in acidic and alkaline media, especially during long term exposure by stimulating spontaneous passivation [150]. Thus, considering the fact that Fe-based alloys can be used as a food-contact surface, that is constantly

affected by corrosive environment caused by food constituents; the influence of phosphorous on corrosion resistance was investigated. The detailed experimental conditions and composition of the plating baths in which sodium hypophosphite was introduced as a source of phosphorous are described in *Article VI*. In order to improve the physical appearance of Fe-W-P coating, also the influence of organic additives, such as Rokafenol-10 and N-butindiol was investigated as well.

Finally, the improvement of alloys electrochemical performance was examined through nanostructurization of Co-W alloy by applying electrodeposition into nanoporous templates. A well-ordered nanowires arrays may offer many advantages for catalysis, including the increased catalyst loading amount and surface area, reduced internal resistance, shortened ionic diffusion path, and favourable boundary for gas bubble release [151,152]. However, regarding the synthesis of NWs, a challenge in depositing metal/alloy into nanometer structures rises because of inherent hydrogen evolution (side reaction). Thus, in order to improve the efficiency of the electrolysis process and uniform deposition of Co-W alloy, glycine was added to the plating solution as a complexing agent. It was shown that it stabilizes the pH close to the electrode surface in both alkaline and acidic electrolyte [153]. At the same time glycine is a non-toxic, easily obtained and, upon degradation, effluent treatment is easier [154]. What is more, the viability of a novel Co-W nanowire/Au nanoparticle hybrid composite is presented (more details are given in *Article VII*).

2.2 Electrodeposition procedure

Coatings described in this work were electrodeposited onto stainless steel (type 304) substrate foils (2 cm²), and on stainless steel rods (1 cm²), depending on the requirements for coatings characterization. The composition of the both substrates is the following (in wt.%): Fe-70, Cr-19, Ni-8, Mn-2, other: Si, Al, P-1. The electrodeposition of Mo-rich coatings was carried out on copper substrates. Electrodeposition has been performed in a standard three-electrode cell. A platinized titanium mesh was used as a counter and Ag/AgCl/KCl_{sat} as a reference electrode, respectively. Prior to electrodeposition the stainless steel substrate was washed with detergent and rinsed with water and acetone in an ultrasound bath in order to remove any contaminants from the surface. For the better adhesion of the alloys to the substrate, a nickel seed layer (thickness of ~ 30 nm) was electrodeposited from an electrolyte containing 1.0 M NiCl₂ and 2.2 M HCl, at the room temperature at the cathodic current density of 10 mA cm⁻². The thickness of all synthesized coatings was calculated based on gravimetric and elemental

analysis results [155], and was ~ 10-15 μm . The cathodic current efficiencies (CCE) were determined based on the charge passed, the mass and chemical composition of the deposited alloys using Faraday's law [155]. Notable, in this work alloys' composition is given in at.%.

2.3 Characterization of alloys

The morphology of deposits was investigated by SEM Hitachi TM3000 and high resolution Hitachi SU-70 (*Articles I-VI*). The chemical composition was measured with an INCA energy dispersive X-ray spectroscopy detector (Oxford Instruments) at an accelerating voltage of 20 kV. Transmission electron microscopy (TEM) results for deeper understanding of the nature of W-rich alloys structure were obtained using Talos F200X (200kV, field emission) HRTEM microscope. Meanwhile the specific operating TEM analysis conditions for Co-W nanowires are given in *Article VII*. The structural changes of alloy coatings described in *Articles I-VI* were analysed using diffractometer Rigaku MiniFlex II. Analysis of the spectra was carried out using PDXL software. The crystallite size of the alloys was calculated by using Sherrer's equation [78].

2.4 Electrochemical analysis methods

Hydrogen evolution and electrochemical corrosion behaviour of the electrodeposited alloys were investigated by means of potentiodynamic polarization and electrochemical impedance spectroscopy (EIS) using AUTOLAB302 device and GPES software (*Articles I, II, IV, VI*). Cyclic voltammetry (CV) measurements were employed for investigation of Co-W electrodes towards methanol electro-oxidation as described in *Article III*.

2.5 Summary

Good experimental infrastructure is necessary to explore and understand the relationship between composition and structure of obtained materials and their properties, and how this relationship is affected by processing parameters. Firstly, to characterize adequately and understand the characteristics of metals and alloys, each specimen is desired be of the highest quality and properly controlled so it would be possible to manipulate it, when necessary. Once prepared, several surface analytical techniques (SEM-EDS, TEM, XRD) are available to investigate compositional, morphological and structural peculiarities. Meanwhile different electrochemical methods (potentiodynamic polarization, CV, EIS) may be applied for the evaluation of material's functional properties.

3. RESULTS AND DISCUSSIONS

This chapter briefly summarises the major findings that can be outlined on the base of the accomplished research on the electrochemical properties (alkaline HER, MOR and corrosion behaviour in acidic solution) of nanocrystalline iron group metals (Co, Ni, Fe) alloys with W/Mo. A thorough discussion of the results can be found in the appended eight publications (referred in the text by their Roman numerals).

3.1 Interdependences between composition, structure and morphology

Electrochemical properties, such as catalysis towards HER, MOR and corrosion behaviour, are controlled by the surface reactions and comprehensive understanding of such processes needs a good knowledge of microstructure and nature of the surface of the electrodes. Accordingly, in this subchapter the compositional, structural and morphological investigation of electrodeposited iron group metals alloys with refractory metals (W and Mo) is presented. This investigation was a primary step for guided selection of the sample for further evaluation of the catalytic activity (MOR, HER) and corrosion properties.

W-based alloys. The properties of the alloys depend on many factors. The most important is the chemical composition, due to the synergistic effect of the constituents of an alloy, which will influence on structure and properties. It is known, that alloy's composition depends on the ratio of the partial current densities of the constituents. However, the ones are controlled by a number of factors, such as the bath chemistry, total current density or applied potential, temperature, etc. Thus, in order to map the composition-properties interdependencies, iron group metals alloys with tungsten content varying in a wide range were electrodeposited from a citrate-based electrolyte. More specifically, the binary iron group metals alloys having 2 – 33 at.% of W have been prepared by changing the electrodeposition parameters, i.e. cathodic current density or deposition potential, pH and temperature of the plating bath. The interdependencies between the investigated parameters schematically are shown in Fig. 7. As it can be seen, the increment of the bath temperature from 20°C to 60°C decreases polarization, which can increase the concentration of metals in the cathode diffusion layer [156] and thus, leading to an increase of the partial current densities for W deposition and its content in the coating. Therefore, the maximum W content that can be reached at 20°C, and it not exceeds 25 at.% of W.

The variations of W content in Co-W alloys with pH were more thoroughly investigated at 60°C by varying the pH from 5 to 8 at the fixed current density. As can be seen from Fig. 7 for the given electroplating bath composition the increase of the W content in the alloy with pH growth is noticed. This correlates well with the rapid raise in the concentration of some W(VI)-citrate complexes such as $(\text{WO}_4)(\text{HCitr})\text{H}^{4-}$ at $\text{pH} > 5$ [7]. The maximum percentage of W co-deposited with iron group metals in this work reaches ~ 30 at.% at pH 8. The further increase of pH it is not rational as can lead to the decrease in tungsten content due to the drop in $(\text{WO}_4)(\text{HCitr})\text{H}^{4-}$ concentration in cost of increase in concentration of “free” WO_4^{2-} ions [7]. Probably, WO_4^{2-} ions are less electrochemically active than $(\text{WO}_4)(\text{HCitr})\text{H}^{4-}$, so the content of W in the alloys as a function of pH usually has maxima [36].

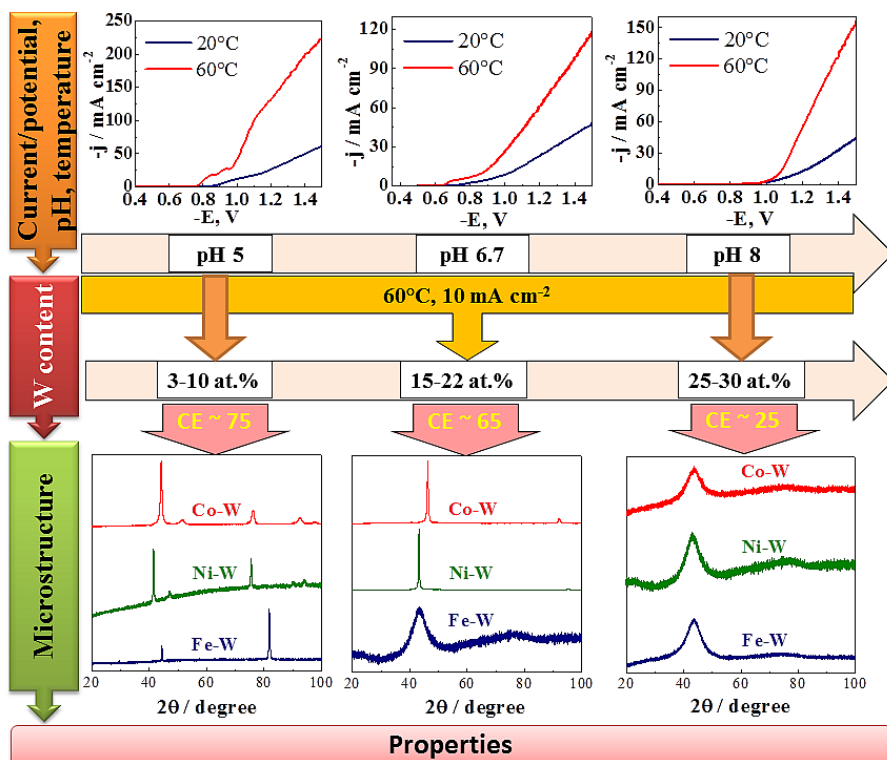


Fig. 7. Mapping of the composition and structure of Co-W coatings with electroplating variables.

7 pav. Co-W lydinių sudėties ir struktūros priklausomybė nuo elektronusodinimo sąlygų.

On the other hand, it was found that the current efficiency depends rather on the alloy composition than on the bath temperature. It was concluded that

CE decreases as the higher amount of tungsten in the coatings is deposited. This could be attributed to an increase of hydrogen evolution during deposition with the higher W content in the deposit [157]. The crystallinity of W alloys with iron group metals is associated to W content. Coatings with low tungsten percentage (< 10 at.%) show diffraction patterns typical to an fcc Ni, hcp Co or bcc Fe structure (Fig. 7). Notable, the diffraction peaks shift to the lower diffraction angle range with an increase in W content in the deposits; it indicates that bigger W atoms are incorporated into crystalline lattice of Ni, Co or Fe and corresponding solid solutions are formed. At W contents above 22 % at.% for Ni-W and Co-W and 15 at.% for Fe-W alloys the diffraction spectra showed halo patterns, which are characteristic to an “amorphous-like” structure. In fact, the crystallite size decreases from 27 nm to ~ 1.5 nm for Co-W alloy; from 15 to ~ 4 nm for Ni-W alloy; from 41 nm to ~ 1.5 nm for Fe-W alloy with increasing the W percentage from 0 % (iron group metals) to ~ 30 at.%.

The values of crystallite sizes were confirmed by diffraction patterns obtained by TEM (see *Article I*). Thus, in this study the alloys that are characterized by one broad peak on their diffractograms, compared to the crystalline ones, are named ultra-nanocrystalline. While the mapping of elements showed that both iron group metal and W are distributed almost evenly onto the entire surface at nanometric scale. However, there are some regularly located spots with higher W amount. Probably, it is due to mixed structure obtaining by electrodeposition: tungsten solution in nickel and intermetallic compounds, namely Ni_4W [93–95], Co_3W [7,57], Fe_2W [57] and W solid solutions in Ni, Co, Fe form in W-rich Ni-W, Co-W and Fe-W alloys, respectively. Notable, it is difficult to determine to which particular phase the broad peak is attributed, because the characteristic peaks for W solid solutions in iron group metals and corresponding intermetallic phases are fully overlapped [7]. Thus, for the deeper investigation of the structure the more advanced instrumental analysis has to be applied. For instance, in the case of Fe-W coatings the Mössbauer spectroscopy supported the abovementioned presumption and suggested that amorphous deposits consist of a mixture of molybdenum solid solution in α -Fe and intermetallic phases, e.g. Fe_3W , Fe_2W [67].

It is important to highlight, that “amorphisation” of the alloys structure can be controlled not only by chemical composition, but also by tuning the temperature of the plating bath. More specifically, the electrodeposition of Co-W alloys at the 60°C leads to the formation of “amorphous-like” structure at lower W content, i.e. above 13 at.%, in comparison to the electroplating at the room temperature (Fig. 8). Analogous results have been

obtained for Fe-W alloys electrodeposition from citrate-glycolic electrolyte [158]. Apparently, this is due to the higher polarization which is realized at lower temperature leading to generation of higher number of nucleation sites and in such a way, coarsening of the crystallites size. In addition, the lower temperature of the electrolyte negatively affects the quality of the coatings due to the promoted hydrogen embrittlement. A visual analysis has shown that the coatings deposited at 20°C are cracked and can be easily stripped off mechanically from the substrate, while those electrodeposited at 60°C temperature are free of cracks and well adhered to the substrate.

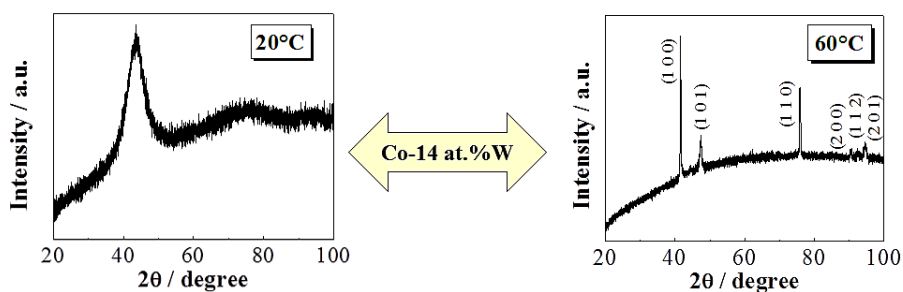


Fig. 8. X-ray diffraction patterns recorded on Co–W electrodeposits having 14 at.% of W and electrodeposited at different temperatures.

8 pav. Skirtingose temperatūrose elektrochemiškai nusodintų Co-14at.%W lydinių Rentgeno spindulių difraktogramos.

Some representative SEM images are shown in Fig. 9, in which the influence of the W content on morphology of investigated coatings is provided. In general, for all alloys the morphology evolves from angular/faceted growth, which is typical to pure iron group metals (content of W is < 20 at.%) to nodular growth (content of W > 20 at.%). Notable, the W-rich iron group metals alloys are characterized by more homogeneous and denser morphology. The surface roughness measurements revealed that the addition of W leads to the reduction of the average surface roughness (R_a) from ~ 600-700 nm (for pure Ni and Fe) to ~ 300 nm for Ni-W and Fe-W alloys with 30 at.% of W. In contrary, the R_a of electrodeposited Co-W coatings shows the tendency to increase with the higher W percentage in the alloys composition and changes from ~ 300 nm for electrodeposited Co to maximum of 487 nm for Co-33at.% W. The “cauliflower” type structures that appear as aggregates of the smaller grains are clearly observed in the SEM image of this Co-W alloy coating (Fig. 9c). Important to note that a subsequent release of hydrogen results in high tensile stress, which develops micro cracking on Ni-W surface (see insets of Fig. 9 d-f).

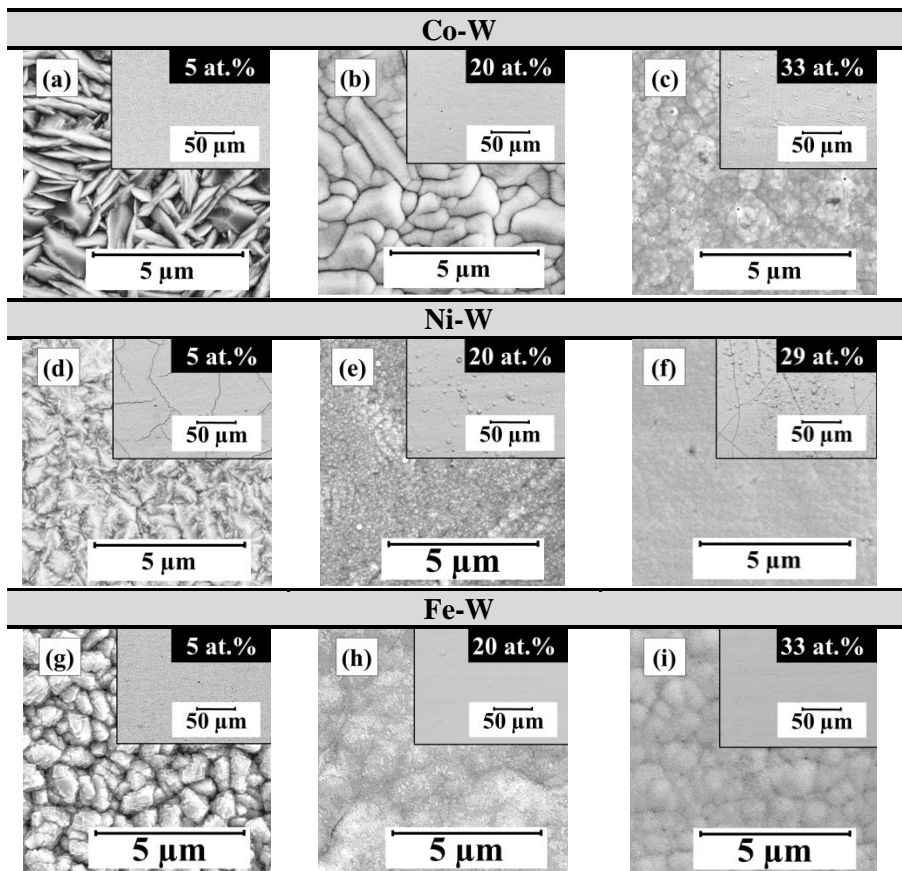


Fig. 9. SEM images of iron group metals alloys deposited at 60°C and having different W content in the alloys. Images are made at higher (x6000) and lower (x500, inserts) magnifications.

9 pav. Skirtingos sudėties geležies grupės metalų lydinių, elektrochemiškai nusodintų 60°C temperatūroje, SEM nuotraukos, esant didesniam (x6000) ir mažesniam (x500, tarpai) didinimui.

Mo-based alloys. It is known that the substitution of W by Mo significantly increases the content of refractory metal in iron group metal alloys [143,159]. Indeed, in this work it was found that the Mo content in alloy can be tuned from 30 at.% to 78 at.% by decreasing molar ratio [Ni(II)]:[Mo(VI)] in the saturated acetate electrolyte from 1.0 to 0.25 and increasing the cathodic current density from 30 to 100 mA cm⁻². Notable, such Mo amount is significantly higher than reported in the previous works reported for Mo-based alloys electrodeposition from aqueous electrolytes and it is close to had been determined for Ni-Mo alloys prepared by metallurgical [145] or mechanical alloying technique [160]. However, the side reaction (hydrogen evolution) is also increased under these conditions

and it results in larger micro-cracks propagation. Accordingly, in order to obtain Mo-rich alloys without visible defects, the applied cathodic current density of 30 mA cm^{-2} and ratio $[\text{Ni(II)}]:[\text{Mo(VI)}]$ of 0.5 were accepted as optimum conditions that allowed to electrodeposit Mo-rich coatings ($\sim 50 \text{ at.}\%$) coupled with suitable morphology (crack-free coatings with less rough globular surface) and reasonable efficiency ($\sim 50 \%$) (Fig. 10).

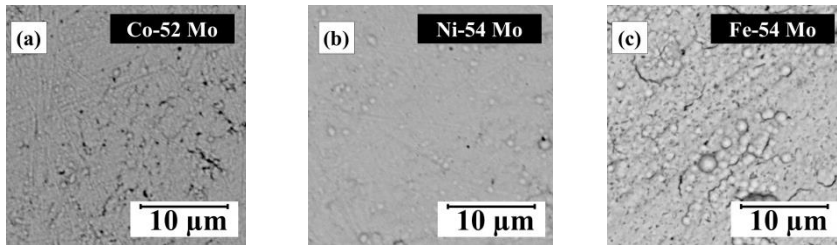


Fig. 10. SEM images of electrodeposited alloys of: Ni-Mo (a), Co-Mo (b) and Fe-Mo (c) alloys.

10 pav. Elektrochemiškai nusodintų Ni-Mo (a), Co-Mo (b) and Fe-Mo (c) lydinių SEM nuotraukos.

As it was expected, the characteristic single broad peaks indicating the ultra-nanocrystalline structure for obtained Co-52at.%Mo, Ni-54at.%Mo and Fe-54at.%Mo have been depicted (Fig.11).

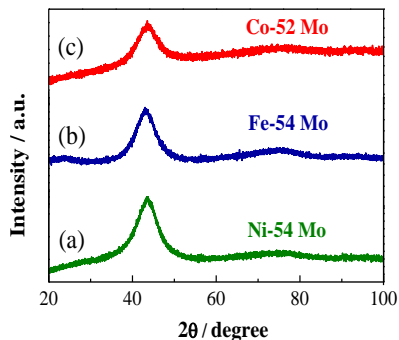


Fig. 11. XRD pattern for: (a) Ni-54 Mo, (b) Fe-54 Mo and (c) Co-52 Mo electrodeposits.

11 pav. Elektrochemiškai nusodintų molibdeno lydinių Rentgeno spindulių difraktogramos: (a) Ni-54 Mo, (b) Fe-54 Mo, (c) Co-52 Mo.

Based on the previous results, the formation of intermetallic Ni_4Mo , Ni_3Mo and NiMo compounds in line with a solid solution of Ni in Mo become possible for Ni-Mo alloys having $> 25 \text{ at.}\%$ of Mo [161,162]. In the case of Co-Mo alloys with $> 27 \text{ at.}\%$ of Mo, some of the studies reported that Mo solid solution in cobalt and intermetallic Co_3Mo are formed [133]. While for

Fe-Mo, analogously to the “amorphous-like” Fe-W alloy, the Mössbauer spectroscopy shows that deposits having more than 17 at.% of Mo consists of a mixture of molybdenum solid solution in α -Fe and intermetallic phases, e.g. Fe₃Mo, Fe₂Mo [163].

3.2 Electrochemical properties

3.2.1 Hydrogen evolution reaction (HER)

Based on the results obtained in the previous section, the iron group metals alloys with the distinct microstructures, i.e. nanocrystalline coatings having 3 at. % and 18 at. % of W and ultra-nanocrystalline alloys with ~ 30 at.% of W, have been selected for the catalytic experiments towards hydrogen evolution reaction in an alkaline environment. The comparative studies were performed on the electrodeposited Ni, Co and Fe coatings and metallurgical Pt under the same experimental conditions. The LSV measurements to determine the kinetic parameters of the HER were performed in 30 wt.% NaOH solution at $25 \pm 2^\circ\text{C}$ and the corresponding electrochemical parameters (Tafel slope (b_c), apparent exchange current density (j_0), and polarization at $j = -200 \text{ mA cm}^{-2}$ (η_{200})) obtained from the linear part of semi-logarithmic polarization plots are summarized in **Article I**.

Generally, it was found that the apparent ECDs on binary W alloys are considerably higher than that for pure Ni, Co and Fe electrodeposits. Particularly, the higher values of hydrogen evolution rate were observed with increasing W content in the coatings, i.e the catalytic activity for all coatings follows the sequence: $> 5 \text{ at.\% W} > 20\text{at.\% W} > \sim 30 \text{ at.\% W}$. As it was shown in previous section (Section 4.1), W-rich (~ 30 at.%) alloys are characterized by the finely refined grained (ultra-nanocrystalline) structure that probably offer the greater activity due to the better dispersion of the catalyst active sites and higher affinity for hydrogen absorption [164,165]. In addition, it was claimed that the higher activity of an “amorphous-like” iron group metal based HER catalyst originates from a change in its electronic structure caused by the absorption of hydrogen.

The highest catalytic activity determined for Ni-29at.%W alloy could be attributed to the structure peculiarities, more specifically the presence of the intermetallic Ni₄W phase, which in previous works was characterized by the fast water dissociation kinetics that allows improving of the HER performance [166]. Indeed, the computational and experimental results revealed the fact that the kinetic energy barrier of the initial Volmer step is substantially reduced on the such type intermetallic phase catalysts [166].

Furthermore, it was demonstrated that Ni₄W phase is more stable under liquid phase reactions [167,168].

It is known that the temperature of alkaline bath plays an important role on the increase of the catalytic activity of W(Mo)-based cathodes towards the HER [169]. Hence, the electrodeposited Ni-29at.% W, Co-33at.% W and Fe-30at.% W electrodes demonstrated the higher catalytic activity, and were tested at temperatures ranged from 25 to 65°C by applying 10°C increments. The temperature has a significant influence on the HER (Table 3). For comparison, the apparent ECD obtained for metallurgical Pt was 9.1 mA cm⁻² with the Tafel slope value of 119 mV dec⁻¹ and η_{200} of 106 mV dec⁻¹ at 65°C.

Table 3. Experimental values j_0 (mA cm⁻²) and Tafel slopes (b_c , mV dec⁻¹) for as-deposited alloy electrodes at different 30 wt.% NaOH solution temperatures.

3 lentelė. Eksperimentiškai nustatytos elektrochemiškai nusodintų geležies grupės metalų lydinių j_0 vertės (mA cm⁻²) ir Tafelio nuolinkiai (b_c , mV dec⁻¹), esant skirtingoms 30 sv.% NaOH tirpalo temperatūroms.

Electrode	25°C		35°C		45°C		55°C		65°C	
	j_0	b_c	j_0	b_c	j_0	b_c	j_0	b_c	j_0	b_c
Ni-29 W	0.55	142	1.5	134	2.9	118	5.9	97	14.5	78
Co-33 W	0.29	146	0.91	139	1.2	134	2.7	101	6.0	93
Fe-30 W	0.016	176	0.019	160	0.041	149	0.12	143	0.29	139

The obtained results agree with the previous studies certifying that the catalytic activity for hydrogen evolution is qualitatively proportional to the refractory metal content in the alloys with iron group metals [145–147]. Following this phenomenon the Ni-, Co- and Fe- Mo alloys with the higher refractory metal content, namely 50 at.% of Mo, were tested as the catalytic material for alkaline HER at the same conditions. Among all investigated systems, the Co–52 at.% Mo electrode demonstrates the best performance towards the HER, particularly at temperatures higher than 45 °C (Table 4). These results correspond well with findings published in [119], where it was confirmed that Co–Mo co-deposits are characterized by a higher catalytic activity and stability in alkaline water electrolysis than Ni–Mo, Co–W and Ni–W alloy electrodes.

Moreover, in [170], it was shown that catalytic activity depends on the metal-hydrogen bond strength and absorption sites in the alloy available to hydrogen and thus the electrochemically charged H content decreases in the series of Co–Mo > Co–W > Ni–Mo.

Table 4. Experimental values of j_0 (in mA cm^{-2}) and Tafel slopes (b_c , in mV dec^{-1}) for electrodeposited Ni–54Mo, Co–52Mo and Fe–54Mo alloy electrodes at different 30 wt.% NaOH solution temperatures.

4 lentelė. Eksperimentiškai nustatytos elektrochemiškai nusodintų Ni–54Mo, Co–52Mo and Fe–54Mo lydinų j_0 vertės (mA cm^{-2}) ir Tafelio nuolinkiai (b_c , mV dec^{-1}), esant skirtingoms 30 sv.% NaOH tirpalo temperatūroms.

Electrode	25°C		35°C		45°C		55°C		65°C	
	j_0	b_c	j_0	b_c	j_0	b_c	j_0	b_c	j_0	b_c
Ni-54 Mo	0.62	128	3.21	128	7.32	119	14.7	116	25.4	123
Co-52 Mo	1.90	132	9.53	130	17.1	128	32.0	121	46.2	119
Fe-54 Mo	0.23	152	0.99	148	4.33	142	5.83	139	14.6	145

Furthermore, comparing Co–Mo, Co–W and Ni–Mo electrodeposits, the thermal desorption of hydrogen occurs at the lowest temperature on Co–Mo showing a faster recombination step of H atoms possible on this alloy, thus improving its electrocatalytic performance [170]. In general, the present study shows that the catalytic activity for the Ni–Mo alloy is comparable to previously reported samples under similar experimental conditions (see *Article II*).

3.2.2 Methanol oxidation (MOR)

Extending the application of iron group metal alloys in electrocatalysis, the possibility to apply Co–W electrodes for MOR has been investigated. For this purpose alloy samples with characteristic compositions, i.e. Co-3at.%W, Co-18 at.%W (nanocrystalline structure) and Co-30at.%W (ultrananocrystalline structure), were chosen for electrodeposition. The catalytic results were interpreted by means of CV measurements in 1 M $\text{CH}_3\text{OH} + 0.1 \text{ M H}_2\text{SO}_4$ solution at $22 \pm 2^\circ\text{C}$.

It was found that as-deposited Co-3at.% W and Co-18 at.% W coatings are totally inactive for methanol oxidation since the CV curves in both cases are almost linear (Fig. 12). It is presumed that the high current density (up to 350 mA cm^{-2}) can be detected due to the continuous dissolution of Co–W alloys that occurs through the whole alloy layer (based on EDS analysis).

Meanwhile when the W content in the deposit is $\sim 30 \text{ at.}\%$, only the top surface layer of the alloy takes part in the corrosion process. More specifically, in this case after experiment in 1 M CH_3OH and 0.1 M H_2SO_4 solution the Co content in the alloys decreased from 70 to 67 at.%, accordingly W content in composition increased from 30 to 33 at.%. After polishing the surface layer of the alloy W content in composition was the

same as it was in surface layer before experiment in the tested solution, i.e. ~ 30 at.%. Apparently, the coatings having such high amount of W in their composition are more corrosion resistant and the synergistic effect by the interaction between Co and W prevents the active Co dissolution during the methanol oxidation reaction. Consequently, the Co-30at.%W alloy can be considered as possible electrocatalyst for methanol oxidation. Indeed, in the case of Co-30at.%W alloy the oxidation reaction occurs at about 0.67 V (the catalytic activity was evaluated from this peak current) and this potential and the shape of CV curve is similar to the typical CV shape determining on Pt electrode (Fig. 12 (c)), whereas no peak at this potential was noticed in the voltammogram for Co-30at.%W deposit in the absence of methanol (see *Article III*).

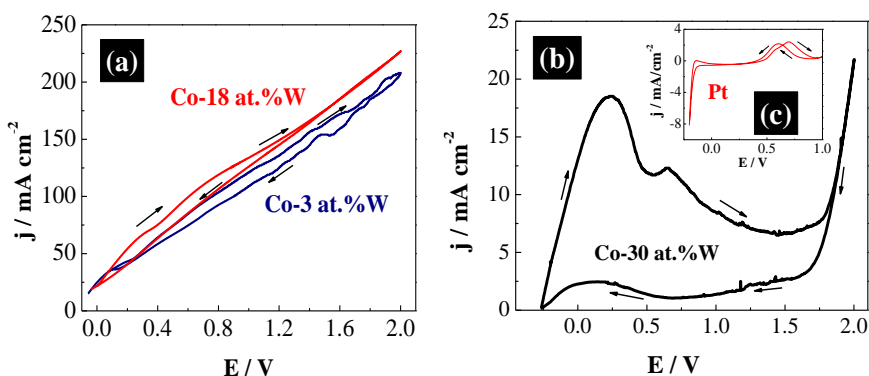


Fig. 12. Cyclic voltammograms recorded on the Co-W electrodes with (a) 3 and 18 at.% of W and (b) 30 at.% of W in the mixture of 0.1 M H₂SO₄ and 0.1 M CH₃OH at 22 ± 2°C. Arrows show the potential scan direction.

12 pav. Co-3at.%W ir Co-18at.%W (a) ir Co-30at.%W (b) elektrodų ciklinės voltamperogramos, užrašytos 0.1 M H₂SO₄ ir 0.1 M CH₃OH tirpale 22 ± 2°C temperatūroje. Rodyklėmis pažymėtos potencialo skleidimo kryptys.

After polishing the surface layer of the alloy W content in composition was the same as it was in surface layer before experiment in the tested solution, i.e. ~ 30 at.%. Apparently, the coatings having such high amount of W in their composition are more corrosion resistant and the synergistic effect by the interaction between Co and W prevents the active Co dissolution during the methanol oxidation reaction. Consequently, the Co-30at.%W alloy can be considered as potential electrocatalyst for methanol oxidation.

It was shown that after thermal treatment the catalytic activity of Co-W alloy for methanol oxidation in both acidic and alkaline media increases because of improved their crystalline structure and new phases are formed [112]. The catalytic activity was studied on the oxidized alloys too.

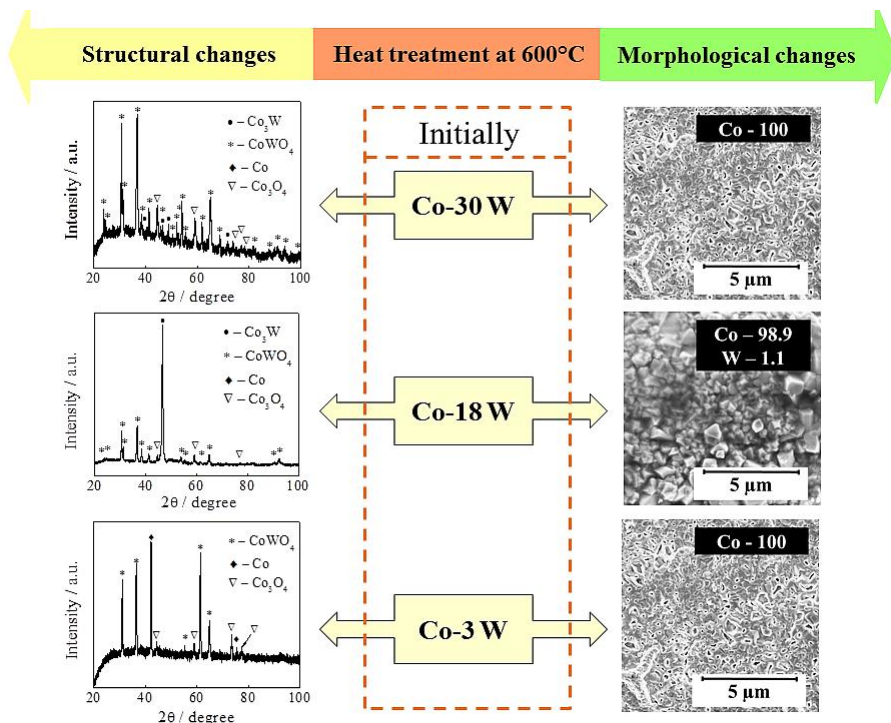


Fig 13. Effect of heat treatment on morphology and structure of Co-W alloys.
13 pav. Atkaitintų Co-W lydinų morfologijos ir struktūros pokyčiai.

Thus, in order to prepare oxidized samples, Co-W alloys were heated for 1 h at 600°C in air atmosphere. This temperature has been chosen as optimal, since at the lower temperature “amorphous-like” structure of Co-30at.%W alloys remains stable and no corresponding peaks for oxides were noticed. After heat treatment at the higher temperature, the coatings were poorly adhered to the stainless steel substrate and many cracks on the surface were observed. In general, XRD analysis confirmed the crystalline structure of all investigated coatings after heating at 600°C in an open air. New phases were noticed (Co₃O₄, CoWO₄) coupled to a decrease of tungsten content (up to several at.%) in the alloy due to the volatilization of tungsten oxides. Notable, the dramatic reduction of W content in turn changed the morphology of the deposits (Fig. 13) compared to that of as-deposited ones.

Electrocatalytic properties of the heat-treated and oxidized Co-W alloy electrodes toward methanol oxidation were investigated under the same conditions as for as-deposited alloys, and corresponding CV curves are shown in Fig. 14. As it was envisaged, Co-W deposits that initially contained ≤ 18 at.% of W, after heating still remains totally inactive for methanol oxidation reaction. Whereas, the annealed Co-W alloy that initially

contained 30 at.% of W demonstrates a methanol oxidation peak at 0.7 V in sulfuric acid and methanol mixture. However, the peak current density of the methanol oxidation on the heat treated Co-W electrode is around 0.135 mA cm⁻², which is sufficiently lower than indicated for as-deposited Co-30at.%W alloy coating (12.3 mA cm⁻²) or pure Pt electrode (2.4 mA cm⁻²). The decrease in catalytic activity might be attributed to the reduction of tungsten content in the alloy and the inhomogeneity of surface morphology.

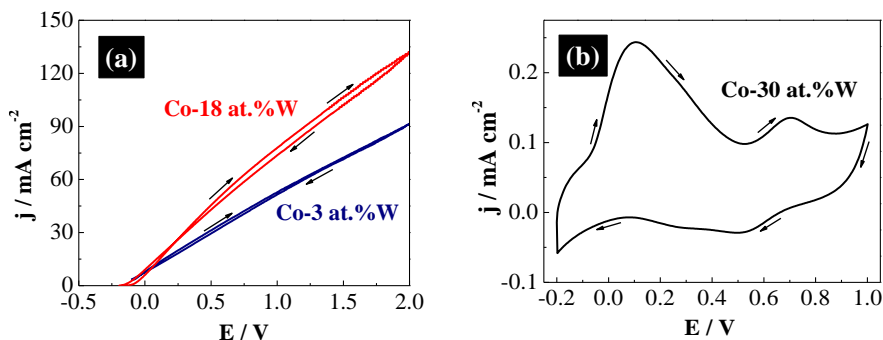


Fig. 14. Cyclic voltammograms recorded on the annealed Co-W catalyst in the mixture of 0.1 M H₂SO₄ and 0.1 M CH₃OH at 22 ± 2°C. Composition is provided for as-deposited alloys. Arrows show a potential scan direction.

14 pav. Atkaitintų Co-W elektrodų ciklinės voltamperogramos, užrašytos 0.1 M H₂SO₄ ir 0.1 M CH₃OH tirpale 22 ± 2°C temperatūroje. Pateikiama lydinių sudėtis nustatyta prieš atkaitinimo procedūrą. Rodyklėmis pažymėtos potencialo skleidimo kryptys.

Electro-oxidation of methanol can be retarded by the strong adsorption of reaction intermediates (e.g. CO, formaldehyde, formic acid, etc.) formed on the electrode surface [171]. Thus, in order to identify the presence of formaldehyde (if the case) during oxidation the following experiments have been carried out. A mixture of H₂SO₄ and methanol was electrolyzed for 2 h at 100 mA cm⁻² using a Co-30at.%W alloy as the anode. The resulting reaction mixture was mixed with zinc sulphate solution and cyclic voltammetric experiments were conducted on a platinum electrode. This solution was chosen based on the results presented in [112], where zinc sulphate in the presence of formaldehyde provides a characteristic peak on the platinum electrode. As can be seen, CV curves obtained with a reference solution of formaldehyde and in the presence of the oxidation mixture are almost identical (Fig. 15). This demonstrates the participation of formaldehyde as an intermediate during electro-oxidation of methanol on ultra- nanocrystalline W-rich Co-W electrodes.

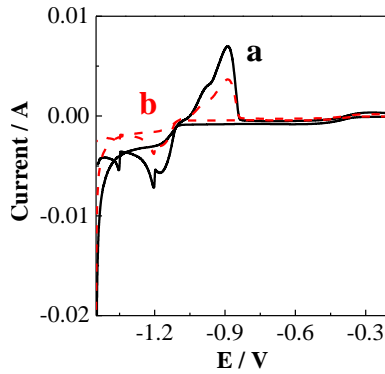


Fig. 15. Cyclic voltammograms obtained on Co–30 at.%W alloy at a scan rate 25 mV s^{-1} and temperature $22 \pm 2^\circ\text{C}$: (a) $0.02 \text{ M ZnSO}_4 + 0.01 \text{ M Na}_2\text{SO}_4 +$ formaldehyde; (b) oxidized mixture of methanol in H_2SO_4 .

15 pav. Co-30at.%W lydinio ciklinės voltamperogramos, užrašytos $22 \pm 2^\circ\text{C}$ temperatūroje (a) $0.02 \text{ M ZnSO}_4 + 0.01 \text{ M Na}_2\text{SO}_4 +$ formaldehido tirpale ir (b) metanolio oksidacijos reakcijos mišinyje su H_2SO_4 . Potencialo skleidimo greitis 25 mV s^{-1} .

3.2.3 Corrosion properties in H_2SO_4

Sulfuric acid is used extensively as electrolyte solution in methanol fuel cell technology [172]. Consequently, the main pre-requisite requirement for electrode materials in order to perform effectively in such fuel cells is good corrosion resistance in the acidic media. Thus, in order to validate the Co–W alloy as effective anode material for methanol oxidation reaction in the mixture of $\text{H}_2\text{SO}_4 + \text{CH}_3\text{OH}$, the corrosion behaviour in H_2SO_4 solution is discussed briefly.

The corrosion resistance of Co-W alloys having different W content has been evaluated in H_2SO_4 solution by using potentiodynamic polarization and EIS. For comparison with the behaviour of the deposited alloys, the experiments on pure electrodeposited Co has been recorded as well. The polarization curves recorded for the samples with the characteristic chemical composition, prepared at different temperatures are given in Fig. 16. As the shape of voltammograms is not symmetric and it is complicated to estimate corrosion parameters, i.e. corrosion potential E_{corr} and corrosion current density j_{corr} , by applying lines extrapolation in Tafel region, each curve was transformed into Allen-Hickling coordinates that enable to determine the corrosion parameters in a narrow range of potentials. The corrosion data extracted from polarization curves for all investigated alloys are reported in Table 5.

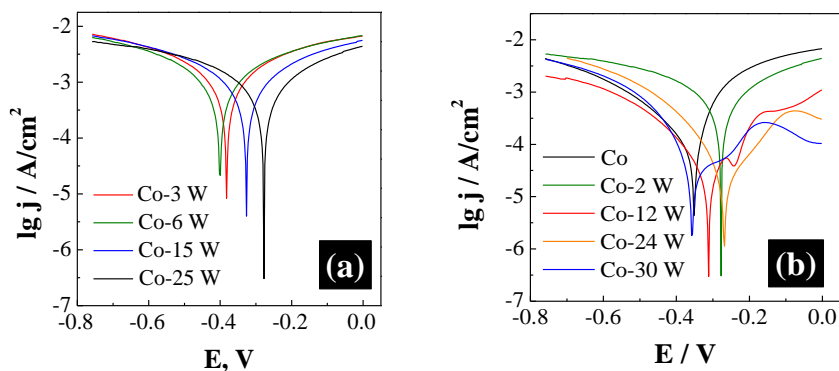


Fig. 16. Potentiodynamic polarization curves in 0.01 M H_2SO_4 for Co and Co-W coatings deposited at: (a) 20°C; (b) 60°C.

16 pav. Co ir 20°C (a) bei 60°C (b) temperatūrose nusodintų skirtingos sudėties Co-W poliarizacinės kreivės 0.01 M H_2SO_4 tirpale.

Table 5. Extracted corrosion parameters of Co and Co-W coatings at different deposition temperatures and various compositions.

5 lentelė. Co ir 20 bei 60°C temperatūrose nusodintų skirtingos sudėties Co-W elektrolitinių dangų korozijos parametrai.

Sample	T, °C	E_{corr} , V	j_{corr} , A cm^{-2}	R_{corr} , $\Omega \cdot cm^2$
Co	60	-0.31	$6.5 \cdot 10^{-5}$	132.0
Co-2 W		-0.28	$1.7 \cdot 10^{-4}$	21.9
Co-5 W		-0.32	$1.1 \cdot 10^{-5}$	18.3
Co-12 W		-0.31	$1.5 \cdot 10^{-5}$	347.2
Co-17 W		-0.18	$5.0 \cdot 10^{-6}$	555.9
Co-20 W		-0.19	$4.9 \cdot 10^{-6}$	682.3
Co-24 W		-0.27	$4.1 \cdot 10^{-6}$	985.0
Co-28 W		-0.26	$1.9 \cdot 10^{-5}$	848.9
Co-31 W		-0.35	$1.8 \cdot 10^{-5}$	620.9
Co-3 W	20	-0.38	$2.5 \cdot 10^{-4}$	3.7
Co-6 W		-0.40	$2.3 \cdot 10^{-4}$	7.4
Co-15 W		-0.36	$2.1 \cdot 10^{-4}$	9.5
Co-25 W		-0.28	$2.2 \cdot 10^{-5}$	19.6
Stainless steel	-	-0.039	$9.1 \cdot 10^{-7}$	6567

As it seen, the corrosion potential is located in the range from -0.40 to -0.18 V and does not show any clear correlation as a function of alloys composition. This is not surprisingly, because it is driven by the equal rates of both cathodic and anodic reactions. In this particular case, the cathodic reaction is hydrogen evolution reaction, and the anodic reaction is the rather active electrolytic dissolution, because sufficient current drops in the anodic part of voltammogram caused by the transferring into passive state were not

detected (Fig. 16). The rates of both reactions depend on the corrosion media, and chemical composition of electrode material. Furthermore, the rate of hydrogen evolution reaction depends on the state of the surface. Thus, due to the different hydrogen overvoltage on variously obtained Co–W alloys the corrosion potential may vary over some range without correlation with corrosion rate.

Meanwhile, the calculated corrosion current densities testify that corrosion rate of Co-W deposits decreases from $1.7 \cdot 10^{-4}$ to $4.1 \cdot 10^{-6}$ A cm^{-2} with increasing the W content from 2 to 24 at.%, respectively. At the even higher W content (in at.%) the corrosion rate increases again. This can be related to the formation of intermetallic Co_3W phase at this W content as it was indicated above. These observations correspond well to the results presented in Section 4.2.2 showing that the corrosion rate of the coatings with ≤ 20 at.% in acidic media is really high and electrocatalytic response towards MOR was not observed. Notable, for Co-W samples deposited at the room temperature the higher corrosion current densities can be observed (Table 5). This may be related to the fact that Co-W alloys obtained at 20°C are characterized by the cracked surface.

The EIS spectra in Nyquist coordinates and fitting results of corresponding equivalent circuits that validate the model describing the corrosion processes of investigated alloys are presented in the *Article IV*. Notable, for comprehensive understanding of the corrosion processes, the EIS measurements were performed at OCP and within the anodic polarisation of 0.05 and 0.10 V vs. corresponding OCP. In general, they contain similar stages and comprise similar processes such as formation of double electric layer, the presence of ohmic resistance, charge transfer resistance of electrochemical reaction or corrosion resistance, adsorbed layers formed by intermediates of complex electrochemical reactions. Hence, EIS reveals that the corrosion of Co and Co–W alloys occurs via an intermediate adsorption stage.

The corrosion resistance values (R_{corr}) for investigated samples were extracted from the fitting results and are summarized in Table 5. It can be noticed, that the best anti-corrosive behaviour has been determined for Co-24 at.% W ($R_{corr} = 985 \Omega \cdot \text{cm}^2$). Important to mention that Co–W alloys deposited at room temperature were investigated as well, but the adhesion of them to the substrate is very poor, and thus, no good fitting curves have been obtained (for more details see *Article IV*). Accordingly, the corrosion resistance of such samples is very poor (Table 5).

EDS analysis showed that the oxygen content in the alloy significantly increases after the corrosion experiments. This indicates that the electrochemical corrosion process occurs via an intermediate stage of forming oxide-containing compounds on the surface. It was found that the thickness of the adsorbed oxide layer increases with increasing the W content and reaches maximum at 25 at.% of W (Fig. 17).

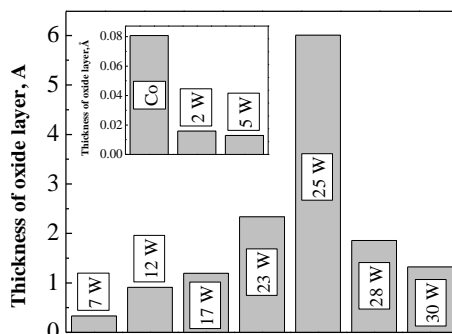


Fig. 17. Effect of tungsten content in Co–W alloys on oxide layer thickness; Co–W alloys were deposited at 60°C.

17 pav. 60°C temperatūroje nusodintų Co–W lydinių paviršiuje susidarančio oksidinio sluoksnio storio priklausomybė nuo W kiekio.

Thus, can be assumed that the corrosion stability of such alloy could be linked to the formation of thicker protective surface oxide layer (e.g. CoOOH). The higher W content in composition (> 25 at.%) leads to the formation of thinner and less protected oxide coating on the surface, accordingly, the corrosion rate increases. For more details related to the calculation of the oxide thickness, see **Article IV**.

3.3 Modification of binary alloys

3.3.1 Addition of the third metal

The poor corrosion resistance of the alloys for targeted applications is one of the main obstacles preventing their widespread usage [173]. It is well known that the introduction of the third element into a binary alloy system can affect its chemical and structural characteristics and, thus improve their mechanical and anti-corrosive properties [156]. Consequently, there are some studies focused on Ni-Fe-W [142,174,175], Ni-Co-W [156,176] and Co-Fe-W [177] alloys' electrodeposition. Though the characteristics of copper, e.g. good electrical conductivity, ductility, low expansion coefficient and enhanced wear resistance, may be expected significantly to expand the range of it's possible applications, as far as it is known, the papers

concerning electrodeposited Co–Cu–W alloys are rather scarce hitherto [149,178]. Accordingly, in this study the efforts to prepare novel Co-Cu-W alloy coatings from abovementioned citrate electrolyte with variable compositions have been made. For comparison, Co-W and Cu-W alloys were electrodeposited under the same experimental conditions.

The suitable cathodic potentials for Co-Cu-W and Cu-W alloy coatings electrodeposition have been selected based on the cathodic scan plots that are widely described in *Article V*. The general dependency of deposition potential on elemental composition of W-based alloys prepared at 60°C is presented in Fig 18a. Notable, the W percentage in alloys fabricated at 20°C in the whole tested range of cathodic potential was extremely low (< 4 at.%) and did not change significantly with the cathodic potential (for more information see *Article V*). While at the elevated temperature the W content in Cu-W and Co-Cu-W deposits reaches the maximum values of 6 at.% and 12 at.% (depending on the applied potential), respectively. The same, as in binary alloys case, the CE decreases with increasing the W content in the deposit (Fig. 18b).

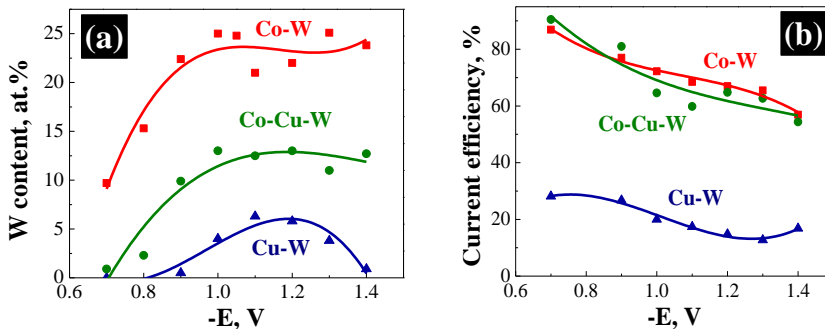


Fig. 18. Effect of deposition potential on (a) tungsten content and (b) current efficiency for Cu-W, Co-W and Co-Cu-W alloys.

18 pav. W kiekio (a) ir srovinės išeigos (b) priklausomybė nuo Cu-W, Co-W ir Co-Cu-W lydiniių nusodinimo potencialo.

X-ray diffraction patterns of the as-deposited Cu-W and Co–Cu–W alloy coatings, as well as metallic Co and Cu for comparison are shown in Fig. 19. As it can be seen, the pure Cu coating is characterized by face-centered cubic (fcc) lattice with {111}, {200}, {220} and {311} crystal orientations. After the co-deposition of Cu with W a solid solution of Cu-W with a typical Cu-type fcc lattice is formed. A small shift to lower 2Θ values can be seen, This may be attributed to the incorporation of larger W atoms into Cu lattice that causes the changes in lattice parameter, since the atomic radius for W and Cu being 140 pm and 128 pm, respectively. Similarly, for ternary Co-Cu-W alloy having low content of tungsten fcc Cu phase is formed, however

the additional lines that reflect the formation of W solid solution in hpc Co with increasing the W percentage can be seen. This agrees well to the fact that solubility limit of W in Co is around 17.5 at.%.

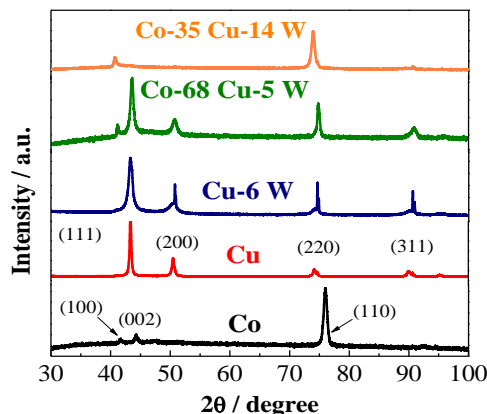


Fig. 19. XRD patterns of deposited Co, Cu, Co-W, Cu-W and Co-Cu-W coatings deposited at 60°C and having similar W content.

19 pav. 60°C temperatūroje nusodintų Co, Cu, Co-W, Cu-W and Co-Cu-W lydinių Rentgeno spindulių difraktogramos.

All deposited coatings visibly are cracks-free on the surface, well adhered to the substrate. Meanwhile, the variability in the morphology of the deposits having similar W content in their composition (5-6 at.%) was noticed, Some representative SEM images of Cu-W and Co-Cu-W alloys are given in Fig. 20. Cu-W coatings are characterized by rough cauliflower-type nodules that are composed from smaller grains. The incorporation of Co into the alloy leads to the formation of rougher morphology composed of larger semi-spherical clusters. While, for the Co-5 at.% W electrodeposit (Fig. 9a) a needle-like structure with extended acicular grains that is typical for electrodeposited pure cobalt coatings can be noticed.

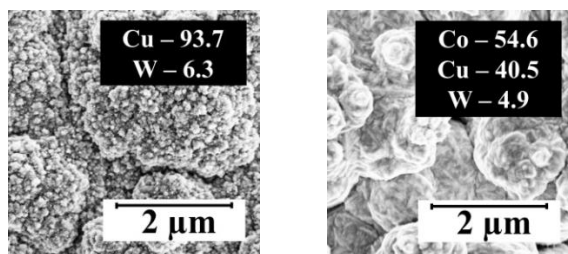


Fig. 20. SEM images of Cu-W and Co-Cu-W alloy coatings deposited at 60°C and having similar W content.

20 pav. 60°C temperatūroje nusodintų Cu-W ir Co-Cu-W lydinių, turinčių panašų W kiekį sudėtyje, SEM nuotraukos.

The further step was to study the corrosion parameters of Co-41 Cu-5 W (in at.%) and to compare the results with Cu-W and Co-W having the same W content. Polarization curves of the samples tested in 0.01 M H₂SO₄ solution at the room temperature are shown in Fig. 21. It was found, that after the addition of Cu to Co-W alloy the corrosion current density decreased from $1.9 \cdot 10^{-4}$ to $6.9 \cdot 10^{-6}$ A cm⁻², while for Cu-W this value was close to $5.8 \cdot 10^{-6}$ A cm⁻². The EDS analysis showed that after the corrosion test in the ternary alloy W content increased from 5 to 8 at.%, Cu from 41 to 51 at.%, correspondingly Co percentage was reduced from 54 at.% to 41 at.%. Apparently, the Cu may precipitate from the ions that were dissolved as Cu²⁺ or Cu⁺ and then reduced [179]. Also, it is likely that the enhanced corrosion resistance associated with Cu involves the selective dissolution of active alloying elements such as Co and formation of the protective surface film enriched with the noble metal [180].

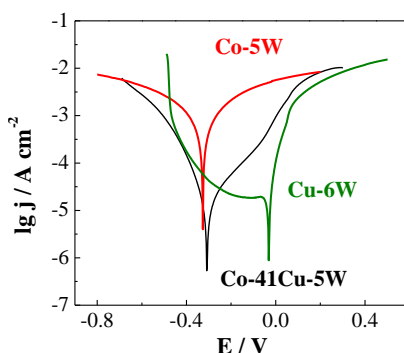


Fig. 21. Potentiodynamic polarization behaviour for Co-5W, Cu-6W and Co-41Cu-5W deposits in 0.01 M H₂SO₄.

21 pav Co-5W, Cu-6W ir Co-41Cu-5W lydinių poliarizacinės kreivės 0.01 M H₂SO₄ tirpale.

3.3.2 Addition of phosphorus

W based alloys are well recognized for their hardness, ability to resist deformations, and long-term service [181]. Therefore, they can be used as blades for the cutting and slitting of fruits, vegetables, etc. In this context environmentally and human-friendly Fe-W alloys are of significant importance because contrary to Co-W and Ni-W coatings, they meet the general safety requirements for materials that can come into direct contact with food [182]. Moreover, earlier our group showed that the nanohardness of as-plated Fe-W coatings reaches 13 GPa that is comparable to the hardness of electrodeposited chromium [2]. Fe-W coatings also could achieve excellent wear resistance which is much greater than that of

electrolytic chromium, TiB₂, TiN and TiAlN coatings measured under the same conditions and perform well in the rigorous food processing industry [183]. However, in order to withstand continuous use and heat created from the friction of fast moving cutting tools in acidic environment corrosion phenomenon becomes a critical factor. Though based on the literature we can see that the corrosion resistance is the weak point of Fe-W alloys and seems to be lower than in the case of other W-based coatings [96]. It was reported that the corrosion resistance of W alloys with iron group metals can be enhanced by the addition of phosphorus to alloys composition by stimulating spontaneous passivation in acidic and alkaline media [184,185]. Furthermore, the previous tribological studies showed that that the addition of phosphorous into Fe-W system leads to the formation of more wear resistant coating and improve the adhesion to the substrate [186]. On the other hand, it was reported that ternary W alloys with phosphorous are characterized by lower hardness than binary ones without phosphorous [72]. Thus, our work was aimed to find the optimum Fe-W-P electrodeposition conditions in order to prepare coatings with the synergy of high hardness and improved corrosion resistance in the light of their potential application for cutting tools in food industry.

For W-based alloys has been reported that the addition of sodium hypophosphite to electroplating solution causes a sudden drop in tungsten content in composition as well as in cathodic current efficiency [187]. Therefore, in order to study the effect of sodium hypophosphite on Fe-W system electrodeposition, the experimental conditions corresponding to the preparation of an alloy with the high tungsten content has been applied. Consequently, the deposition current density of 30 mA cm⁻², which according to previous studies [72,188] corresponds to the Fe-W alloy with the highest tungsten content that could be deposited with Fe, namely up to 33 at.%, and the highest cathode current efficiency (38%), has been selected. In order to improve the physical appearance of Fe-W-P coating, also the influence of organic additives, such as Rokafenol-10 and N-butindiol, on functional properties has been evaluated. The detailed experimental conditions and composition of plating bath are described in **Article VI**, in which sodium hypophosphite was used as the source of phosphorous.

Fig. 22 shows the effect of sodium hypophosphite influence on the composition of tertiary Fe-W-P alloy. As it can be noticed, W content increases with an addition of hypophosphite to the solution. Important to mention that in this system the effect of sodium hypophosphite on tungsten content is not so drastic as it has been observed for analogous Ni-W-P

system [174]. Obvious, the wetting and brightening agents presented in the bath slightly increase the phosphorous percentage in the deposit. Generally, Fe-W-P alloy coatings are uniform and free of cracks. It is clearly seen that the addition of phosphorous in the composition leads to refining the structure and the deposits become tight, compact and dense.

XRD patterns of electrodeposited pure Fe deposit exhibit texture with the preferred orientation of {211}. Meanwhile, the introduction of the high W content (> 26 at.%) in composition after alloying with Fe results in the formation of “amorphous-like” phase (Fig. 23). Analogous tendency can be seen for ternary Fe-W-P alloy having the similar W content.

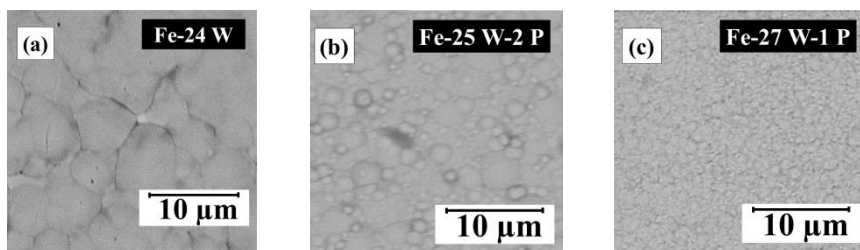


Fig. 22. SEM images of Fe-W and Fe-W-P alloy coatings electrodeposited from: solution without additives (a) and (b); solution containing 1,4-butindiol and Rokafenol-10 (c).

22 pav. Fe-W ir Fe-W-P SEM nuotraukos; lydinių, nusodintų iš elektrolito be organinių priedų (a) ir (b); iš elektrolito, kurio sudėtyje yra 1,4-butindiolio ir Rokafenolio-10 (c).

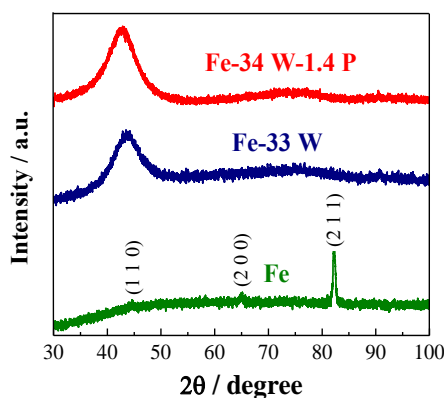


Fig. 23. XRD diffraction patterns for Fe-W-P, Fe-W and Fe coatings.

23 pav. Elektrolitinių Fe-W-P, Fe-W ir Fe lydinių dangų Rentgeno spindulių difraktogramos.

In respect to the potential iron-based tungsten alloys application in food industry, the corrosion measurements of as-deposited Fe-33at.-% W and Fe-

34W-1.4P (in at.%) coatings have been performed in 0.012 M Na₂SO₄ and 0.027 M NaCl solution (pH 5) at 90°C. The polarization curves have been evaluated in terms of corrosion potential E_{corr} and corrosion current density j_{corr} , that were calculated by applying Tafel fit to Allen-Hickling equation. The graphs are presented in **Article VI**, meanwhile the obtained data is summarized in Table 6. Generally, it can be seen that the addition of phosphorous in composition results in nobler E_{corr} and lower j_{corr} , and thus potentially better corrosion resistance of Fe-34W-1.4P (in at. %) in the tested media in comparison with metallic Fe and Fe-33 at. % W coatings.

Table 6. Extracted corrosion parameters from E vs. $\log i$ plots for stainless steel and electrodeposited Fe-based coatings having various compositions.

6 lentelė. Fe, Fe-W ir Fe-W-P lydinių korozijos parametrai.

Sample	E_{corr} , V	j_{corr} , A cm ⁻²	R_{corr} , Ohm cm ⁻²
Fe	-0.616	$3.9 \cdot 10^{-5}$	335.9
Fe-33 W	-0.746	$4.3 \cdot 10^{-5}$	380.7
Fe-34 W-1.4 P	-0.613	$1.8 \cdot 10^{-5}$	388.9

Notable, similarly to the Co-W corrosion in H₂SO₄ solution (see Section 4.2.3), the used equivalent circuit for fitting of the obtained EIS data of Fe-based alloys in Cl⁻ and SO₄²⁻-media suppose the complicated mechanism of alloy corrosion involving intermediate stages probably containing adsorbed oxygen compounds; that can explain an increase in oxygen content in the alloys and some changes in tungsten content obtained after corrosion tests (see **Article VI**).

3.3.3 Nanostructures

Taking into account the advantages of electrochemical deposition (see Section 2.1), this chapter presents how the Co-W alloy synthesis can be turned from plane coatings to one-dimensional nanomaterials, namely nanowires by applying the template-assisted deposition technique

A great interest of nanostructure-based devices is associated with their high surface area, and excellent optical, electrochemical and electronic properties, leading to numerous and various potential applications [189,190]. For instance, the high catalytic activity promise its use as an integrated 3D cathodes with the highest performance–price ratio in electrochemical water splitting for large-scale hydrogen fuel production [191]. Accordingly, in this work the strategy to consistently enhance the HER catalysis of iron group metals alloys though nanostructurization by applying template assisted deposition has been presented. As it is illustrated in Fig 24a, the process begins with a conductive layer of Au sputtering on the one side of the

polycarbonate foil. Co-W segments were grown from electrolyte containing CoSO_4 , Na_2WO_4 , $\text{Na}_3\text{C}_6\text{H}_5\text{O}_7$, $\text{C}_2\text{H}_5\text{NO}_2$ and $M \text{ NaOH}$ (pH 10) with an applied cathodic pulsed current density of 80 mA cm^{-2} with a 5 s on-time and a 10 s off-time current (Fig. 24b). Notable, with a goal to maintain kinetic control and avoiding gas accumulation and concentration gradients within the pores, thinner polycarbonate films were used instead of AAO, and a relaxation, or off-time, was chosen to be twice as longer as the on-time. The current density was chosen in such manner that Co-W with low W content would be deposited because as it was demonstrated in [7], the highest saturation magnetization and coercivity were found for Co-W samples with the low W content.

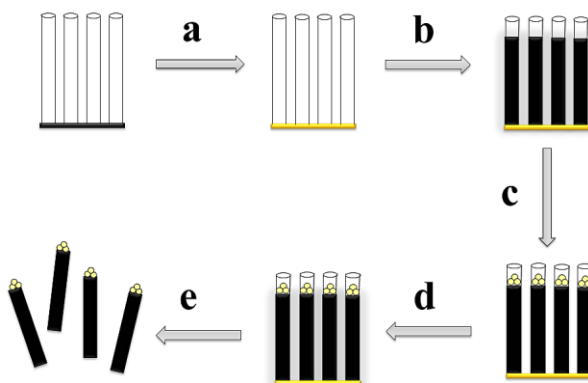


Fig. 24. Schematic route of the development of nanowire-nanoparticle composites: (a) sputtering a layer of gold; (b) pulsed electrodeposition of Co-W nanowires; (c) adding colloidal gold nanoparticles; (d) pulsed electrodeposition of Co-W alloy; (e) dissolving the membrane.

24 pav. Nanovielų-nanodalelių kompozitų formavimo schema: (a) Au sluoksnio užpurškimas; (b) impulsinis Co-W nanovielų nusodinimas; (c) Au nanodalelių įvedimas; (d) impulsinis Co-W lydinių nusodinimas į poras; (e) membranos tirpinimas.

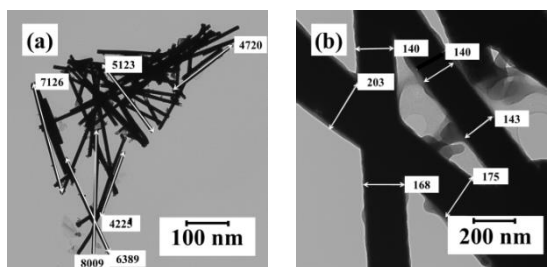


Fig. 25. TEM images of Co-W nanowires with measured (a) length and (b) diameter.

25 pav. Co-W nanovielų TEM nuotraukos, kuriose išmatuotas jų ilgis (a) ir skersmuo (b).

A typical example of released nanowires after dissolving membrane in dichloromethane is shown in Fig. 25 (a, b). Subsequent use of this membrane as a template for the growth of nanowires allow to expect that the length of these nanostructures is proportional, not higher than the aforementioned thickness (6-7 μm). Meanwhile the average diameter of the Co-W nanowires is about 130 nm, which is slightly bigger than the pore size of the PC templates (100 nm).

The catalytic properties were determined by applying the same procedure as in the case of Co-5at.%W thin film. Fig. 26 shows the polarization curves recorded for different forms of electrodes. It was found that the exchange current density for the Co-5at.%W nanowires is considerably higher than that of the flat Co-W coatings with the same W percentage, namely 3.7 mA cm^{-2} for NWs and 0.02 mA cm^{-2} for plane deposits. This can be attributed to the more exposed active sites because of their high surface area-to-volume ratio and the direct contact of nanowires to the underneath conductive substrate which ensures each nanowire to participate in the reaction [192]. Besides the improved functional properties surface (bio)functionalization of the nanowires with the appropriate ligands or biomolecules are often desired to tune the nanostructures towards a biomedical/biotechnological applications. Up to now, surface modification was mostly applied onto the entire surface of the nanostructures [193–195].

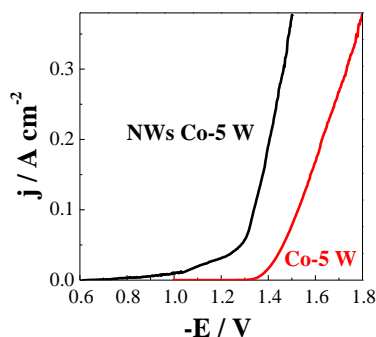


Fig. 26. Cathodic polarization curves of different configuration Co-W electrodes in 30 wt.% NaOH. The scan rate is 2 mV s^{-1} .

26 pav Skirtingos konfiguracijos Co-W lydinių poliatrizacinės kreivės 30 sv.% NaOH tirpale. Potencialo skleidimo greitis 2 mV s^{-1} .

Though, selective functionalization of NW arrays with several active segments offers a unique ability to combine a number of functionalities and/or properties while avoiding molecular interference due to randomly distributed functional groups that could lead to multifunctionality of the system [196]. Regarding metallic NWs, the most frequently and successful

reported selective functionalization strategies rely on individual multi-component nanowires that are composed of different material segments. For instance, the magnetic part of iron group metal was found to be responsible for the magnetic interactions and controlled positioning of the NWs, while the gold segment provides possible functioning with the biological entities, e.g thiol-containing molecules [197,198]. On the other hand, gold is a well-established material that displays attractive optical properties, biological compatibility, catalytic activity, and excellent surface effects. Accordingly, it was anticipated that the combination of Co, Ni or Fe and Au segments in a hybride structure on the nanoscale would produce a new nanostructured material that reveal properties beyond those of their individual components, thereby opening up the area of bio-magnetic applications.

Indeed, the multilayered iron group metals and gold nanowires were electrodeposited in [199–201]. Talking about the iron group metal alloys with W/Mo, the possibility to fabricate Co-W nanostructures inside the pores of AAO from citrate-ammonia and citrate solutions was demonstrated in [27,202], while the electrodeposition of Ni-W alloys from ammonia-free electrolytes containing citrate and boric acid in a deep recess was reported in [203]. However, no reports of electrodeposited iron group metal alloy nanowires with W/Mo modified with gold segments exist so far. Thus, in this work not only an improvement in electrodeposition of Co-W alloy nanowires from both an ammonia-free and boric acid-free electrolyte and their catalytic activity towards alkaline HER, but a novel approach to assemble with two functional sections, the Co-W alloy and Au nanoparticle segment, for possible assembling and sensing functions, respectively, is presented.

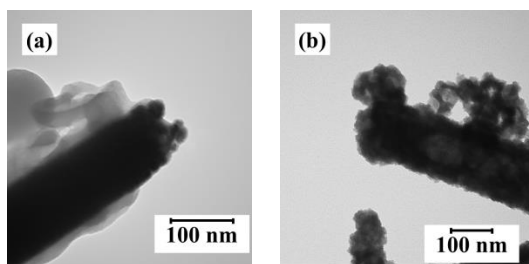


Fig. 27. TEM images of Co-W nanowires with (a) Au nanoparticles, (b) FeO nanoparticles captured at the nanowire tip.

27 pav. Co-W lydinių nanovielių kompozitai su Au nanodalelėmis (a) ir FeO nanodalelėmis (b).

For such purpose after the electrodeposition of Co-W nanowires, the electrolyte was flushed with water. Then the nanoparticle solution was added

to the membrane with formed nanowire electrodes and vacuum was applied for 1 minute in order to attach the NPs (Fig. 24c). The nanoparticles were fixed on the surface by deposition of an additional Co-W alloy layer while applying 20 pulses in the same pulse mode as described previously (Fig. 24d). The last step (Fig. 24e) is the release of the wires from the polycarbonate membrane by dissolving the membrane in dichloromethane. Fig. 27a shows that gold nanoparticles were indeed attached to the top of Co-W nanowires.

In this study the Au NPs were chosen for their inert nature and possible functioning with biological entities that allows them to serve as the labels for the detection of biological species. However, the Au NPs segment can be easily interchangeable with a variety of other materials, such as metal oxides. More specifically, the iron oxide nanoparticles with superparamagnetic properties are being developed as specific contrast agents in magnetic resonance capable of wide-ranging applications, including imaging of cancer tumours in live animal models [204]. Following this example, the Co-W nanowires modified with FeO nanoparticles are shown in Fig. 27b. The ability to incorporate a wide range of materials as a functional segment provides the feasibility to fabricate different functional devices using the same platform reported herein.

4. CONCLUSIONS

The extensive research on the intrinsic (electrochemical conditions-tungsten content-structure) and extrinsic (electrochemical properties) interdependencies of the alloys of iron group metals (Me) with W/Mo have been carried out in order to elucidate the opportunities for further design/application of those alloys, including with very high content of refractory metal. The following conclusions can be outlined:

- The well-thought conditions of electrodeposition of alloys of iron group metal with W/Mo permitted to obtain homogeneous, compact, well adhered to the substrate coatings having up to ~ 30 at.% of W and ~ 50 at.% of Mo, which are characterized by ultra-nanocrystalline structure (the crystallite size < 5 nm), having two phases: W/Mo solid solution in Me and corresponding intermetallic compound.
- Hydrogen evolution reaction (HER) on W/Mo-rich ultra-nanocrystalline alloys in 30 wt.% NaOH solution is much higher than the activity of their individual components and crystalline counterparts having low refractory metal content. The values of apparent exchange current density (ECD) reduces in the following order for investigated alloys: (in at.%): Co-52Mo > Ni-54Mo > Fe-54Mo > Ni-29W > Co-33W > Fe-30W.
- The highest apparent ECD (46.2 mA cm^{-2}) was obtained for Co-52at.%Mo coating which could be attributed to the formation of the intermetallic Co_3Mo phase ensuring the larger number of the active sites for HER. The another way to increase ECD was shown through template electrodeposition of Co-W nanowires (NWs): ECD for Co-5at.%W electrode increased from 0.02 mA cm^{-2} (coating) to 3.7 mA cm^{-2} (NWs).
- The highest corrosion resistance in H_2SO_4 was determined for Co-24at.%W alloy, in which the phase transition from W solid solution in Co to Co_3W intermetallide occurs. The Co_3W phase provides superior corrosion resistance to Co-W coatings that was successfully used for catalytic anodic oxidation of methanol in H_2SO_4 . The anodic peak current density of methanol oxidation was $12.3 \text{ mA}\cdot\text{cm}^{-2}$ which is higher than on Pt (2.4 mA cm^{-2}).
- The modification of the binary alloys by introducing the third element (P, Cu, Au) allows to improve the applicability of those alloys. Thus, j_{corr} of Co-Cu-W alloy can be decreased in 300 times, while j_{corr} of Fe-W-P alloy only in 2 times in comparison to their binary counterparts. Another opportunity was gathered by fabrication of a novel nano-composite NWs arrays, where Co-W matrix was modified with Au nanoparticles in order to design new material for sensing application.

5. SANTRAUKA

Įvadas

Geležies grupės metalų (Co, Ni, Fe) lydiniai su W/Mo pasižymi vertingomis mechaninėmis, antikorozinėmis, magnetinėmis, tribologinėmis savybėmis. Pvz. nanokristalinių didelį W/Mo kiekį (≥ 23 at.%) sudėtyje turinčių lydinių kietumas siekia 10 GPa esant 20 mN apkrovai. Pažymėtina, jog ši vertė yra artima elektrolitinio chromo dangoms esant toms pačioms eksperimentinėms sąlygoms. Be to, geležies grupės metalų lydiniai su W/Mo būdingas išskirtinis atsparumas trinčiai ir geras lankstumas (visiškai sulenkama 180 kampu be įtrūkimų), o tempimo stipris siekia net iki 2333 Pa. Yra duomenų apie jų gebėjimą katalizuoti elektrocheminę vandenilio išsiskyrimo iš vandens reakciją. Taip pat didelis W/Mo kiekis lydiniuose ženkliai padidina jų lydymosi temperatūrą, kuri gali siekti net iki 2500°C. Taigi, nenuostabu, kad tokių lydinių praktinio pritaikymo galimybės technologijoje priklauso nuo konkrečių jų funkcinių savybių: vieni jų naudojami dėl terminio atsparumo, kiti – dėl magnetinių savybių, dar kiti – dėl išskirtinio kietumo, ir t.t. Vis dėlto, šiuolaikiniame pasaulyje vis daugiau dėmesio susilaukia daugiafunkcinėmis savybėmis pasižyminčios lydinių dangos, kurios ne tik leidžia sumažinti išlaidas, susijusias su nusodinimo procesais, tačiau taip pat sąlygoja efektyvesnę įrenginių panaudojimą. Šiame kontekste geležies grupės metalų lydiniai su W/Mo sulaukia didžiulio susidomėjimo dėl galimybės net keletą anksčiau minėtų technologiniu požiūriu svarbių charakteristikų sujungti į vieną lydinį. Gerai žinoma, kad lydinių funkcinės savybės yra susijusios su jų chemine sudėtimi. Ir nors mechaninės, tribologinės ir terminės Co, Ni ir Fe lydinių su W/Mo savybės yra gana plačiai ištirtos ir aprašytos, rezultatai, susiję su jų elektrocheminėmis savybėmis yra gana prieštaringi. Kitaip tariant, nepakanka duomenų koreliacijai tarp lydinių sudėties ir konkrečių elektrocheminių savybių nustatyti, pvz. katalizinio aktyvumo vandenilio išsiskyrimo reakcijoje ar korozijos greičio. Pirmiausia tai susiję su skirtingais lydinių paruošimo būdais. Deja, elektrocheminių savybių interpretavimas net ir electrochemiškai nusodintiems lydiniai yra gana komplikotas, nes paprastai skirtingi autoriai lydinių nusodinimui naudoja skirtingas elektrolizės sąlygas, kurios įtakoja nevienodus morfologijos ir struktūros ypatumus, o šie savo ruožtu, lemia skirtingas elektrochemines savybes. Literatūroje netgi pasitaiko tokių atvejų, kai labai artimos ar netgi vienodos cheminės sudėties lydiniai yra apibūdinami skirtingais kataliziniais aktyvumais vandenilio išsiskyrimo reakcijoje ar skirtinga korozine elgsena.

Atsižvelgiant į tai, šis darbas yra skirtas sistemingam elektrocheminių geležies grupės metalų lydinių su W/Mo elektrocheminių savybių ištyrimui. Nusodinimo sąlygos buvo parenkamos taip, kad sunkialydzio metalo kiekis, t.y. W ar Mo, lydinyje būtų kuo įvairesnis esant panašioms nusodinimo sąlygoms. Arba panašus esant skirtingoms nusodinimo sąlygoms, siekiant įvertinti geležies grupės metalo įtaką konkrečioms elektrocheminėms savybėms.

Darbo tikslas: atlikti išsamų geležies grupės metalų lydinių su W/Mo elektronusodinimo tyrimą – nustatyti, kaip šių lydinių morfologija, sudėtis ir kristalinė struktūra įtakoja jų elektrochemines savybes, t.y. katalizinį aktyvumą vandenilio išsiskyrimo reakcijoje šarminėje terpėje, metanolio oksidacijos reakciją ir korozinį atsparumą rūgštiniame tirpale.

Uždaviniai:

1. Optimizuoti skirtingos sudėties lydinių elektrolizės sąlygas (tirpalo pH, srovės tankį/potencialą, temperatūrą), siekiant nusodinti skirtingos sudėties Co, Ni ir Fe lydinius su W/Mo ir nustatyti jų sudėties-morfologijos-struktūros sąryšius;
2. Įvertinti, kaip lydinių sudėtis, morfologija ir struktūra įtakoja geležies grupės metalų (Co, Ni, Fe) lydinių su W/Mo katalizines savybes vandenilio išsiskyrimo reakcijoje šarminėje terpėje;
3. Nustatyti optimalią Co-W lydinio, efektyviai katalizuojančio metanolio oksidacijos reakciją H_2SO_4 tirpale, sudėtį;
4. Ištirti Co-W lydinių korozinę elgseną ir nustatyti, kaip ji kinta priklausomai nuo jų cheminės sudėties bei struktūros;
5. Atlikti Co-W lydinių nanovielų nusodinimą į porėtas polikarbonatines membranas ir modifikuoti suformuotas nanostruktūras Au nanodalelėmis siekiant sukurti naujus nanovielų-nanodalelių kompozitus.

EKSPERIMENTŲ METODIKA

Darbe taikyta tyrimų metodologija schematiškai yra pavaizduota 6 pav. (34 psl.). Geležies grupės metalų (Co, Ni, Fe) lydinių su W/Mo elektronusodinimui naudotų tirpalų cheminės sudėtys yra pateiktos 2 lentelėje (35 psl.).

Lydinių elektronusodinimas. Elektrocheminis nusodinimas atliktas naudojant įprastinę trijų elektrodų sistemą. Darbiniai elektrodai W lydinių nusodinimui buvo gaminami iš nerūdijančio plieno vielos (1 cm^2) ar plokštelių (2 cm^2). Mo lydiniai buvo nusodinami and vario vielos (1 cm^2)

arba vario plokštelių (2 cm^2), priklausomai nuo dangų tyrimo metodo. Visais atvejais palyginamuoju naudotas Ag/AgCl elektrodas sočiame KCl tirpale, pagalbinis – platinuoto titano tinklelis. Elektronusodinimas buvo vykdomas 20 ir 60°C ($\pm 2^\circ$) temperatūrose. Elektrodai prieš matavimus buvo nuriebalinami ultragarso vonelėje vaitspirito ir acetono tirpaluose. Sukibimui pagerinti, ant pagrindo buvo nusodinamas plonas Ni sluoksnis iš $240 \text{ g l}^{-1} \text{ NiCl}_2 \cdot 6\text{H}_2\text{O} + 80 \text{ g l}^{-1} \text{ HCl}$ (nusodinimo laikas 1 minutė), srovės tankis 10 mA cm^{-2} .

Paviršiaus morfologija, sudėtis ir struktūra. Nusodintų dangų morfologija buvo tiriama skenuojančiais elektroniniais mikroskopais Hitachi TM-3000 ir Hitachi SU-70. Elementinė dangų buvo nustatoma SEM-EDS metodu (programinė įranga Swift ED-3000), o fazinė sudėtis identifikuojama remiantis Rentgeno spindulių difrakcinės analizės duomenimis (difraktometras Rigaku MiniFlex II, programinė įranga PDXL). Lydinius sudarančių kristalinių dydis buvo apskaičiuotas taikant Šererio lygtį. Išsamesni struktūros tyrimai buvo atliekami interpretuojant didelės skiriamosios gebos transmisiniu elektroniniu mikroskopu Talos F200X gautus vaizdus.

Elektrocheminiai tyrimai. Vandens skirimosi greičio nustatymo ir elektrocheminės korozijos tyrimai buvo atliekami tiesinės voltamperometrijos ir elektrocheminio impedanso spektroskopijos (EIS) metodais naudojant universalią elektrocheminių tyrimų sistemą AUTOLAB302 bei programinę įrangą GPES ir FRA. Ciklinės voltamperometrijos matavimai buvo taikomi analizuojant Co-W katalizinį aktyvumą metanolio išsiskyrimo reakcijoje.

REZULTATŲ APTARIMAS

Lydinių sudėties, morfologijos ir struktūros sąryšiai

Naudojant tos pačios sudėties citratinį elektrolitą ir keičiant tik elektrolizės sąlygas (tirpalo pH, srovės tankį bei temperatūrą), nusodinamos kokybiškos elektrolitinės Co, Ni ir Fe lydinių su W dangos, kuriose W kiekis kinta pakankamai plačiame intervale, t.y. nuo 0 iki 33 at.%. Yra žinoma, kad aukštesnė elektrolito temperatūra sumažina poliarizaciją, sumažina metalų koncentracijų skirtumus difuziniame sluoksnyje prie katodo, dėl to padidėja dalinis W srovės tankis ir atitinkamai nusodinamas didesnis jo kiekis lydinyje. Tokiu būdu kambario temperatūroje nusodintose dangose didžiausias nusodinamo W kiekis siekia 25 at.%, tuo tarpu 60°C temperatūroje šis kiekis gali būti padidintas iki 33 at.%.

Pastebėta, kad W kiekis lydiniuose su geležies grupės metalais įtakoja jų paviršiaus morfologiją, t.y. didėjant W kiekiui nuo 2 iki 7 at.%, lydinį sudarantys kristalinių aglomeratai smulkėja, pasikeičia jų forma. Kai W kiekis padidėja nuo 7 iki 17 at.%, paviršiuje vyrauja įvairaus dydžio kamuoti, netaisyklingos formos kristalitiniai, o esant ≥ 23 at.% W, lydiniai būdinga smulkiakristalinė grūdėta struktūra. Verta atkreipti dėmesį, kad kambario temperatūroje nusodintos dangos yra sutrūkinėjusios ir prastai sukibusios su nerūdijančio plieno paviršiumi. Prasta dangų kokybė turi neigiamos įtakos jų funkcinėms savybėms, tad toliau tyrimams buvo pasirinkti 60°C temperatūroje suformuoti lydiniai paviršiai.

Morfologijos pokyčiai susiję ir su lydinio struktūros ypatybėmis. Kaip matyti iš 7 pav. (40 psl.) pateiktų difraktogramų, kai W kiekis yra mažesnis nei 20 at.%, nusodinami nanokristaliniai Co-W, Ni-W ir Fe-W lydiniai, kurių struktūra artima atitinkamai hcp Co, fcc Ni ir bcc Fe struktūrai. Tiesa, lyginant su elektrochemiškai nusodintų geležies grupės metalų smailėmis, atitinkamuose lydiniuose su W pastebimas jų poslinkis į mažesnių kamuų pusę. Tai aiškinama W kietojo tirpalo geležies grupės metalo kristalinėje gardelėje susidarymu, kai Co-W, Ni-W ir Fe-W lydiniuose yra nedidelis W kiekis. Kai W kiekis padidėja iki ~ 24 at.% Co-W ir Ni-W lydiniams bei 17 at.% Fe-W lydinio atveju, Rentgeno spindulių difraktogramoje lieka viena plati smailė. Žinoma, jog toks smailės išplatėjimas siejamas su kristalinių kamuų sumažėjimu. Iš tiesų, buvo nustatyta, kad didėjant W kiekiui lydinyje kristalinių kamuų dydis mažėja nuo maždaug 60-50 nm (elektrochemiškai nusodinti gryni geležies grupės metalai) iki 2-5 nm (esant ~ 30 at.% W). Didelį sunkialydzio metalo kiekį turinčių Co-W, Ni-W ir Fe-W lydinio kristalinių kamuų dydžių vertės buvo patvirtintos taikant TEM analizę. Pažymėtina, kad šiame darbe lydiniai, sudaryti iš tokių mažų kristalinių kamuų (< 5 nm), yra vadinama ultra-nanokristaline.

Siekiant padidinti sunkialydzio metalo kiekį geležies grupės metalų lydiniuose, šiame darbe tai pat buvo nustatytos optimalios elektrolizės sąlygos, kuomet nusodinamos homogeniškos, be įtrūkimų ir gerai su pagrindu sukibusios net apie 50 at.% Mo sudėtyje turinčios lydiniai su Co, Ni ir Fe dangos su priimtina srovine išeiga (~ 50 at.%) (10 pav., 44 psl.). Kaip ir buvo tikėtasi, tokių didelį sunkialydzio metalo kiekį turinčių lydiniai pasižymi ultra-nanokristaline struktūra (kristalinių kamuų dydis siekia 2 nm) (11 pav., 44 psl.).

Elektrocheminės savybės

Vandenilio išsiskyrimo reakcija. Paprastai katalizatorių efektyvumas vandenilio išsiskyrimo reakcijoje vertinamas lyginat vandenilio mainų

srovės tankio reikšmes, kurios apskaičiuojamos ekstrapoliuojant Tafelio tieses iki taško, kuriame viršitampis yra lygus 0. Žinoma, jog didesnės mainų srovės tankio vertės reiškia lengvesnę vandenilio jonų redukciją – turi būti suteiktas mažesnis viršitampis, kad būtų generuojama didesnė srovė.

Darbe buvo nustatyta, kad geležies grupės metalų lydiniai su W pasižymi didesniu kataliziniu aktyvumu 30 sv.% NaOH tirpaluose, lyginant su grynais geležies grupės metalais. Atsižvelgiant į lydinų morfologiją, vidutinio šiurkštumo matavimus bei tikrąjį lydinų paviršiaus plotą visai tirtais atvejais galima daryti išvadą, jog lydinams būdingas didesnis katalizinis aktyvumas yra susijęs su sinergetiniu efektu, kuomet formuojantis dvinariui lydiniai pasikeičia elektroninis tankis d-lygmenyje ir tai teigiamai veikia vandenilio išsiskyrimo kinetiką. Taip pat nustatyta, kad ultra-nanokristaliniai didelį sunkialydzio metalo kiekį sudėtyje turintys lydiniai yra aktyvesni už nanokristalinės struktūros geležies grupės metalų lydinių su W elektrodus. Katalizinis visų geležies grupės metalų lydinių su W aktyvumas didėja tokia tvarka: 5 at.% W < 20 at.% W < 30 at.% W. Tokia tendencija gali būti siejama su struktūros ypatumais, kuomet formuojantis ultra-nanokristalinei struktūrai susidaro ne tik daugiau aktyvių centrų, galinčių dalyvauti reakcijoje, bei susidaro atitinkami stabilūs intermetaliniai junginiai.

Teigiamas efektas tiriant katalizinį ultra-nanokristalinių geležies grupės metalų lydinių su W aktyvumą buvo pastebėtas keliant elektrolito temperatūrą: didinant temperatūrą nuo 25 iki 65°C visų turtų lydinių atvejais mainų srovės tankio vertės didėja. Didžiausias katalizinis aktyvumas nustatytas ultra-nanokristaliniam Ni-W lydiniai: vandenilio mainų srovė siekia 14.5 mA cm⁻² esant 65°C (3 lentelė, 46 psl.).

Taip pat dideliu kataliziniu aktyvumu vandenilio išsiskyrimo reakcijoje pasižymi geležies grupės metalų lydiniai su Mo. Pritaikius tą pačią tyrimų metodiką, kaip ir lydinių su W atveju, buvo apskaičiuotos Mo pagrindu nusodintų lydinių vandenilio mainų srovės tankio vertės, esant skirtingoms natrio šarmo tirpalo temperatūroms. Rezultatai parodė, jog Co-52at.%Mo lydinys tirtame temperatūrų intervale pasižymi didžiausiu kataliziniu aktyvumu: vandenilio mainų srovė siekia 46.2 mA cm⁻² esant 65°C (4 lentelė, 47 psl.).

Svarbu pažymėti, kad lyginant su literatūroje publikuotais analogiškų lydinių rezultatais, gautais esant panašioms eksperimentinėms sąlygoms, šiame darbe suformuotoms Mo elektrodams būdingos didesnės vandenilio mainų srovės vertės.

Metanolio oksidacijos reakcija. Metanolio oksidacijos reakcijos tyrimui buvo pasirinkti charakteringos sudėties ir struktūros Co-W lydiniai (t.y.

nanokristaliniai mėginiai, turintys 3, 18 at.% W ir ultra-nanokristalinės struktūros lydinys, turintis 30 at.% W). Nustatyta, kad ant mažą W kiekį (3 ir 18 at.%) turinčių elektrodų nevyksta metanolio oksidacija ir srovės padidėjimas siejamas su Co-W lydinio tirpimu (12a pav., 48 psl.). Tuo tarpu atliekant analogiškus bandymus su ~ 30 at.% W turinčiais Co-W lydiniais buvo pastebėtas anodinė smailė ties 0.6 V (12b pav., 48 psl.), kuri buvo aptikta ir palyginamosiose kreivėse ant platinos elektrodo (12c pav., 48 psl.) – vieną efektyviausių oksidavimui naudojamų elektrodų. Lydinių sudėties po metanolio oksidavimo reakcijos tyrimai parodė, kad šiuo atveju reakcijos metu korozija paveikia tik viršutinį elektrodo sluoksnį ir nustatytas 3 at.% W kiekio padidėjimas paviršiuje lyginant su pradine lydinio sudėtimi. Švelniai su švitriniais popieriumi nuvalius viršutinį sluoksnį buvo pakartota sudėties analizė, ir rezultatai sutapo su pradinės, nusodintos dangos sudėtimi. Taigi, galime manyti, jog ultra-nonkristalinės struktūros lydiniai, kuriuos sudaro intermetalinis Co_3W junginys ir W kietasis tirpalas Co kristalinėje gardelėje, apsaugo nuo kobalto tirpimo ir lydinys gali dalyvauti katalizinėje reakcijoje.

Korozinės savybės H_2SO_4 tirpale. Elektrocheminės korozijos tyrimuose buvo vertinami įvairios sudėties Co-W lydinių korozijos parametrai: korozijos srovė, korozijos potencialas ir korozijos varža. Korozijos parametrai šiame darbe buvo apskaičiuojami iš poliarizacinių matavimų (16 pav., 52 psl.) naudojantis Alleno-Hicklingo aproksimacija. Paaiškėjo, jog korozijos varža keičiasi analogiškai su korozijos srovės tankio vertėmis. Didžiausias korozinis atsparumas buvo nustatytas Co-W lydiniai, turinčiam 24 at.% W (5 lentelė, 52 psl.).

Po korozijos tyrimo visais atvejais deguonies kiekis Co-W dangose ženkliai išauga. Jose taip pat nustatytas didesnis W kiekis. Atsižvelgiant į gautus rezultatus bei oksidinio sluoksnio storio pokyčius, atskaičiuotus remiantis plokščiojo kondensatoriaus talpos formule, galima spręsti apie tai, jog elektrocheminės korozijos metu vyksta anodinis Co tirpimas, o W oksiduojasi susidarant tarpiniams produktams su deguonimi. Apskaičiuotas Co-W korozijos metu susidarancio oksidinio sluoksnio storis didėja, kai lydinyje auga W kiekis, ir pasiekia maksimalią vertę, ties 24 at.% W (17 pav., 54 psl.). Šis oksidas efektyviausiai apsaugo Co nuo tirpimo.

Binarinių lydinių modifikavimas

Trečiojo metalo įvedimas į lydinį. Literatūroje randama duomenų, jog funkcinės dvinarių lydinių savybės gali būti ženkliai pageriamos į sistemą įvedant trečiąją komponentą. Turint omenyje didelį Cu atsparumą korozijai,

buvo nuspręsta atlikti naujo, literatūroje dar neaprašyto Co-Cu-W lydinio elektronusodinimą. Elektronusodinimas buvo atliktas potenciostatinėmis sąlygomis. 18 pav. (55 psl.) galima matyti lydinių cheminės sudėties ir išeigos pagal srovę sąryšius su nusodinimo potencialo vertėmis. Trinario Co-Cu-W lydinio charakteristikos buvo lyginamos kartu su binariniais Co-W ir Cu-W lydiniais. Kadangi didžiausias W kiekis, kurį pavyko nusodinti su Cu yra 6 at.%, palyginamiesiems korozijos atsparumo tyrimams 0.01 M H₂SO₄ tirpale buvo pasirinkti būtent tokį W kiekį turintys Co-Cu-W ir Co-W lydiniai. Cu-W lydinio atveju susidaro W kietasis tirpalas Cu kristalinėje gardelėje, tuo tarpu trinario lydinio difraktogramoje pastebimos ir heksagoninio Co smailės (19 pav, 56 psl.). Morfologijos tyrimai parodė, kad Cu-6W ir Co-41Cu-5W lydinių paviršiaus vaizdas ženkliai skiriasi nuo panašų W kiekį turinčio Co-W lydinio (9a pav., 43 psl.): dangų, kurių sudėtyje yra Cu, paviršių sudaro grūdėti aglomeravusių kristalitų agregatai (20 pav., 56 psl.).

Pasirinktų lydinių korozinė elgsena buvo tiriama lyginant korozijos srovės vertes, apskaičiuotas analizuojant poliarizacines kreives (21 pav., 57 psl.) bei Alleno-Hicklingo pasiūlytą metodą. Nustatyta, kad įvedus Cu į Co-W lydinį korozijos srovės tankis ženkliai sumažėja apie 300 kartų. Po eksperimento atlikta cheminės sudėties analize parodė, kad trinariame lydinyje išauga Cu ir W kiekis, bei atitinkamai sumažėja Co kiekis. Galima manyti, kad į tirpalą perėję Cu jonai proceso metu vėl yra redukuojami iki metalinės formos. Taip pat, remiantis literatūroje pateiktais duomenimis, galima daryti prielaidą, kad korozinis Co-Cu-W atsparumas, lyginant su tokį patį W kiekį turinčiu Co-W lydiniu, išauga dėl apsauginės plėvelės, kurios sudėtyje yra Cu, susidarymo paviršiuje.

Fosforo įvedimas į lydinį. Volframo lydiniai gali būti naudojami pramoninių peilių, skirtų vaisių (alyvuogių) smulkinimui, gamyboje. Perspektyvūs yra geležies pagrindu paruošti lydiniai, nes priešingai, nei kobalto arba nikelio lydinių atveju, juos leidžiama naudoti maisto pramonėje. Šiame darbe korozinė elektrochemiškai nusodintų Fe, Fe-W ir Fe-W-P lydinių elgsena buvo tiriama 0.012 M Na₂SO₄ + 0.027 M NaCl tirpale 90°C temperatūroje, t.y. atsižvelgiant į realias panaudojimo sąlygas, siekiant lydinius potencialiai pritaikyti maisto apdirbimo pramonėje. Lydinių elektronusodinimo sąlygos buvo parenkamos taip, kad juose būtų didelis W kiekis (apie 30 at.%). Fe-W dangos kokybei pagerinti į elektrolitą buvo pridėta organinių priedų: 1,4-butindiolio ir Rokafenolio-10. Nustatyta, kad fosforo įvedimas į Fe-W lydinį ryškios įtakos paviršiaus morfologijai neturi, susiformuoja tik kiek smulkesnis grūdėtų aglomeratų paviršius (22 pav., 59 psl.). Tuo tarpu

dangos, nusodintos iš elektrolito, kuriame yra organinės kilmės priedų, pasižymėjo dar smulkesne struktūra. Visais atvejais buvo gautos ultra-nanokristalinės struktūros lydiniai (23 pav., 59 psl.).

Skirtingos sudėties Fe pagrindu nusodintų lydinių korozijos srovės buvo nustatomos naudojantis voltamperinėmis kreivėmis. Nustatyta, kad net ir nežymus P įvedimas į Fe-W lydinį sąlygoja didesnę paviršiaus atsparumą elektrocheminei korozijai: Fe-W-P paviršiui nustatyta 2 kartus mažesnė korozijos srovė, nei elektrolitinėms Fe ir Fe-33 at.% W dangomis (6 lentelė, 60 psl.). Atlikus palyginamuosius Co-W ir Fe-W lydinių korozijos tyrimus 0.012 M Na₂SO₄ + 0.027 M NaCl tirpale 90°C temperatūroje pastebėta, kad nanokristalinės struktūros Co-31 at.% W lydiniai būdinga mažesnė korozijos srovė, nei tokios pačios struktūros Fe-33 at.% W lydiniai. Tiesa, į Fe-W lydinį įvedus nedidelį kiekį P, korozijos srovė tampa artima anksčiau minėtai Co-31 at.% W danga ($\sim 1.7 \cdot 10^{-5}$ A cm⁻²).

Nanostruktūrizavimas. Galiausiai buvo pritaikytas dar vienas lydinių modifikavimo metodas, t.y. nansotuktūrizavimas atliekant elektronusodinimą naudojant nanoporų membranų šabloną. Laidumui užtikrinti pirmiausia buvo užpurškiamas plonas Au sluoksnis. Tuomet nanoporos elektrochemiškai buvo užpildytos Co-W lydiniais.

Nusodintos nanovielos buvo panaudotos kataliziniams tyrimams vandenilio išsiskyrimo reakcijoje. Ir kaip ir buvo tikėtasi dėl išaugusio paviršiaus ploto Co-5 at.%W lydinio nanovielų vandenilio mainų srovės tankis, lyginant su plonais sluoksniais, turinčiais tą pačią sudėtį, t.y., išauga net apie 300 kartų (26 pav., 62 psl.).

Šiame darbe pirmą kartą buvo pasiūlyta idėja nusodintas nanovielas modifikuoti Au nanodalelėmis, kuomet atskiros nanodalelės yra įtvirtinamos ant nanovielos viršūnėlės (27 pav., 63 psl.). Tokių kompozitų gamybos schema schematiškai yra pavaizduota 24 pav., 61 psl. Tokios naujoviškos nanostruktūros gali būti pritaikytos jutiklių gamyboje, mat Au nanodalelės gali būti modifikuojamos įvairiomis biologinėmis funkcinėmis grupėmis.

IŠVADOS

1. Keičiant elektrolizės sąlygas, buvo suformuotos homogeniškos, kompaktiškos, gerai su pagrindu sukibusios geležies grupės metalų lydinių dangos, turinčios 30 at.% W ir 50 at.% Mo. Tokių lydinių struktūra yra ultra-nanokristaline, ir ją sudaro dvi fazės: W/Mo kietasis tirpalas geležis grupės metalo gardelėje ir atitinkami intermetaliniai junginiai.
2. Visi tirti W/Mo lydiniai pasižymi didesniu kataliziniu aktyvumu vandenilio išsiskyrimo reakcijoje 30 sv.% NaOH tirpale, nei grynai geležies grupės metalai, o jų vandenilio mainų srovės vertės mažėja tokia tvarka: Co-52Mo > Ni-54Mo > Fe-54Mo > Ni-29W > Co-33W > Fe-30W (sudėtis pateikiama at.%). Didžiausias vandenilio mainų srovės tankis (46.2 mA cm^{-2}) buvo nustatytas Co-52at.%Mo elektrodui, ir tai gali būti susiję su stabilios Co_3Mo intermetalinės fazės, kuriai būdingas didesnis aktyvių vandenilio išsiskyrimo reakcijos centrų skaičius, susidarymu. Lydinių nanostruktūrizavimas elektronusodinimo į poringas membranas metu, susidarant lydinių nanovieloms leidžia dar labiau padidinti katalizinį aktyvumą, t.y. vandenilio mainų srovės tankis padidėja nuo 0.02 mA cm^{-2} (Co-5at.%W ploni sluoksniai) iki 3.7 mA cm^{-2} (Co-5at.%W nanovielos).
3. Didžiausiu atsparumu korozijai pasižymi Co-W lydinys, turintis 24 at.% W, kuomet pastebimas perėjimas iš nanokristalinės į ultra-nanokristalinę struktūrą, ir susidaro stabilus intermetalinis Co_3W junginys. Dėka minėtų pokyčių ir padidėjusio atsparumo korozijai, Co-W elektrodas gali katalizuoti metanolio oksidacijos reakciją rūgtiniame tirpale: Co-30at.%W lydinio anodinės smailės srovės tankis siekia $12,3 \text{ mA}\cdot\text{cm}^{-2}$, tuo tarpu Pt $\sim 2,4 \text{ mA cm}^{-2}$, t.y. apie 5 kartus mažesnis.
4. Binarinių lydinių modifikavimas įvedant į sistemą trečiąjį komponentą (P, Cu, Au) sąlygoja didesnę atsparumą korozijai, pvz. trinariam Co-Cu-W lydiniai būdinga 300 kartų mažesnis korozijos srovės tankis, nei Co-W lydiniai; Fe-W-P lydiniai nustatytas korozijos srovės tankis yra 2 kartus mažesnis, nei Fe-W lydinio atveju. Taip pat buvo suformuotas naujas nano-kompozitas, sudarytas iš elektronusodintų Co-W nanovielų bei Au nanodalėlių, kuris galėtų sėkmingai būti modifikuotas organinėmis funkcinėmis grupėmis ir tokiu būdu pritaikytas jutiklių kūrimui.

6. REFERENCES

- [1] D. Sobha Jayakrishnan, Electrodeposition: the versatile technique for nanomaterials, in: V. S. Saji, R. Cook (Eds.) Corrosion protection and control using nanomaterials, Elsevier, (2012) 86–125.
- [2] N. Tsyntaru, J. Bobanova, X. Ye, H. Cesiulis, A. Dikusar, I. Prosycevas, J. P. Celis, Iron–tungsten alloys electrodeposited under direct current from citrate–ammonia plating baths, *Surf. Coat. Technol.* 203 (2009) 3136–3141.
- [3] N. Tsyntaru, Tribological Behaviour of Co-W Under Dry and Lubricating Conditions, in: Proc. 8th Int. Sci. Conf. BALTRIB2015, Aleksandras Stulginskis University, Lithuania (2015).
- [4] T. Yamasaki, High-strength nanocrystalline Ni-W alloys produced by electrodeposition, *Mater. Phys. Mech.* 1 (2000) 127-132.
- [5] T. Nasu, M. Sakurai, T. Kamiyama, T. Usuki, O. Uemura, K. Tokumitsu, T. Yamasaki, Structural comparison of M–W (M = Fe, Ni) alloys produced by electrodeposition and mechanical alloying, *Mater. Sci. Eng. A.* 375–377 (2004) 163–170.
- [6] N. Tsyntaru, H. Cesiulis, A. Budreika, X. Ye, R. Juskenas, J. P. Celis, The effect of electrodeposition conditions and post-annealing on nanostructure of Co–W coatings, *Surf. Coat. Technol.* 206 (2012) 4262–4269.
- [7] N. Tsyntaru, H. Cesiulis, E. Pellicer, J. P. Celis, J. Sort, Structural, magnetic, and mechanical properties of electrodeposited cobalt–tungsten alloys: Intrinsic and extrinsic interdependencies, *Electrochim. Acta.* 104 (2013) 94–103.
- [8] T. Sadat, G. Dirras, D. Tingaud, M. Ota, T. Chauveau, D. Faurie, S. Vajpai, K. Ameyama, Bulk Ni–W alloys with a composite-like microstructure processed by spark plasma sintering: Microstructure and mechanical properties, *Mater. Des.* 89 (2016) 1181–1190.
- [9] B. B. Bokhonov, A. V. Ukhina, D. V. Dudina, A. G. Anisimov, V. I. Mali, I. S. Batraev, Carbon uptake during Spark Plasma Sintering: investigation through the analysis of the carbide “footprint” in a Ni-W alloy, *RSC Adv.* 5 (2015) 80228-80237.
- [10] M. Metikoš-Huković, Z. Grubač, N. Radić, A. Tonejc, Sputter deposited nanocrystalline Ni and Ni-W films as catalysts for hydrogen evolution, *J. Mol. Catal. Chem.* 249 (2006) 172–180.
- [11] J. M. V. Nsanzimana, Y. Peng, M. Miao, V. Reddu, W. Zhang, H. Wang, B. Y. Xia, X. Wang, An Earth-Abundant Tungsten–Nickel Alloy Electrocatalyst for Superior Hydrogen Evolution, *ACS Appl. Nano Mater.* 1 (2018) 1228–1235.
- [12] E. R. Gonzalez, A. Mota-Lima, Catalysts for methanol oxidation, in: R. Corti, E.R. Gonzalez (Eds.), *Direct Alcohol Fuel Cells – Materials, Performance, Durability and Applications*, Springer Science + Business Media, Dordrecht (2014) 33.
- [13] A. Genç, M. L. Öveçoğlu, M. Baydoğan, S. Turan, Fabrication and characterization of Ni–W solid solution alloys via mechanical alloying and pressureless sintering, *Mater. Des.* 42 (2012) 495–504.
- [14] A. O. Aning, Z. Wang, T. H. Courtney, Tungsten solution kinetics and amorphization of nickel in mechanically alloyed Ni-W alloys, *Acta Metall. Mater.* 41 (1993) 165–174.

- [15] N. Petrov, Y. Sverdlov, Y. Shacham-Diamand, Electrochemical Study of the Electroless Deposition of Co(P) and Co(W,P) Alloys, *J. Electrochem. Soc.* 149 (2002) C187-C194.
- [16] J. Jiang, H. Chen, Y. Wang, L. Zhu, Y. Sun, H. Lin, S. Han, Y. Luo, W. Qian, Effect of ultrasonication and Na₂MoO₄ content on properties of electroless Ni–Mo–P coatings, *Surf. Eng.* 35 (2019) 1–10.
- [17] A. Brenner, P. Burkhead, E. Seegmiller, Electrodeposition of tungsten alloys containing iron, nickel, and cobalt, *J. Res. Natl. Bur. Stand.* 39 (1947) 351.
- [18] O. Pourret, M. P. Faucon, Cobalt, in: P. Bobrowsky, B. Marker (Eds.), *Encyclopedia of Geochemistry*, Springer International Publishing, Cham, (2016) 1–3.
- [19] K. Akira, Tungsten Coating for Thermal Fusion Material Produced by Gas Tunnel Type Plasma Spraying, *Transactions of JWRI*, 37 (2008) 63–67.
- [20] I. M. Dharmadasa, J. Haigh, Strengths and Advantages of Electrodeposition as a Semiconductor Growth Technique for Applications in Microelectronic Devices, *J. Electrochem. Soc.* 153 (2006) G47–G52.
- [21] G. Zangari, Electrodeposition of Alloys and Compounds in the Era of Microelectronics and Energy Conversion Technology, *Coatings*. 5 (2015) 195–218.
- [22] W. Giurlani, G. Zangari, F. Gambinossi, M. Passaponti, E. Salvietti, F. Di Benedetto, S. Caporali, M. Innocenti, Electroplating for Decorative Applications: Recent Trends in Research and Development, *Coatings*. 8 (2018) 260–285.
- [23] I. Gurrappa, L. Binder, Electrodeposition of nanostructured coatings and their characterization—A review, *Sci. Technol. Adv. Mater.* 9 (2008) 043001.
- [24] T. H. Tsai, J. H. Huang, Electrochemical investigations for copper electrodeposition of through-silicon via, *Microelectron. Eng.* 88 (2011) 195–199.
- [25] F. Wang, Z. Zhao, N. Nie, F. Wang, W. Zhu, Dynamic through-silicon-via filling process using copper electrochemical deposition at different current densities, *Sci. Rep.* 7 (2017) 1–9.
- [26] X. Z. Li, X. W. Wei, Y. Ye, Template electrodeposition to cobalt-based alloys nanotube arrays, *Mater. Lett.* 63 (2009) 578–580.
- [27] N. Tsyntaru, S. Silkin, H. Cesiulis, M. Guerrero, E. Pellicer, J. Sort, Toward uniform electrodeposition of magnetic Co-W mesowires arrays: direct versus pulse current deposition, *Electrochim. Acta.* 188 (2016) 589–601.
- [28] R. Bogue, MEMS sensors: past, present and future, *Sens. Rev.* 27 (2007) 7–13.
- [29] C. M. Ho, Y. C. Tai, Review: MEMS and Its Applications for Flow Control, *J. Fluids Eng.* 118 (1996) 437–447.
- [30] M. Asadnia, A. G. P. Kottapalli, R. Haghghi, A. Cloitre, P. V. Alvarado, J. Miao, M. Triantafyllou, MEMS sensors for assessing flow-related control of an underwater biomimetic robotic stingray, *Bioinspir. Biomim.* 10 (2015) 036008.
- [31] B. R. Donald, C. G. Levey, C. D. McGray, I. Paprotny, D. Rus, An Untethered, Electrostatic, Globally Controllable MEMS Micro-Robot, *J. Microelectromechanical Syst.* 15 (2006) 1–15.
- [32] G. Ciuti, L. Ricotti, A. Menciassi, P. Dario, MEMS Sensor Technologies for Human Centred Applications in Healthcare, Physical Activities, Safety and

- Environmental Sensing: A Review on Research Activities in Italy, *Sensors*. 15 (2015) 6441–6468.
- [33] S. Aravamudhan, MEMS for in vivo sensing, in: *Mems for Biomedical Applications*, Woodhead Publishing Limited (2012) 81–96.
- [34] A. Brenner, *Electrodeposition of Alloys: Principles and Practice*, Academic Press Inc., New York (1963).
- [35] K. S. Jackson, A. S. Rssell, J. L. Merrill, The electrolytic deposition of tungsten at a mercury cathode, *J. Chem. Soc.* (1929) 2394–2398.
- [36] N. Tsyntsaru, H. Cesiulis, M. Donten, J. Sort, E. Pellicer, E.J. Podlaha-Murphy, Modern trends in tungsten alloys electrodeposition with iron group metals, *Surf. Eng. Appl. Electrochem.* 48 (2012) 491–520.
- [37] T. Akiyama. H. Fukushima, Recent Study on the Mechanism of the Electrodeposition of Iron-group Metal Alloys, *ISIJ Int.* 32 (1992) 787–798.
- [38] H. Fukushima, T. Akiyama., S. Akagi, K. Higashi, Role of Iron-group Metals in the Induced Codeposition of Molybdenum from Aqueous Solution, *Trans JTM.* 20 (1979) 358–364.
- [39] M. L. Holt, L. E. Vaaler, Electrolytic Reduction of Aqueous Tungstate Solutions, *J. Electrochem. Soc.* 94 (1948) 50-58.
- [40] E. Gileadi, N. Eliaz, The Mechanism of Induced Codeposition of Ni-W Alloys, in: *ECS Trans.*, ECS, Denver, Colorado (2007) 337–349.
- [41] O. Younes-Metzler, L. Zhu, E. Gileadi, The anomalous codeposition of tungsten in the presence of nickel, *Electrochim. Acta.* 48 (2003) 2551–2562.
- [42] D. P. Weston, S. J. Harris, P. H. Shipway, N. J. Weston, G. N. Yap, Establishing relationships between bath chemistry, electrodeposition and microstructure of Co–W alloy coatings produced from a gluconate bath, *Electrochim. Acta.* 55 (2010) 5695–5708.
- [43] S. S. Belevskii, S. P. Yushchenko, A. I. Dikusar, Anomalous electrodeposition of Co-W coatings from a citrate electrolyte due to the formation of multinuclear heterometallic complexes in the solution, *Surf. Eng. Appl. Electrochem.* 48 (2012) 97–98.
- [44] A. T. Vasko, in: A. J. Bard (Eds.) *Encyclopedia of Electrochemistry of the Elements*, Marcel Dekker, New York (1986) 69.
- [45] V. L. Krasikov, A. V. Krasikov, Mechanism for induced codeposition of alloys and some single refractory metals, *Bull. St. Petersburg State Inst. Technol. Tech. Univ.* 37 (2016) 8–14.
- [46] H. Cesiulis, A. Budreika, Electroreduction of Ni(II) and Co(II) from Pyrophosphate Solutions, *Mater. Sci. Medz.* 16 (2010) 52-56.
- [47] S. Oue, H. Nakano, S. Kobayashi, H. Fukushima, Structure and Codeposition Behavior of Ni–W Alloys Electrodeposited from Ammoniacal Citrate Solutions, *J. Electrochem. Soc.* 156 (2009) D17-D22.
- [48] E. J. Podlaha, D. Landolt, II. A Mathematical Model Describing the Electrodeposition of Ni-Mo Alloys, *J. Electrochem. Soc.* 143 (1996) 893-898.
- [49] E. J. Podlaha, D. Landolt, III. Molybdenum Alloys with Nickel, Cobalt, and Iron, *J. Electrochem. Soc.* 144 (1997) 1672-1680.
- [50] Y. Zeng, Z. Li, M. Ma, S. Zhou, In situ surface Raman study of the induced codeposition mechanism of Ni–Mo alloys, *Electrochem. Commun.* 2 (2000) 36–38.

- [51] Z. J. Niu, S. B. Yao, S. M. Zhou, In situ surface Raman investigation on induced-codeposition of an Fe–Mo alloy, *J. Electroanal. Chem.* 455 (1998) 205–207.
- [52] V. Vasauskas, J. Padgurskas, R. Rukuiža, H. Cesiulis, D. Mil, Cracking behavior of electrodeposited nanocrystalline tungsten-cobalt and tungsten-iron coatings, *Mechanika*. 72 (2008) 21-27.
- [53] I. Matsui, Y. Takigawa, T. Uesugi, K. Higashi, Effect of additives on tensile properties of bulk nanocrystalline Ni–W alloys electrodeposited from a sulfamate bath, *Mater. Lett.* 99 (2013) 65–67.
- [54] M. Benaicha, M. Allam, A. Dakhouche, M. Hamla, Electrodeposition and Characterization of W-rich NiW Alloys from Citrate Electrolyte, *Int. J. Electrochem. Sci.* 11 (2016) 7605 – 7620.
- [55] S. Hayata, S. Oue, H. Nakano, T. Takahashi, Effect of Annealing on the Structure and Hardness of Electrodeposited Ni–W Alloys, *ISIJ Int.* 55 (2015) 1083–1090.
- [56] L. Elias, A. Chitharanjan Hegde, Electrodeposition of laminar coatings of Ni–W alloy and their corrosion behaviour, *Surf. Coat. Technol.* 283 (2015) 61–69.
- [57] M. Donten, Bulk and surface composition, amorphous structure, and thermocrystallization of electrodeposited alloys of tungsten with iron, nickel, and cobalt, *J. Solid State Electrochem.* 3 (1999) 87–96.
- [58] Y. Ruan, S. Yao, M. Kowaka, Amorphization of electrodeposited Fe-W alloy films and electrochemical behavior, *J. Non-Cryst. Solids.* 117–118 (1990) 752–755.
- [59] J. Druga, M. Kašiarová, E. Dobročka, M. Zemanová, Corrosion and tribological properties of nanocrystalline pulse electrodeposited Ni–W alloy coatings, *Trans. IMF.* 95 (2017) 39–45.
- [60] E. Navarro-Flores, Z. Chong, S. Omanovic, Characterization of Ni, NiMo, NiW and NiFe electroactive coatings as electrocatalysts for hydrogen evolution in an acidic medium, *J. Mol. Catal. Chem.* 226 (2005) 179–197.
- [61] O. Younes, Electroplating of High Tungsten Content Ni/W Alloys, *Electrochem. Solid-State Lett.* 3 (1999) 543.
- [62] K. H. Hou, Y. F. Chang, S. M. Chang, C. H. Chang, The heat treatment effect on the structure and mechanical properties of electrodeposited nano grain size Ni–W alloy coatings, *Thin Solid Films.* 518 (2010) 7535–7540.
- [63] I. Mizushima, P. T. Tang, H. N. Hansen, M. A. J. Somers, Residual stress in Ni–W electrodeposits, *Electrochim. Acta.* 51 (2006) 6128–6134.
- [64] P. de Lima-Neto, A. N. Correia, R. A.C. Santana, R. P. Colares, E. B. Barros, P. N. S. Casciano, G. L. Vaz, Morphological, structural, microhardness and electrochemical characterisations of electrodeposited Cr and Ni–W coatings, *Electrochim. Acta.* 55 (2010) 2078–2086.
- [65] L. M. Chang, Z. T. Wang, S. Y. Shi, W. Liu, Study on microstructure and properties of electrodeposited Ni–W alloy coating with glycolic acid system, *J. Alloys Compd.* 509 (2011) 1501–1504.
- [66] K. R. Sriraman, S. Ganesh Sundara Raman, S. K. Seshadri, Corrosion behaviour of electrodeposited nanocrystalline Ni–W and Ni–Fe–W alloys, *Mater. Sci. Eng. A.* 460–461 (2007) 39–45.
- [67] A. Nicolenco, N. Tsyntaru, J. Fornell, E. Pellicer, J. Reklaitis, D. Baltrunas, H. Cesiulis, J. Sort, Mapping of magnetic and mechanical properties of Fe-

- W alloys electrodeposited from Fe(III)-based glycolate-citrate bath, *Mater. Des.* 139 (2018) 429–438.
- [68] N. Fathollahzade, K. Raeissi, A comparative study on the electrochemical behaviour of amorphous and nanocrystalline cobalt–tungsten electrodeposited coatings, *Trans. IMF.* 92 (2014) 253–261.
- [69] L. Ma, X. Xi, Z. Nie, T. Dong, Y. Mao, Electrodeposition and Characterization of Co-W Alloy from Regenerated Tungsten Salt, *Int. J. Electrochem. Sci.* 12 (2017) 1034–1051.
- [70] M. Svensson, U. Wahlström, G. Holmbom, Compositionally modulated cobalt–tungsten alloys deposited from a single ammoniacal electrolyte, *Surf. Coat. Technol.* 105 (1998) 218–223.
- [71] M. Zemanová, M. Krivosudská, M. Chovancová, V. Jorik, Pulse current electrodeposition and corrosion properties of Ni–W alloy coatings, *J. Appl. Electrochem.* 41 (2011) 1077–1085.
- [72] N. Tsyntsaru, A. Dikumar, H. Cesiulis, J. P. Celis, Zh. Bobanova, S. Sidel'nikova, S. Belevskii, Yu. Yapontseva, O. Bersirova, V. Kublanovskii, Tribological and corrosive characteristics of electrochemical coatings based on cobalt and iron superalloys, *Powder Metall. Met. Ceram.* 48 (2009) 419–428.
- [73] A. Królikowski, E. Płońska, A. Ostrowski, M. Donten, Z. Stojek, Effects of compositional and structural features on corrosion behavior of nickel–tungsten alloys, *J. Solid State Electrochem.* 13 (2009) 263–275.
- [74] M. Obradovic, J. Stevanovic, A. Despic, R. Stevanovic, J. Stoch, Characterization and corrosion properties of electrodeposited Ni-W alloys, *J. Serbian Chem. Soc.* 66 (2001) 899–912.
- [75] C. L. Aravinda, V. S. Muralidharan, S. M. Mayanna, Electrodeposition and dissolution of Co–W alloy films, *J. Appl. Electrochem.* 30 (2000) 601–606.
- [76] T. Omi, H. Yomamoto, Structure of Noncrystalline Co-25 a/o W Electrodeposit, *J. Electrochem. Soc.* 119 (1972) 168–173.
- [77] S. Wang, C. Zeng, Y. Ling, J. E. G. Xu, Phase transformations and electrochemical characterizations of electrodeposited amorphous Fe–W coatings, *Surf. Coat. Technol.* 286 (2016) 36–41.
- [78] M. Donten, Z. Stojek, H. Cesiulis, Formation of Nanofibers in Thin Layers of Amorphous W Alloys with Ni, Co, and Fe Obtained by Electrodeposition, *J. Electrochem. Soc.* 150 (2003) C95–C98.
- [79] K. R. Sriraman, S. G. Sundara Raman, S. K. Seshadri, Synthesis and evaluation of hardness and sliding wear resistance of electrodeposited nanocrystalline Ni–Fe–W alloys, *Mater. Sci. Technol.* 22 (2006) 14–20.
- [80] C. A. Schuh, T. G. Nieh, H. Iwasaki, The effect of solid solution W additions on the mechanical properties of nanocrystalline Ni, *Acta Mater.* 51 (2003) 431–443.
- [81] N. Hansen, Hall–Petch relation and boundary strengthening, *Scr. Mater.* 51 (2004) 801–806.
- [82] C. N. Panagopoulos, E. P. Georgiou, D. A. Lagaris, V. Antonakaki, The effect of nanocrystalline Ni-W coating on the tensile properties of copper, *AIMS Mater. Sci.* 3 (2016) 324–338.
- [83] A. Giga, Y. Kimoto, Y. Takigawa, K. Higashi, Demonstration of an inverse Hall–Petch relationship in electrodeposited nanocrystalline Ni–W alloys through tensile testing, *Scr. Mater.* 55 (2006) 143–146.

- [84] A. S. M. A. Haseeb, U. Albers, K. Bade, Friction and wear characteristics of electrodeposited nanocrystalline nickel–tungsten alloy films, *Wear*. 264 (2008) 106–112.
- [85] N. I. Tsyntaru, Zh. I. Bobanova, D. M. Kroitoru, V. F. Cheban, G. I. Poshtaru, A. I. Dikumar, Effect of a multilayer structure and lubrication on the tribological properties of coatings of Fe-W alloys, *Surf. Eng. Appl. Electrochem.* 46 (2010) 538–546.
- [86] K. Watabe, K. City, Iron Tungsten Alloy Plating with Low Friction and Wear Resistance, *NASF Surface Technology White Papers*. 81 (2017) 1-9.
- [87] H. Chen, X. R. Ren, X. H. Zhang, J. H. Li, Wear and Corrosion Properties of Crystalline Ni-W Alloy Coatings Prepared by Electrodeposition, *Mater. Sci. Forum*. 849 (2016) 671–676.
- [88] H. Capel, P. H. Shipway, S. J. Harris, Sliding wear behaviour of electrodeposited cobalt–tungsten and cobalt–tungsten–iron alloys, *Wear*. 255 (2003) 917–923.
- [89] T. Yamasaki, P. Schloßmacher, K. Ehrlich, Y. Ogino, Formation of amorphous electrodeposited Ni-W alloys and their nanocrystallization, *Nanostructured Mater.* 10 (1998) 375–388.
- [90] S. Eskin, O. Berkh, G. Rogalsky, J. Zahavi, Co-W Alloys for Replacement Of Conventional Hard Chromium, *Plating Surf. Finish*. 85 (1998) 79-83.
- [91] A. J. Detor, C. A. Schuh, Microstructural evolution during the heat treatment of nanocrystalline alloys, *J. Mater. Res.* 22 (2007) 3233–3248.
- [92] A. Mulone, A. Nicolenco, J. Fornell, E. Pellicer, N. Tsyntaru, H. Cesiulis, J. Sort, U. Klement, Enhanced mechanical properties and microstructural modifications in electrodeposited Fe-W alloys through controlled heat treatments, *Surf. Coat. Technol.* 350 (2018) 20–30.
- [93] H. Okamoto, Ni-W(Nickel-Tungsten), *J. Phase Equilibria USA*. 12 (1991) 706.
- [94] H. Okamoto, Co-W (Cobalt-Tungsten), *J. Phase Equilibria Diffus.* 29 (2008) 119–119.
- [95] B. Predel, Fe-W (Iron-Tungsten), in: Madelung O Eds Dy-Er – Fr-Mo, *Landolt-Börnstein - Group IV Physical Chemistry (Numerical Data and Functional Relationships in Science and Technology)*, Springer, Berlin, Heidelberg (1995) 1-4.
- [96] S. Yao, S. Zhao, H. Guo, M. Kowaka, A New Amorphous Alloy Deposit with High Corrosion Resistance, *Corrosion*. 52 (1996) 183–186.
- [97] A. Subramanian, G. N. Kousalya, V. S. Muralidharan, T. Vasudevan, Cobalt tungsten alloy electrodeposition and characterization, *Indian J. Chem. Technol.* 9 (2002) 513–518.
- [98] A. Chianpairot, G. Lothongkum, C.A. Schuh, Y. Boonyongmaneerat, Corrosion of nanocrystalline Ni–W alloys in alkaline and acidic 3.5 wt.% NaCl solutions, *Corros. Sci.* 53 (2011) 1066–1071.
- [99] Yu. S. Yapontseva, A. I. Dikumar, V. S. Kyblanovskii, Study of the composition, corrosion, and catalytic properties of Co-W alloys electrodeposited from a citrate pyrophosphate electrolyte, *Surf. Eng. Appl. Electrochem.* 50 (2014) 330–336.
- [100] V. Kublanovsky, O. Bersirova, A. Dikumar, Z. Bobanova, H. Cesiulis, J. Sinkeviciute, I. Prosycevas, Electrodeposition and Corrosion Properties of Nanocrystalline Fe-W alloys, *Problems of corrosion and corrosion protection of materials*. 7 (2008) 308–314.

- [101] V. S. Kublanovskii, Yu. S. Yapontseva, Yu. N. Troshchenkov, V. A. Gromova, Corrosion and magnetic properties of electrolytic Co-Mo alloys, *Russ. J. Appl. Chem.* 83 (2010) 440–444.
- [102] X. Liu, Z. Xiang, J. Niu, K. Xia, Y. Yang, B. Yan, W. Lu, The Corrosion Behaviors of Amorphous, Nanocrystalline and Crystalline Ni-W Alloys Coating, *Int. J. Electrochem. Sci.* 10 (2015) 7.
- [103] H. B. Lee, Synergy Between Corrosion and Wear of Electrodeposited Ni–W Coating, *Tribol. Lett.* 50 (2013) 407–419.
- [104] M. Donten, Z. Stojek, Pulse electroplating of rich-in-tungsten thin layers of amorphous Co-W alloys, *J. Appl. Electrochem.* 26 (1996) 665–672.
- [105] M. Donten, Voltammetric, Optical, and Spectroscopic Examination of Anodically Forced Passivation of Cobalt-Tungsten Amorphous Alloys, *J. Electrochem. Soc.* 140 (1993) 3417.
- [106] A. Bodaghi, J. Hosseini, Corrosion resistance and electrocatalytic properties of Co–W alloy coatings, *Surf. Eng.* 28 (2012) 632–635.
- [107] C. N. Panagopoulos, G. D. Plainakis, M. G. Tsoutsouva, Corrosion of Nanocrystalline Ni-W Coated Copper, *J. Surf. Eng. Mater. Adv. Technol.* 5 (2015) 65–72.
- [108] A. Laszczyńska, W. Tylus, J. Winiarski, I. Szczygieł, Evolution of corrosion resistance and passive film properties of Ni-Mo alloy coatings during exposure to 0.5 M NaCl solution, *Surf. Coat. Technol.* 317 (2017) 26–37.
- [109] N. Shakibi Nia, J. Creus, X. Feaugas, C. Savall, Influence of metallurgical parameters on the electrochemical behavior of electrodeposited Ni and Ni–W nanocrystalline alloys, *Appl. Surf. Sci.* 370 (2016) 149–159.
- [110] C. N. Tharamani, P. Beera, V. Jayaram, N. S. Begum, S. M. Mayanna, Studies on electrodeposition of Fe–W alloys for fuel cell applications, *Appl. Surf. Sci.* 253 (2006) 2031–2037.
- [111] F. S. Hoor, C. N. Tharamani, M. F. Ahmed, S. M. Mayanna, Electrochemical synthesis of Fe–Mo and Fe–Mo–Pt alloys and their electrocatalytic activity for methanol oxidation, *J. Power Sources.* 167 (2007) 18–24.
- [112] T. Shobba, S. M. Mayanna, C. A. C. Sequeira, Preparation and characterization of Co–W alloys as anode materials for methanol fuel cells, *J. Power Sources.* 108 (2002) 261–264.
- [113] A. Züttel, A. Borgschulte, L. Schlapbach, Hydrogen as a future energy carrier, in: Wiley-VCH Verl. GmbHCo, KGaA, Weinheim (2008).
- [114] N. Mahmood, Y. Yao, J. W. Zhang, L. Pan, X. Zhang, J. J. Zou, Electrocatalysts for Hydrogen Evolution in Alkaline Electrolytes: Mechanisms, Challenges, and Prospective Solutions, *Adv. Sci.* 5 (2018) 1700464.
- [115] M. M. Jakšić, Hypo–hyper-d-electronic interactive nature of synergism in catalysis and electrocatalysis for hydrogen reactions, *Electrochim. Acta.* 45 (2000) 4085–4099.
- [116] A. Kawashima, E. Akiyama, H. Habazaki, K. Hashimoto, Characterization of sputter-deposited Ni-Mo and Ni-W alloy electrocatalysts for hydrogen evolution in alkaline solution, *Mater. Sci. Eng. A.* 226–228 (1997) 905–909.
- [117] M. P. Marceta Kaninski, D. P. Saponjic, V. M. Nikolic, D. L. Zugic, G. S. Tasic, Energy consumption and stability of the Ni–Mo electrodes for the alkaline hydrogen production at industrial conditions, *Int. J. Hydrog. Energy.* 36 (2011) 8864–8868.

- [118] M. Sheng, W. Weng, Y. Wang, Q. Wu, S. Hou, Co-W/CeO₂ composite coatings for highly active electrocatalysis of hydrogen evolution reaction, *J. Alloys Compd.* 743 (2018) 682–690.
- [119] C. Fan, D. L. Piron, Abderrahman Sleb, P. Paradis Study of Electrodeposited Nickel-Molybdenum, Nickel-Tungsten, Cobalt-Molybdenum, and Cobalt-Tungsten as Hydrogen Electrodes in Alkaline Water Electrolysis, *J. Electrochem. Soc.* 141 (1994) 382.
- [120] C. González-Buch, I. Herraiz-Cardona, E. M. Ortega, J. García-Antón, V. Pérez-Herranz, Development of Ni-Mo, Ni-W and Ni-Co Macroporous Materials for Hydrogen Evolution Reaction, *Chem. Eng. Trans.* 32 (2013) 865-870.
- [121] M. R. Gennero de Chialvo, A. C. Chialvo, Hydrogen evolution reaction on smooth Ni(1-x)+Mo(x) alloys (0≤x≤0.25), *J. Electroanal. Chem.* 448 (1998) 87–93.
- [122] O. Aaboubi, Hydrogen evolution activity of Ni–Mo coating electrodeposited under magnetic field control, *Int. J. Hydrog. Energy.* 36 (2011) 4702–4709.
- [123] I. Arul Raj, V. Venkatesan, Characterization of nickel-molybdenum and nickel-molybdenum-iron alloy coatings as cathodes for alkaline water electrolyzers, *Int. J. Hydrog. Energy.* 13 (1988) 215–223.
- [124] L. Huang, F. Yang, S. Xu, S. Zhou, Studies of Structure and Electrocatalytic Hydrogen Evolution on Electrodeposited Nanocrystalline Ni-Mo Alloy Electrodes, *Trans. IMF.* 79 (2001) 136–139.
- [125] M. Manazoğlu, G. Hapçı, G. Orhan, Effect of electrolysis parameters of Ni–Mo alloy on the electrocatalytic activity for hydrogen evaluation and their stability in alkali medium, *J. Appl. Electrochem.* 46 (2016) 191–204.
- [126] S. Shetty, M. Mohamed Jaffer Sadiq, D. K. Bhat, A. C. Hegde, Electrodeposition and characterization of Ni-Mo alloy as an electrocatalyst for alkaline water electrolysis, *J. Electroanal. Chem.* 796 (2017) 57–65.
- [127] G. S. Tasic, S. P. Maslovara, D. L. Zugic, A. D. Maksic, M. P. Marceta Kaninski, Characterization of the Ni–Mo catalyst formed in situ during hydrogen generation from alkaline water electrolysis, *Int. J. Hydrog. Energy.* 36 (2011) 11588–11595.
- [128] Q. Han, S. Cui, N. Pu, J. Chen, K. Liu, X. Wei, A study on pulse plating amorphous Ni–Mo alloy coating used as HER cathode in alkaline medium, *Int. J. Hydrog. Energy.* 35 (2010) 5194–5201.
- [129] T. Mikolajczyk, B. Pierozynski, Influence of Electrodeposited Ni-Mo Alloy on Hydrogen Evolution Reaction at Nickel Foam Cathode, *Int. J. Electrochem. Sci.* 13 (2018) 621–630.
- [130] J. Panek, A. Budniok, Ni + Mo composite coatings for hydrogen evolution reaction, *Surf. Interface Anal.* 40 (2008) 237–241.
- [131] S. Shetty, M. M. J. Sadiq, D. K. Bhat, A. C. Hegde, Electrodeposition of Ni–Mo–rGO composite electrodes for efficient hydrogen production in an alkaline medium, *New J. Chem.* 42 (2018) 4661–4669.
- [132] V. V. Kuznetsov, A. A. Kalinkina, T. V. Pshenichkina, V. V. Balabaev, Electrocatalytic properties of cobalt-molybdenum alloy deposits in the hydrogen evolution reaction, *Russ. J. Electrochem.* 44 (2008) 1350–1358.
- [133] P. N. S. Casciano, R. L. Benevides, R. A. C. Santana, A. N. Correia, P. de Lima-Neto, Factorial design in the electrodeposition of Co-Mo coatings and their evaluations for hydrogen evolution reaction, *J. Alloys Compd.* 723 (2017) 164–171.

- [134] Q. F. Zhou, L. Y. Lu, L. N. Yu, X. G. Xu, Y. Jiang, Multifunctional Co–Mo films fabricated by electrochemical deposition, *Electrochim. Acta.* 106 (2013) 258–263.
- [135] V. S. Kublanovsky, Y. S. Yapontseva, Electrocatalytic Properties of Co-Mo Alloys Electrodeposited from a Citrate-Pyrophosphate Electrolyte, *Electrocatalysis.* 5 (2014) 372–378.
- [136] N. R. Elezović, V. D. Jović, N. V. Krstajić, Kinetics of the hydrogen evolution reaction on Fe–Mo film deposited on mild steel support in alkaline solution, *Electrochim. Acta.* 50 (2005) 5594–5601.
- [137] A. W. Jeremiassi, J. Bergsma, J. M. Kleijn, M. Saakes, C. J. N. Buisman, M. Cohen Stuart, H. V. M. Hamelers, Performance of metal alloys as hydrogen evolution reaction catalysts in a microbial electrolysis cell, *Int. J. Hydrog. Energy.* 36 (2011) 10482–10489.
- [138] W. Schwarzacher, Electrodeposition: A Technology for the Future, *Electrochem. Soc. Interface.* 4 (2006) 32–35.
- [139] N. Tsyntaru, Electrodeposition of cobalt–tungsten alloys and their application for surface engineering, *Russ. J. Electrochem.* 52 (2016) 1041–1047.
- [140] N. Tsyntaru, S. Belevsky, A. Dikumar, J.-P. Celis, Tribological behaviour of electrodeposited cobalt–tungsten coatings: dependence on current parameters, *Trans. IMF.* 86 (2008) 301–307.
- [141] N. I. Tsyntaru, S. S. Belevskii, G. F. Volodina, O. L. Bersirova, Yu.S. Yapontseva, V. S. Kublanovskii, A. I. Dikumar, Composition, structure, and corrosion properties of coatings of Co-W alloys electrodeposited under direct current, *Surf. Eng. Appl. Electrochem.* 43 (2007) 312–317.
- [142] M. Donten, H. Cesiulis, Z. Stojek, Electrodeposition and properties of Ni-W, Fe-W and Fe-Ni-W amorphous alloys. A comparative study, *Electrochim. Acta.* 45 (2000) 3389–3396.
- [143] J. Niedbała, Production of Ni-Mo+Mo composite coatings with increased content of embeded Mo, *Arch. Mater. Sci.* 27 (2006) 121–127.
- [144] S. Sun, E. J. Podlaha, Electrodeposition of Mo-Rich, MoNi Alloys from an Aqueous Electrolyte, *J. Electrochem. Soc.* 159 (2012) D97–D102.
- [145] J. M. Jakšić, M. V. Vojnović, N. V. Krstajić, Kinetic analysis of hydrogen evolution at Ni–Mo alloy electrodes, *Electrochim. Acta.* 45 (2000) 4151–4158.
- [146] K. Mech, P. Zabinski, M. Mucha, R. Kowalik, Electrodeposition of Catalytically Active Ni-Mo Alloys / Elektroosadzanie Aktywnych Katalitycznie Stopów Ni-Mo, *Arch. Metall. Mater.* 58 (2013) 227–229.
- [147] S. Martinez, M. Metikoš-Huković, L. Valek, Electrocatalytic properties of electrodeposited Ni–15Mo cathodes for the HER in acid solutions: Synergistic electronic effect, *J. Mol. Catal. Chem.* 245 (2006) 114–121.
- [148] T. J. Morley, L. Penner, P. Schaffer, T. J. Ruth, F. Bénard, E. Asselin, The deposition of smooth metallic molybdenum from aqueous electrolytes containing molybdate ions, *Electrochem. Commun.* 15 (2012) 78–80.
- [149] Y. H. Li, Z. C. Guo, B. F. Huang, H. Huang, Feasibility Analysis of Electrodeposited Cu-W-Co Alloys, *Adv. Mater. Res.* 881–883 (2014) 702–707.
- [150] T. A. Aljohani, A. M. Almayouf, A. I. Almarshad, Enhancement of corrosion resistance of ternary Ni-W-P alloys using nanocoating, *Mater. Sci. Eng.* 3 (2009) 54–59.

- [151] Z. Chen, D. Cummins, B. N. Reinecke, E. Clark, M. K. Sunkara, T. F. Jaramillo, Core-shell MoO₃-MoS₂ Nanowires for Hydrogen Evolution: A Functional Design for Electrocatalytic Materials, *Nano Lett.* 11 (2011) 4168–4175.
- [152] J. Tian, Q. Liu, N. Cheng, A. M. Asiri, X. Sun, Self-Supported Cu₃P Nanowire Arrays as an Integrated High-Performance Three-Dimensional Cathode for Generating Hydrogen from Water, *Angew. Chem. Int. Ed.* 53 (2014) 9577–9581.
- [153] M. C. Esteves, P. T. A. Sumodjo, E. J. Podlaha, Electrodeposition of CoNiMo thin films using glycine as additive: anomalous and induced codeposition, *Electrochim. Acta.* 56 (2011) 9082–9087.
- [154] İ. H. Karahan, Effects of pH Value of the Electrolyte and Glycine Additive on Formation and Properties of Electrodeposited Zn-Fe Coatings, *Sci. World J.* 2013 (2013) 1–7.
- [155] P. Radhakrishnamurthy, Current efficiency of alloy plating and the electrochemical equivalent of an alloy, *Bulletin Of Electrochemistry.* 15 (1999) 252–256.
- [156] R. A. C. Santana, A. R. N. Campos, E. A. Medeiros, A. L. M. Oliveira, L. M. F. Silva, S. Prasad, Studies on electrodeposition and corrosion behaviour of a Ni-W-Co amorphous alloy, *J. Mater. Sci.* 42 (2007) 9137–9144.
- [157] L. Elias, P. Cao, A. C. Hegde, Magneto-electrodeposition of Ni-W alloy coatings for enhanced hydrogen evolution reaction, *RSC Adv.* 6 (2016) 111358–111365.
- [158] A. Nicolenco, N. Tintaru, H. Cesiulis, Electrodeposition of Fe-W alloys from environmentally-friendly bath and their characterization, *J. Electrochem. Soc.* 164 (2017) D590–D596.
- [159] E. J. Podlaha, D. Landolt, I. An Experimental Investigation of Ni-Mo Alloys, *J. Electrochem Soc.* 143 (1996) 885–892.
- [160] L. M. Rodríguez-Valdez, I. Estrada-Guel, F. Almeraya-Calderón, M. A. Neri-Flores, A. Martínez-Villafañe, R. Martínez-Sánchez, Electrochemical performance of hydrogen evolution reaction of Ni-Mo electrodes obtained by mechanical alloying, *Int. J. Hydrog. Energy.* 29 (2004) 1141–1145.
- [161] M. Donten, H. Cesiulis, Z. Stojek, Electrodeposition of amorphous/nanocrystalline and polycrystalline Ni-Mo alloys from pyrophosphate baths, *Electrochim. Acta.* 50 (2005) 1405–1412.
- [162] S. Costovici, A. C. Manea, T. Visan, L. Anicai, Investigation of Ni-Mo and Co-Mo alloys electrodeposition involving choline chloride based ionic liquids, *Electrochim. Acta.* 207 (2016) 97–111.
- [163] V. V. Kuznetsov, K. E. Golyanin, Yu. Sh. Ladygina, T. V. Pshenichkina, B. F. Lyakhov, K. V. Pokholok, Electrodeposition of iron-molybdenum alloy from ammonium-citrate solutions and properties of produced materials, *Russ. J. Electrochem.* 51 (2015) 748–757.
- [164] M. Stancheva, S. Manev, D. Lazarov, M. Mitov, Catalytic activity of nickel based amorphous alloys for oxidation of hydrogen and carbon monoxide, *Appl. Catal. Gen.* 135 (1996) L19–L24.
- [165] S. H. Hong, S. H. Ahn, J. Choi, J. Y. Kim, H. Y. Kim, H. J. Kim, J. H. Jang, H. Kim, S. K. Kim, High-activity electrodeposited NiW catalysts for hydrogen evolution in alkaline water electrolysis, *Appl. Surf. Sci.* 349 (2015) 629–635.

- [166] J. Zhang, T. Wang, P. Liu, Z. Liao, S. Liu, X. Zhuang, M. Chen, E. Zschech, X. Feng, Efficient hydrogen production on MoNi₄ electrocatalysts with fast water dissociation kinetics, *Nat. Commun.* 8 (2017) 15437.
- [167] J. Hou, Y. Wu, S. Cao, Y. Sun, L. Sun, Active Sites Intercalated Ultrathin Carbon Sheath on Nanowire Arrays as Integrated Core-Shell Architecture: Highly Efficient and Durable Electrocatalysts for Overall Water Splitting, *Small*. 13 (2017) 1702018.
- [168] E. Soghrati, C. Kok Poh, Y. Du, F. Gao, S. Kawi, A. Borgna, C–O Hydrogenolysis of Tetrahydrofurfuryl Alcohol to 1,5-Pentanediol Over Bi-functional Nickel-Tungsten Catalysts, *ChemCatChem*. 10 (2018) 4652–4664.
- [169] M. P. Marceta Kaninski, S. M. Miulovic, G. S. Tasic, A. D. Maksic, V. M. Nikolic, A study on the Co–W activated Ni electrodes for the hydrogen production from alkaline water electrolysis – Energy saving, *Int. J. Hydrog. Energy*. 36 (2011) 5227–5235.
- [170] D. Lupu, P. Mărginean, A.R. Biriş, Hydrogen in some synergetic electrocatalysts, *J. Alloys Compd.* 245 (1996) 146–152.
- [171] H. Matsui, A. Kunugi, The scheme of methanol oxidation at a platinum electrode in an acid solution, *J. Electroanal. Chem. Interfacial Electrochem.* 292 (1990) 103–113.
- [172] A. Hamnett, P. Stevens, G.I. Troughton, The effect of zirconium (IV) oxide on the electrocatalytic activity of carbon supported Pt/Ru porous electrodes for the electrochemical oxidation of methanol in acid electrolyte, *Catal. Today*. 7 (1990) 219–228.
- [173] E. D. D. Doring, A Collection of Illustrated Case Histories, in: *Corrosion Atlas*, 2nd ed., Elsevier, Amsterdam (1988) 300.
- [174] J. Ahmad, K. Asami, A. Takeuchi, D. V. Louzguine, A. Inoue, High Strength Ni-Fe-W and Ni-Fe-W-P Alloys Produced by Electrodeposition, *Materials Transactions*. 44 (2003) 1942–1947.
- [175] J. K. Yu, J. Zhao, M. Q. Yu, H. L. Luo, Q. Qiao, S. Zhai, Z. F. Xu, K. Matsugi, Properties of ternary NiFeW alloy coating by jet electrodeposition, *Bull. Mater. Sci.* 41 (2018) 1-7.
- [176] M. A. Farzaneh, K. Raeissi, M. A. Golozar, Effect of current density on deposition process and properties of nanocrystalline Ni–Co–W alloy coatings, *J. Alloys Compd.* 489 (2010) 488–492.
- [177] R. Della Noce, A. V. Benedetti, M. Magnani, E. C. Passamani, H. Kumar, D. R. Cornejo, C. A. Ospina, Structural, morphological and magnetic characterization of electrodeposited Co–Fe–W alloys, *J. Alloys Compd.* 611 (2014) 243–248.
- [178] N. Tsyntaru, S. Belevsky, H. Cesiulis, A. Dikusar, J. P. Celis, Feasibility Analysis of Electrodeposited Cu-W-Co Alloys, *Adv. Mater. Res.* 881–883 (2014) 702–707.
- [179] S. T. Kim, Y.S. Park, Effect of Copper Addition on Corrosion Behavior of High-Performance Austenitic Stainless Steel in Highly Concentrated Sulfuric Acid Solution—Part 1, *Corrosion*. 63 (2007) 114–126.
- [180] J. S. Lee, S. T. Kim, I. S. Lee, G. T. Kim, J. S. Kim, Y. S. Park, Effect of Copper Addition on the Active Corrosion Behavior of Hyper Duplex Stainless Steels in Sulfuric Acid, *Mater. Trans.* 53 (2012) 1048–1055.

- [181] B. W. Kwon, C. Ellefson, J. Breit, J. Kim, M. Grant Norton, S. Ha, Molybdenum dioxide-based anode for solid oxide fuel cell applications, *J. Power Sources*. 243 (2013) 203–210.
- [182] S. Keitel, Metals and alloys used in food contact materials and articles. European Directorate for the Quality of Medicines & HealthCare (EDQM), (2013).
- [183] B. Prakash, Low friction and wear resistance of plasma immersed ion implanted boron based layers under sliding conditions, PhD Thesis, (2004).
- [184] H. Zhou, Z. Liao, C. Fang, H. Li, B. Feng, S. Xu, G. Cao, Y. Kuang, Pulse electroplating of Ni-W-P coating and its anti-corrosion performance, *Trans. Nonferrous Met. Soc. China*. 28 (2018) 88–95.
- [185] B. Łosiewicz, M. Popczyk, M. Szklarska, P. Osak, Effect of Phosphorus on the Corrosion Resistance of Nickel Electrocoatings, *Solid State Phenom.* 228 (2015) 310–316.
- [186] E. Vernickaite, Z. Z. Antar, A. Nicolenco, R. Kreivaitis, N. Tsyntaru, H. Cesiulis, Tribological and Corrosion Properties of Iron-Based Alloys, in: *Proc. 8th Int. Sci. Conf. BALTTTRIB 2015*, Aleksandras Stulginskis University, Aleksandras Stulginskis University, Lithuania (2015).
- [187] J. Ahmad, K. Asami, A. Takeuchi, A. Inoue, Effect of Sodium Hypophosphite on the Structure and Properties of Electrodeposited Ni-W-P Alloys, *Mater. Trans.* 44 (2003) 705–708.
- [188] Zh. I. Bobanova, A.I. Dikumar, H. Cesiulis, J.-P. Celis, N.I. Tsyntaru, I. Prosycevas, Micromechanical and tribological properties of nanocrystalline coatings of iron-tungsten alloys electrodeposited from citrate-ammonia solutions, *Russ. J. Electrochem.* 45 (2009) 895–901.
- [189] Y. P. Ivanov, A. Chuvilin, S. Lopatin, J. Kosel, Modulated Magnetic Nanowires for Controlling Domain Wall Motion: Toward 3D Magnetic Memories, *ACS Nano*. 10 (2016) 5326–5332.
- [190] Y. Ma, W. Gao, H. Shan, W. Chen, W. Shang, P. Tao, C. Song, C. Addiego, T. Deng, X. Pan, J. Wu, Platinum-Based Nanowires as Active Catalysts toward Oxygen Reduction Reaction: In Situ Observation of Surface-Diffusion-Assisted, Solid-State Oriented Attachment, *Adv. Mater.* 29 (2017) 1703460.
- [191] P. Jiang, Q. Liu, Y. Liang, J. Tian, A.M. Asiri, X. Sun, A Cost-Effective 3D Hydrogen Evolution Cathode with High Catalytic Activity: FeP Nanowire Array as the Active Phase, *Angew. Chem. Int. Ed.* 53 (2014) 12855–12859.
- [192] X. Yan, K. Li, L. Lyu, F. Song, J. He, D. Niu, L. Liu, X. Hu, X. Chen, From Water Oxidation to Reduction: Transformation from $\text{Ni}_x\text{Co}_{3-x}\text{O}_4$ Nanowires to NiCo/NiCoO_x Heterostructures, *ACS Appl. Mater. Interfaces*. 8 (2016) 3208–3214.
- [193] A. Gupta, B.C. Kim, E. Edwards, C. Brantley, P. Ruffin, Functionalization of ZnO Nanowires for Potential *p*-Nitrophenol Sensing Applications, *Adv. Mater. Res.* 567 (2012) 228–231.
- [194] N. Liu, Y. Yao, J. J. Cha, M. T. McDowell, Y. Han, Y. Cui, Functionalization of silicon nanowire surfaces with metal-organic frameworks, *Nano Res.* 5 (2012) 109–116.
- [195] M. W. Shao, H. Wang, Y. Fu, J. Hua, D. D. D. Ma, Surface functionalization of HF-treated silicon nanowires, *J. Chem. Sci.* 121 (2009) 323–327.

- [196] C. Chattaway, D. Magnin, E. Ferain, S. Demoustier-Champagne, K. Glinel, Spatioselective functionalization of gold nanopillar arrays, *Nanoscale Adv.* (2019).
- [197] X. Wang, C. S. Ozkan, Multisegment Nanowire Sensors for the Detection of DNA Molecules, *Nano Lett.* 8 (2008) 398–404.
- [198] T. S. Ramulu, R. Venu, B. Sinha, S. S. Yoon, C. G. Kim, Electrodeposition of CoPtP/Au Multisegment Nanowires: Synthesis and DNA Functionalization., *Int. J. Electrochem Sci.* 7 (2012) 8.
- [199] J. H. Lee, J. H. Wu, H. L. Liu, J. U. Cho, M. K. Cho, B. H. An, J. H. Min, S. J. Noh, Y. K. Kim, Iron–Gold Barcode Nanowires, *Angew. Chem. Int. Ed.* 46 (2007) 3663–3667.
- [200] C. M. Hangarter, N. V. Myung, Magnetic Alignment of Nanowires, *Chem. Mater.* 17 (2005) 1320–1324.
- [201] L. Qin, L. He, J. Zhao, B. Zhao, Y. Yin, Y. Yang, Synthesis of Ni/Au multilayer nanowire arrays for ultrasensitive non-enzymatic sensing of glucose, *Sens. Actuators B Chem.* 240 (2017) 779–784.
- [202] H. Cesiulis, E. J. Podlaha-Murphy, Electrolyte Considerations of Electrodeposited Ni-W Alloys for Microdevice Fabrication, *Materials Science (Medžiagotyra)* 9 (2003) 324 – 327.
- [203] W. Ehrfeld, V. Hessel, H. Löwe, C. Schulz, L. Webe, Materials of LIGA technology, *Microsyst. Technol.* 5 (1999) 105 – 112.
- [204] L. Arias, J. Pessan, A. Vieira, T. Lima, A. Delbem, D. Monteiro, Iron Oxide Nanoparticles for Biomedical Applications: A Perspective on Synthesis, Drugs, Antimicrobial Activity, and Toxicity, *Antibiotics.* 7 (2018) 46.

ACKNOWLEDGEMENTS

I would like to thank the people and institutions that so generously contributed to the work presented in this thesis.

First of all, I would like to express my deep gratitude to my supervisor prof. Henrikas Cesiulis and scientific consultant associate prof. dr. Natalia Tsyntaru who have guided, assisted and encouraged me throughout my doctoral studies. Both extremely knowledgeable, organised and inspiring together they form an ideal supervision team, and have ignited in me a keen to thrive for excellence and nothing less.

The appreciation goes to the members of the Department of Physical Chemistry at Vilnius University and to the administration personnel for their kindness and help. I acknowledge the colleagues Modestas Vainoris and Ramūnas Levinas for their energy, promoting a good climate of work. Thanks for letting me be myself! A very special gratitude goes to dr. Aliona Nicolenco for being with me in ups and downs of professional and personal adventures. I find myself extremely lucky to have a friend like her in my life.

I wish to acknowledge the help provided by the co-authors of the joint articles: prof. Elizabeth Podlaha-Murphy, prof. habil. dr. Arūnas Ramanavičius, dr. Urtė Samukaitė-Bubnienė, dr. Oksana Bersirova. Furthermore, I thank the colleagues in Belarusian State University (head of the group prof. Genady Ragoisha) (Belarus), Research Center CIDETEC (head of the group dr. E. Garcia-Lecina) (Spain) and JSC TOPAZ (Moldova) for their hospitality and beneficial advices during the secondments.

I am grateful to the members of my committee for their patience and support in overcoming numerous obstacles in the presented research.

Finally, I would like to thank my family, especially my mother, who has provided me through moral and emotional support in my life. I am also grateful to my friends Vita, Evelina and Laura who have been there for me since the beginning of this scientific journey, supported me along the way and provided a lot of happy distractions to rest my mind outside of the research. My special thanks to dr. Vaida Linkuvienė for her sisterly affection during the doctoral studies. This accomplishment would not have been possible without her encouragement.

CURRICULUM VITAE

AFFILIATION

Department of Physical Chemistry,
Faculty of Chemistry and Geosciences,
Vilnius University
Naugarduko str. 24, Vilnius, Lithuania
Tel. +370 (5) 2193183, e-mail: info@chgf.vu.lt

ACADEMIC EDUCATION

- PhD student in Chemistry, Vilnius University, Lithuania** 2014 - present
Supervisors: prof. dr. H. Cesiulis, assoc. prof. dr. N. Tsyntsaru
Thesis: Electrochemical properties of iron group metals alloys with high W/Mo content
- M.Sc. in Chemistry, Vilnius University, Lithuania** 2012 - 2014
Supervisor: prof. dr. H. Cesiulis
Thesis: Structural and corrosion characterisations of electrodeposited Co-W alloy coatings
- B.Sc. in Chemistry, Vilnius University, Lithuania** 2008 - 2012
Supervisor: prof. dr. H. Cesiulis
Thesis: Electrochemical codeposition in the systems containing cobalt-copper-tungsten

ACADEMIC AFFILIATIONS

- Vilnius University, Faculty of Chemistry, junior researcher 2018 - 2019
Vilnius University, Faculty of Chemistry, junior assistant 2017 - 2018
Vilnius University, Faculty of Chemistry, junior researcher 2013 - 2016

INTERNSHIPS

- Belarusian State University**, Minsk (Belarus) April – May 2019
November – December 2018
July – August 2018
- JSC “**Topaz**”, Chisinau (Moldova) September – October 2018
- “**CIDETEC**”, San Sebastian (Spain) June 2018

TRAINING SCHOOLS

- 3rd Training school **MP1407 e-MINDS** project, Siófok (Hungary) March 2018
- 2nd Training school **MP1407 e-MINDS** project, Schwäbisch Gmünd (Germany) April 2017
- 18th International school **Advanced Materials and Technologies**, Palanga (Lithuania) August 2016

PROJECTS

HORIZON 2020 program Research and Innovation Staff Exchanges (RISE) project “**SMARTELECTRODES**”
Project No. MIP-031/2014 „**Electrochemical nanomaterials for energy conversion and catalysis**“ (Lithuanian Research Council) 2018-present
2014-2016

INTERNATIONAL CONFERENCES

E. Vernickaitė, Z. Antar, A. Nicolenco, R. Kreivaitis, H. Cesiulis. Tribological and corrosion properties of iron-based alloys. *International Conference BALTRIB 2015*. Akademija, Kaunas district, Lithuania; November 27-26, 2015 (*oral*)

E. Vernickaitė, O. Bersirova, M. Lelis, H. Cesiulis. Preparation and characterization of molybdenum based alloy electro- catalysts for hydrogen evolution in alkaline media. *International Conference E-MRS Fall Meeting*. Warsaw, Poland; September 19-22, 2016. (*oral*)

E. Vernickaitė, N. Tsyntsaru, H. Cesiulis. Electrocatalytic properties of Co-W alloy deposits for methanol oxidation reaction in the acidic solution. *8th International Conference Materials Science and Condensed Matter Physics*. Chisinau, Moldova; September 12-16, 2016. (*oral*)

E. Vernickaitė, H. Cesiulis, N. Tsyntsaru. Evaluation of corrosion and tribological behavior of electrodeposited tungsten alloys. *International Conference BALTRIB 2017*. Akademija, Kaunas district, Lithuania; November 16-17, 2017. (*oral*).

E. Vernickaitė, Electrochemical hydrogen evolution on electrodeposited W-based alloy electrodes. *32nd International Conference on Surface Modification Technologies*. San Sebastian, Spain; June 27-29, 2018. (*oral*)

E. Vernickaitė, N. Tsyntsaru, H. Cesiulis. Electrodeposited high W-content Co-W, Ni-W and Fe-W cathodes for efficient hydrogen evolution in alkaline medium. *69th Annual ISE Meeting*. Bologna, Italy; September 2-7, 2018. (*oral*)

E. Vernickaitė, N. Tsyntsaru, H. Cesiulis. Electrodeposited iron-group metals alloys with W and Mo for alkaline hydrogen evolution reaction. *9th International Conference Materials Science and Condensed Matter Physics*. Chisinau, Moldova; September 24-28, 2018. (*oral*)

E. Vernickaitė, O. Bersirova, M. Lelis, H. Cesiulis. Electrocatalytic properties of electrodeposited molybdenum alloys for hydrogen evolution reaction. *International Conference Chemistry and Chemical Technology*. Vilnius, Lithuania; April 28-29, 2016. (*poster*)

E. Vernickaitė, N. Tsyntsaru, H. Cesiulis. Electrochemical co-deposition of tungsten with cobalt and copper: peculiarities of binary and ternary alloy coatings. *18th International Conference-School Advanced Materials and Technologies 2016*. Palanga, Lithuania; August 27-31, 2016. (*poster*)

Article I

**Electrodeposited tungsten-rich Ni-W, Co-W and Fe-W cathodes for
efficient hydrogen evolution in alkaline medium**

E. Vernickaite, N. Tsyntaru, K. Sobczak, H. Cesiulis

Electrochimica Acta 318 (2019) 597-606



Electrodeposited tungsten-rich Ni-W, Co-W and Fe-W cathodes for efficient hydrogen evolution in alkaline medium

E. Vernickaite^a, N. Tsyntaru^{a,*}, K. Sobczak^b, H. Cesiulis^{a,**}

^a Department of Physical Chemistry, Vilnius University, Naugarduko str. 24, LT, 03225, Vilnius, Lithuania

^b Faculty of Chemistry, Biological and Chemical Research Centre, University of Warsaw, Żwirki i Wigury 101 Str., PL-02-089, Warsaw, Poland



ARTICLE INFO

Article history:

Received 17 February 2019

Received in revised form

27 May 2019

Accepted 14 June 2019

Available online 17 June 2019

Keywords:

electrodeposition

Tungsten alloys

Iron group metal alloys

Electrocatalysis

Hydrogen evolution reaction

ABSTRACT

The search of active, stable and cost-effective non-noble electrocatalysts for hydrogen evolution reaction (HER) is essential for sustainable energy systems. In this study, the electrodeposited Ni-W, Co-W and Fe-W coatings having 5–30 at.% of W were examined as an alternative electrocatalysts for hydrogen evolution. The electrocatalytic efficiency of the electrodes was investigated on the basis of electrochemical data obtained from steady-state polarization technique in 30 wt% NaOH solution. It was found that with increasing of tungsten content in the deposits up to ~30 at.% a crystal-to-ultra-nanocrystalline transition takes place and the crystal grain size decreases up to 2–4 nm. The high content of W leads to coarse-grained coatings. These morphological and structural changes showed remarkable impact on the catalytic activity. The maximum catalytic performance was obtained for ultra-nanocrystalline W coatings. Among them the Ni-29at.%W demonstrated the highest apparent exchange current density (ECD) at the room temperature, i.e. 0.55 mA cm⁻², thus indicating more favorable hydrogen reduction. A significant improvement of catalytic activity of all tested cathodes with increasing the temperature of NaOH solution was noticed. Among investigated Co-33at.%W, Fe-30at.%W and Ni-29at.%W cathodes, the last one showed the best performance towards HER (ECD = 14.5 mA cm⁻² at 65 °C).

© 2019 Elsevier Ltd. All rights reserved.

1. Introduction

Hydrogen is a clean, environmentally friendly and renewable energy carrier [1]. Therefore hydrogen generation for energy systems is poised to be the best alternative to depleting fossil fuel reserves in the future [2]. From this point of view electrocatalytic water splitting attracts extensive attention compared to other hydrogen production approaches (e.g. steam reforming, coal gasification) due to its technological simplicity and ecological cleanliness [3], smaller costs [4] and reasonable efficiencies [5]. Consequently, the hydrogen evolution reaction (HER) in both acidic and alkaline media is one of the most explored fields of electrochemistry. However, application of acidic electrolysis for hydrogen production remains limited by the high cost of proton exchange membranes that are used in an electrolyzer system and low stability caused by corrosion issues [6]. On the other hand, compared

with acidic media, HER in alkaline solution generally requires higher overpotentials and is associated with lower efficiency and larger energy consumption. Thus, the effective state-of-the-art catalysts that work well in acidic media can considerable lose the catalytic performance in an alkaline media [7]. Therefore, the water electrolysis industry is mainly focused on improving the efficiency of HER in basic environment by the proper selection of electrode materials that allow enhancing the hydrogen reaction kinetics. The mainstream characteristics that the electrodes should possess: exceptional electrocatalytic activity; good electrical conductivity; low hydrogen overpotential at rather high current densities (1–2 A cm⁻²); long-term stability during electrolysis process and high corrosion resistance. In this context platinum and other precious metals are unconquerable catalysts, since they are characterized by superior surface stability and require very small overpotentials, e.g. –12 mV to reach the current density of 10 mA cm⁻² in 1 M KOH and –47 mV in 0.1 M KOH [8]. Unfortunately the deficiency and high price limit their large-scale application in water electrolysis. This opens the window for alternative, durable, cost-effective materials that would be suitable for replacement of noble metals. Among various alternatives, W(Mo)-

* Corresponding author.

** Corresponding author.

E-mail addresses: ashra_nt@yahoo.com (N. Tsyntaru), henrikas.cesiulis@chf.vu.lt (H. Cesiulis).

based alloys with iron group metals, namely Ni, Co and Fe, have attracted considerable research attention during the last decades because of their high electrocatalytic activity [9–11], superior mechanical [12,13], tribological [14–16], anti-corrosion properties [15] and thermal resistance [18,19]. W(Mo) alloy electrodes with iron group metals have been prepared by various methods, such as magnetron sputtering [10,20,21], hydrothermal treatment [22], arc melting [23], mechanical alloying [24–27] and electrodeposition [28–30]. Among them, electrodeposition is considered as rather simple and inexpensive technique which does not require a sophisticated equipment or large energy expenditure. Furthermore, W(Mo)-based alloys prepared by electrodeposition showed the highest electrocatalytic activity and stability in long-term operations [31].

It was reported that Co-W thin films show better performance for the HER than Ni-W deposits [32]. Meantime to the best of our knowledge, no works are available on the electrocatalytic performance of Fe-W alloy as a cathode for alkaline water electrolysis. This could be related to its stability issues under working conditions in terms of corrosion [33]. The ability of an electrode to catalyze the HER is usually measured by the exchange current density (ECD), which is the rate of hydrogen evolution per surface area at the electrode potential, where the reaction is at equilibrium. According to different authors the ECD for Ni-W and Co-W electrodes for the HER in alkaline solution varies in the range of 10^{-5} – 10^{-2} A cm⁻² [11] and fundamentally depends on corresponding alloy's chemical composition, morphology, structure and physicochemical properties. It was shown that the ECD rises with increasing W content in Ni-W [20] and Co-W [23] alloys and becomes maximal at 10 at.%. A general explanation of this tendency was based on the local density-functional theory of the transition metal alloys, indicating that the increase in electrochemical activity is attributed to the modification of the density of states of the host metal [23]. The main contribution to the density of states comes from d-electrons. The optimal catalytic activity for the HER on the Ni(Co)-W alloy 10 at.% W coincides with an increase in the density of states at Fermi level of the 3d Ni band. The increased electron density around Ni-sites influences proton discharge at the Ni(Co)-W surface and Ni sites can serve as a hydrogen source for the neighboring W sites in which the ion/atom recombination and molecular hydrogen desorption are promoted more efficiently [20,23]. Similarly in Ref. [34] the best HER activity in 30 wt% NaOH solution was observed for Ni-W alloy having about 14 at.% W (ECD = 0.3 mA cm⁻²), while the W-richest Ni-W alloy (31.7 at.%) was described as the weakest HER electrocatalyst under the same conditions (ECD = 0.02 · 10⁻² mA cm⁻²). These findings agree well with the conclusions in Ref. [10], suggesting that in order to obtain more active W-based electrodes with iron group metals it is necessary to prepare them with less than 19 at.% of W. Although, it is possible to find some controversial information defining the optimal composition of Ni-W or Co-W alloys for the alkaline HER. For instance, a significant improvement in the electrocatalytic efficiency was observed for ultra-nanocrystalline Ni-W electrodes containing >32 at.% of W most likely due to the absorption of a larger amount of hydrogen into their specific structures [35,36]. The positive effect on the catalytic activity for HER of amorphous Ni-W alloys' nature was also confirmed by Ref. [37]. Notable, in the case of Co-W alloys, the ECD for hydrogen evolution as a function of the W content denoted a minimum corresponding to a transition from polycrystalline to nanocrystalline structure, namely at around 25 at.% of W [38]. However, for similar tungsten content (~24–26 at.%) disagreeing results were obtained [39]. Namely, acknowledging the better catalytic performance towards HER in 20 wt% KOH of those coatings.

Thus, despite the large amount of research data collected in this

field, no univocal dependence of electrocatalytic activity on the chemical composition of the W-based alloy coatings can be determined. The discrepancies in ECDs on alloys with similar chemical composition reported from author to author can be found. This confirms the sensitivity of alloys' characteristics to the provided conditions of electrolysis that influence not only chemical but also phase composition, which in turn, influence the catalytic properties as a whole. Hence, for the first time a comprehensive analysis and comparison of the performance of Ni-W, Co-W and Fe-W alloys (W: from 5 to 30 at.%) which have been prepared from the same initial citrate-based electrolyte by applying the minor changes in electrodeposition conditions (in order to obtain similar W content) for the HER in 30 wt% NaOH solution in the temperature range from 25 to 65 °C is presented. The kinetics towards the HER of the as-deposited electrodes was studied by using steady-state polarization measurements.

2. Experimental

2.1. Electrodeposition

Co-W, Ni-W, Fe-W alloy coatings were electrodeposited under galvanostatic mode by using a standard three electrodes configuration. Ag/AgCl/KCl (sat) electrode has been used as a reference electrode (RE) and all potentials presented in this study are referred to this electrode. As a counter electrode (CE) was a platinized titanium mesh (~20 cm²). Notable, W-based alloys were deposited from non-volatile citrate-borate electrolytes, proposed in our previous works [40,41]. All solutions were prepared from chemicals of analytical grade purity dissolved in distilled water. The pH was adjusted by adding concentrated solutions of NaOH or H₂SO₄. The composition and pH of the applied plating baths used for alloys' electrodeposition are presented in Table 1. The deposits in all cases were obtained at the current density of 10 mA cm⁻² and temperature of 60 °C. Electrodeposition in all cases was carried out on stainless steel substrate foils (2 cm²), and on stainless steel rods (1 cm²), depending on the requirements for coatings' characterization. The stainless steel (with composition in wt.%, Fe-70, Cr-19, Ni-8, Mn-2, Si, Al, P-1) was chosen as a substrate in order to avoid the corrosion. The stainless steel substrate was chemically degreased and cleaned in an ultrasonic bath with acetone, ethanol and finally rinsed with distilled water. In order to improve the adhesion of the alloys to the substrates, a thin nickel seed layer (~30 nm) was electrodeposited from an electrolyte containing 1 M NiCl and 2.2 M HCl, at a cathodic current density of 10 mA cm⁻² for 1 min. The electrodeposition time for W-based alloys and iron group metals was controlled in a way until the desired coating thickness of around 10 μm was achieved. The given thickness allows to avoid any interference from the stainless steel substrate.

2.2. Structural and morphological characterization

Surface morphology of electrodeposits and chemical composition were examined by scanning electron microscope (SEM, Hitachi SU-70) combined with an INCA energy dispersive X-ray spectroscopy detector (EDS, Oxford Instruments) operated at 20 kV (1 μm penetration depth). After determining the composition of the as-deposited alloys by EDS, the current efficiency (CE) was calculated according to the Faradays' law using following formula:

$$CE (\%) = \frac{F \cdot m}{I \cdot t} \left[\frac{x_i \cdot n_i}{M_i} + \frac{x_W \cdot n_W}{M_W} \right] \cdot 100\%, \quad (1)$$

where F – Faradays constant (96485C); m – measured mass (g); I – current flowing through the plating solution (A); t –

Table 1
Composition of the plating baths used for electrodeposition of Ni-W, Co-W, Fe-W alloys; and Co, Ni and Fe coatings.

Coating	W, at.%	Concentration, mol l ⁻¹					pH
		(Co/Fe/Ni)SO ₄	C ₆ H ₈ O ₇	Na ₂ C ₆ H ₅ O ₇	H ₃ BO ₃	Na ₂ WO ₄	
Co/Ni/Fe	-	0.2	0.04	0.25	0.65	-	6.7
Co-W	5	0.2	0.04	0.25	0.65	0.2	5.0
	20						6.7
	30						8.0
	30						5.0
Ni-W/Fe-W	5	0.04	0.04	0.2	0.16	0.24	5.0
	20	0.02					
	30						6.7

electrodeposition duration (s); x_i , n_i , M_i – content (wt.%), electron number, molecular weight (g mol⁻¹) of i -th component of the alloy (Ni, Co or Fe); x_W , n_W , M_W – content, wt.%, electron number, molecular weight of tungsten (W).

The thickness of the electrodeposits in all cases was around 10–15 μm and was calculated from gravimetric and elemental analysis data using the following equation:

$$d = \frac{m}{A} \left[\frac{x_i \cdot m}{\rho_i} + \frac{x_W \cdot m}{\rho_W} \right], \quad (2)$$

where d – thickness (cm); A – surface area of the cathode (cm²); ρ_i – density of i -th component of the alloy (Ni, Co or Fe) (g cm⁻³); ρ_W – density of W (g cm⁻³).

The structural changes of the thin films were analyzed by X-ray diffraction method (XRD: Rigaku MiniFlex II). XRD patterns were produced with Cu K α radiation ($\lambda = 1.5406 \text{ \AA}$) in a 2 θ scanning mode from 20° to 100° with the step of 0.01°. Analysis of the spectra was carried out using PDXL software. The crystallite size of all obtained coatings was calculated based on the broadening of XRD peaks by using Sherrer's equation [42]. The roughness of the deposits was estimated by interpreting the atomic force microscopy (AFM, BioscopeII/Catalyst) results, as their average roughness (R_a). The R_a of the stainless steel substrate was 12 nm before electrodeposition of metals (Co, Ni, Fe) and alloys (Co-W, Ni-W, Fe-W).

Transmission electron microscopy (TEM) results were obtained using a Talos F200X (200 kV, field emission) HRTEM microscope equipped with four detector super-EDS systems (FEI).

2.3. Electrocatalytic evaluation

The electrocatalytic activity of the deposited electrodes towards the HER was evaluated by the following kinetic parameters: the apparent ECD (j_0), the Tafel slope (b_c), the overpotential at the current density of 300 mA cm⁻² (η_{300}) and the apparent activation energy (E_a). The voltammetric measurements for determining the kinetic parameters of the deposited samples were performed in 30% NaOH solution at 25–65 °C in a thermostated cell. A platinum foil has been used as an auxiliary electrode, and Ag/AgCl/KCl (sat) electrode was used as the reference electrode. The geometrical area of all investigated working electrodes was 1 cm² and the experimental results are referred to this geometric surface area. Potentiodynamic polarization hydrogen evolution curves were recorded at the sweep rate of 2 mV s⁻¹. Before starting the measurement, each sample was left in the solution to attain a steady state, which was indicated as open circuit potential (OCP). The cathode potential was scanned from OCP up to -1 V. Voltammetric curves were recorded using potentiostat/galvanostat AUTOLAB equipped with GPES software (version 4.9).

Extrapolation of the polarization curves obtained at different temperatures, in the coordinates $\lg j - \eta$ to the value $\eta = 0$ made it possible to determine the ECD. The overvoltage, η , was calculated

from the following equation:

$$\eta = E - E_r, \quad (3)$$

$$E_r = - \left(\frac{2.3RT}{F} \right) \text{pH} \quad (4)$$

where η is an overpotential of the HER (V), E is an experimental potential value at which the reaction takes place (V); E_r is the reversible potential value calculated from the Nernst equation (V), R is the universal gas constant (8.3144 J K⁻¹ mol⁻¹); T is the temperature (K); F is the Faraday constant (96 485 J mol⁻¹).

For the calculation of overpotentials at temperatures other than 25 °C, the tabulated data [43] of the temperature dependence of the potential of the saturated Ag/AgCl/KCl (sat) electrode vs. the hydrogen electrode, were used.

The oxide film layer formed in the 30 wt% NaOH solution was investigated using the electrochemical impedance spectroscopy (EIS). The thickness of the oxide layer was calculated from the capacitive behavior of the film by using the relation:

$$d = \frac{\epsilon_0 \epsilon_r S}{C} \quad (5)$$

where d is the thickness of the oxide layer (m), C is the capacitance of the oxide layer (F), S is the surface area (m²), ϵ_0 is the electric constant ($\epsilon_0 \approx 8.854 \times 10^{-12} \text{ F m}^{-1}$); ϵ_r is the dielectric constant of Co/Ni/Fe and W oxides.

Because the dielectric constants of iron group metals (Co, Ni, Fe) and W significantly differ, the total ϵ_r was calculated using the following equation:

$$\epsilon_r = x_{Me} \epsilon_{MeO} + x_W \epsilon_{WO_3} \quad (6)$$

where x_{Me} and x_W are atomic fractions of iron group metal (Ni, Co, Fe) and tungsten in the corresponding alloy, respectively. Taking $\epsilon_r = 11.9$; 12.9 and 14.2 for NiO, CoO and FeO, respectively, and $\epsilon_r = 300$ for WO₃.

3. Results and discussion

3.1. Characterization of Ni-W, Co-W and Fe-W alloy coatings

Morphology. The electrocatalytic activity of alloys depends on the surface roughness that enhances the specific surface area available for the HER [44]. Consequently, both alloy composition and surface morphology determined by electrolysis conditions have remarkable influence on the catalytic activity. Based on reports [45–47] certifying that the catalytic activity for hydrogen evolution is qualitatively proportional to the refractory metal (W/Mo) content in the alloys with iron group metals (Ni, Co, Fe) the main approach of this work was to increase the W content in Ni-W, Co-W and Fe-W coatings, namely from 5 to 30 at.%, and thereby to

investigate its influence on electrocatalytic performance towards HER. In order to vary the composition of alloys the pH of the corresponding plating bath was changed in the range of 5.0–8.0 (Table 1). The influence of pH on the chemistry of electrolytes and composition of W alloys with the iron group metals are comprehensively described in Refs. [40,48]. In order to compare the electrocatalytic properties of the obtained W-alloys, Ni, Co and Fe also were deposited under the same electrolysis conditions. In this case the pH of 6.7 chosen for electrodeposition, because it is an initial value which is settled after mixing the components of corresponding solutions. The representative SEM top-view images of the various compositions of Ni-W, Co-W and Fe-W alloys along with Ni, Co and Fe metals for comparison are shown in Table 2.

As it can be seen, the iron group metal coatings have the surface morphology clearly different from their binary alloys with W. In general, with increasing the W content a transition in the surface morphology from the deposits with angular/faceted structure (characteristic to Ni, Co and Fe) to nodular nature coatings (specific to W-rich alloys) was determined. Notable, the alloys are characterized by more homogenous and denser morphology. The surface roughness measurements (Table 3) further reveals that the addition of W can smooth the Ni-W and Fe-W alloy surfaces. In these cases the average surface roughness (R_a) decreases from ~600 to 700 nm (for iron group metals) to ~300 nm (at 30 at.% W). These observations are in a good agreement with the characteristics expected for ultra-nanocrystalline alloys with increased W content in the alloy's composition [49–51]. Unlike, the R_a of electrodeposited Co-W coatings shows the tendency to increase with the higher W percentage in the alloy's composition and attain its maximum for Co-

Table 3

The average roughness, current efficiency and grain size of the as-deposited coatings.

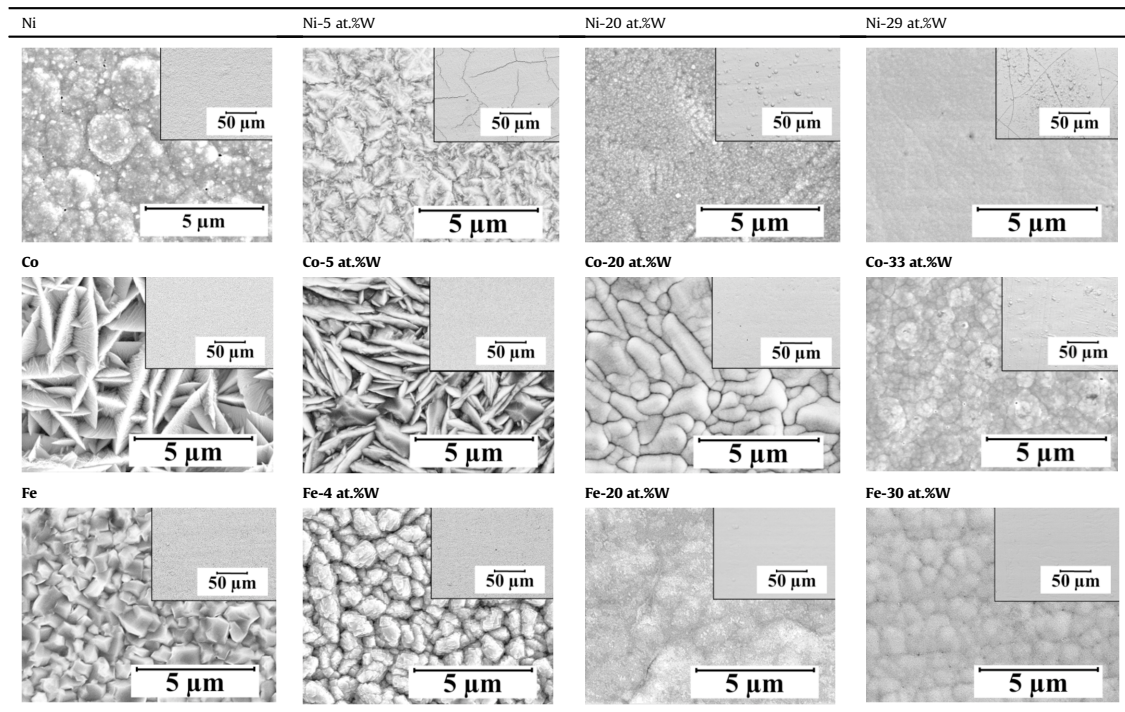
Sample	Roughness, nm	Current efficiency, %	Grain size, nm
Ni	686	47.6	22.7
Ni-5 at.% W	639	44.2	14.9
Ni-20 at.% W	397	31.1	10.0
Ni-30 at.% W	270	21.8	4.3
Co	322	91.3	33.7
Co-4 at.% W	171	89.6	27
Co-20 at.% W	416	83.0	23.7
Co-33 at.% W	487	35.5	1.5
Fe	556	66.5	41.8
Fe-5 at.% W	410	50.2	21.4
Fe-20 at.% W	256	46.9	1.5
Fe-31 at.% W	310	37.4	1.5

33at.%W ($R_a = 487$ nm). The “cauliflower” type structures that appear as aggregates of the smaller grains are clearly observed in the SEM picture of this surface.

It is well known that the electrodeposition of W-based alloys from aqueous electrolytes occurs with the significant hydrogen release, resulting in the distortion of coating's structure due to the hydrogen saturation, which provokes the cracking of the coatings [52]. The presence of the microcracks on the surface results in a decrease of fatigue life and localized corrosion problem that is one of the main limitations of using W alloy coatings for the target purposes [15,28]. Though there is some data declaring that the

Table 2

SEM micrographs of Ni, Co, Fe and Ni-W, Co-W, Fe-W electrodeposits made at higher (x6000) and lower (x500, inserts) magnifications.



formation of the microcracks leads to the higher electrocatalytic activity of electrode for HER. The reason behind that cracks, being filled with electrolyte, render a greater part of the internal surface of the electrode accessible to electrochemical gas evolution [53,54]. From the SEM images made at lower magnification the presence of the cracks on Ni-W surfaces at 5 and 29 at.% W can be noticed, whilst the electrodeposited Co-W and Fe-W coatings having similar composition are uniform and no cracks can be observed (Table 2). This could be attributed to the lower cathodic current efficiency of Ni-W alloys (Table 3), and consequently, more intensive hydrogen evolution during the deposition due to the higher initial Ni catalytic activity towards HER in comparison with the Co and Fe. The Ni-5 at.% W coating has the cracking pattern characterized by the highest density. Since the formation of spherical nodular structure becomes more favorable for Ni-29at.%W, the crack density decreases. Similar observations have been made in Ref. [28].

Structure. The catalytic activity of electrodes is also strongly influenced by their crystal structure, especially, nanocrystalline or amorphous states have been reported as the most attractive towards HER [35]. Furthermore, amorphous alloys are known to exhibit higher hardness, better tribological properties [55] and also a better corrosion behavior compared to those of crystalline ones [56]. The X-ray diffraction (XRD) spectra of the deposits are given in Fig. 1. It was established that the crystallinity of W alloys with iron group metals is associated to W content, i.e. Ni-W and Co-W coatings with a low tungsten percentage (≤ 22 at.%) have the crystalline structure and coatings with the higher tungsten content are ultra-nanocrystalline. Notable, the crystalline to ultra-nanocrystalline transition for Fe-W alloy is occurs at lower W content, namely 15–17 at.%, that value is slightly lower than it was reported by other authors [24,57]. The alloys having low-W content did not show any evidence of additional diffraction lines relating to elemental tungsten or W- compounds, only those for hcp Co, fcc Ni or bcc Fe lattice. Furthermore, a shift of Co, Ni and Fe peaks towards smaller diffraction angles is observed. This suggests that during tungsten co-deposition with iron group metals bigger W atoms are incorporated into crystalline lattice of Ni, Co or Fe and corresponding solid solutions are formed. These observations agree with the previous works in which W-based alloys were prepared from gluconate or saccharin containing bath [30,58,59]. Meanwhile at the high tungsten content (~ 30 at.% for Ni-W and Co-W; ≥ 20 at.% for Fe-W) the single broad peaks revealing the ultra-nanocrystalline (the crystallite size is less than 4 nm) structure can be observed. In the literature it is widely described that such peak broadening is attributed to the reduction of the crystallite size of an alloy with an increase in the amount of tungsten [40,51]. Indeed, the crystallite sizes decreases from 27 nm to ~ 1.5 nm for Co-W alloy; from 15 to ~ 4 nm for Ni-W alloy; from 41 nm to ~ 1.5 nm for Fe-W alloy with increasing the W percentage from 0% (iron group metals) to 30 at.% (Table 3). However, in the case of the broad peak in XRD pattern it is difficult to strictly determine to which phase it is attributed. Nevertheless, based on the equilibrium phase diagrams [60–62] and previous investigations, it can be assumed that

the W solid solutions in Ni, Co or Fe together with their corresponding thermodynamically stable intermetallic phases of Co_3W [40,63], Fe_2W [57], Ni_4W [17,64]. It was shown that different intermetallic phases have an impact on their activity for the HER [65,66].

The values of crystallite sizes is confirmed by diffraction patterns obtained by TEM (see Fig. 2). It shows that alloys consist of few nanometers sized crystallites, and the crystallinity of Co-W alloy is more evident in comparison with Ni-W alloy.

The metal distribution was also examined. Here we present the characteristic results obtained for NiW alloy. As it seeming from comparison of the TEM images of Ni-W alloy spot presenting mapping of elements (see Fig. 3), both Ni and W are present onto entire sample (see Fig. 3 c and d). However, as it is shown in Fig. 3 b, there are some regularly located (several nanometers in diameter) spots with significantly higher amount of W are present. It was also proved that the spots with higher concentration of W are crystalline (see inset in Fig. 3a). The TEM results suggest that material obtained in electrodeposition process consists of two phases: tungsten solution in nickel (amorphous phase with lower tungsten content) and intermetallic, crystalline phase of intermetallic compounds containing higher percentage of tungsten, e.g. NiW. Detailed identification of the stoichiometry of the crystalline phase require more advanced TEM and XRD measurements and will be a subject of further examination.

3.2. Electrocatalytic hydrogen evolution on Ni-W, Co-W and Fe-W coatings

The steady-state equilibrium method is one of the simplest techniques for investigating the electrocatalytic activity in the alkaline water electrolysis [67]. Hence, in order to investigate the catalytic activity of the prepared Ni-W, Co-W and Fe-W electrocatalysts having different W content, linear sweep voltammetry measurements were performed in 30 wt% NaOH solution at 25 ± 2 °C. The polarization curves of the investigated samples are presented in Fig. 4(a–c). The corresponding electrochemical parameters (Tafel slope (b), apparent exchange current density (j_0), and overpotential at $j = -200 \text{ mA cm}^{-2}$ (η_{200})) obtained from the linear part of semi-logarithmic polarization plots (Fig. 4(d and e)) are summarized in Table 4. The comparative studies were performed on the electrodeposited Ni, Co and Fe coatings and metallurgical Pt under the same experimental conditions. It was found that Tafel slopes vary in the range from -185 to -142 mV dec^{-1} for Ni-W, from -189 to -146 mV dec^{-1} for Co-W and from -233 to -176 mV dec^{-1} for Fe-W alloy coatings with increasing the W percentage from 0 to ~ 30 at.%. These values are in a good agreement with previous works based on W(Mo) and iron group metal

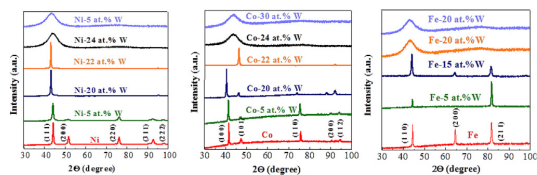


Fig. 1. XRD patterns of as-deposited Ni, Co, Fe and Ni-W, Co-W, Fe-W coatings. Composition of alloys is given in at.%.

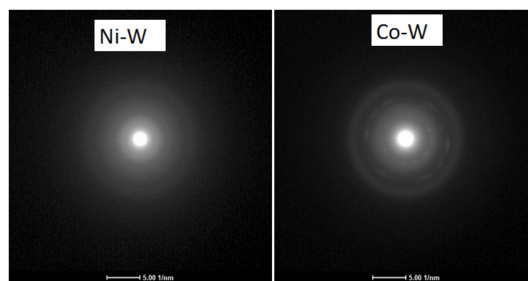


Fig. 2. Diffraction patterns obtained by high resolution TEM of Ni-29at.%W and Co-33at.%W alloys.

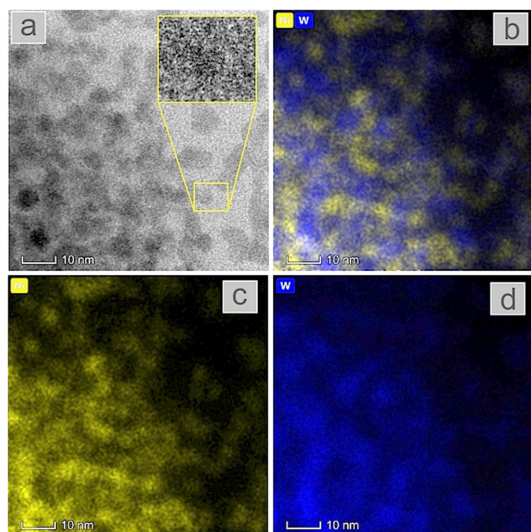


Fig. 3. High resolution TEM images of the Ni-W sample: (a) bright field TEM image of examined spot; (b) EDX map of Ni and W distribution; (c) EDX map of Ni distribution; (d) EDX map of W distribution.

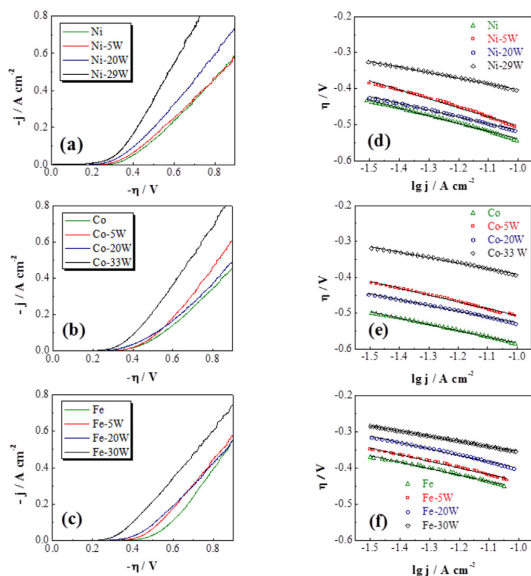


Fig. 4. Cathodic polarization curves of hydrogen evolution in 30 wt% NaOH at 25 ± 2 °C for electrodeposited coatings with different chemical compositions (a–c) and the plots in semi-logarithmic coordinates (d–f). The scan rate is 2 mV s^{-1} . The composition of alloys are given in at.%.

catalysts for the HER [23,31,68,69]. It is widely accepted that the HER kinetics in alkaline medium involves the electron-coupled water dissociation (the Volmer step for the formation of adsorbed hydrogen) and the combination of adsorbed hydrogen into molecular hydrogen via either the interaction of the H atom and water

Table 4

Electrochemical parameters at 25 ± 2 °C for as-deposited coatings and metallurgical Pt.

Electrode	$b_j/\text{mV dec}^{-1}$	$j_0/\text{mA cm}^{-2}$	η_{200}/mV
Ni	185	$1.5 \cdot 10^{-2}$	-586
Ni-5 at.%W	175	$2.4 \cdot 10^{-2}$	-584
Ni-20 at.%W	160	$7.3 \cdot 10^{-2}$	-503
Ni-29 at.%W	142	$5.5 \cdot 10^{-1}$	-419
Co	189	$3.5 \cdot 10^{-3}$	-664
Co-5 at.%W	184	$1.6 \cdot 10^{-2}$	-621
Co-20 at.%W	176	$3.8 \cdot 10^{-2}$	-611
Co-33 at.%W	146	$2.3 \cdot 10^{-1}$	-490
Fe	233	$1.0 \cdot 10^{-3}$	-673
Fe-5 at.%W	204	$1.9 \cdot 10^{-3}$	-637
Fe-20 at.%W	182	$9.1 \cdot 10^{-3}$	-517
Fe-30 at.%W	176	$1.6 \cdot 10^{-2}$	-488
Pt	122	$2.6 \cdot 10^1$	-363

molecule (Heyrovsky step), or the combination of two H atoms (Tafel step) [70]. Each step can determine the overall rate of the reaction. According to this general model, the Tafel slope of 118 mV dec^{-1} at 20 °C indicates that the process is controlled by the Volmer reaction step. While if the Tafel slope is ~ 40 or $\sim 30 \text{ mV dec}^{-1}$, the rate-determining step would be Heyrovsky or Tafel reactions, respectively [47]. Table 4 shows the Tafel slopes are close to 118 mV dec^{-1} , and thus indicating that the Volmer reaction step is the controlling step of the HER in the alkaline solution in this study. The Tafel slopes greater than the theoretically predicted is related to the presence of the barrier-type oxide film on the electrode surfaces that causes additional potential drop [31,47]. The smaller Tafel slopes indicate the minor change in electrode overpotential for the larger increase in HER current. According to this can be assumed that the W-rich (~ 30 at.%) electrodes are characterized by faster hydrogen gas production.

At the same time, the apparent ECD values on the active electrocatalyst are desired to be as large as possible, because the higher ECD reflects the faster kinetics toward the redox reaction, i.e. lower overvoltage must be applied to create a significant current flow [71]. It was found that the apparent ECDs on binary W alloys are considerably higher than in the case of Ni, Co and Fe electrodeposits (see Table 4). Especially higher values of the hydrogen evolution rate were observed with increasing W content in the coatings. As it was shown in previous section, W-rich (~ 30 at.%) alloys are characterized by a refined grained (ultra-nanocrystalline) structure that probably offer the greater activity due to the better dispersion of the catalyst active sites and higher affinity for hydrogen absorption [35,72]. Indeed, both increased surface area and intrinsic reactivity can have significant effect on the enhanced catalytic behavior of a target material. Thus, in order to evaluate the intrinsic activity of the electrode in the HER, it is very important to estimate its real electrochemically active area. However, in our case the higher roughness of the electrode surface that has been observed by SEM imaging and surface topography measurements for the alloys rich in iron group metals (Ni, Co, Fe) did not show the enhancement of the electrochemically active surface area. Contrary, the most active W-rich electrodes characterized by relatively low surface roughness ($\sim 300 \text{ nm}$ for Ni-30at.%W and Fe-31at.%W), compact and homogenous morphology, without any pronounced pores or cavities demonstrated the highest catalytic activity. This phenomenon is comprehensively described in Ref. [73] where it is concluded that the geometric effects of the alloys can be used only for a ‘fine-tuning’ of the catalytic behavior. Hence, the main factor influencing outstandingly high electrocatalytic activity of the W(Mo) alloys

with iron group metals towards HER could be explained by the synergistic electronic effects [74]. Generally, it was explained that the metals of the left half of the transition series in the periodic table with empty or less-filled d-orbitals (e.g. W/Mo) are alloyed with metals of the right half of the series with more filled d-bands (e.g. Ni, Co, Fe) and the maximum in bond strength and stability of the intermetallic alloy phases is expected [75,76]. Although the corresponding intermetallic compounds are formed in all W-based alloys at the highest co-deposited W content, the influence of the iron group metal nature on the apparent hydrogen ECDs can be noticed. Ni-29at.%W coatings have shown to be the best overall catalyst. Notable, in Ref. [35] the higher catalytic activity of the ultra-nanocrystalline Ni-W alloy was proposed to occur due to the presence of cracks or/and discontinuities on the surface that lead to the higher affinity for hydrogen absorption. Meanwhile in our case even the crack-free Ni-20at.%W electrodeposition showed the higher apparent ECD compared to Co-20at.%W and Fe-20at.%. This suggests that the surface area of the cathode is not the main factor which controls the catalytic behavior. Thus, the origin of the enhanced electrocatalytic activity of Ni-29at.%W could be attributed to the structure peculiarities, more specifically the presence of the intermetallic Ni₄W phase which in previous works was characterized by the fast water dissociation kinetics that allows improving of the HER performance [77]. Indeed, the computational and experimental results revealed the fact that the kinetic energy barrier of the initial Volmer step is substantially reduced on the such type intermetallic phase catalysts [77]. What is more, it was demonstrated that Ni₄W phase is more stable under liquid phase reactions [78,79]. Finally, based on the bipolar electrodes method calculations [80] was concluded that Ni-based electrodes produce the higher number of active sites for the HER than those containing Co and Fe. These assumptions correspond well to previous works reporting the higher catalytic activity for refractory metal alloys with Ni than those containing Co in their composition [81,82]. Notable, the apparent ECD values of Fe-W alloys are of magnitude lower than those determined for Ni-W and Co-W deposits with the analogous compositions (Table 5). This can be related to the higher iron-based compounds affinity to the oxygen and formation of the natural oxide film on the surface which leads to the reduced conductivity [83]. Whilst oxygen affinity for Ni and Co is less than for Fe [84]. Thus, the least compact oxide film is expected to form on Ni-W alloys [85]. To sum up, the apparent ECDs of ultra-nanocrystalline W coatings are higher than that of crystalline ones and the most active electrodes follow the sequence: Ni-29 at.%W > Co-33 at.%W > Fe-30 at.%W.

It is known that the ECD characterizes the electrocatalytic activity of the electrode at equilibrium conditions. However, a certain current density is required for the HER to proceed at a measurable rate. Therefore, in order to compare the electrocatalytic activity of electrodes, it has been suggested to compare rather the overvoltage at the fixed current density [86]. In the light of these facts, in this study the overpotentials at -200 mA cm⁻² (η_{200}) were investigated in order to compare the apparent activity of the electrodeposited

tungsten-based alloys. The results showed that the overpotential reduction at the above mentioned current density for all coatings follows the sequence of chemical composition: iron group metals > 5 at.%W > 20 at.%W > ~30 at.%W, thereby confirming the previous conclusions that the ultra-nanocrystalline electrodes are characterized by the highest electrocatalytic activity for the HER in 30 wt% NaOH at 25 ± 2 °C.

Effect of electrolyte temperature. It is known that the temperature of alkaline bath plays an important role on the increase of the catalytic activity of W(Mo)-based cathodes towards the HER [11,87]. Hence, the electrodeposited Ni-29at.%W, Co-33at.%W and Fe-30at.%W alloy electrodes that demonstrate the higher apparent catalytic activity were tested at the temperature range from 25 to 65 °C by applying 10 °C increments. The characteristic polarization curves obtained for the HER in 30 wt% NaOH on the different electrodes at 25, 45 and 65 °C are displayed in Fig. 5 (a, c, e). Kinetic parameters determined from the linear part of the Tafel curves (Fig. 5 (b, d, f)), i.e. apparent exchange current density, Tafel slopes, and η_{200} are presented in Table 5. The higher temperature exhibits the significant effect on the HER, leading to the distinct reduction of Tafel slopes which is opposite the prediction of classical theory. Apparently, the catalytic activity depends not only on the synergistic effect and/or increased surface area, but also on the surface characteristics. It was determined that an increase in the bath's temperature induces the formation of a thicker oxide layer, i.e. from 0.02 to 0.7 Å for Ni-29at.%W, from 0.1 to 0.46 Å for Co-33at.%W, from 2.6 to 7.1 Å for Fe-30at.%W. As revealed by XPS analysis [17], the electrodeposited iron group metals alloys of high W-content are covered with a surface layer of the tungsten-based oxides. It is known that tungsten oxide, WO₃, has been long accepted as a promising non-precious-metal electrocatalyst for hydrogen

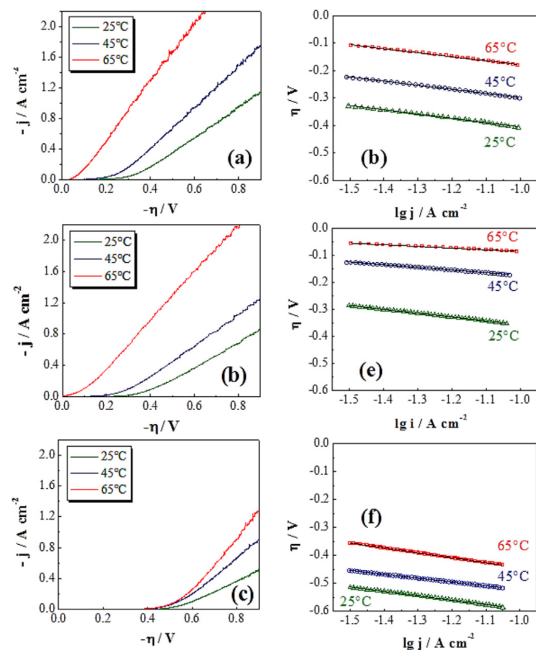


Fig. 5. Influence of the temperature on cathodic polarization curves and plots in semi-logarithmic coordinates for Ni-29at.%W (a–b), Co-33at.%W (c–d), Fe-30at.%W (e–f) electrodeposits. The scan rate is 2 mV s⁻¹.

Table 5

Experimental values of the apparent ECD (j_0 , mA cm⁻²) and Tafel slopes (b_c , mV dec⁻¹) for as-deposited alloy electrodes at different temperatures (composition is given in at.%).

Electrode	25 °C		35 °C		45 °C		55 °C		65 °C	
	j_0	b_c	j_0	b_c	j_0	b_c	j_0	b_c	j_0	b_c
Ni-29 W	0.55	142	1.5	134	2.9	118	5.9	97	14.5	78
Co-33 W	0.29	146	0.91	139	1.2	134	2.7	101	6.0	93
Fe-30 W	0.016	176	0.019	160	0.041	149	0.12	143	0.29	139

production [90]. Thus, can be assumed that during the HER at the higher temperature of the solution the thicker oxide layer characterized by catalytic activity results in the lower Tafel slopes. Also the oxide layer can influence the process of hydrogen adsorption. On this basis the real contribution of oxides for catalytic activity is yet another area of enquiry for future investigation. In addition, there is a significant increase in the apparent ECD for all investigated ultra-nanocrystalline electrodes towards HER with increasing temperature. The highest apparent ECD of 14.5 mA cm^{-2} and the lowest Tafel slope of 78 mV dec^{-1} presented in Table 5 were determined for Ni-29at.%W sample at 65°C , indicating that this catalyst is the most active for the HER among the Co-33at.%W and Fe-30at.%W under similar conditions. This was confirmed by the lower overpotential value at -200 mA cm^{-2} determined for Ni-29at.%W electrode ($\eta_{200} = -120 \text{ mV}$) than that determined for Co-33at.%W and Fe-30at.%W ($\eta_{200} = -146$ and -429 mV , respectively). For comparison, the apparent ECD obtained for metallurgical Pt was 9.1 mA cm^{-2} with the Tafel slope value of 119 mV dec^{-1} and η_{200} of 106 mV at 65°C .

In order to better compare the electrocatalytic activity of the most active ultra-nanocrystalline W alloy electrodes, the apparent activation energy (E_a) for the HER in accordance with the Arrhenius relation (Fig. 6) was also estimated. The calculations revealed the following activation energies: 23.5 kJ mol^{-1} for Ni-29at.%W, 26.0 kJ mol^{-1} for Co-33at.%W and 29.8 kJ mol^{-1} for Fe-30at.%W. It is known that the lower the E_a value is, the lower the energy requirements for hydrogen production are. Hence, the above mentioned results suggest the best catalytic performance of electrodeposited Ni-29at.%W catalyst which is highly comparable to that for Pt under the similar experimental conditions ($E_a = 19.2 \text{ kJ mol}^{-1}$).

Notable, the apparent ECDs for W alloys towards HER at 65°C found in this study in some cases seem to be much higher than that in other works, implying higher catalytic activity of the electrodeposited coatings (Table 6). This could be related to the different experimental conditions, i.e. higher concentration of the alkaline solution, elevated bath temperature, surface condition, etc. Nevertheless, the obtained results are of a significant importance, because the enhanced catalytic performance described above

Table 6

Comparison of the ECDs derived from the literature for W-based alloy electrodes.

Sample	W content, at.%	Media	j_0 , mA cm^{-2}	Reference
Co-W	18.9	1.0 KOH, 65°C	$1.1 \cdot 10^{-2}$	[11]
Co-W	10	1.0 M NaOH, 25°C	$7.65 \cdot 10^{-2}$	[23]
Co-W	27.3	1 M NaOH	$1.13 \cdot 10^{-2}$	[89]
Co-W	22.6	30 wt% KOH, 25°C	$1.2 \cdot 10^{-3}$	[32]
Ni-W	18.1		$6.5 \cdot 10^{-3}$	
Ni-W	10	1.0 M NaOH, 30°C	$5.0 \cdot 10^{-2}$	[20]
Ni-W	Not specified	30 wt% KOH, 80°C	2.83	[75]
Ni-W	40	33 wt% KOH, 25°C	143.5	[35]
Ni-W	29	30 wt. NaOH, 65°C	14.5	This work
Co-W	33		6.0	
Fe-W	30		$2.9 \cdot 10^{-1}$	

supplements the previous findings showing the outstanding mechanical [14,40], anti-corrosion [28,88] of W-rich alloys and allows proposing them as suitable materials not only for effective cathodes for HER, but also for the design of the electrodes with multifunctional capability.

4. Conclusions

The electrocatalytic performance of electrodeposited Ni-W, Co-W and Fe-W alloys (0–30 at.% W) as the effective cathodes for the HER was investigated using linear voltammetry technique in 30 wt % NaOH at the temperatures ranging from 25 to 65°C . It was found that alloying of Ni, Co, Fe with W results in the increased electrocatalytic activity towards HER when compared to single iron group metals. Furthermore, it was demonstrated that the higher content of W results in an enhanced HER catalytic activity and electrodes with ~30 at.% of W demonstrated the lowest η_{200} values and the highest apparent ECDs at 25°C . This could be related to the formation of the stable ultra-nanocrystalline intermetallic compounds and the occurrence of a so-called synergistic effect. At the elevated temperature of NaOH solution a significant improvement of catalytic activity leading to the distinct reduction of the overpotential and the enhancement of the apparent ECD of the ultra-nanocrystalline cathodes was noticed. The apparent ECD values at 65°C reduced in the following order: Ni-29at.%W > Co-33at.%W > Fe-30at.%W. Moreover, the Ni-29at.%W electrode was characterized by the lower activation energy (23.5 kJ mol^{-1}) than the Co-33at.%W (26.0 kJ mol^{-1}) and Fe-30at.%W (29.8 kJ mol^{-1}) coatings. Such catalytic activity of Ni-29at.%W that is comparable to that of metallurgical Pt probably could be link to the higher number of active sites for the HER and stability of intermetallic Ni_4W phase.

Acknowledgements

This research has received funding from Horizon 2020 research and innovation program under MSCA-RISE-2017 (No. 778357) and from the Research Council of Lithuania (LMTLT), agreement No 09.3.3-LMT-K-712-08-0003. The TEM images were obtained using the equipment purchased within CePT Project No.: POIG.02.02.00-14-024/08-00. Authors thanks Prof. Mikolaj Donten from Faculty of Chemistry, University of Warsaw (Poland) for valuable discussions.

References

- [1] A. Züttel, A. Borgschulte, L. Schlapbach, O. Friedrichs, Hydrogen as a future energy carrier, *Phil. Trans. R. Soc. A* 368 (2010) 3329.
- [2] A.G. Stern, A new sustainable hydrogen clean energy paradigm, *Int. J. Hydrogen Energy* 43 (2018) 4244.
- [3] S.E. Hosseini, M.A. Wahid, Hydrogen production from renewable and sustainable energy resources: promising green energy carrier for clean development, *Renew. Sustain. Energy Rev.* 57 (2016) 850.
- [4] I. Vincent, D. Bessarabov, Low cost hydrogen production by anion exchange

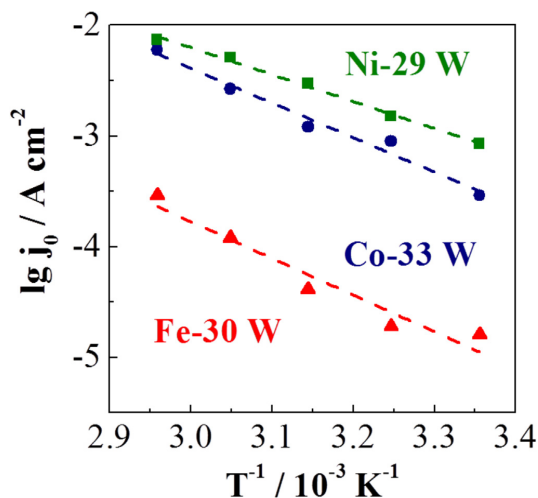


Fig. 6. Arrhenius plots for ultra-nanocrystalline Ni-29at.%W, Co-33at.%W and Fe-30at.%W alloys.

- membrane electrolysis: a review, *Renew. Sustain. Energy Rev.* 81 (2018) 1690.
- [5] V.M. Nikolic, G.S. Tasic, A.D. Maksic, D.P. Saponjic, S.M. Miulovic, M.P. Marceta Kaninski, Raising efficiency of hydrogen generation from alkaline water electrolysis – energy saving, *Int. J. Hydrogen Energy* 35 (2010) 12369.
- [6] Y. Naimi, A. Antar, Hydrogen Generation by water electrolysis, in: M. Eyvaz (Ed.), *Adv. Hydrot. Gener. Technol.*, InTech, 2018.
- [7] N. Mahmood, Y. Yao, J.W. Zhang, L. Pan, X. Zhang, J.J. Zou, Electrocatalysts for hydrogen evolution in alkaline electrolytes: mechanisms, challenges, and prospective solutions, *Adv. Sci.* 5 (2018) 1700464.
- [8] B. Lu, L. Guo, F. Wu, Y. Peng, J.E. Lu, T.J. Smart, N. Wang, Y.Z. Finfrock, D. Morris, P. Zhang, N. Li, P. Gao, Y. Ping, S. Chen, Ruthenium atomically dispersed in carbon outperforms platinum toward hydrogen evolution in alkaline media, *Nat. Commun.* 10 (2019) 631.
- [9] E. Vernickaite, O. Bersirova, H. Cesulius, N. Tsyntsaru, Design of highly active electrodes for hydrogen evolution reaction based on Mo-rich alloys electrodeposited from ammonium acetate bath, *Coatings* 9 (2019) 85.
- [10] A. Kawashima, E. Akiyama, H. Habazaki, K. Hashimoto, Characterization of sputter-deposited Ni-Mo and Ni-W alloy electrocatalysts for hydrogen evolution in alkaline solution, *Mater. Sci. Eng. A* 226–228 (1997) 905.
- [11] M.P. Marceta Kaninski, S.M. Miulovic, G.S. Tasic, A.D. Maksic, V.M. Nikolic, A study on the Co–W activated Ni electrodes for the hydrogen production from alkaline water electrolysis – energy saving, *Int. J. Hydrogen Energy* 36 (2011) 5227.
- [12] K.R. Sriraman, S.G. Sundara Raman, S.K. Seshadri, Synthesis and evaluation of hardness and sliding wear resistance of electrodeposited nanocrystalline Ni–Fe–W alloys, *Mater. Sci. Technol.* 22 (2006) 14.
- [13] A. Mulone, A. Nicolenco, J. Fornell, E. Pellicer, N. Tsyntsaru, H. Cesulius, J. Sort, U. Klement, Enhanced mechanical properties and microstructural modifications in electrodeposited Fe–W alloys through controlled heat treatments, *Surf. Coating Technol.* 350 (2018) 20.
- [14] F. Su, P. Huang, Microstructure and tribological property of nanocrystalline Co–W alloy coating produced by dual-pulse electrodeposition, *Mater. Chem. Phys.* 134 (2012) 350.
- [15] L. Xu, H. Guan, D. Li, L. Wang, Tribological properties of electroplated crack Ni–W alloy coatings, *Proc. Inst. Mech. Eng. Part J. J. Eng. Tribol.* 229 (2015) 1372.
- [16] A. Mulone, A. Nicolenco, N. Imaz, V. Martinez-Nogues, N. Tsyntsaru, H. Cesulius, U. Klement, Improvement in the wear resistance under dry friction of electrodeposited Fe–W coatings through heat treatments, *Coatings* 9 (2019) 66.
- [17] M. Obradovic, J. Stevanovic, A. Despic, R. Stevanovic, J. Stoch, Characterization and corrosion properties of electrodeposited Ni–W alloys, *J. Serb. Chem. Soc.* 66 (2001) 899.
- [18] N. Tsyntsaru, H. Cesulius, A. Budreika, X. Ye, R. Juskenas, J.-P. Celis, The effect of electrodeposition conditions and post-annealing on nanostructure of Co–W coatings, *Surf. Coating Technol.* 206 (2012) 4262.
- [19] N. Sunwang, P. Wangyao, Y. Boonyongmaneerat, The effects of heat treatments on hardness and wear resistance in Ni–W alloy coatings, *Surf. Coating Technol.* 206 (2011) 1096.
- [20] M. Metikos-Hukovic, Z. Grubač, N. Radić, A. Tonejc, Sputter deposited nanocrystalline Ni and Ni–W films as catalysts for hydrogen evolution, *J. Mol. Catal. A Chem.* 249 (2006) 172.
- [21] M. Lagarde, A. Billard, J. Creus, X. Feaugas, J.L. Grosseau-Poussard, S. Touzain, C. Savall, Electrochemical behavior of Ni–W alloys obtained by magnetron sputtering, *Surf. Coating Technol.* 352 (2018) 581.
- [22] J.M.V. Nsanzimana, Y. Peng, M. Miao, V. Reddu, W. Zhang, H. Wang, B.Y. Xia, X. Wang, An earth-abundant tungsten–nickel alloy electrocatalyst for superior hydrogen evolution, *ACS Appl. Nano Mater.* 1 (2018) 1228.
- [23] F. Rosalbino, D. Macciò, A. Saccone, G. Scavino, Study of Co–W crystalline alloys as hydrogen electrodes in alkaline water electrolysis, *Int. J. Hydrogen Energy* 39 (2014) 12448.
- [24] T. Nasu, M. Sakurai, T. Kamiyama, T. Usuki, O. Uemura, K. Tokumitsu, T. Yamasaki, Structural comparison of M–W (M = Fe, Ni) alloys produced by electrodeposition and mechanical alloying, *Mater. Sci. Eng. A* 375–377 (2004) 163.
- [25] T.D. Shen, K.Y. Wang, M.X. Quan, J.T. Wang, Amorphous phase transition mechanism by the mechanical alloying of the Fe–W system, *J. Appl. Phys.* 71 (1992) 1967.
- [26] A. Genç, M.L. Öveçoğlu, M. Baydoğan, S. Turan, Fabrication and characterization of Ni–W solid solution alloys via mechanical alloying and pressureless sintering, *Mater. Des.* 42 (2012) 495.
- [27] M.A. Dominguez-Crespo, M. Plata-Torres, A.M. Torres-Huerta, E.M. Arce-Estrada, J.M. Hallen-López, Kinetic study of hydrogen evolution reaction on Ni₃₀Mo₇₀, Co₃₀Mo₇₀, Co₃₀Ni₇₀ and Co₁₀Ni₂₀Mo₇₀ alloy electrodes, *Mater. Char.* 55 (2005) 83.
- [28] H. Alimadadi, M. Ahmadi, M. Aliofkhaizraei, S.R. Younesi, Corrosion properties of electrodeposited nanocrystalline and amorphous patterned Ni–W alloy, *Mater. Des.* 30 (2009) 1356.
- [29] A. Nicolenco, N. Tsyntsaru, H. Cesulius, Fe (III)-based ammonia-free bath for electrodeposition of Fe–W alloys, *J. Electrochem. Soc.* 164 (2017) D590.
- [30] D.P. Weston, S.J. Harris, P.H. Shipway, N.J. Weston, G.N. Yap, Establishing relationships between bath chemistry, electrodeposition and microstructure of Co–W alloy coatings produced from a gluconate bath, *Electrochim. Acta* 55 (2010) 5695.
- [31] G. Abuin, R. Coppola, L. Diaz, Ni–Mo alloy electrodeposited over Ni substrate for HER on water electrolysis, *Electrocatalysis* 10 (2019) 17.
- [32] C. Fan, D.L. Piron, A. Sleb, P. Paradis, Study of electrodeposited nickel-molybdenum, nickel-tungsten, cobalt-molybdenum, and cobalt-tungsten as hydrogen electrodes in alkaline water electrolysis, *J. Electrochem. Soc.* 141 (1994) 382.
- [33] N. Tsyntsaru, A. Dikusar, H. Cesulius, J.P. Celis, Z. Bobanova, S. Sidelnikova, S. Belevskii, Y. Yapontseva, O. Bersirova, V. Kublanovskii, Tribological and corrosive characteristics of electrochemical coatings based on cobalt and iron superalloys, *Powder Metall. Met. Ceram.* 48 (2009) 419.
- [34] M. Benaïcha, M. Allam, A. Dakhouche, M. Hamla, Electrodeposition and characterization of W-rich Ni/W alloys from citrate electrolyte, *Int. J. Electrochem. Sci.* 11 (2016) 7605.
- [35] S.H. Hong, S.H. Ahn, J. Choi, J.Y. Kim, H.Y. Kim, H.-J. Kim, J.H. Jang, H. Kim, S.-K. Kim, High-activity electrodeposited Ni/W catalysts for hydrogen evolution in alkaline water electrolysis, *Appl. Surf. Sci.* 349 (2015) 629.
- [36] V.S. Kublanovskiy, Y.S. Yapontseva, Electrochemical properties of Co–Mo alloys electrodeposited from a citrate-pyrophosphate electrolyte, *Electrocatalysis* 5 (2014) 372.
- [37] M. Wang, Z. Wang, Z. Guo, Z. Li, The enhanced electrocatalytic activity and stability of Ni/W films electrodeposited under super gravity field for hydrogen evolution reaction, *Int. J. Hydrogen Energy* 36 (2011) 3305.
- [38] H. Cesulius, N. Tsyntsaru, A. Budreika, N. Skridaila, Electrodeposition of CoMo and CoMoP alloys from the weakly acidic solutions, *Электронная обработка материалов* 9 5 (2010) 17.
- [39] S. Voskanyan, G. Pchelarov, R. Rashkov, K. Petrov, Co and W alloys as catalysts for evolution of H₂ at elevated temperatures, *Bulg. Chem. Commun.* 48 (2016) 78.
- [40] N. Tsyntsaru, H. Cesulius, E. Pellicer, J.P. Celis, J. Sort, Structural, magnetic, and mechanical properties of electrodeposited cobalt–tungsten alloys: intrinsic and extrinsic interdependencies, *Electrochim. Acta* 104 (2013) 94.
- [41] M. Donten, H. Cesulius, Z. Stojek, Electrodeposition and properties of Ni–W, Fe–W and Fe–Ni–W amorphous alloys. A comparative study, *Electrochim. Acta* 45 (2000) 3389.
- [42] B.D. Cullity, S.R. Stock, *Elements of X-Ray Diffraction*, third ed., Prentice Hall, Upper Saddle River, New Jersey, 2001.
- [43] H. Kahlert, Reference electrodes, in: F. Scholz (Ed.), *Electroanalytical Methods*, Springer, Berlin, Heidelberg, 2005, p. 261.
- [44] S.H. Ahn, I. Choi, H.Y. Park, S.J. Hwang, S.J. Yoo, E. Cho, H.J. Kim, D. Henskensmeier, S.W. Nam, S.K. Kim, J.H. Jang, Effect of morphology of electrodeposited Ni catalysts on the behavior of bubbles generated during the oxygen evolution reaction in alkaline water electrolysis, *Chem. Commun.* 49 (2013) 9323.
- [45] L. Elias, P. Cao, A.C. Hegde, Magnetelectrodeposition of Ni–W alloy coatings for enhanced hydrogen evolution reaction, *RSC Adv.* 6 (2016) 111358.
- [46] K. Mech, P. Zabinski, M. Mucha, R. Kowalik, Electrodeposition of catalytically active Ni–Mo Alloys, *Arch. Metall. Mater.* 58 (2013) 227.
- [47] J. Jakišić, M. Vojnović, N. Krstajić, Kinetic analysis of hydrogen evolution at Ni–Mo alloy electrodes, *Electrochim. Acta* 45 (2000) 4151.
- [48] N. Tsyntsaru, H. Cesulius, M. Donten, J. Sort, E. Pellicer, E.J. Podlaha-Murphy, Modern trends in tungsten alloys electrodeposition with iron group metals, *Surf. Eng. Appl. Electrochem.* 48 (2012) 491.
- [49] T. Yamasaki, P. Schlofmacher, K. Ehrlich, Y. Ogino, Formation of amorphous electrodeposited Ni–W alloys and their nanocrystallization, *Nanostruct. Mater.* 10 (1998) 375.
- [50] M. Donten, Z. Stojek, H. Cesulius, Formation of nanofibers in thin layers of amorphous W alloys with Ni, Co, and Fe obtained by electrodeposition, *J. Electrochem. Soc.* 150 (2003) C95.
- [51] K.H. Hou, Y.F. Chang, S.M. Chang, C.H. Chang, The heat treatment effect on the structure and mechanical properties of electrodeposited nano grain size Ni–W alloy coatings, *Thin Solid Films* 518 (2010) 7535.
- [52] S. Lee, M. Choi, S. Park, H. Jung, B. Yoo, Mechanical properties of electrodeposited Ni–W thin films with alternate W-rich and W-poor multilayers, *Electrochim. Acta* 153 (2015) 225.
- [53] Th. Borucinski, S. Rausch, H. Wendt, Raney nickel activated H₂-electrodes Part II: correlation of morphology and effective catalytic activity of Raney-nickel coated cathodes, *J. Appl. Electrochem.* 22 (1992) 1031.
- [54] L. Elias, A.C. Hegde, Electrodeposition and electrocatalytic study of Ni–W alloy coating, *Mater. Sci. Forum* 830–831 (2015) 651.
- [55] Y. Wu, Q. Luo, J. Jiao, X. Wei, J. Shen, Investigating the wear behavior of Fe-based amorphous coatings under nanoscratch tests, *Metals* 7 (2017) 118.
- [56] S. Yao, S. Zhao, H. Guo, M. Kowaka, A new amorphous alloy deposit with high corrosion resistance, *Corrosion* 52 (1996) 183.
- [57] A. Nicolenco, N. Tsyntsaru, J. Fornell, E. Pellicer, J. Reklaitis, D. Baltrunas, H. Cesulius, J. Sort, Mapping of magnetic and mechanical properties of Fe–W alloys electrodeposited from Fe(III)-based glycolate-citrate bath, *Mater. Des.* 139 (2018) 429.
- [58] F. Su, C. Liu, Q. Zuo, P. Huang, M. Miao, A comparative study of electrodeposition techniques on the microstructure and property of nanocrystalline cobalt deposit, *Mater. Chem. Phys.* 139 (2013) 663.
- [59] F. Su, C. Liu, P. Huang, Friction and wear of nanocrystalline Co and Co–W alloy coatings produced by pulse reverse electrodeposition, *Wear* 300 (2013) 114.
- [60] H. Okamoto, Ni–W (Nickel–Tungsten), *J. Phase Equilibria* 12 (1991) 706.
- [61] H. Okamoto, Co–W (Cobalt–Tungsten), *J. Phase Equilibria Diffusion* 29 (2008) 119.
- [62] B. Predel, Fe–W (Iron–Tungsten), in: O. Madelung (Eds.), *Dy-Er – Fr–Mo, Vol.*

- vol. 5, Springer, Berlin, Heidelberg, p. 1.
- [63] M. Dönten, Bulk and surface composition, amorphous structure, and thermocrystallization of electrodeposited alloys of tungsten with iron, nickel, and cobalt, *J. Solid State Electrochem.* 3 (1999) 87.
- [64] T.M. Sridhar, N. Eliaz, E. Gileadi, Electroplating of Ni₄W, *Electrochim. Solid State Lett.* 8 (2005) C58.
- [65] M.M. Jakić, Advances in electrocatalysis for hydrogen evolution in the light of the Brewer-Engel valence-bond theory, *J. Mol. Catal.* 38 (1986) 161.
- [66] M.M. Jakić, Electrocatalysis of hydrogen evolution in the light of the brewer–engel theory for bonding in metals and intermetallic phases, *Electrochim. Acta* 29 (1984) 1539.
- [67] L. Elias, K. Scott, A.C. Hegde, Electrolytic synthesis and characterization of electrocatalytic Ni-W alloy, *J. Mater. Eng. Perform.* 24 (2015) 4182.
- [68] V.V. Kuznetsov, A.A. Kalinkina, T.V. Pshenichkina, V.V. Balabaev, Electrocatalytic properties of cobalt-molybdenum alloy deposits in the hydrogen evolution reaction, *Russ. J. Electrochem.* 44 (2008) 1350.
- [69] G.S. Tasić, U. Lačnjevac, M.M. Tasić, M.M. Kaninski, V.M. Nikolić, D.L. Žugić, V.D. Jović, Influence of electrodeposition parameters of Ni–W on Ni cathode for alkaline water electrolyser, *Int. J. Hydrogen Energy* 38 (2013) 4291.
- [70] T. Shinagawa, A.T. Garcia-Esparza, K. Takanahe, Insight on Tafel slopes from a microkinetic analysis of aqueous electrocatalysis for energy conversion, *Sci. Rep.* 5 (2015) 13801.
- [71] Q. Ding, B. Song, P. Xu, S. Jin, Efficient electrocatalytic and photo-electrochemical hydrogen generation using MoS₂ and Related Compounds, *Chem* 1 (2016) 699.
- [72] M. Stancheva, S. Manev, D. Lazarov, M. Mitov, Catalytic activity of nickel based amorphous alloys for oxidation of hydrogen and carbon monoxide, *Appl. Catal. Gen.* 135 (1996) L19.
- [73] M. Armbrüster, R. Schlögl, Y. Grin, Intermetallic compounds in heterogeneous catalysis—a quickly developing field, *Sci. Technol. Adv. Mater.* 15 (2014), 034803.
- [74] S. Martínez, M. Metikoš-Huković, L. Valek, Electrocatalytic properties of electrodeposited Ni–15Mo cathodes for the HER in acid solutions: synergistic electronic effect, *J. Mol. Catal. A Chem.* 245 (2006) 114.
- [75] C. González-Buch, I. Herraiz-Cardona, E.M. Ortega, J. García-Antón, V. Pérez-Herranz, Development of Ni–Mo, Ni–W and Ni–Co macroporous materials for hydrogen evolution reaction, *Chem. Eng. Trans.* 32 (2013) 865.
- [76] G. Lu, P. Evans, G. Zangari, Electrocatalytic properties of Ni-based alloys toward hydrogen evolution reaction in acid media, *J. Electrochem. Soc.* 150 (2003) A551.
- [77] J. Zhang, T. Wang, P. Liu, Z. Liao, S. Liu, X. Zhuang, M. Chen, E. Zschech, X. Feng, Efficient hydrogen production on MoNi₃ electrocatalysts with fast water dissociation kinetics, *Nat. Commun.* 8 (2017) 15437.
- [78] J. Hou, Y. Wu, S. Cao, Y. Sun, L. Sun, Active sites intercalated ultrathin carbon sheath on nanowire arrays as integrated core-shell architecture: highly efficient and durable electrocatalysts for overall water splitting, *Small* 13 (2017) 1702018.
- [79] E. Soghrati, C. Kok Poh, Y. Du, F. Gao, S. Kawi, A. Borgna, C–O hydrogenolysis of tetrahydrofurfuryl alcohol to 1,5-pentanediol over bi-functional nickel-tungsten catalysts, *ChemCatChem* 10 (2018) 4652.
- [80] S.E. Fosdick, S.P. Berglund, C.B. Mullins, R.M. Crooks, Evaluating electrocatalysts for the hydrogen evolution reaction using bipolar electrode arrays: bi- and trimetallic combinations of Co, Fe, Ni, Mo, and W, *ACS Catal.* 4 (2014) 1332.
- [81] D. Goranova, E. Lefterova, R. Rashkov, Electrocatalytic activity of Ni–Mo–Cu and Ni–Co–Cu alloys for hydrogen evolution reaction in alkaline medium, *Int. J. Hydrogen Energy* 42 (2017) 28777.
- [82] A.W. Jeremiasse, J. Bergsma, J.M. Kleijn, M. Saakes, C.J.N. Buisman, M. Cohen Stuart, H.V.M. Hamelers, Performance of metal alloys as hydrogen evolution reaction catalysts in a microbial electrolysis cell, *Int. J. Hydrogen Energy* 36 (2011) 10482.
- [83] S.S. Brenner, Oxidation of iron-molybdenum and nickel-molybdenum alloys, *J. Electrochem. Soc.* 102 (1955) 7.
- [84] H. Yildirim, H. Morcali, A. Turan, Nickel pig iron (NPI) production from lateritic nickel ores, in: 13th International Ferro Alloys Congress, Almaty, Kazakhstan, 2013, p. 8, 9–13 June.
- [85] E. Navarro-Flores, Z. Chong, S. Omanovic, Characterization of Ni, NiMo, NiW and NiFe electroactive coatings as electrocatalysts for hydrogen evolution in an acidic medium, *J. Mol. Catal. A Chem.* 226 (2005) 179.
- [86] T. Boiadjieva-Scherzer, H. Kronberger, G. Faflek, M. Monev, Hydrogen evolution reaction on electrodeposited Zn–Cr alloy coatings, *J. Electroanal. Chem.* 783 (2016) 68.
- [87] P.N.S. Casciano, R.L. Benevides, R.A.C. Santana, A.N. Correia, P. de Lima-Neto, Factorial design in the electrodeposition of Co–Mo coatings and their evaluations for hydrogen evolution reaction, *J. Alloy. Comp.* 723 (2017) 164.
- [88] M.P.Q. Argañaraz, S.B. Ribotta, M.E. Folquer, L.M. Gassa, G. Benítez, M.E. Vela, R.C. Salvarezza, Ni–W coatings electrodeposited on carbon steel: chemical composition, mechanical properties and corrosion resistance, *Electrochim. Acta* 56 (2011) 5898.
- [89] M. Sheng, W. Weng, Y. Wang, Q. Wu, S. Hou, Co–W/CeO₂ composite coatings for highly active electrocatalysis of hydrogen evolution reaction, *J. Alloy. Comp.* 743 (2018) 682.
- [90] T. Zheng, W. Sang, Z. He, Q. Wei, B. Chen, H. Li, C. Cao, R. Huang, X. Yan, B. Pan, S. Zhou, J. Zeng, Conductive tungsten oxide nanosheets for highly efficient hydrogen evolution, *Nano Lett.* 17 (12) (2017) 7968, 13.

Article II



Design of Highly Active Electrodes for Hydrogen Evolution Reaction Based on Mo-Rich Alloys Electrodeposited from Ammonium Acetate Bath

E. Vernickaite, O. Bersirova, H.Cesiulis, N.Tsyntsaru

Coatings 2019, 9(2), 85

Article

Design of Highly Active Electrodes for Hydrogen Evolution Reaction Based on Mo-Rich Alloys Electrodeposited from Ammonium Acetate Bath

Edita Vernickaite¹, Oksana Bersirova², Henrikas Cesiulis¹  and Natalia Tsyntsaru^{1,3,*} 

¹ Department of Physical Chemistry, Vilnius University, Naugarduko str. 24, LT-03225 Vilnius, Lithuania; edita.vernickaite@chf.vu.lt (E.V.); henrikas.cesiulis@chf.vu.lt (H.C.)

² V.I. Vernadsky Institute of General and Inorganic Chemistry, 32-34 Acad. Palladina ave., 03680 Kiev, Ukraine; bersirova@nas.gov.ua

³ Institute of Applied Physics, Academiei str. 5, MD-2028 Chisinau, Moldova

* Correspondence: ashra_nt@yahoo.com; Tel.: +370-672-28632

Received: 15 January 2019; Accepted: 29 January 2019; Published: 30 January 2019



Abstract: The given research was driven by prospects to design Mo-rich coatings with iron group metals electrodeposited from a highly saturated ammonium acetate bath. The obtained coatings could be employed as prominent electrodes for the hydrogen evolution reaction (HER). It was found that the Mo content in Ni–Mo alloys can be tuned from 30 to 78 at.% by decreasing the molar ratio [Ni(II)]:[Mo(VI)] in the electrolyte from 1.0 to 0.25 and increasing the cathodic current density from 30 to 100 mA/cm². However, dense cracks and pits are formed due to hydrogen evolution at high current densities and that diminishes the catalytic activity of the coating for HER. Accordingly, smoother and crack-free Ni–54 at.% Mo, Co–52 at.% Mo and Fe–54 at.% Mo alloys have been prepared at 30 mA/cm². Their catalytic behavior for HER has been investigated in a 30 wt.% NaOH solution at temperatures ranging from 25 to 65 °C. A significant improvement of electrocatalytic activity with increasing bath temperature was noticed. The results showed that the sequence of electrocatalytic activity in alkaline media decreases in the following order: Co–52 at.% Mo > Ni–54 at.% Mo > Fe–54 at.% Mo. These peculiarities might be linked with different catalytic behavior of formed intermetallics (and active sites) in electrodeposited alloys. The designed electrodeposited Mo-rich alloys have a higher catalytic activity than Mo and Pt cast metals.

Keywords: Ni–Mo; Co–Mo; Fe–Mo alloys; electrodeposition; hydrogen evolution reaction; electrocatalysis

1. Introduction

Hydrogen is a clean fuel and an energy carrier that can be used for energy conversion and storage and is considered as a possible substitute for fossil fuels [1]. Electrocatalytic water splitting offers an ideal approach for highly pure hydrogen production. However, despite the multitude of on-going research, the development of an optimized, cost-effective and sustainable catalyst, which possesses a high catalytic activity for hydrogen evolution reaction (HER) is still rather appealing. Commonly, the ability of a given metal to catalyze the HER is estimated based on the exchange current density (ECD), i.e., the current density in the absence of net electrolysis at zero overpotential (at formal equilibrium potential for hydrogen evolution reaction in the particular solution). It is known, that the higher the ECD, the lower the overvoltage that must be applied to create a significant current flow. Hence, elaborated electrocatalysts should manifest exchange current densities equivalent or analogous to the ECD of polycrystalline platinum ($\sim 1 \times 10^{-3}$ A/cm² in alkaline electrolytes) [2].

A considerable part of research on the design of effective cathode materials for HER has been focused on Mo alloys with iron group metals (Ni, Co, Fe) due to their superior catalytic performance in alkaline media [3–5], stability at elevated temperatures [6] and reasonable corrosion and oxidation resistance [7–10]. These characteristics, combined with good electrical conductivity, easy usage and reasonable price, are attractive parameters for selecting the cathode material for water electrolysis. It was revealed that the activity of the Ni- x at.% Mo ($12 \leq x \leq 29$) alloy for HER is much higher than that of separate metallic nickel and molybdenum electrodes [11–15]. This phenomenon is attributed to the synergistic effect of Mo dispersed in the Ni matrix, which increases the real surface area of the electrode [12,16]. In addition, the enhancement of the catalytic activity for the HER of the Ni-15 at.% Mo alloy was ascribed to the modification of electron density in d-orbitals upon alloying nickel with molybdenum [17]. In other words, this model implies that some of the electrons of the iron group metal (Ni, Fe, Co) with more filled d-bands are shared with Mo having less-filled d-orbitals. This leads to maximal bond strength and stability of the intermetallic alloy phases [18,19].

Commonly, Mo alloys with iron group metals (Ni, Co, Fe) can be synthesized by applying mechanical alloying [3,20–22], powder metallurgy [11,23,24], spraying [25] and laser cladding techniques [26]. However, fabrication processes in aqueous media are often considered as simpler, cheaper and more environmentally friendly fabrication methods than those requiring sophisticated apparatus, volatile and corrosive chemicals and extra energy that must be incurred to keep the system in a liquid state. Thus, molybdenum can be successfully co-electrodeposited in the presence of iron group metal ions (Ni(II), Co(II), Fe(II)) and appropriate complexing agents from an aqueous electrolyte. It is assumed that the molybdate ions are reduced to molybdenum oxide or hydroxide, which in the presence of iron group metal (Ni, Fe or Co) species allows the formation of the corresponding binary alloy deposits. The effective Mo alloys electrodeposition with iron group metals were carried out from citrate [3,5,7,27], citrate–ammonia [10,12], citrate–gluconate [28], ammonia [29] and pyrophosphate [30,31] aqueous electrolytes.

Moreover, it was claimed that Ni–Mo electrodes show higher electrocatalytic activity than other Ni-based binary alloys such as Ni–Co, Ni–Fe, Ni–Zn and Ni–Cr [5,29]. For a given reason, the fabrication of Ni–Mo alloys possessing the highest activity for effective hydrogen production was the target for the vast research in the last decades. There are numerous reports certifying that the catalytic activity for hydrogen evolution is qualitatively proportional to the Mo content in Mo-based alloys [11,13,17]. Therefore, researchers' efforts were directed to optimize the plating bath vs. deposition conditions in order to obtain Mo-rich alloys as effective catalysts for the HER. It was shown that electrodeposition from ammonia based aqueous solutions produces Mo alloys with up to ~41 at.% of Mo [32–36]. Coatings containing more than 40 at.% Mo have been electrodeposited from ammonium-citrate solution in the presence of imidazolium-based ionic liquids as an additive [37]. Ammonia is frequently added to improve the cathode current efficiency, however, there is also some data about its effect on decreasing the Mo content in bimetallic Mo system with iron group metal (Ni, Co, Fe) [34]. Thus, despite the reduced current efficiency, typically ammonia-free electrolytes are used for the preparation of Mo-rich coatings, e.g., the Fe–Mo electrodes containing up to 59 at.% of Mo have been prepared from a pyrophosphate bath [38,39]. Binary Fe–Mo alloys with 49 at.% of Mo have been electrochemically formed from an aqueous trisodium nitrilotriacetate bath [40]. A considerable increase in Mo content, i.e., up to 70 at.%, can be caused by the addition of Mo powder to the electrolyte [41]. In addition, it has been noted that Mo content in alloys composition can be increased by carrying out the electrodeposition under the pulse current mode [42]. The highest Mo content, 74 at.%, achieved so far by induced electrodeposition in aqueous citrate electrolyte was reported for a Ni–Mo alloy [43].

Therefore, based on the mentioned above, the given research was focused on the electrodeposition of Ni-, Co- and Fe- Mo-rich alloys from a highly saturated ammonium acetate bath. The electrolyte's composition given in Reference [44] was adapted for the electrodeposition of binary Mo-containing alloys. In order to determine the influence of the nature of the iron group metal on the catalytic activity of target coatings (Ni-, Co- and Fe- Mo-rich alloys) the electrochemical conditions were tuned

in such way to ensure deposition of alloys with similar content of Mo. The catalytic activity of the electrochemically fabricated Mo-based alloy electrodes for the HER was explored in a 30 wt.% NaOH solution. In order to compare the electrochemical activity with other typical electrode materials, experiments were also performed using bare platinum electrode (same geometrical area) under the same conditions.

2. Materials and Methods

2.1. Mo-Rich Alloys Electrodeposition

Mo-rich alloys, namely Ni–Mo, Co–Mo and Fe–Mo, were prepared from highly saturated ammonium acetate electrolytes (Table 1) based on bath composition proposed in Reference [44] for Mo films deposition. All solutions were prepared from chemicals of analytical grade (A.R.) dissolved in demineralized water. The electrodeposition of coatings was carried out at 30 °C in order to lower the viscosity of the concentrated solutions and to avoid salt precipitation. Cu rod (surface area of 1 cm²), platinum sheet (3 × 7 cm²) and a saturated Ag/AgCl electrode were used as a working, counter and reference electrodes, respectively. Prior to the electrodeposition, Cu rods were washed and cleaned in an ultrasonic bath for 6–7 min and etched in an HNO₃:CH₃COOH:H₃PO₄ (1:1:1) solution at 60 °C. The thickness of the prepared Mo alloy coatings with iron group metals was calculated from gravimetric and elemental analysis data. Further, the electrocatalytic activity for the HER in 30 wt.% NaOH of fabricated cathodes has been investigated.

Table 1. Composition of electrolytes for Ni–Mo (Baths No. 1–3), Co–Mo (Bath No. 4) and Fe–Mo (Bath No. 5) coatings electrodeposition.

Bath	CH ₃ CO ₂ K	CH ₃ CO ₂ NH ₄	(NH ₄) ₂ MoO ₄	NiSO ₄ ·7H ₂ O	CoSO ₄ ·7H ₂ O	FeSO ₄ ·7H ₂ O	pH
1				0.001 M			
2				0.002 M	–	–	8.2
3	10.2 M	10.4 M	0.004 M	0.004 M			
4				–	0.002 M		
5					–	0.002 M	8.3

2.2. Morphological and Structural Study

The surface morphology and chemical composition of the prepared Mo-based deposits were examined with the scanning electron microscope (SEM, Hitachi TM3000, Tokyo, Japan) equipped with an INCA energy dispersive X-ray spectroscopy detector (EDS, Oxford Instruments, Buckinghamshire, UK) at an accelerating voltage of 20 kV, respectively. Based on the chemical composition of the obtained alloys, the current efficiency (CE) was calculated according to the Faradays' law:

$$CE (\%) = \frac{Fm}{It} \frac{x_i n_i}{M_i} + \frac{x_{Mo} \cdot n_{Mo}}{M_{Mo}} \times 100\% \quad (1)$$

where F is Faradays constant (96485 C); m is the weight of the electrodeposit (g); I is an applied current (A); t is the time of electrodeposition (s); x_i , n_i , M_i is the content (wt.%), electrons transferred per ion, and molecular weight (g/mol) of Ni, Co or Fe, respectively; x_{Mo} , n_{Mo} , M_{Mo} is the content, wt.%, electrons transferred per particular ion, respectively; molecular weight of Mo.

The structure of the electrodeposited alloys was investigated by X-ray diffraction (XRD) methods (Rigaku MiniFlex II, Tokyo, Japan). XRD patterns were produced with Cu K α radiation (1.5406 Å) in 2 θ scanning mode from 20 to 100° with a step of 0.01°.

2.3. Electrochemical Measurements

The voltammetric measurements for the evaluation of the kinetic parameters of Mo-rich alloys for the HER were performed in a 30 wt.% NaOH solution at several temperatures (25–65 °C, with the increment of 10 °C) in a thermostatic cell. A platinum wire was used as an auxiliary electrode and a saturated Ag/AgCl electrode was used as the reference electrode. All potentials are given with respect to the Ag/AgCl reference electrode. Potentiodynamic polarization hydrogen evolution curves were recorded at the sweep rate of 2 mV/s. The cathode potential was scanned from its open circuit potential (OCP) up to -1 V. Voltammetric curves were recorded using a potentiostat/galvanostat AUTOLAB equipped with GPES software (version 4.9). Extrapolation of the polarization curves obtained at different temperatures, in the coordinates $\lg i - \eta$ to value $\eta = 0$ give the possibility to determine the ECD (i_0). The overvoltage, η , was calculated from the following equation:

$$\eta = E - E_r \quad (2)$$

$$E_r = - \frac{2.3RT}{F} \text{pH} \quad (3)$$

where η is an overpotential of the HER (V), E is an experimental potential value at which the reaction takes place (V); E_r is the reversible potential value calculated from the Nernst equation (V), R is the universal gas constant (8.314472 J/K mol); T is the temperature (K); F is the Faraday constant (96,485 J/mol).

For the calculation of overpotentials at temperatures other than 25 °C, the tabulated data [45] of the temperature dependence of the potential of the saturated Ag/AgCl electrode vs. the hydrogen electrode, were used.

3. Results and Discussion

3.1. Design of Mo-Rich Alloys Coatings

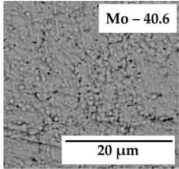
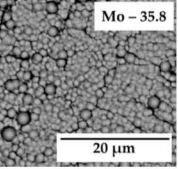
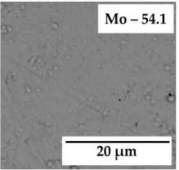
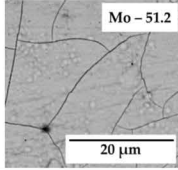
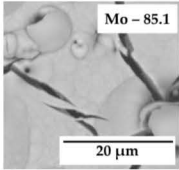
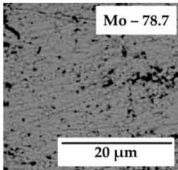
The high percentage of molybdenum in Mo-based alloy electrodeposits leads commonly to the growth of the ECD value but also has a positive influence on their corrosion resistance and microhardness [10]. On the other hand, the electrodeposition of coatings having a very high molybdenum content (>38 at.% of Mo) is more sensitive to side reactions, namely the evolution of hydrogen, which can lead to the appearance of a dense net of cracks, bumps and small pits that diminish practical application of such coatings for the HER. Thus, the first step of the given research was dedicated to the selection of the optimum electrochemical conditions (bath chemistry, applied current density) in order to obtain high-quality Mo-rich alloys with a reasonable deposition rate. The first investigated system was Ni–Mo (Table 1, Baths 1–3) since a high amount of publications have reported [15,46,47] that the Ni–Mo alloy is the most promising non-noble catalysts for the HER among other refractory metal-based electrodes.

Previously, it was shown that if the ratio [Ni(II)]:[Mo(VI)] is approaching 10, the amount of Mo in the Ni–Mo deposit decreases dramatically from 65 to 20 at.% [48]. Therefore, in order to obtain Mo-rich alloys, the ratio was kept at 0.25, 0.5, 1.0. Another parameter, which influences the refractory metal content in the alloys is the applied current density. Based on a preliminary study, two cathodic current densities, namely 30 and 100 mA/cm², have been chosen for electrodeposition of Mo-rich alloys.

Taking these parameters into account, the dependence of Mo content on the [Ni(II)]:[Mo(VI)] ratio and the cathodic current density was evaluated (Table 2). Namely, as it was anticipated, the amount of Mo in the alloys decreases from ~85 to 36 at.% as the Ni(II) increased in the bath. Here it should be mentioned, that only the content of the metallic phase was taken into account for the evaluation regardless of the ambiguous values of oxygen and other light elements detected by the EDS analysis. The highest content of molybdenum in the Ni–Mo deposits, around 85 at.%, was achieved at a [Ni(II)]/[Mo(VI)] ratio equal to 0.25 in the plating bath. This Mo amount is significantly higher

in comparison with previous works reported for Ni–Mo alloys obtained from aqueous electrolytes and is close to that found for Ni–Mo alloys prepared by metallurgical [11] or mechanical alloying techniques [49]. In order to reveal the interdependencies between bath chemistry and applied current densities, partial current densities (PSD) for Ni_{PCD}, Mo_{PCD} reduction and hydrogen evolution were also evaluated based on Faraday's law (Table 2).

Table 2. Dependence of composition, morphology and partial current densities of electrodeposited Ni–Mo alloys on the [Ni(II)]:[Mo(VI)] ratio and applied cathodic current density. Molybdenum at.% content is specified on the SEM images.

[Ni(II)]: [Mo(VI)] Ratio	Applied Cathodic j , 30 mA/cm ²		Applied Cathodic j , 100 mA/cm ²	
	SEM	Partial Cathodic j , mA/cm ²	SEM	Partial Cathodic j , mA/cm ²
1		$j_{Ni} = 0.6$ $j_{Mo} = 1.3$ $j_{H_2} = 28.1$		$j_{Ni} = 1.3$ $j_{Mo} = 2.2$ $j_{H_2} = 96.5$
0.5		$j_{Ni} = 0.3$ $j_{Mo} = 1.2$ $j_{H_2} = 28.5$		$j_{Ni} = 0.6$ $j_{Mo} = 2.1$ $j_{H_2} = 97.3$
0.25		$j_{Ni} = 0.02$ $j_{Mo} = 0.27$ $j_{H_2} = 29.71$		$j_{Ni} = 0.2$ $j_{Mo} = 2.3$ $j_{H_2} = 97.5$

Namely, the increase of the [Ni(II)]:[Mo(VI)] ratio increases the Ni_{PCD} and consequently Ni content in the deposit the higher applied current density (overpotential) accelerates the reduction of Ni(II) rather than Mo(VI) compounds. The side reaction is accelerated by a higher Mo content in the alloy that leads to the propagation of large micro-cracks, especially for Ni–Mo alloys deposited at a [Ni(II)]/[Mo(VI)] ratio ≤ 0.5 and having more than 50 at.% of Mo. Our results are in a good agreement with Reference [50], where it was shown that the cracks in the Ni–Mo alloys deposited from a citrate solution have been tracked at a Mo content higher than ~ 30 at.% but from an ammonium-citrate electrolyte [3] they appear even at lower Mo content (~ 21 at.%).

Hence, in order to obtain Mo-rich alloys without visible defects, the applied current density of 30 mA/cm² and a [Ni(II)]:[Mo(VI)] ratio of 0.5 should be viewed as the optimum conditions. This ratio allows for a four times increase in the Mo_{PCD} in comparison with the ratio of 0.25. It suggests that the electroactive complex should contain both molybdenum and nickel species. At the higher ratio (higher Ni(II) concentration), the Mo_{PCD} does not change significantly but the Mo content in the alloy decreases (from 54 to 40 at.%). Notably, at a current density of 100 mA/cm², the Mo_{PCD} is practically the same for all investigated [Ni(II)]:[Mo(VI)] ratios, suggesting that electroactive Mo-containing species under such conditions reaches saturation and has no significant effect on alloy electrodeposition. Furthermore, at a higher applied current density, an additional roughening due to the pronounced nodular structure of the coatings is obtained, that can be interconnected with abundant hydrogen evolution, which leads to cracks and holes on the surface (Table 2). On the one hand, in Reference [51], it was shown that the

cracked surfaces are characterized by higher HER activity and ascribed to an increased surface area of the active centers due to the microcracks but on the other hand, a certain amount of the hydrogen enters the open pores (cracks) of the deposit and it starts peeling off around the pores. Hence, it is obvious that the application of such coatings in the industrial processes is not recommendable [30]. Moreover, due to high PCDs for hydrogen reduction, the current efficiency in all investigated cases is rather low (<10%). This is a common characteristic for Ni–Mo co-deposition [52] that is associated with the formation of a mixed Mo oxides layer in the presence of an excess of Mo(VI) ions in the bath, which hinders the further reduction.

Accordingly, based on the experimental results obtained for Ni–Mo alloys, the following optimal conditions were adapted for electrodeposition of Co–Mo and Fe–Mo alloys: cathodic current density 30 mA/cm² and [Me(II)]/Mo(VI) = 0.5. This allowed for the electrodeposition of Mo-rich coatings (Co–52 at.% Mo and Fe–54 at.% Mo) coupled with suitable morphology (crack-free coatings with a less rough globular surface) and to evaluate the influence of iron group metal on the catalytic activity for HER in alkaline media. The obtained morphology of Mo-rich alloys was quite similar regardless of the iron group metal (Figure 1).

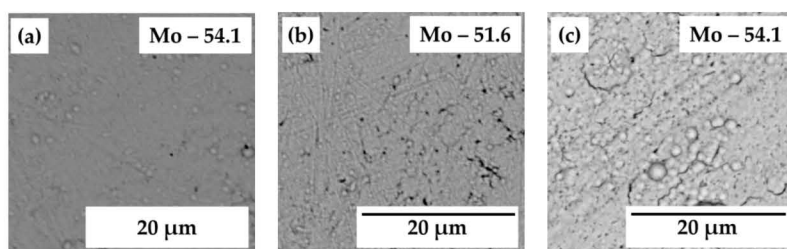


Figure 1. SEM images of electrodeposited at 30 mA/cm² and [Me(II)]/[MoO₄²⁻] = 0.5 coatings: Ni–Mo (a), Co–Mo (b) and Fe–Mo (c). The time of electrolysis was 1 h and the thickness of all deposits was ~10 μm.

The structure and crystallite size was evaluated by XRD analysis. A characteristic broad peak at $2\theta = 43^\circ\text{--}44^\circ$ was obtained for Ni–54 at.% Mo and is depicted in Figure 2a. According to the thermodynamic equilibrium data, the solubility limit of Mo in the fcc Ni structure at room temperature is ~17 at.%. When the Mo content exceeds this limit, an amorphous microstructure can be noticed and the formation of intermetallic Ni₄Mo, Ni₃Mo, NiMo compounds becomes possible for Ni–Mo alloys having >25 at.% of Mo [31,53]; a line with a solid solution of Ni in Mo. It is also known that the broadening of the XRD peak is related to the refinement of crystallite size that typically occurs with an increasing Mo content [31]. According to the literature, the mean crystallite size of Ni–Mo coatings can decrease from 50 to 2 nm by increasing the Mo content from 1 to 38 at.%, respectively [35,37,54]. This corresponds to a crystallite size of the investigated Ni–Mo coatings as small as ~2 nm. Notably, Ni–Mo deposits consisting of such small crystallites can have a lower overpotential for hydrogen evolution due to the larger concentration of crystal lattice defects and dislocations, which are considered as active centers for HER [12,19].

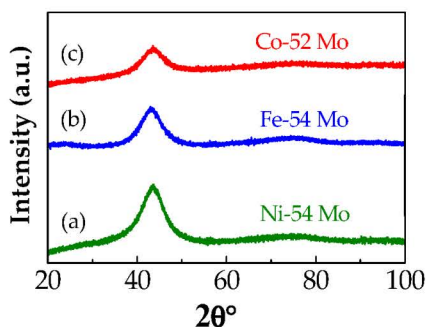


Figure 2. XRD pattern for: (a) Ni-54 Mo, (b) Fe-54 Mo and (c) Co-52 Mo electrodeposits (composition is given in at.%).

The XRD patterns for Fe-54 at.% Mo and Co-52 at.% Mo alloys showed the analogous crystalline structure to the Ni-54 at.% Mo coating (Figure 2b,c). Since the presence of one broad peak in the X-ray diffraction patterns makes it difficult to interpret the results, it can be only proposed that a mixture of Mo solid solution in the iron group metal and corresponding intermetallic compounds were formed. For the Fe-Mo (also Fe-W) system, the Mössbauer spectroscopy supports this presumption and suggests that deposits having more than 17 at.% of refractory metal consists of a mixture of molybdenum solid solution in α -Fe and intermetallic phases, e.g., Fe_3Mo , Fe_2Mo [55,56]. In the case of the Co-Mo alloy, some of the studies reported that a Mo solid solution in cobalt and intermetallic Co_3Mo is formed [36,57].

The different intermetallic phases should have an impact on their activity for the HER. It was emphasized that the maximum electrocatalytic activity could be achieved for intermetallic phases of highest symmetry and minimal entropy, such as Laves phases or A_3B types (Co_3Mo , Ni_3Mo , Fe_3Mo) and the Brewer theory for intermetallic bonding predicts as the most stable systems [58]. Thus, it was reported that films consisting of a Co_3Mo phase (for Co- x at.% Mo, $18 \leq x \leq 28$) have the best electrocatalytic properties among other Co-Mo alloys having lower molybdenum contents [59]. Furthermore, in Reference [60], it was concluded that Co_3Mo intermetallic compounds are more stable in a hot alkaline solution than other Co-Mo phases. Similarly, in the case of the Fe-Mo alloy system, the lowest overvoltage for hydrogen evolution at a current density of 200 mA/cm^2 has been observed for the Fe-47 at.% Mo sample with a predominant Fe_3Mo intermetallic compound phase [38].

3.2. Catalytic Behavior

The electrocatalytic activity for hydrogen evolution in 30 wt.% NaOH of Ni-Mo, Co-Mo and Fe-Mo samples containing ~52–54 at.% of Mo in their composition was evaluated using a linear scan voltammetry method that allows for the determination of the apparent exchange current densities. Polarization curves and semi-logarithmic coordinates of all chosen systems obtained at 25 °C are presented in Figure 3. In order to compare the catalytic behavior of Mo-rich Ni-, Co-, Fe-Mo coatings, the cast Mo and Pt electrodes were used. Table 3 summarizes the calculated apparent exchange current densities (i_0), the overpotentials at a selected current density of 200 mA/cm^2 ($\eta_{0,2}$) and the current densities obtained at an overpotential of 0.3 V ($i_{0,3}$); calculated Tafel slopes (b_c).

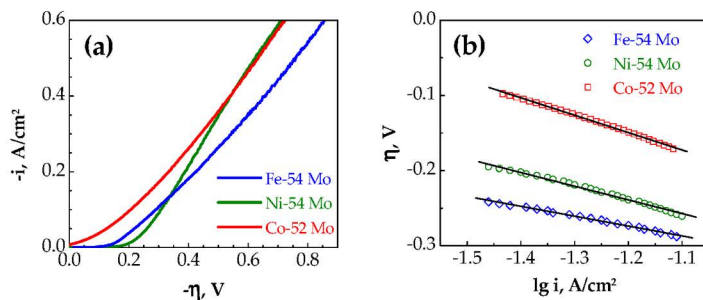


Figure 3. Cathodic polarization curves of (a) Mo-rich electrodeposits in 30 wt.% KOH at 25 °C and (b) plots in semi-logarithmic coordinates. The scan rate was 2 mV/s (composition is given in at.%).

Table 3. Calculated apparent exchange current densities (i_0), Tafel slopes (b_c), overpotentials (η_i) at $i = 0.3 \text{ A/cm}^2$ and current densities (i_{η}) at $\eta = -0.3 \text{ V}$ for hydrogen evolution different electrodes (composition is given in at.%).

Parameter	Electrode				
	Ni-54 Mo	Co-52 Mo	Fe-54 Mo	Mo	Pt
i_0 (mA/cm ²)	0.62	1.90	0.23	2.90×10^{-5}	2.63
b_c (mV/dec)	128	132	152	231	122
η_i (V)	0.46	0.43	0.54	0.67	0.48
i_{η} (A/cm ²)	9.1×10^{-2}	1.8×10^{-1}	9.3×10^{-2}	5.4×10^{-4}	8.2×10^{-2}

Binary Mo alloy cathodes possess 10^5 times higher apparent exchange current densities than cast Mo, thus are more active for the HER. However, all alloys demonstrated lower apparent exchange current densities for the HER at 25 °C in comparison with a bare Pt electrode. However, the overpotentials required to obtain current densities of 300 mA/cm² and current densities at -0.3 V for active bimetallic Mo alloys were similar to those determined for Pt, making them competitive electrodes for hydrogen production. Notably, as it was mentioned above, the nature of the iron group metal affects the catalytic activity for the HER and the cathodic current density for the Co-52 at.% Mo coating is higher in comparison to that of Ni-54 at.% and Fe-54 at.% Mo, thus indicating the best catalytic performance among the synthesized electrodes, which is consistent with the lowest $\eta_{0.2}$ and $i_{0.3}$ values.

It is well known that the lower Tafel slope implies a lower electrochemical electrode polarization during the HER process, particularly at a high current density. The values of the Tafel slope for Ni-54 at.% Mo and Co-52 at.% Mo deposits under high polarization conditions are 128 mV/s and 132 mV/dec, respectively. Meanwhile, the Tafel slope for Fe-54 at.% Mo under these conditions shifted to more positive values, i.e., increased up to 152 mV/dec and it can be related to the higher iron affinity to the air and the presence of a thin oxide film on the surface that is characterized by a lower conductivity that impedes the electron transfer rate [15].

An improvement of catalytic activity for the HER with the operation temperature, as is desired for practical industrial alkaline electrolysis has been reported [36,42]. Accordingly, in the present study, the electrodeposited alloy electrodes were tested at temperatures ranging from 25 to 65 °C by applying 10 °C increments. A general comparison of the performance of electrodeposited Ni-54 at.% Mo, Fe-54 at.% Mo, Co-52 at.% Mo and cast separate metals in the temperature range 25–65 °C is given in Figure 4. The apparent exchange current densities were calculated from the linear region at low overpotential values and are presented in Table 4. As it was expected, the electrocatalytic activity of Ni-54 at.% Mo, Fe-54 at.% Mo and Co-52 at.% Mo is significantly higher than cast Mo in the whole tested temperature range. Moreover, the results suggest that at an elevated temperature (>35 °C) Mo-rich alloys have a more prominent HER outperformance than Pt investigated in our

laboratory. Although the HER activity, namely i_0 , was found to increase with temperature, the Tafel slopes for the Mo-based alloys remained almost constant and varied in the range of 120–150 mV/dec. This phenomenon has been discussed in terms of the entropic contribution towards free energy of activation [61]. Among all investigated systems, the Co–52 at.% Mo electrode demonstrates the best performance towards the HER, particularly at temperatures higher than 45 °C. These results correspond well with findings published in Reference [62] where it was confirmed that Co–Mo co-deposits are characterized by a higher catalytic activity and stability in alkaline water electrolysis than Ni–Mo, Co–W and Ni–W alloy electrodes. Moreover, in Reference [63], it was shown that catalytic activity depends on the metal-hydrogen bond strength and absorption sites in the alloy available to hydrogen and thus the electrochemically charged H content decreases in the series of Co–Mo > Co–W > Ni–Mo. Furthermore, comparing Co–Mo, Co–W and Ni–Mo electrodeposits, the thermal desorption of hydrogen occurs at the lowest temperature on Co–Mo showing a faster recombination step of H atoms possible on this alloy, thus improving its electrocatalytic performance [63].

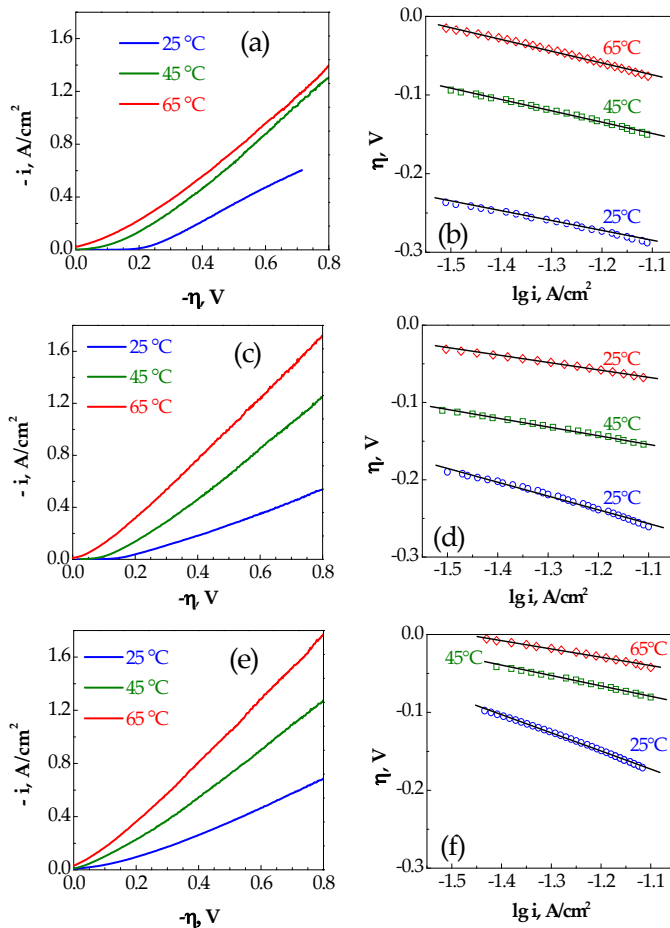


Figure 4. Effect of temperature on cathodic polarization curves at Ni–54 Mo (a), Fe–54 Mo (c), Co–52 Mo (e) electrodeposits in 30 wt.% KOH at different temperatures and plots in semi-logarithmic coordinates for Ni–54 Mo (b), Fe–54 Mo (d), Co–52 Mo (f) electrodes. The scan rate was 2 mV/s (composition is given in at.%).

Table 4. Experimental values of the apparent exchange current (i_0 , in mA/cm²) and Tafel slopes (b_c , in mV/dec) for Ni–54 Mo, Co–52 Mo and Fe–54 Mo alloy electrodes at different temperatures (composition is given in at.%).

Sample	Measurement temperature (°C)									
	25		35		45		55		65	
	i_0	b_c	i_0	b_c	i_0	b_c	i_0	b_c	i_0	b_c
Ni–54 Mo	0.62	128	3.21	128	7.32	119	1.47	116	25.4	123
Fe–54 Mo	0.23	152	0.99	148	4.33	142	5.83	139	14.6	145
Co–52 Mo	1.90	132	9.53	130	17.1	128	32.0	121	46.2	119
Mo	2.9×10^{-2}	231	8.3×10^{-2}	220	1.9×10^{-1}	220	2.1×10^{-1}	215	2.3×10^{-1}	221
Pt	2.63	122	3.68	129	6.51	120	2.63	125	11.5	125

In many previous publications the Ni–Mo alloy coatings are characterized by a lower overpotential value, as compared to the Co–Mo [14]. Though, there is also some information suggesting that Co–Mo coatings have a better catalytic activity for the HER compared to Ni–Mo deposits [62,64]. At the first glance, these controversial results could be attributed to the different alloy preparation techniques that are capable of yielding an uneven composition, morphology and structure of the prepared samples and thus, directly influence the catalytic properties of the samples. However, the clear tendency between the nature of the iron group metal effect during alloying with Mo and catalytic behavior also cannot be easily defined even for the Ni–Mo, Co–Mo and Fe–Mo cathodes fabricated using the same electrodeposition technique (Table 5). As it can be seen, the exchange current densities, even for alloys having a similar chemical composition, vary depending on the selected alkaline media and temperature.

In general, the present study shows the catalytic activity for the Ni–Mo alloy is comparable to previously reported samples under similar experimental conditions (Figure 5). Moreover, in the case of the Co–Mo and Fe–Mo system, the apparent exchange current density calculated in our work is significantly higher than it was expected from other authors observations (the corresponding columns are not given in the figure due to a significantly lower value). This could be attributed to the more concentrated alkaline media and higher temperature used in the present study.

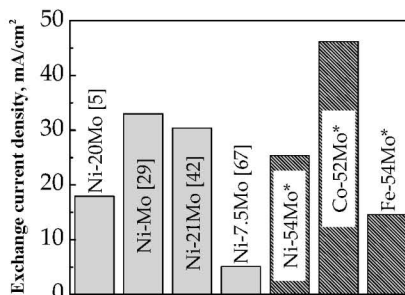


Figure 5. The comparison of apparent exchange current densities (i_0) towards the HER on Mo alloys with iron group metals determined in this study (*) with the published data. The experiments were performed in NaOH at 60–65 °C. The composition of alloys is given in at.%.

Notably, the Fe–Mo coating demonstrates lower exchange current densities for the HER in an alkaline environment among other electrodes investigated in this study. This may be related to the higher iron affinity to the air by forming an oxide, hydroxide, or mixed film that physically separates the metal surface from the electrolyte.

Table 5. Comparison of the HER apparent exchange current density values, i_0 , extracted from the published data for electrodeposited Ni–Mo, Co–Mo and Fe–Mo alloy electrodes.

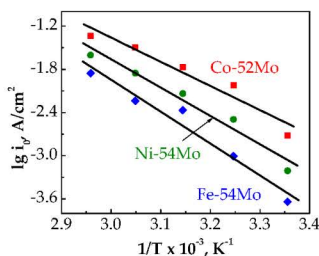
Sample	Mo content (at.%)	Media	i_0 (mA/cm ²)	Reference
Ni–Mo	26	8.25 M NaOH, 85 °C	44.4	[4]
	20	6 M KOH; 80 °C	18.62	[5]
	33.8	7 M KOH, 25 °C	2.8	[19]
	–	7 M KOH, 80 °C	55.24	[29]
	25	2 M NaOH, 30 °C	3.1×10^{-2}	[32]
	20.8	11 M NaOH; 80 °C	42.4	[42]
	29.8	1 M NaOH, 30 °C	11.1	[65]
	27.5	1 M KOH	3.18×10^{-3}	[66]
NiMo-modified Ni foam	2.5	0.1 M NaOH, 25 °C	4.1×10^{-2}	[28]
Ni + Mo composite	44	5 M KOH; 25 °C	1.0	[68]
Ni–Mo–rGO	30.8	1 M KOH; 25 °C	4.31×10^{-3}	[69]
Ni–Mo	10.4	7 M KOH, 25 °C	2.6×10^{-2}	[62]
Co–Mo	21.4		2.3×10^{-2}	
Co–Mo	40.9	1 M NaOH	1.5	[33]
	32	0.5 M NaOH; 60 °C	6.9×10^{-3}	[36]
	25	1 M NaOH, 25 °C	0.13	[59]
	19	1 M KOH, 25 °C	0.36	[70]
	33	1 M NaOH, 30 °C	5.0×10^{-2}	[71]
Fe–Mo	59.3	1 M NaOH, 25 °C	2.4×10^{-3}	[39]

In order to obtain a more complete picture of electrocatalytic behavior for the HER, the corresponding E_a values for all tested systems have been calculated considering the linear dependence $\lg(i_0) = f(1/T)$ using Arrhenius equation:

$$E_a = -2.303R \frac{\partial(\lg i_0)}{\partial(1/T)} \quad (4)$$

where E_a is the activation energy (J/mol), i_0 —apparent exchange current density, T —temperature (K).

Figure 6 shows the Arrhenius plots for the as-deposited Ni–54 at.% Mo, Co–52 at.% Mo and Fe–54 at.% Mo electrodes. From the slope of these plots E_a values of 36.6, 32.5 and 27.9 kJ/mol for Fe–Mo, Ni–Mo and Co–Mo electrodes were determined, respectively. It is known that the lower the E_a value is, the lower the energy requirements for hydrogen production. Thus, it is obvious that the charge transfer rate is favored by Co–52 at.% Mo alloys electrodeposition, since this electrode showed slightly lower activation energy than that of the Ni–54 at.% Mo and Fe–54 at.% Mo coatings.

**Figure 6.** Arrhenius plots for Ni–54 Mo, Co–52 Mo and Fe–54 Mo electrocatalysts (composition is given in at.%).

4. Conclusions

- The electrodeposition of Mo-rich (36–82 at.%) alloys with iron group metals (Ni, Co, Fe) from highly saturated ammonium acetate aqueous electrolytes is reported. The composition was affected by the [Ni(II)]/[Mo(VI)] ratio in the plating bath and cathodic current density.
- The electro-catalytic activity towards cathodic hydrogen evolution in 30 wt.% NaOH solution in the temperature range of 25–65 °C on the electrodeposited Ni–54 at.% Mo, Co–52 at.% Mo, Fe–54 at.% Mo and Co–52 at.% Mo alloy coatings characterized by amorphous-like structure has been investigated.
- Bimetallic Mo-based alloys are considered as more active for the HER in comparison with the cast Mo and Pt since they demonstrate higher apparent exchange current densities in the tested temperature range. The apparent exchange current density of hydrogen for Co–52 at.% Mo deposits were considerably higher than those for Ni–54 at.% Mo and Fe–54 at.% Mo alloy coatings and this can be attributed to the formation of stable intermetallic Co₃Mo phase which ensures optimal Co and Mo distribution over the surface and produces larger active sites for the HER.
- The calculated activation energy values suggest that the Mo alloy coating with iron group metals shows promising electrocatalytic activity for the HER and among all investigated samples, the Co–52 at.% Mo electrode is characterized by a lower activation energy (27.9 kJ/mol) than the Ni–54 at.% Mo (32.5 kJ/mol) and Fe–54 at.% Mo (36.6 kJ/mol) coatings.

Author Contributions: Investigation, E.V. and O.B.; Methodology, E.V. and O.B.; Supervision, H.C. and N.T.; Visualization, E.V.; Writing—Original Draft Preparation, E.V.; Writing—Review & Editing, E.V., H.C. and N.T.

Funding: This research has received funding from Horizon 2020 research and innovation program under MSCA-RISE-2017 (No. 778357) and from Research Lithuanian Council project (No 09.3.3-LMT-K-712-08-0003).

Conflicts of Interest: The authors declare no conflict of interest.

References

1. Studer, S.; Stucki, S.; Speight, J.D. Hydrogen as a Fuel. In *Hydrogen as a Future Energy Carrier*; Zittel, A., Borgschulte, A., Schlapbach, L., Eds.; Wiley-VCH Verlag GmbH & Co. KGaA: Weinheim, Germany, 2008; pp. 23–69.
2. Sheng, W.; Gasteiger, H.A.; Shao-Horn, Y. Hydrogen oxidation and evolution reaction kinetics on platinum: Acid vs alkaline electrolytes. *J. Electrochem. Soc.* **2010**, *157*, B1529–B1536. [[CrossRef](#)]
3. Halim, J.; Abdel-Karim, R.; El-Raghy, S.; Nabil, M.; Waheed, A. Electrodeposition and characterization of nanocrystalline Ni–Mo catalysts for hydrogen production. *J. Nanomater.* **2012**, *2012*, 845673. [[CrossRef](#)]
4. Aaboubi, O. Hydrogen evolution activity of Ni–Mo coating electrodeposited under magnetic field control. *Int. J. Hydrogen Energy* **2011**, *36*, 4702–4709. [[CrossRef](#)]
5. Raj, I.A.; Venkatesan, V.K. Characterization of nickel-molybdenum and nickel-molybdenum-iron alloy coatings as cathodes for alkaline water electrolyzers. *Int. J. Hydrogen Energy* **1988**, *13*, 215–223.
6. Kapoor, G.; Huang, Y.; Sarma, V.S.; Langdon, T.G.; Gubicza, J. Influence of Mo alloying on the thermal stability and hardness of ultrafine-grained Ni processed by high-pressure torsion. *J. Mater. Res. Technol.* **2017**, *6*, 361–368. [[CrossRef](#)]
7. Feng, C.; Qian, W.; Liu, J.; Han, S.; Fu, N.; Ye, F.; Lin, H.; Jiang, J. Effect of ultrasonication on Ni–Mo coatings produced by DC electroformation. *RSC Adv.* **2016**, *6*, 30652–30660. [[CrossRef](#)]
8. Laszczyńska, A.; Tylus, W.; Winiarski, J.; Szczygieł, I. Evolution of corrosion resistance and passive film properties of Ni–Mo alloy coatings during exposure to 0.5 M NaCl solution. *Surf. Coat. Technol.* **2017**, *317*, 26–37. [[CrossRef](#)]
9. Chassaing, E.; Portail, N.; Levy, A.-F.; Wang, G. Characterisation of electrodeposited nanocrystalline Ni–Mo alloys. *J. Appl. Electrochem.* **2004**, *34*, 1085–1091. [[CrossRef](#)]
10. Huang, P.-C.; Hou, K.-H.; Wang, G.-L.; Chen, M.-L.; Wang, J.-R. Corrosion resistance of the Ni–Mo alloy coatings related to coating's electroplating parameters. *Int. J. Electrochem. Sci.* **2015**, *10*, 4972–4984.

11. Jakšić, J.M.; Vojnović, M.V.; Krstajić, N.V. Kinetic analysis of hydrogen evolution at Ni–Mo alloy electrodes. *Electrochim. Acta* **2000**, *45*, 4151–4158. [[CrossRef](#)]
12. Xu, C.; Zhou, J.; Zeng, M.; Fu, X.; Liu, X.; Li, J. Electrodeposition mechanism and characterization of Ni–Mo alloy and its electrocatalytic performance for hydrogen evolution. *Int. J. Hydrogen Energy* **2016**, *41*, 13341–13349. [[CrossRef](#)]
13. Mech, K.; Zabinski, P.; Mucha, M.; Kowalik, R. Electrodeposition of catalytically active Ni–Mo alloys/elektroosadzanie aktywnych katalitycznie stopów Ni–Mo. *Arch. Metall. Mater.* **2013**, *58*, 227–229. [[CrossRef](#)]
14. Jeremiasse, A.W.; Bergsma, J.; Kleijn, J.M.; Saakes, M.; Buisman, C.J.N.; Cohen Stuart, M.; Hamelers, H.V.M. Performance of metal alloys as hydrogen evolution reaction catalysts in a microbial electrolysis cell. *Int. J. Hydrogen Energy* **2011**, *36*, 10482–10489. [[CrossRef](#)]
15. Navarro-Flores, E.; Chong, Z.; Omanovic, S. Characterization of Ni, NiMo, NiW and NiFe electroactive coatings as electrocatalysts for hydrogen evolution in an acidic medium. *J. Mol. Catal. A Chem.* **2005**, *226*, 179–197. [[CrossRef](#)]
16. Manazoğlu, M.; Hapçı, G.; Orhan, G. Electrochemical deposition and characterization of Ni–Mo alloys as cathode for alkaline water electrolysis. *J. Mater. Eng. Perform.* **2016**, *25*, 130–137. [[CrossRef](#)]
17. Martinez, S.; Metikoš-Huković, M.; Valek, L. Electrocatalytic properties of electrodeposited Ni–15Mo cathodes for the HER in acid solutions: Synergistic electronic effect. *J. Mol. Catal. A Chem.* **2006**, *245*, 114–121. [[CrossRef](#)]
18. Lu, G.; Evans, P.; Zangari, G. Electrocatalytic properties of Ni-based alloys toward hydrogen evolution reaction in acid media. *J. Electrochem. Soc.* **2003**, *150*, A551–A557. [[CrossRef](#)]
19. Huang, L.; Yang, F.; Xu, S.; Zhou, S. Studies of structure and electrocatalytic hydrogen evolution on electrodeposited nanocrystalline Ni–Mo alloy electrodes. *Trans. IMF* **2001**, *79*, 136–139. [[CrossRef](#)]
20. Kedzierzawski, P.; Oleszak, D.; Janik-Czachor, M. Hydrogen evolution on hot and cold consolidated Ni–Mo alloys produced by mechanical alloying. *Mater. Sci. Eng. A* **2001**, *300*, 105–112. [[CrossRef](#)]
21. González, G.; Sagarzazu, A.; Villalba, R.; Ochoa, J. Comparative study of NiW, NiMo and MoW prepared by mechanical alloying. *J. Alloys Compd.* **2007**, *434–435*, 525–529. [[CrossRef](#)]
22. Schulz, R.; Huot, J.Y.; Trudeau, M.L.; Dignard-Bailey, L.; Yan, Z.H.; Jin, S.; Lamarre, A.; Ghali, E.; Van Neste, A. Nanocrystalline Ni–Mo alloys and their application in electrocatalysis. *J. Mater. Res.* **1994**, *9*, 2998–3008. [[CrossRef](#)]
23. Yang, C.; Muránsky, O.; Zhu, H.; Thorogood, G.J.; Huang, H.; Zhou, X. On the origin of strengthening mechanisms in Ni–Mo alloys prepared via powder metallurgy. *Mater. Des.* **2017**, *113*, 223–231. [[CrossRef](#)]
24. Bhattacharjee, P.P.; Ray, R.K.; Upadhyaya, A. Development of cube texture in pure Ni, Ni–W and Ni–Mo alloys prepared by the powder metallurgy route. *Scripta Materialia* **2005**, *53*, 1477–1481. [[CrossRef](#)]
25. Tang, X.; Xiao, L.; Yang, C.; Lu, J.; Zhuang, L. Noble fabrication of Ni–Mo cathode for alkaline water electrolysis and alkaline polymer electrolyte water electrolysis. *Int. J. Hydrogen Energy* **2014**, *39*, 3055–3060. [[CrossRef](#)]
26. Li, X.; Liu, Z.; Wang, Y. Microstructure and corrosion properties of laser cladding MoNi based alloy coatings. *Sci. China Technol. Sci.* **2014**, *57*, 980–989. [[CrossRef](#)]
27. Aaboubi, O.; Chopart, J.-P. Magnetic field effect on molybdenum based alloys electrodeposition. *ECS Trans.* **2010**, *25*, 27–34.
28. Mikolajczyk, T.; Pierozynski, B. Influence of electrodeposited Ni–Mo alloy on hydrogen evolution reaction at nickel foam cathode. *Int. J. Electrochem. Sc.* **2018**, *13*, 621–630. [[CrossRef](#)]
29. González-Buch, C.; Herraiz-Cardona, I.; Ortega, E.M.; García-Antón, J.; Pérez-Herranz, V. Development of Ni–Mo, Ni–W and Ni–Co macroporous materials for hydrogen evolution reaction. *Chem. Eng. Trans.* **2013**, *32*, 865–870.
30. Krstajic, N.V.; Jovic, V.D.; Gajic-krstajic, L.; Jovic, B.M.; Antozzi, A.L.; Martelli, G.N. Electrodeposition of Ni–Mo alloy coatings and their characterization as cathodes for hydrogen evolution in sodium hydroxide solution. *Int. J. Hydrogen Energy* **2008**, *33*, 3676–3687. [[CrossRef](#)]
31. Donten, M.; Cesilius, H.; Stojek, Z. Electrodeposition of amorphous/nanocrystalline and polycrystalline Ni–Mo alloys from pyrophosphate baths. *Electrochim. Acta* **2005**, *50*, 1405–1412. [[CrossRef](#)]
32. Gennero de Chialvo, M.R.; Chialvo, A.C. Hydrogen evolution reaction on smooth Ni(1–x) + Mo(x) alloys (0 ≤ x ≤ 0.25). *J. Electroanal. Chem.* **1998**, *448*, 87–93. [[CrossRef](#)]

33. Kuznetsov, V.V.; Kalinkina, A.A.; Pshenichkina, T.V.; Balabaev, V.V. Electrocatalytic properties of cobalt-molybdenum alloy deposits in the hydrogen evolution reaction. *Russ. J. Electrochem.* **2008**, *44*, 1350–1358. [[CrossRef](#)]
34. Podlaha, E.J.; Landolt, D. Induced codeposition: 1. An experimental investigation of Ni–Mo alloys. *J. Electrochem. Soc.* **1996**, *143*, 885–892. [[CrossRef](#)]
35. Bigos, A.; Beltowska-Lehman, E.; Kot, M. Studies on electrochemical deposition and physicochemical properties of nanocrystalline Ni–Mo alloys. *Surf. Coat. Technol.* **2017**, *317*, 103–109. [[CrossRef](#)]
36. Casciano, P.N.S.; Benevides, R.L.; Santana, R.A.C.; Correia, A.N.; de Lima-Neto, P. Factorial design in the electrodeposition of Co–Mo coatings and their evaluations for hydrogen evolution reaction. *J. Alloys Compd.* **2017**, *723*, 164–171. [[CrossRef](#)]
37. Allahyazadeh, M.H.; Roozbehani, B.; Ashrafi, A.; Shadizadeh, S.R.; Kheradmand, E. Electrochemically deposition of high Mo content amorphous/nanocrystalline Ni–Mo using ionic liquids as additive. *ECS Trans.* **2012**, *41*, 11–28.
38. Elezović, N.; Grgur, N.B.; Krstajić, N.V.; Jović, V.D. Electrodeposition and characterization of Fe–Mo alloys as cathodes for hydrogen evolution in the process of chlorate production. *J. Serb. Chem. Soc.* **2005**, *70*, 879–889.
39. Elezović, N.R.; Jović, V.D.; Krstajić, N.V. Kinetics of the hydrogen evolution reaction on Fe–Mo film deposited on mild steel support in alkaline solution. *Electrochim. Acta* **2005**, *50*, 5594–5601. [[CrossRef](#)]
40. Barbano, E.P.; de Carvalho, M.F.; Carlos, I.A. Electrodeposition and characterization of binary Fe–Mo alloys from trisodium nitrilotriacetate bath. *J. Electroanal. Chem.* **2016**, *775*, 146–156. [[CrossRef](#)]
41. Niedbala, J. Production of Ni – Mo + Mo composite coatings with increased content of embedded Mo. *Arch. Mater. Sci.* **2006**, *27*, 121–127.
42. Han, Q.; Cui, S.; Pu, N.; Chen, J.; Liu, K.; Wei, X. A study on pulse plating amorphous Ni–Mo alloy coating used as HER cathode in alkaline medium. *Int. J. Hydrogen Energy* **2010**, *35*, 5194–5201. [[CrossRef](#)]
43. Sun, S.; Podlaha, E.J. Electrodeposition of Mo-Rich, MoNi alloys from an aqueous electrolyte. *J. Electrochem. Soc.* **2012**, *159*, D97–D102. [[CrossRef](#)]
44. Morley, T.J.; Penner, L.; Schaffer, P.; Ruth, T.J.; Bénard, F.; Asselin, E. The deposition of smooth metallic molybdenum from aqueous electrolytes containing molybdate ions. *Electrochem. Commun.* **2012**, *15*, 78–80. [[CrossRef](#)]
45. Kahlert, H. Reference electrodes. In *Electroanalytical Methods*, 2nd ed.; Scholz, F., Ed.; Springer: Berlin/Heidelberg, Germany, 2010; pp. 291–308.
46. Fosdick, S.E.; Berglund, S.P.; Mullins, C.B.; Crooks, R.M. Evaluating electrocatalysts for the hydrogen evolution reaction using bipolar electrode arrays: Bi- and trimetallic combinations of Co, Fe, Ni, Mo, and W. *ACS Catal.* **2014**, *4*, 1332–1339. [[CrossRef](#)]
47. Raj, I.A.; Vasu, K.I. Transition metal-based hydrogen electrodes in alkaline solution? electrocatalysis on nickel based binary alloy coatings. *J. Appl. Electrochem.* **1990**, *20*, 32–38. [[CrossRef](#)]
48. Sanches, L.S.; Domingues, S.H.; Marino, C.E.B.; Mascaro, L.H. Characterisation of electrochemically deposited Ni–Mo alloy coatings. *Electrochem. Commun.* **2004**, *6*, 543–548. [[CrossRef](#)]
49. Rodríguez-Valdez, L.; Estrada-Guel, I.; Almeraya-Calderon, F.; Neri-Flores, M.A.; Martínez-Villafane, A.; Martínez-Sánchez, R. Electrochemical performance of hydrogen evolution reaction of Ni–Mo electrodes obtained by mechanical alloying. *Int. J. Hydrogen Energy* **2004**, *29*, 1141–1145. [[CrossRef](#)]
50. Beltowska-Lehman, E. Kinetics of induced electrodeposition of alloys containing Mo from citrate solutions. *Phys. Status Solidi C* **2008**, *5*, 3514–3517. [[CrossRef](#)]
51. Benaicha, M.; Allam, M.; Dakhouche, A.; Hamla, M. Electrodeposition and characterization of W-rich NiW alloys from citrate electrolyte. *Int. J. Electrochem. Sci.* **2016**, *11*, 7605–7620. [[CrossRef](#)]
52. Bigos, A.; Beltowska-Lehman, E.; Kania, B.; Szczerba, M. Ni–Mo alloys electrodeposited under direct current from citrate-ammonia plating bath. *Inżynieria Materiałowa.* **2013**, *34*, 135–139.
53. Costovici, S.; Manea, A.-C.; Visan, T.; Anicai, L. Investigation of Ni–Mo and Co–Mo alloys electrodeposition involving choline chloride based ionic liquids. *Electrochim. Acta* **2016**, *207*, 97–111. [[CrossRef](#)]
54. Karolus, M.; Łągiewka, E. Crystallite size and lattice strain in nanocrystalline Ni–Mo alloys studied by Rietveld refinement. *J. Alloys Compd.* **2004**, *367*, 235–238. [[CrossRef](#)]
55. Kuznetsov, V.V.; Golyanin, K.E.; Ladygina, Y.S.; Pshenichkina, T.V.; Lyakhov, B.F.; Pokholok, K.V. Electrodeposition of iron–molybdenum alloy from ammonium–citrate solutions and properties of produced materials. *Russ. J. Electrochem.* **2015**, *51*, 748–757. [[CrossRef](#)]

56. Nicolenco, A.; Tsyntsaru, N.; Fornell, J.; Pellicer, E.; Reklaitis, J.; Baltrunas, D.; Cesiulis, H.; Sort, J. Mapping of magnetic and mechanical properties of Fe-W alloys electrodeposited from Fe(III)-based glycolate-citrate bath. *Mater. Des.* **2018**, *139*, 429–438. [CrossRef]
57. Kinh, V.Q.; Chassaing, E.; Saurat, M. Electroplating of crack-free corrosion resistant Co–Mo alloy coatings. *Electrodepos. Surf. Treat.* **1975**, *3*, 205–212. [CrossRef]
58. Jakšić, M.M. Advances in electrocatalysis for hydrogen evolution in the light of the Brewer-Engel valence-bond theory. *J. Mol. Catal.* **1986**, *38*, 161–202. [CrossRef]
59. Zhou, Q.F.; Lu, L.Y.; Yu, L.N.; Xu, X.G.; Jiang, Y. Multifunctional Co–Mo films fabricated by electrochemical deposition. *Electrochim. Acta* **2013**, *106*, 258–263. [CrossRef]
60. Lee, C.R.; Kang, S.G. Electrochemical stability of Co–Mo intermetallic compound electrodes for hydrogen oxidation reaction in hot KOH solution. *J. Power Sources* **2000**, *87*, 64–68. [CrossRef]
61. Conway, B.E.; Tessier, D.F.; Wilkinson, D.P. Temperature dependence of the Tafel slope and electrochemical barrier symmetry factor. *J. Electrochem. Soc.* **1989**, *136*, 2486–2493. [CrossRef]
62. Fan, C.; Piron, D.L.; Sleb, A.; Paradis, P. Study of electrodeposited nickel-molybdenum, nickel-tungsten, cobalt-molybdenum, and cobalt-tungsten as hydrogen electrodes in alkaline water electrolysis. *J. Electrochem. Soc.* **1994**, *141*, 382–387. [CrossRef]
63. Lupu, D.; Mărginean, P.; Biriş, A.R. Hydrogen in some synergetic electrocatalysts. *J. Alloys Compd.* **1996**, *245*, 146–152. [CrossRef]
64. Domínguez-Crespo, M.A.; Plata-Torres, M.; Torres-Huerta, A.M.; Arce-Estrada, E.M.; Hallen-López, J.M. Kinetic study of hydrogen evolution reaction on Ni₃₀Mo₇₀, Co₃₀Mo₇₀, Co₃₀Ni₇₀ and Co₁₀Ni₂₀Mo₇₀ alloy electrodes. *Mater. Charact.* **2005**, *55*, 83–91. [CrossRef]
65. Manazoğlu, M.; Hapçı, G.; Orhan, G. Effect of electrolysis parameters of Ni–Mo alloy on the electrocatalytic activity for hydrogen evaluation and their stability in alkali medium. *J. Appl. Electrochem.* **2016**, *46*, 191–204. [CrossRef]
66. Shetty, S.; Mohamed Jaffer Sadiq, M.; Bhat, D.K.; Hegde, A.C. Electrodeposition and characterization of Ni–Mo alloy as an electrocatalyst for alkaline water electrolysis. *J. Electroanal. Chem.* **2017**, *796*, 57–65. [CrossRef]
67. Tasic, G.S.; Maslovara, S.P.; Zugic, D.L.; Maksic, A.D.; Marceta Kaninski, M.P. Characterization of the Ni–Mo catalyst formed in situ during hydrogen generation from alkaline water electrolysis. *Int. J. Hydrogen Energy* **2011**, *36*, 11588–11595. [CrossRef]
68. Panek, J.; Budniok, A. Ni + Mo composite coatings for hydrogen evolution reaction. *Surf. Interface Anal.* **2008**, *40*, 237–241. [CrossRef]
69. Shetty, S.; Sadiq, M.M.J.; Bhat, D.K.; Hegde, A.C. Electrodeposition of Ni–Mo–rGO composite electrodes for efficient hydrogen production in an alkaline medium. *New J. Chem.* **2018**, *42*, 4661–4669. [CrossRef]
70. Kublanovsky, V.S.; Yaponseva, Y.S. Electrocatalytic properties of Co–Mo alloys electrodeposited from a citrate-pyrophosphate electrolyte. *Electrocatalysis* **2014**, *5*, 372–378. [CrossRef]
71. Subramania, A.; Sathiyapriya, A.; Muralidharan, V. Electrocatalytic cobalt–molybdenum alloy deposits. *Int. J. Hydrogen Energy* **2007**, *32*, 2843–2847. [CrossRef]



© 2019 by the authors. Licensee MDPI, Basel, Switzerland. This article is an open access article distributed under the terms and conditions of the Creative Commons Attribution (CC BY) license (<http://creativecommons.org/licenses/by/4.0/>).

Article III

**Electrodeposited Co-W alloys and their prospects as effective anode for
methanol oxidation in acidic media**

E. Vernickaite, N. Tsyntsaru, H. Cesiulis

Surface & Coatings Technology 307 (2016) 1322–1328



Electrodeposited Co-W alloys and their prospects as effective anode for methanol oxidation in acidic media

E. Vernickaite^a, N. Tsyntsaru^{a,b}, H. Cesiulis^{a,*}

^a Vilnius University, Dept. Phys. Chem., Naugarduko str. 24, Vilnius, Lithuania

^b Institute of Applied Physics of ASM, Academiei str. 5, Chisinau, Republic of Moldova

ARTICLE INFO

Article history:

Received 31 March 2016

Revised 15 July 2016

Accepted in revised form 16 July 2016

Available online 18 July 2016

Keywords:

Electrodeposition

Cobalt-tungsten alloys

Anode

Methanol electrooxidation

Annealing

ABSTRACT

Electrodeposited Co-W alloys having different composition and structure were tested as anodes for methanol electrooxidation. The structure of electrodeposited Co-W alloys having various tungsten content is either nano-crystalline (3 and 18 at.% of W) or “amorphous-like” (30 at.% of W). The electrodeposition was performed on the stainless steel substrate from citrate-borate bath at 60 °C and a cathodic current density 10 mA·cm⁻². Alloys having different compositions were obtained by varying pH from 5 to 8. A well-defined crystalline structure was indicated for Co-W having 3 at.% and 18 at.% of W: these deposits have a hexagonal close packed (hcp) structure typical for electrodeposited pure Co. The high content of W in the alloy (~30 at.%) leads to the formation of nano-crystalline structure (“amorphous-like”). The electrocatalytic activity of prepared Co-W alloys was examined by means of cyclic voltammetry in the mixture of 1 M CH₃OH and 0.1 M H₂SO₄. The electrooxidation of methanol depends on the content of W in the alloy. It was found that the crystalline Co-3 W and Co-18 W alloys are inactive for methanol oxidation, and the electrochemical alloys dissolution occurs in the tested media. Whereas, the high content of W (~30 at.%) in the Co-W coating prevents the continuous Co-W alloy dissolution and it might be used as anode for the methanol oxidation in the acidic media. The annealing of Co-W deposits was performed at 600 °C for 1 h in the air and formation of Co₃O₄ and CoWO₄ compounds with simultaneous decrease of tungsten content in the alloys were detected. The annealed Co-W coatings show lower activity toward methanol electrooxidation compared to as-deposited Co-30 at.% W.

© 2016 Elsevier B.V. All rights reserved.

1. Introduction

Fuel cells based on methanol oxidation reaction (MOR) could replace combustion engines for a variety of applications due to their easy transportation, handling, storage, low operating temperatures and higher energy density compared to the hydrogen [1–3]. Methanol oxidation has been extensively investigated since the early 1970's and a multistep oxidation mechanism was determined involving O—H bond scission in methanol followed by sequential dehydrogenation to CH₂O, then to CO or CO₂ [4]. The resulted products of oxidation (CO₂, HCHO, HCOOH and HCOOCH₃) depend on methanol concentration, temperature, electrode roughness and time of electrolysis. Platinum is the most common catalyst for methanol oxidation, but it is very sensitive to the reaction intermediates such as CO as it poisoning losses catalyst activity [5]. It was found that in the acidic media platinum exhibits the higher catalytic activity for the oxidation of methanol and it is more

resistant toward poisoning by CO, so usually perchloric and sulfuric acids are commonly used as the supporting electrolytes for studies of methanol electrooxidation [6]. The interest in investigation of methanol oxidation on platinum electrodes in alkaline media is lower due to its progressive carbonation by CO₂ [7]. Accordingly, the acidic electrolytes are generally preferred for practical application. Nevertheless, the price of pure platinum is relatively high and the search of more active and less expensive catalysts with great stability for the methanol oxidation reaction has resulted in the development of new binary and ternary catalysts based on modifications of Pt with some other metal [4,8]. Therefore, a number of other materials have been investigated for their suitability as methanol oxidation catalysts, including TiO₂ [9] and Cu(111) [10]. Meanwhile, as the small price of electrodes for methanol fuel cells has been still a key factor, only a few studies have been made to investigate electrodeposited alloys as anode materials for possible application in methanol oxidation reaction. Relatively cheap electrodeposition technique offers the possibility to prepare alloy coatings with easy control of their composition, thickness and homogeneity of the surface. In [11] the electro-catalytic activity of electrodeposited Pt-Ni alloy layers on an inert substrate (Au) electrode for methanol oxidation

* Corresponding author.

E-mail address: henrikas.cesiulis@ch.fvu.lt (H. Cesiulis).

reaction was investigated. It was shown that the onset of electrooxidation shifted to less anodic potential values (approximately by 160 mV vs Hg/Hg₂SO₄ electrode), while also the current density values obtained for Pt-Ni alloy surfaces were higher for 15 times than those of pure Pt. In [12] it was demonstrated that the anodic current peak, a measure of oxidation reaction rate of methanol, is considerably higher using the electrochemically prepared Fe-W alloy in comparison with pure Fe. In addition, the electrodeposited Co-W alloy was presented as a promising anodic catalyst for direct methanol fuel cells [13]. Partially amorphous structure Co-W alloys with W content <10 wt.% in the composition exhibited good corrosion resistance and catalytic activity in highly corrosive media such as H₂SO₄ and KOH. It is well known that W alloys with iron group metals, especially Co-W, have drawn much more attention because of their unusual mechanical, tribological, magnetic and anti-corrosion properties toward acidic and alkaline media and ability to improve catalytic properties of alkaline water electrolysis [14,15]. Heat treatment of the electrodeposited Co-W alloys enhances their corrosion resistance and it is attributed to the formation of stoichiometric compounds, surface oxides and the precipitation of stable phases in the microcracks [16]. Moreover, they are considered as environmentally safe alloys and can be easily prepared by simple and effective electrodeposition technique.

Considering the great performance of W alloys for methanol oxidation, the aim of this study was the electrochemical preparation and characterization of optimal composition of Co-W alloys electrodeposited from ammonia-free bath and possibilities to apply these alloys for methanol electrooxidation reaction in the acidic solution.

2. Materials and methods

Co-W deposits were electrodeposited onto stainless steel (type 304) substrates from citrate-borate electrolyte at different pH under galvanostatic mode at 10 mA·cm⁻². The plating bath consisted of (mol·L⁻¹): CoSO₄·7H₂O–0.2, Na₂WO₄·2H₂O–0.2, C₆H₈O₇–0.04, H₃BO₃–0.65, Na₃C₆H₅O₇–0.25. The pH of solutions was adjusted to 5.0, 6.7 and 8 ± 0.1 by concentrated H₂SO₄ and NaOH solutions. The electrolyte temperature was maintained at 60 ± 2 °C by means of a water bath. The thickness of the deposits was calculated from gravimetric and elemental analysis data and in all cases was ~10 μm.

Electrodeposition was performed in a standard three-electrode cell. A platinum mesh was used as a counter electrode, and saturated Ag/AgCl acted as a reference electrode. All electrode potentials in this paper are presented with respect to the saturated Ag/AgCl electrode. Before the electrodeposition, the stainless steel substrates were washed with detergent and rinsed in the ultrasonic bath with water and then with acetone to remove any contaminants from the surface. In order to improve the adhesion of alloys to the substrates, a nickel seed layer was electrodeposited from an electrolyte containing 1 M NiCl₂ and 2.2 M HCl, at a cathodic current density of 10 mA·cm⁻² for 1 min. Co-W alloy coatings were annealed in air atmosphere in a tube furnace at 600 °C under for 1 h.

The morphology and chemical composition of the coatings was examined by scanning electron microscope (SEM) using Hitachi TM3000 equipment complemented with an energy dispersive X-ray spectroscopy (EDS) analyzer for elemental analysis. The structure of the alloys was studied by X-ray diffraction method using Rigaku MiniFlex II diffractometer with Cu Kα radiation in the 2θ range from 30 to 100°.

Cyclic voltammetry measurements were performed using programmable potentiostat/galvanostat (Autolab N302). Experiments were performed in the potential range from –0.2 to 2.0 V in 0.1 M H₂SO₄ + 1 M CH₃OH solution at room temperature at the scan rate 10 mV s⁻¹. A platinum rode was used as a counter electrode and Ag/AgCl was used as a reference electrode. All potentials were measured and presented also against saturated Ag/AgCl electrode.

3. Results and discussions

3.1. Composition, surface morphology and structure of electrodeposited Co-W alloys

In this study the Co-W alloys coatings were electrodeposited from citrate electrolyte. The composition of Co-W alloys from this electrolyte could be varied in a wide range by changing the pH only, because the electrochemical reactions in the given complex system are dependent on a number of Co(II) and W(VI) complexes with citrates and their distribution strongly depends on pH [14,17–20]. Thus, tungsten content is low (<8 at.%) in Co-W alloys electrodeposited at pH 5, increases from 13 to up to 30 at.% with increasing current density at pH 6.7; whereas at pH 8, the amount of tungsten in the Co-W coatings varies only from 30 to 36 at.%. Thereby, in order to reveal the influence of Co-W alloys composition on their effective use as anode in methanol electrooxidation reaction, there were three marginal cases investigated having different tungsten content (see Table 1), namely Co-3 at.% W (case 1, pH 5), Co-18 at.% W (case 2, pH 6.7), and Co-30 at.% W (case 3, pH 8). The coatings were obtained at the same current density of 10 mA·cm⁻² and 60 °C.

Anodic oxidation of methanol is heterogeneous reaction; therefore it is very important to investigate the microstructure and morphology of the surface of anode material. SEM images of as-deposited Co-W coatings are shown in Fig. 1. Obviously, even a small amount of W in the coating considerably changes the surface morphology. A needle-like structure with extended acicular crystallites that is typical for electrodeposited pure cobalt coating (Fig. 1a) is eliminated after an introduction of tungsten into the alloy. Co-W deposit having ~3 at.% of tungsten consists of densely packed polyhedral crystallites with pronounced grain boundaries (Fig. 1b). An increase in W percentage up to 18 at.% does not considerably affect the shape of the crystallites, but results in an increase in their size (Fig. 1c). When tungsten content reaches ~30 at.%, the morphology of the Co-W alloy changes considerably, the structure becomes more compact and a spherical cluster surface consists from large number of smaller size nodular-shape grains (Fig. 1d).

The changes of alloy composition and morphology are directly reflected in the structural changes. XRD patterns of investigated alloys are presented in Fig. 2. Noticeably, that even the small tungsten amount (“case 1”) incorporated into Co lattice significantly changes the texture of hcp Co lattice: the hexagonal close-packed {100}-textured film, which is characteristic for electrodeposited Co, transforms into {110} textured film while texture {100} weakens sufficiently. This small amount of tungsten causes a strong disorientation of blocs, and maximum angle in the electrodeposited films can reach tens of degrees, that facilitates the growth of defects and multi-domain more readily, therefore, decreasing the texture [21].

The “case 2” is preferentially {101} textured film, whereas the texture of {100} characteristic for electrodeposited cobalt was disappeared. The XRD patterns of this Co-W coating demonstrates a strong peak at 2θ = 46.5° which is attributed to Co₃W. A small shift of 2θ position in comparison with indicated in PDF card no 65–3520 occurs probably due to formation of Co solid solution in the Co₃W phase [17]. Nanocrystalline (“amorphous-like”) structure of Co-W alloy was observed, when the tungsten content in the coatings deposited at 60 °C is >25–27 at.%. In this “case 3” only one broad peak in the proximity of 2θ = 43.5° is seen. It is difficult to determine to which phase this peak is attributed because

Table 1
Influence of the electrolyte pH on Co-W alloy composition and cathodic current efficiency.

pH of the plating bath	W content, at.%	Current efficiency, %
5.0	3.0	75.5
6.7	18.0	70.1
8.0	30.0	25.5

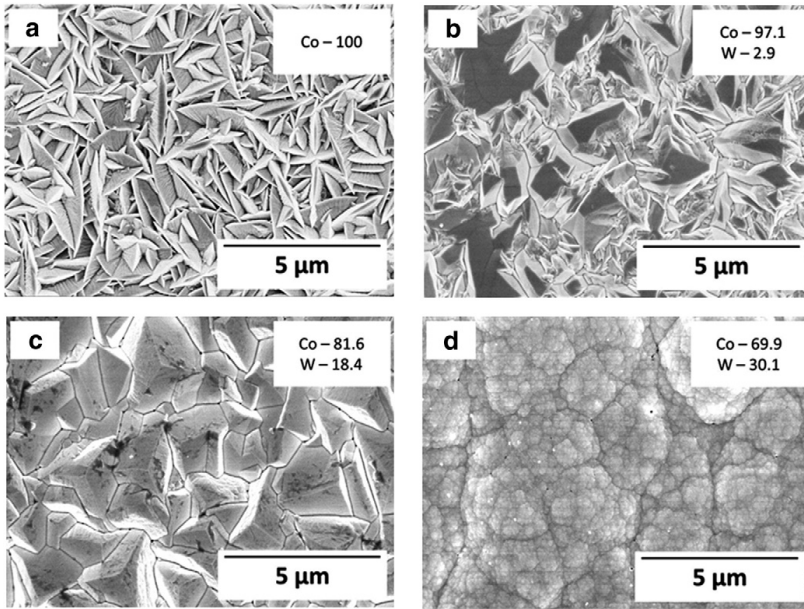


Fig. 1. SEM micrographs of pure Co and Co-W alloys deposited at different pH: (a) 6.7; (b) 5.0; (c) 6.7; (d) 8.0. Compositions of alloys are given in at.%.

the characteristic peaks for Co(W) and Co_3W phase is overlapped. Such peak broadening could be attributed to the reduction of crystallite size of the alloy with an increase of the percentage of W in the deposit.

The abovementioned changes of composition, morphology and structure are the targets of interplay during co-deposition process: the co-deposition of cobalt and tungsten as well as the hydrogen evolution as side reaction undergoes via intermediate adsorption stages and they are interdependent, that lead to increase of W content with increase of pH, lowering of hydrogen overvoltage, and decrease of grain size as follows. Firstly, the increase of the W fraction in the alloy with pH correlates well with the rapid raise in the concentration of some W(VI)-citrate complexes in the solution such as $(\text{WO}_4)(\text{HCitr})\text{H}^{4-}$ at pH > 5. Secondly, the alkalization occurring in the near-electrode zone due to

intense hydrogen evolution during electrolysis, especially at higher pH of solution leads to the increase of tungsten content in the coating, which could be linked to the rise in concentration of electrochemically active W(VI)-citrate complexes with pH. Finally, the formation of adsorbed (heterogeneous) layers on the surface containing intermediates of Co(II) and W(VI) with simultaneous hydrogen evolution facilitate the start the crystallization of Co-W on new spots that causes decrease of the grain size.

Thus, this complex interplay yields the decreasing of both cathodic current efficiency (Table 1) and the grain size with increase in tungsten content with resulted "amorphous-like" structure. Therefore, the alloys obtained at pH 8 contains the highest amount of tungsten (≥ 30 at.%), and due to the intensive hydrogen evolution consist of finest grains

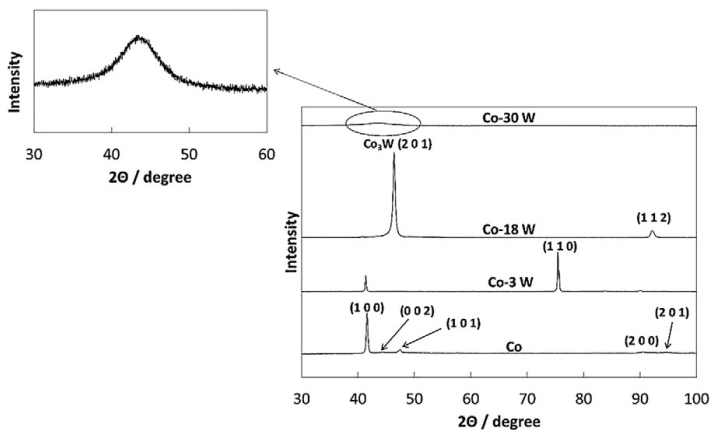


Fig. 2. XRD patterns of as-deposited pure Co and Co-W coatings. Compositions of alloys are given in at.%.

that are smaller than 5 nm and have the low current efficiency (25.5%) in comparison with obtained at pH 5 (75.5%), where they have coarse-grained structure with 5–nm.

3.2. Electrochemical activity of as-deposited Co-W alloys for methanol electrooxidation reaction and their corrosion behavior in acidic medium

In this study, the electro-oxidation of methanol was performed in a mixed solution containing 0.1 M H₂SO₄ and 1 M CH₃OH at room temperature. Typical cyclic voltammograms (CV) curves for different compositions of Co-W catalysts are shown in Fig. 3 (a) and (b). As it can be clearly seen from Fig. 3a, for the cast Co and Co-W alloys having small percentage of W (<18 at.%) the high anodic current densities are observed and they are attributed to the active dissolution of Co-W alloys. The curves were almost linear and no significant peaks of methanol electro-oxidation were observed, which indicates that these Co-W alloys do not possess the electro-catalytic activity toward methanol electro-oxidation reaction.

As it was reported earlier [22], the corrosion resistance of electrodeposited Co-W alloys having <25 at.% of W is very poor. In this case the corrosion rate of the coatings in acidic media is really high and values of anodic current density reach up to 350 mA·cm⁻². According to the literature, due to the oxygen evolution an increase in current density also should be obtained at potentials >1.03 V (vs Ag/AgCl). However, in our case the current density grows mostly because of active Co-W alloys dissolution in acidic media. The corrosion process occurs through the entire alloy layer up to the substrate, and complete coating dissolution is occurred.

When the W content in the deposit is about 30 at.%, only the top surface layer is affected by corrosion process. Thus, after anodization of this alloy in 1 M CH₃OH and 0.1 M H₂SO₄ solution the coating is retained, but Co content in the alloys decreased from 70 to 67 at.%, accordingly W content increased from 30 to 33 at.%, which can be linked with Co faster dissolution. After removing the top layer by gentle polishing, the same W initial content was detected, namely ~30 at.% as it was before the experiment. A baseline CV curve of Co-30 W alloy was also collected in 0.1 M H₂SO₄ (without methanol), and the current (~5 mA·cm⁻²) can be attributed to the corrosion reaction (Fig. 3b), and it is sufficiently smaller than that for Co-W alloys having less content of W.

Thus, Co-W alloy containing 30 at.% of W demonstrates high activity and good stability as a catalyst for methanol oxidation reaction in the acidic media. For comparison the electrooxidation in the same solution on Pt is also shown. Generally, the methanol oxidation on Pt electrode occurs at the potential of 0.15 V and the rate increases considerably at the potentials above 0.4 V, where the hydroxyl groups on a Pt surface are formed. Finally, it was found that methanol oxidation current reached the maximum current density in the potential range of 0.67–0.7 V. The decrease in the oxidation current beyond this potential range is attributed to further oxidation of Pt surface leading to passivation and loss of activity toward methanol oxidation reaction [23]. On the reverse scan, the methanol oxidation peak appeared at an electrode potential of 0.55–0.6 V and the anodically formed oxide film reduces to metallic platinum [23,24]. In this study, the onset of oxide formation was observed at 0.69 V and the oxide reduction peak appeared at 0.6 V. In case of Co-30 W alloy the oxidation reaction occurs at about 0.67 V and this potential and the shape of CV curve is similar to the typical Pt electrode CV shape, whereas no peak at this potential was noticed in the voltammogram for Co-30 W deposit in the absence of methanol. The enhancement in catalytic activity by Co-W catalyst may be attributed to the increase in its real surface area, synergic effect by the interaction between Co and W, which prevents the active Co dissolution during the methanol oxidation reaction.

3.3. Electrochemical performance of oxidized Co-W alloys for methanol oxidation reaction

It was shown [13] that thermal treatment increases the catalytic activity of Co-W alloy for methanol oxidation in both acidic and alkaline media because the thermal treatment of the W alloy coatings improves their crystalline structure and new phases are formed. There are two stable bulk phases of cobalt oxide: the (fcc) type rock salt structure of CoO and the cubic spinel structure of Co₃O₄; they exhibit interesting electronic and magnetic properties and can be used as catalysts in some reactions [25]. In order to prepare oxidized Co-W alloys they were heated for 1 h at 600 °C in air atmosphere. This temperature has been chosen as the optimal for further experiments, because at lower temperature (400 °C) amorphous structure of Co-30 W alloys remains stable and no corresponding peaks for Co oxides were noticed. After heat treatment at higher temperature (700 °C) the coatings were poorly adhered to the stainless steel substrate and many cracks on the surface were observed. The surface morphology after thermal treatment of Co-W catalysts and pure Co at 600 °C is presented in Fig. 4.

As it is seen, the crystalline Co-W coatings having <18 at.% of tungsten in their composition after heat treatment demonstrates similar surface morphology with the presence of open pores and blurry grain boundaries. However, EDS analysis showed that they consist only of elemental Co and O (Fig. 5 a). In contrary, Co-W alloy having 30 at.% of W after annealing contained only ~1 at.% of tungsten (Fig. 5) and this significant decreasing of W content dramatically changes the morphology of the deposit compared to that of as-deposited one. As-deposited Co-30 W coating contains spherical and smooth bright nodules on its surface, and after annealing it demonstrates polyhedral crystallites of the irregular size. In both cases, Co-30 W electrodeposits even after annealing are cracks-free, in comparison with results of work [26].

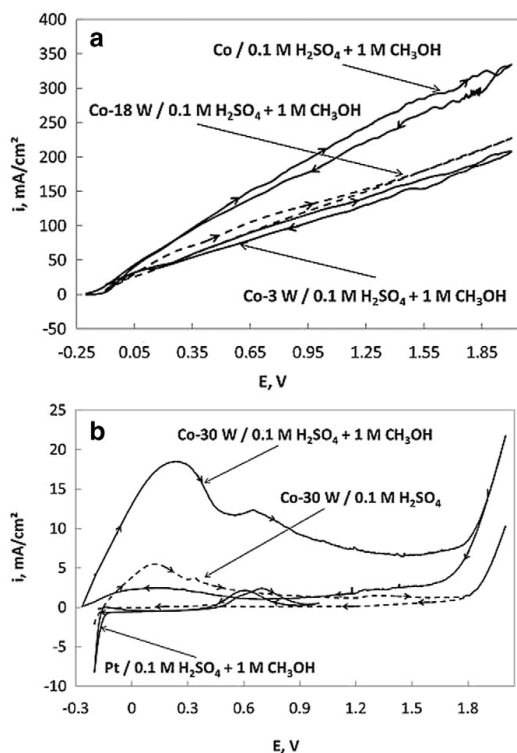


Fig. 3. Cyclic voltammograms recorded on the various as-deposited Co-W alloy catalysts; the composition is given in at.%. Arrows show a potential scan direction.

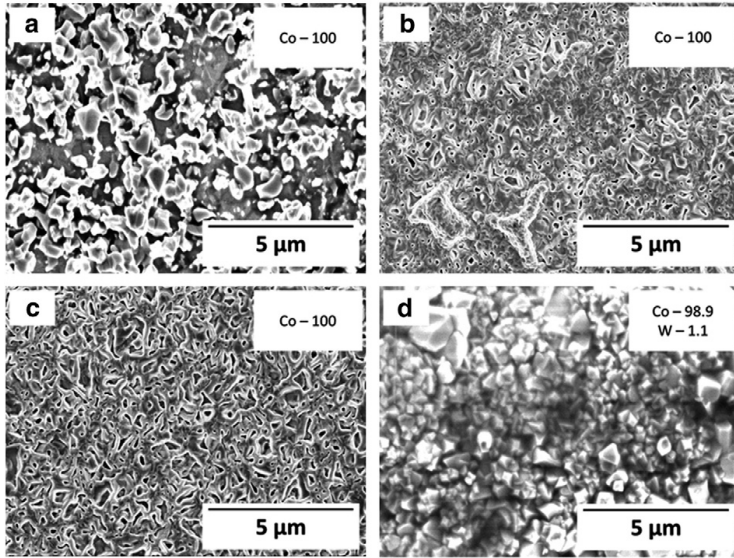


Fig. 4. SEM micrographs of pure Co (a) and Co-W alloys deposited at different pH: 5(b); 6.7 (c); 8(d) after heat treatment at 400 °C for 1 h.

XRD analysis (Fig. 6) confirmed the crystalline structure of all investigated coatings after heating at 600 °C in the open air. The results are similar to previous studies, where it was shown that, the Co-W alloys having high content of W in their composition (24.5 at.%) demonstrates a clear polycrystalline structure after heating for 4 h in vacuum from 400 °C to 800 °C [17]. Meanwhile Co-W deposits containing higher tungsten percentage in their composition recrystallized from

amorphous-like to polycrystalline Co_3W structure at 600 °C. XRD patterns of as-deposited Co-3 at.% W alloy after annealing indicated that are consisting of pure hcp Co and phases of oxidation products (Co_3O_4 and CoWO_4) (Fig. 6). The detected peak positions of CoWO_4 phase is in accordance with [27]. For Co-W alloy coating having higher amount of W a pure hcp Co phase after heat treatment in X-ray spectrum disappears. Interestingly in the case of annealed Co-18 at.% W alloy a strong peak at $2\theta = 46.5^\circ$ corresponding to Co_3W phase was observed like in the same as-deposited coating. Although EDS analysis showed extremely low W content in the alloy after heat treatment at 600 °C in the air a small amount of Co_3W phase also was observed in XRD patterns of annealed Co-30 at.% W sample. This could be attributed to the higher penetration depth of X-ray beam (~4 μm) in course of XRD analysis compared to the EDS technique (~1 μm). As the X-rays penetrate deeper during XRD test, therefore the characterization of the deeper inner layer of the thin film can be performed. It was proven by the EDS analysis

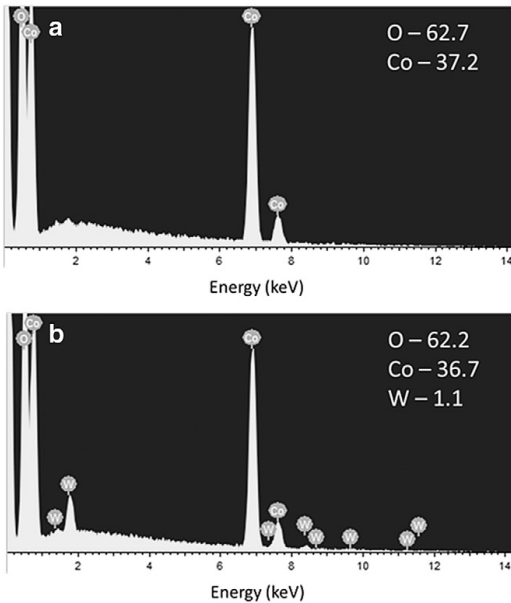


Fig. 5. EDS spectra of (a) Co-18.4 W and (b) Co-30.1 W alloys coating after heat treatment at 600 °C for 1 h. Composition is given in at.%.

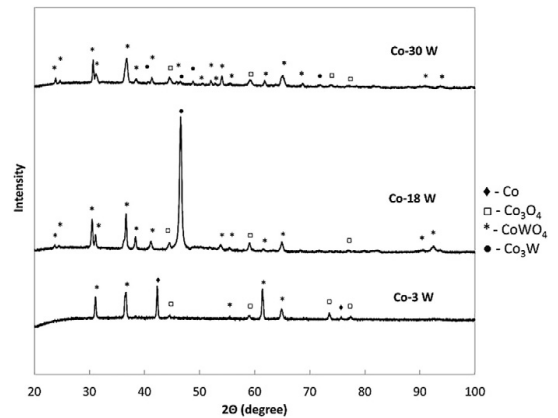


Fig. 6. XRD patterns of Co-W alloys after heating for 1 h at 600 °C in the open air. The composition (in at.%) is given for as-deposited alloys.

performed after gentle polishing of the annealed sample having <2 at.% of W, that inner layer has higher W content of ~19 at.%. This could be the reason of the formation of Co_3W phase in XRD results. Furthermore, the patterns of heat treated Co-30 at.% W alloy coating indicated the formation of Co_3O_4 and CoWO_4 phases as well.

In all investigated cases after heat treatment of Co-W alloys at 600 °C using XRD technique there were no peaks attributed to tungsten oxide phases. That is in contradictory with known fact that pure tungsten starts to oxidize in vacuum by residual oxygen at about 400 °C and above 900 °C the sublimation of WO_3 takes place. This could be attributed to different W structure in pure W metal and in the alloy, which could cause the tungsten sublimation in Co-W alloy at lower temperature (600 °C) in open air. The above-mentioned EDS data show that nanocrystalline alloys sublimate gradually from top to bottom of the coating.

Electrocatalytic properties of the heat-treated and oxidized Co-W alloy electrodes toward methanol oxidation were investigated under the same conditions as for as-deposited alloys, and corresponding cyclic voltammograms are shown in Fig. 7. The cyclic voltammograms for Co-30 W alloys were recorded in the potential range from -0.2 up to 1.0 V in order to prevent the dissolution of cobalt from the surface of the electrode at more positive potentials. A baseline CV curve of annealed Co-W alloy was also recorded in 0.1 M H_2SO_4 solution (without methanol). In this case, Co-W deposit shows an oxidation peak at 0.11 V which corresponds to the Co dissolution from the alloy. This behavior is similar to the noticed for as-deposited Co-W coating. As it was expected, Co-W deposits initially contained <18 at.% of W, after heating became totally inactive for methanol oxidation reaction (Fig. 7 (a)). Whereas the annealed Co-W alloy with having initially 30 at.% of W demonstrates a small methanol oxidation peak at 0.7 V in sulfuric acid and methanol mixture (Fig. 7 b). In this case the peak current density of the methanol

oxidation on the heat treated Co-W electrode is $0.135 \text{ mA} \cdot \text{cm}^{-2}$, which is sufficiently lower than indicated for as-deposited Co-30 W alloy coating ($12.3 \text{ mA} \cdot \text{cm}^{-2}$) or pure Pt electrode ($2.4 \text{ mA} \cdot \text{cm}^{-2}$). The decrease in catalytic activity might be attributed to the reduction of tungsten content in the alloy and the inhomogeneity of surface morphology. In addition, the significant increase in cathodic current density during the reverse scan was not observed as for as-deposited alloys probably due to irreversible oxidation of methanol.

4. Conclusions

Electrodeposited Co-W alloys having various tungsten content and structure ranged from nanocrystalline (3 and 18 at.% of W) and "amorphous-like" (30 at.% of W) had been electrodeposited from citrate-based solutions and tested as anodes for methanol electrooxidation in the mixture of 1 M CH_3OH and 0.1 M H_2SO_4 . As-deposited Co-3 at.% and Co-18 at.% coatings were totally inactive for methanol oxidation, and the electrochemical alloys dissolution occurs in the tested media. Only Co-30 at.% W alloy is an active electrocatalysts for methanol oxidation. It is more effective electrode for methanol electrooxidation than pure Pt because of higher anodic peak current density ($12.3 \text{ mA} \cdot \text{cm}^{-2}$) attributed to the electrooxidation of methanol. After heating for 1 h at 600 °C in air atmosphere the structure of Co-W coatings transformed from "amorphous-like" (nanocrystalline) to crystalline one and new phases are occurred (Co_3O_4 , CoWO_4) simultaneously with decrease of tungsten content in the alloy due to the volatilization of tungsten oxides. It was found that heating resulted the lower Co-W alloy activity toward methanol electrooxidation compared to both "as-deposited" Co-30 at.% W and pure Pt electrodes.

Acknowledgement

The authors acknowledge funding from the Research Council of Lithuania (MIP-031/2014) and Moldavian National Project 15.817.02.05A.

References

- [1] J.R.C. Salgado, E. Antolini, E.R. Gonzalez, Carbon supported Pt-Co alloys as methanol-resistant oxygen-reduction electrocatalysts for direct methanol fuel cells, *Appl. Catal., B* 57 (2005) 283–290.
- [2] E. Antolini, J.R.C. Salgado, E.R. Gonzalez, The methanol oxidation reaction on platinum alloys with the first row transition metals: the case of Pt-Co and -Ni alloy electrocatalysts for DMFCs: a short review, *Appl. Catal., B* 63 (2006) 137–149.
- [3] E.R. Gonzalez, A. Mota-Lima, Catalysts for methanol oxidation, in: R. Corti, E.R. Gonzalez (Eds.), *Direct Alcohol Fuel Cells – Materials, Performance, Durability and Applications* Springer Science + Business Media Dordrecht 2014, pp. 33–62.
- [4] T. Iwasita, Electroanalysis of methanol oxidation, *Electrochim. Acta* 47 (2002) 3663–3674.
- [5] Z. Jusys, T.J. Schmidt, L. Dubau, K. Lasch, L. Jörissen, J. Garche, R.J. Behm, Activity of PtRuMeOx (Me = W, Mo or V) catalysts towards methanol oxidation and their characterization, *J. Power Sources* 105 (2002) 297–304.
- [6] M. Metikos-Hukovic, R. Babic, Y. Piljac, Kinetics and electrocatalysis of methanol oxidation on electrodeposited Pt and Pt₇₀Ru₃₀ catalysts, *J. New Mater. Electrochem. Syst.* 7 (2004) 179–190.
- [7] A.V. Tripković, K.D. Popović, J.D. Lović, V.M. Jovanović, A. Kowal, Methanol oxidation at platinum electrodes in alkaline solution: comparison between supported catalysts and model systems, *J. Electroanal. Chem.* 572 (2004) 119–128.
- [8] T. Iwasita, H. Hostler, A. John-Aacker, W.F. Lin, W. Vielstich, Methanol oxidation on PtRu electrodes. Influence of surface structure and Pt-Ru atom distribution, *Langmuir* 16 (2000) 522–529.
- [9] A. Serov, C. Kwak, Review of non-platinum anode catalysts for DMFC and PEMFC application, *Appl. Catal., B* 90 (2009) 313–320.
- [10] Z.J. Zuo, L. Wang, P.D. Han, W. Huang, Insights into the reaction mechanisms of methanol decomposition, methanol oxidation and steam reforming of methanol on Cu(111): a density functional theory study, *Int. J. Hydrog. Energy* 39 (4) (2014) 1664–1679.
- [11] J. Mathiyarasu, A.M. Remona, A. Mani, K.L.N. Phani, V. Yegnaman, Exploration of electrodeposited platinum alloy catalysts for methanol electro-oxidation in 0.5 M H_2SO_4 : Pt-Ni system, *J. Solid State Electrochem.* 8 (2004) 968–975.
- [12] C.N. Tharamani, P. Beera, V. Jayaram, N.S. Begum, S.M. Mayanna, Studies on electrodeposition of Fe-W alloys for fuel cell applications, *Appl. Surf. Sci.* 253 (2006) 2031–2037.
- [13] T. Shobba, S.M. Mayanna, C.A.C. Sequeira, Preparation and characterization of Co-W alloys as anode materials for methanol fuel cells, *J. Power Sources* 108 (2002) 261–264.

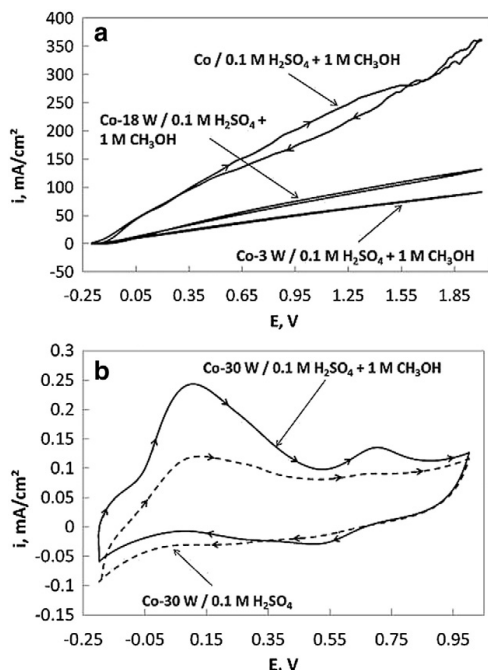


Fig. 7. Cyclic voltammograms recorded on the annealed Co-W catalyst in the mixture of 0.1 M H_2SO_4 and 0.1 M methanol at room temperature. Composition (in at.%) is provided for as-deposited alloys (prior heating at 600 °C). Arrows show a potential scan direction.

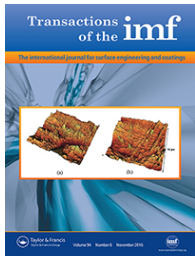
- [14] N. Tsyntsar, H. Cesiulis, M. Donten, J. Sort, E. Pellicer, E.J. Podlaha-Murphy, Modern trends in tungsten alloys electrodeposition with iron group metals, *Surf. Eng. Appl. Electrochem.* 48 (2012) 13–44.
- [15] C. Fan, D.L. Piron, A. Sleb, P. Paradis, Study of electrodeposited nickel-molybdenum, nickel-tungsten, cobalt-molybdenum, and cobalt-tungsten as hydrogen electrodes in alkaline water electrolysis, *J. Electrochem. Soc.* 141 (1994) 382–387.
- [16] P. Bera, H. Seenivasan, K.S. Rajam, V.K.W. Grips, XRD, FESEM and XPS studies on heat treated Co–W electrodeposits, *Mater. Lett.* 76 (2012) 103–105.
- [17] N. Tsyntsar, H. Cesiulis, A. Budreika, X. Ye, R. Juskenas, J.P. Celis, The effect of electrodeposition conditions and post-annealing on nanostructure of Co–W coatings, *Surf. Coat. Technol.* 206 (2012) 4262–4269.
- [18] F. Su, C. Liu, P. Huang, Effect of complexing agents and pH on microstructure and tribological properties of Co–W coatings produced by double pulse electrodeposition, *Appl. Surf. Sci.* 258 (2012) 6550–6557.
- [19] N. Tsyntsar, G. Kaziukaitis, C. Yang, H. Cesiulis, H.G.G. Philipsen, M. Lelis, J.-P. Celis, Co–W nanocrystalline electrodeposits as barrier for interconnects, *J. Solid State Electrochem.* 18 (2014) 3057–3064.
- [20] N. Tsyntsar, H. Cesiulis, E. Pellicer, J.-P. Celis, J. Sort, Structural, magnetic, and mechanical properties of electrodeposited cobalt-tungsten alloys: intrinsic and extrinsic interdependencies, *Electrochim. Acta* 104 (2013) 94–103.
- [21] L.S. Palatnik, M. Ya, V.M. Fuks, Kosevich, *Mekhanizm Obrazovaniya i Substruktura Kondesirovannykh Plenok*, Izdatel'stvo Nauka, Moscow, 1972 (in Russian).
- [22] H. Cesiulis, A. Budreika, Hydrogen evolution and corrosion of W and Mo alloys with Co and Ni, *Physicochem. Mech. Mater.* 8 (2010) 808–814.
- [23] G. Hou, J. Parrondo, V. Ramani, J. Prakash, Kinetic and mechanistic investigation of methanol oxidation on a smooth polycrystalline Pt surface, *J. Electrochem. Soc.* 161 (2014) F252–F258.
- [24] M. Metikos-Hukovic, R. Babic, Y. Piljac, Kinetics and electrocatalysis of methanol oxidation on electrodeposited Pt and Pt70Ru30 catalysts, *J. New Mater. Electrochem. Syst.* 7 (2004) 179–190.
- [25] M.M. Natile, A. Glisenti, Study of surface reactivity of cobalt oxides: interaction with methanol, *Chem. Mater.* 14 (2002) 3090–3099.
- [26] P. Bera, H. Seenivasan, K.S. Rajam, V.K.W. Grips, XRD, FESEM and XPS studies on heat treated Co–W electrodeposits, *Mater. Lett.* 76 (2012) 103–105.
- [27] X. Chun Song, E. Yang, R. Ma, H. Fang Chen, Y. Zhao, Sodium dodecyl sulfate-assisted synthesis of CoWO₄ nanorods, *J. Nanopart. Res.* 10 (2008) 709–713.

Article IV

Electrodeposition and corrosion behavior of nanostructured cobalt tungsten alloy coatings

E.Vernickaite, N. Tsyntsaru, H. Cesiulis

Transactions of the IMF, 94 (6) (2016) 313-321



Electrodeposition and corrosion behaviour of nanostructured cobalt–tungsten alloys coatings

E. Vernickaite, N. Tsyntsaru & H. Cesiulis

To cite this article: E. Vernickaite, N. Tsyntsaru & H. Cesiulis (2016) Electrodeposition and corrosion behaviour of nanostructured cobalt–tungsten alloys coatings, Transactions of the IMF, 94:6, 313-321, DOI: [10.1080/00202967.2016.1220071](https://doi.org/10.1080/00202967.2016.1220071)

To link to this article: <https://doi.org/10.1080/00202967.2016.1220071>



Published online: 09 Nov 2016.



Submit your article to this journal [↗](#)



Article views: 54



View related articles [↗](#)



View Crossmark data [↗](#)



Citing articles: 3 View citing articles [↗](#)

Full Terms & Conditions of access and use can be found at
<http://www.tandfonline.com/action/journalInformation?journalCode=ytim20>

Electrodeposition and corrosion behaviour of nanostructured cobalt–tungsten alloys coatings

E. Vernickaite¹, N. Tsyntsaru^{1,2} and H. Cesiulis^{*1}

Theoretical and practical studies of tungsten alloys with iron group metals continue to be carried out because of their unique combination of tribological, magnetic and electrical properties. The electrodeposition of Co–W alloys was performed in a citrate–borate solution at pH 5–8; $t = 20$ and 60°C. The electrochemical corrosion was studied in 0.01 M H₂SO₄, and stainless steel was selected as a substrate. For the mapping of the properties alloy deposits having various contents of W (2.4–30 at.-%) and crystallite size varying from polycrystalline (<60 nm) to ‘amorphous-like’ (2–5 nm) were prepared. Co–W alloys possessing the highest corrosion resistance should contain 17–24 at.-% of W, i.e. have a structure close to intermetallic phase Co₃W. The corrosion occurs via an intermediate adsorbed stage by forming oxygen-containing compounds; the estimated thickness of the adsorbed layer varies in the range 0–1.6 Å.

Keywords: Cobalt–tungsten alloys; Electrodeposition; Corrosion; EIS; Oxide layer

Introduction

Nanostructured materials generate much excitement in the scientific community for the enhanced properties associated with a nanoscaled grain structure offering new opportunities for challenging industrial applications.¹ Many synthesis techniques for nanostructured materials have been developed over the past 20 years,^{2,3} such as electrodeposition, hydrothermal-electrochemical process, and a hydrothermal-mechanical-chemical process. Among these techniques, electrodeposition is a most appropriate one since it is a low-cost process easy to upscale so that transfer from technology to industry is feasible. Among a number of options of different materials, currently theoretical and practical studies on the codeposition of tungsten with iron group metals are being conducted worldwide.^{1–3} Tungsten alloys of iron group metals have a high melting point and are often considered as superalloys or high-performance alloys, and the interest in those has been driven by their outstanding properties and multiple possible applications, overviewed in Lassner and Schubert.¹ That research is encouraged by the pronounced mechanical, tribological and magnetic properties as well as the corrosion resistance of tungsten alloys.³ The magnetic properties of electrodeposited Me–W alloys are of interest in recording media^{4,5} and remotely actuated micro-/nano-electromechanical systems (MEMS/NEMS), such as microactuators, micromotors, sensors, microgears or micromechanical

magnetometers.^{6,7} A semi-hard ferromagnetic behaviour of electrodeposited Co–W alloys with a coercivity of ~470 Oe along the perpendicular-to-plane direction is observed for Co–W alloys containing small amounts of W in the range of ~2–3 at.-%; at higher tungsten contents the coatings are magnetically softer, and the electrodeposits become non-ferromagnetic beyond ~30 at.-% W.⁸ In other words, electrodeposited tungsten alloys are suitable candidates to meet many technological demands.

Corrosion is a deteriorating phenomenon of metals and alloys, which often dictates the life of a product. Owing to a large surface area-to-volume ratio of thin films, as compared to that of bulk materials, the properties of thin films, as a rule, significantly differ from the bulk (macroscaled) materials behaviour. Indeed, a fundamental requirement for materials in microtechnology is that they have to show an extremely high corrosion resistance. This is due to the continuous decrease in the component size, down to the micrometer range. Under such conditions, the resistance to device failure due to even a small amount of ionic contaminants may become a key issue in terms of lifetime and reliability. Film composition, microstructure and density are very much dependent on preparation methods and conditions, and the variation in corrosion rates and other properties of the surfaces with the fabrication method and structure are well known.^{9,10} Additionally, differences in corrosion properties between cast iron group metals and the corresponding electrodeposited metals have been observed. The values of corrosion potential (open circuit potential (OCP)) are more negative for the electrodeposited metals than for the corresponding cast metals. Furthermore, higher corrosion currents are obtained in electrodeposited metals.¹¹ Therefore, the examination of the corrosion

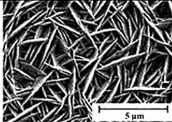
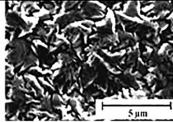
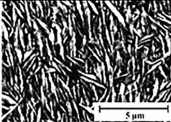
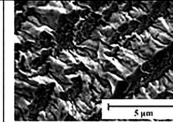
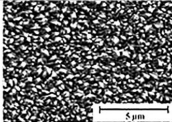
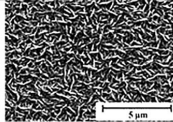
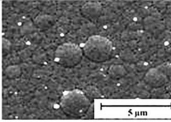
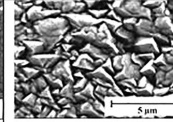
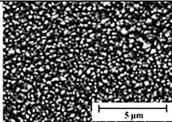
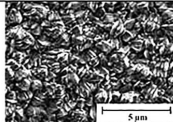
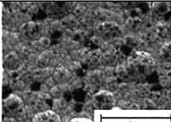
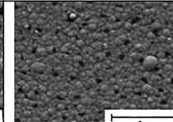
¹Vilnius University, Faculty of Chemistry, Naugarguko 24, Vilnius LT-03325, Lithuania

²Institute of Applied Physics, Academy of Sciences of Moldova, Academiei 5, Chisinau MD-2028, Moldova

*Corresponding author: email henrikas.cesiulis@chf.vu.lt

Table 1 Electrodeposition conditions and contents of obtained Co–W alloys

Composition of electrolyte	Electrodeposition conditions				Composition of metallic phase
	pH	i /mA cm ⁻²	Deposition time/min	Temperature/°C	
0.2 M CoSO ₄ ·7H ₂ O	5.0	10	60	60	Co–3 at.-% W
0.2 M Na ₂ WO ₄ ·2H ₂ O	6.0	5	120		Co–9 at.-% W
0.65 M H ₃ BO ₃	6.7	5	95		Co–14 at.-% W
0.25 M Na ₃ C ₆ H ₅ O ₇	6.7	10	75		Co–19 at.-% W
0.04 M C ₆ H ₆ O ₇	6.7	15	65		Co–24 at.-% W
	8.0	5	370		Co–30 at.-% W
	6.7	5	135	20	Co–13 at.-% W
	8.0	5	285		Co–25 at.-% W
	6.7	5	120	60	Co
0.2 M CoSO ₄ ·7H ₂ O					
0.65 M H ₃ BO ₃					
0.25 M Na ₃ C ₆ H ₅ O ₇					
0.04 M C ₆ H ₆ O ₇					

Co		i , mA cm ⁻²	Co–W	
20°C	60°C		20°C	60°C
		1		
			8 at.-%W	13 at.-%W
		5		
			17 at.-%W	18 at.-%W
		10		
			21 at.-%W	24 at.-%W

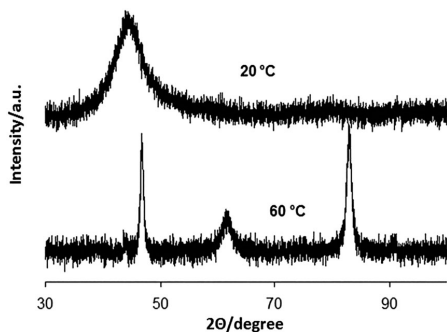
1 Morphology of Co and Co–W electrodeposited coatings obtained at pH 6.7

properties of the obtained materials is an integral part of modern materials science and crucial in terms of technological applications.

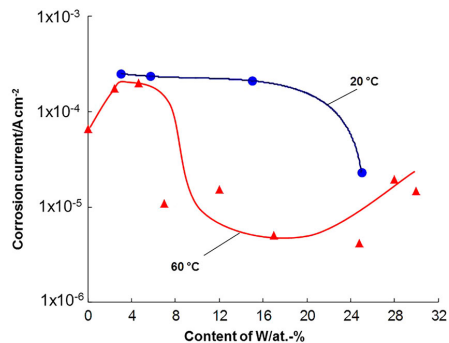
The corrosion behaviour of nanocrystalline tungsten alloys including ‘amorphous like’ is intriguing, as one can expect that the increase of the amount of tungsten in the coating will increase its corrosion resistance. However, it can be noted that they hardly transfer into a passive state in neutral solutions;^{12–16} in both cases, freshly deposited and after exposing these materials for 15 days in open air, the corrosion potential shifts towards more positive potentials by only 100–200 mV and remains relatively negative. Thus, the rubbing of surfaces does not promote corrosion, i.e. tribocorrosion of such alloys is

relatively weak. On the other hand, tungsten alloys show a relatively low hydrogen overvoltage and clear correlation between exchange current for H₂ evolution is obtained for the Co–W alloys with relative high content of W.¹⁷ Moreover, taking into account that corrosion of tungsten alloys with iron group metals occurs with hydrogen depolarisation, and the absolute values of both hydrogen evolution reaction and anodic reaction have to be the same during resting of alloy in corrosive media, the weak passivity of tungsten and molybdenum alloys obtained in air and neutral solutions¹³ may govern the high corrosion rate of these alloys.

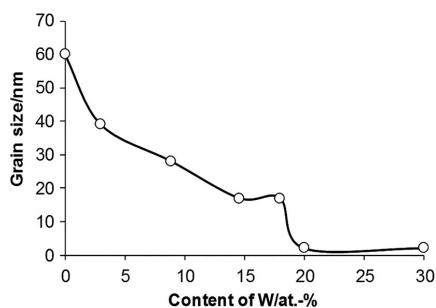
The mapping of corrosion behaviour is a critical step towards an implementation of such materials in modern



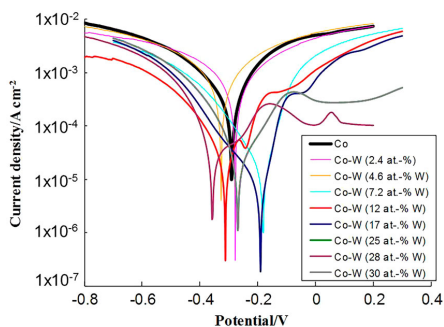
2 X-ray diffraction patterns recorded on Co–W electrodeposits having 14 at.-% of W and electrodeposited at various temperatures



5 Corrosion current for Co and Co–W as a function of the content of tungsten. Electrodepositing temperature is indicated in figure



3 Effect of tungsten content on the average grain size of Co–W alloys



4 Linear sweep voltammograms for Co and Co–W alloys electrodeposited at 60 °C. The scan rate was 2 mV s⁻¹

devices. Indeed, such mapping is important to establish interdependencies between intrinsic and extrinsic properties/parameters. It is well known that the key factor determining the structure and properties of an alloy is its chemical composition.⁸

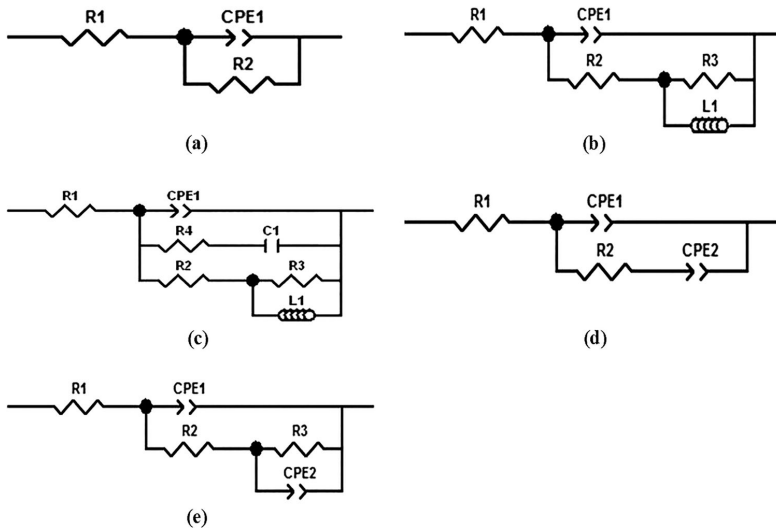
This study is devoted to the Co–W electrodeposition from citrate–borate solution containing a relatively high concentration of CoSO₄ and Na₂WO₄ and mapping the corrosion properties as a function of both the content varying in a wide range (from 0 up to 30 at.-% of W) and the structure of deposits obtained.

Experimental

A galvanostat/potentiostat AUTOLAB 302 in combination with the software GPES and FRA was employed for electrodeposition and for corrosion study. Thicker coatings of about 10 μm were electrodeposited to accurately measure the corrosion resistance. For the corrosion study the registration of electrochemical impedance spectra (EIS) and voltammetric data was started after stabilisation of the OCP within 15 min in the test medium, 0.01 M H₂SO₄. The amplitude of the sinusoidal voltage was 5 mV and the spectrum was obtained in the frequency range: 10 kHz–0.01 Hz. The thickness of the electrodeposits was calculated from gravimetric and elemental analysis data. The surface morphology of the coatings and content of alloys was investigated by scanning electron microscopy (Hitachi TM-3000 equipped with EDS analyser and software Swift ED-3000). Pure Co coatings were electrodeposited from the same solution but free of Na₂WO₄ in order to be compared with Co–W coatings.

The electrodeposition and corrosion tests were performed in a three-electrode cell with a platinised mesh as a counter electrode and saturated Ag/AgCl electrode as the reference electrode. All potential values are expressed vs. this reference electrode. Stainless steel substrates of the following composition (in wt.-%) Fe-70, Cr-19, Ni-8, Mn-2, other: Si, Al, P-1 were used. In all experiments a stationary working electrode has been used. Prior to electrodeposition, the steel substrates were mechanically polished using a diamond paste followed by an ultrasonic cleaning in ethanol to remove any contamination from the surface. In order to improve the adhesion of Co–W coatings to the substrates, a nickel seed-layer was electrodeposited from an electrolyte containing 1 M NiCl₂ + 2.2 M HCl, at a cathodic current density of 20 mA cm⁻² for 1 min. A platinum mesh was used as anode for Ni and Co–W electrodeposition.

Co–W coatings were obtained by electrodeposition under galvanostatic mode from a citrate–borate electrolyte.⁸ The pH was adjusted to 5.0, 6.7 or 8.0 by the addition of concentrated H₂SO₄ or NaOH. The plating temperature was kept at 20 and 60 °C to observe the influence of temperature on the process of nucleation and properties of coatings.



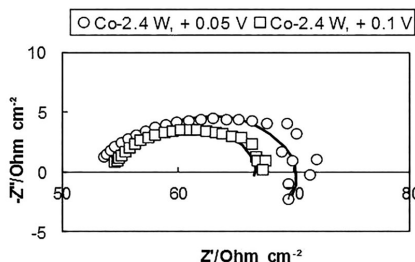
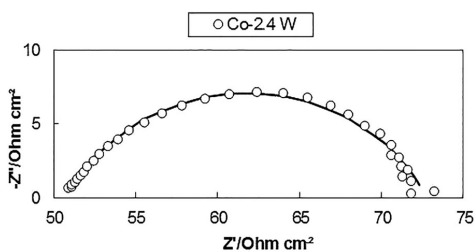
6 Equivalent circuits used for EIS fitting; R1 is solution (uncompensated) resistance; R2 is charge transfer resistance (having meaning of corrosion resistance); CPE1 is a constant phase element having meaning of the capacity of double electric layer on the electrode; R3 and CPE2 are related to adsorption of reaction intermediate resistance and capacitance, respectively; L1 is inductance

Electrochemical corrosion measurements of coatings obtained were performed in 0.01 M H₂SO₄ solution at 23 ± 1°C. The solution was open to air. The exposed area of the sample was 1 cm². In order to estimate the repeatability of corrosion currents and EIS parameters the measurements have been performed on parallel samples obtained under the same conditions. The average fluctuations of corrosion parameters were in the range of ±15%.

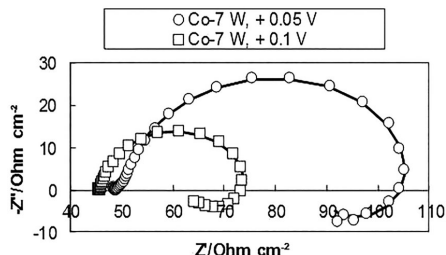
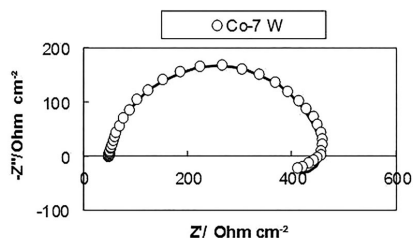
Results and discussion

Content and structure of alloys

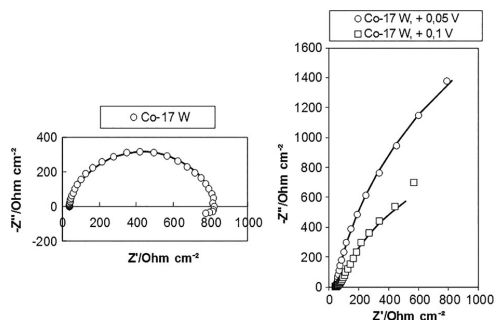
The content of solutions, current densities, and content of obtained alloys are providing in Table 1. The authors considered the composition of the electrodeposited alloys as fractions of metallic phases only, although the presence of oxygen was detected, and this has been discussed recently.¹⁸



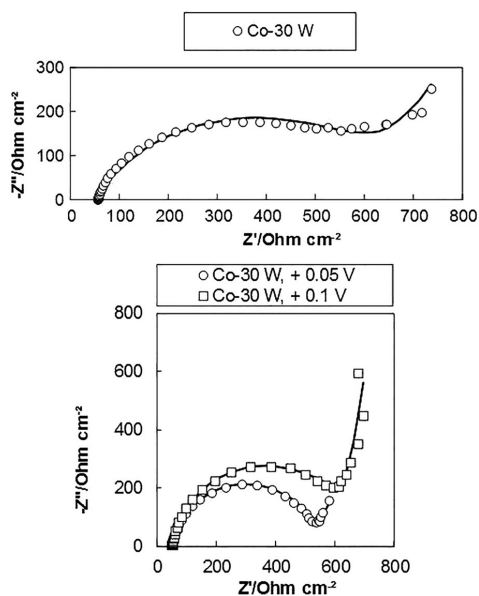
7 Nyquist plots for Co–2.4 at.-% W coatings deposited at 60°C at OCP, equivalent circuit is shown in Fig. 6a; at 0.05 and 0.10 V from OCP, equivalent circuit is shown in Fig. 6b



8 Nyquist plots for Co–7 at.-% W coatings deposited at 60°C at OCP, equivalent circuit is shown in Fig. 6b; at 0.05 V from OCP, equivalent circuit is shown in Fig. 6c; at 0.10 V from OCP, equivalent circuit is shown in Fig. 6b



9 Nyquist plots for Co–17 at.% W coatings deposited at 60°C at OCP, equivalent circuit is shown in Fig. 6c; at 0.050 V from OCP, equivalent circuit is shown in Fig. 6e; at 0.10 V from OCP, equivalent circuit is shown in Fig. 6e



10 Nyquist plots for Co–30 at.% W coatings deposited at 60°C at OCP, equivalent circuit is shown in Fig. 6d; at 0.05 V from OCP, equivalent circuit is shown in Fig. 6d; at 0.10 V from OCP, equivalent circuit is shown in Fig. 6d

Some representative SEM images of electrodeposits are shown in Fig. 1, in which the influence of the solution temperature and current density on pure Co and Co–W coating morphology is evident. It is seen that morphology evolves from coarse-grained lenticular growth (content of W is 0–8 at.-%) to nodular growth (content of W > 8 at.-%). Moreover, the tungsten presenting in the alloy modifies the crystallographic texture to nanocrystalline ('amorphous-like'). In detail, the structure of Co–W alloys electrodeposited at 60°C is discussed in the authors' previous studies.^{8,18} However, it should be noticed, that alloys electrodeposited at 20°C become 'amorphous-like' with lower content of W, i.e. above 13 at.-%, that was not detected in our previous studies, and XRD spectra for comparison of alloys containing 14 at.-% W but

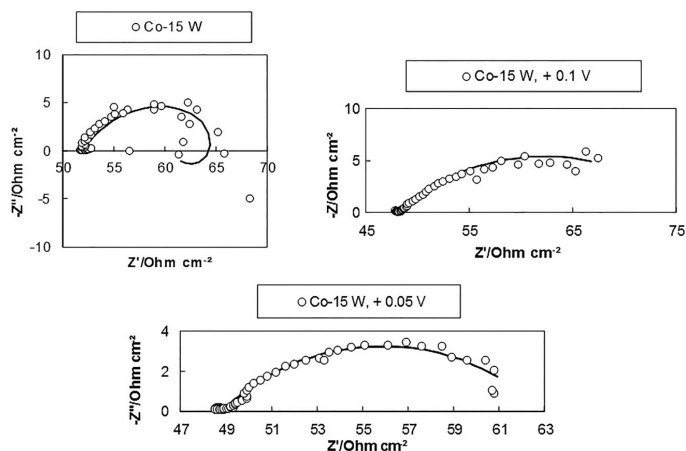
electrodeposited at various temperatures are presented in Fig. 2.

The mean grain size as a function of the tungsten content estimated from XRD data by using Scherrer's equation is shown in Fig. 3. The grain size depends rather on the tungsten content than on the electrodeposition conditions. A transition from a relatively coarse grain size of ~20 to 3–6 nm occurs in a narrow range of tungsten content, namely between 18 and 20 at.-% W. That tungsten range corresponds to the tungsten content range where the dominating phase is the intermetallic Co_3W compound. Electrodeposited Co–W coatings with the smallest grain sizes have a bright appearance.

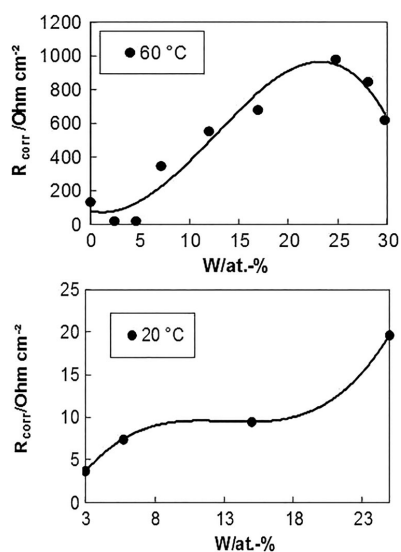
Corrosion

Voltammetric studies for Co–W alloys and compared with cast Co and W were carried out to evaluate the actual corrosion rate. Some representative curves for Co–W alloys obtained at 60°C are presented in Fig. 4. As is seen, the corrosion potential (or so-called 'OCP') is located in the range from –0.40 to –0.18 V and does not show any gradual tendency as a function of alloy composition. This is not surprising, because it is driven by the rates of cathodic and anodic reactions and at these potentials the rates of both reactions are equal. In the studied case, the cathodic reaction is hydrogen evolution reaction, and the anodic reaction is the rather active electrolytic dissolution, because sufficient current drops in the anodic part of voltammogram caused by the transferring into passive state were not detected. The rates of both reactions depend on the corrosion media, and chemical composition of electrode material. Furthermore, the rate of hydrogen evolution reaction depends on the state of the surface. Thus, due to the different hydrogen overvoltage on variously obtained Co–W alloys the corrosion potential may vary over some range without correlation with corrosion rate.

Usually the corrosion current is determined by the extrapolation current from the Tafel region to corrosion potential. However, as is shown in Fig. 4, this procedure might be applied for electrodeposited pure Co and Co–W alloys containing low content of tungsten (up to 7 at.-%). When the contents of tungsten in the Co–W alloys are higher the voltammograms are asymmetric. In these cases each curve was transformed into Allen-Hickling coordinates that enable a corrosion rate to be estimated using a narrow range of potentials. In detail, this method is described previously.¹⁹ The shapes of voltammograms for Co–W alloys electrodeposited at 20°C are similar but placed in the range of higher current densities that result in higher corrosion current densities. The dependencies of corrosion current densities for Co–W alloys are summarised in Fig. 5. As is seen, the lowest corrosion currents are obtained for Co–W alloys electrodeposited at 60°C, because those electrodeposited at room temperature are cracked and can be easily stripped off mechanically. The lowest corrosion current density was observed for Co–25 at.-% W alloy coating, which is slightly lower than that of the Co–17 at.-% W coating, i.e. in the range of contents where thermodynamically stable intermetallic compound Co_3W is formed.¹⁸ By increasing the tungsten content from 23 to 25 at.-%, corrosion current densities increase and this can be related to the change of alloy structure (from crystalline to 'amorphous-like'). The results showed that the Co–W alloy



11 Nyquist plots for Co–15 at.% W coatings deposited at room temperature at OCP, equivalent circuit is shown in Fig. 6b; at 0.05 V from OCP, equivalent circuit is shown in Fig. 6a; at 0.10 V from OCP, equivalent circuit is shown in Fig. 6a



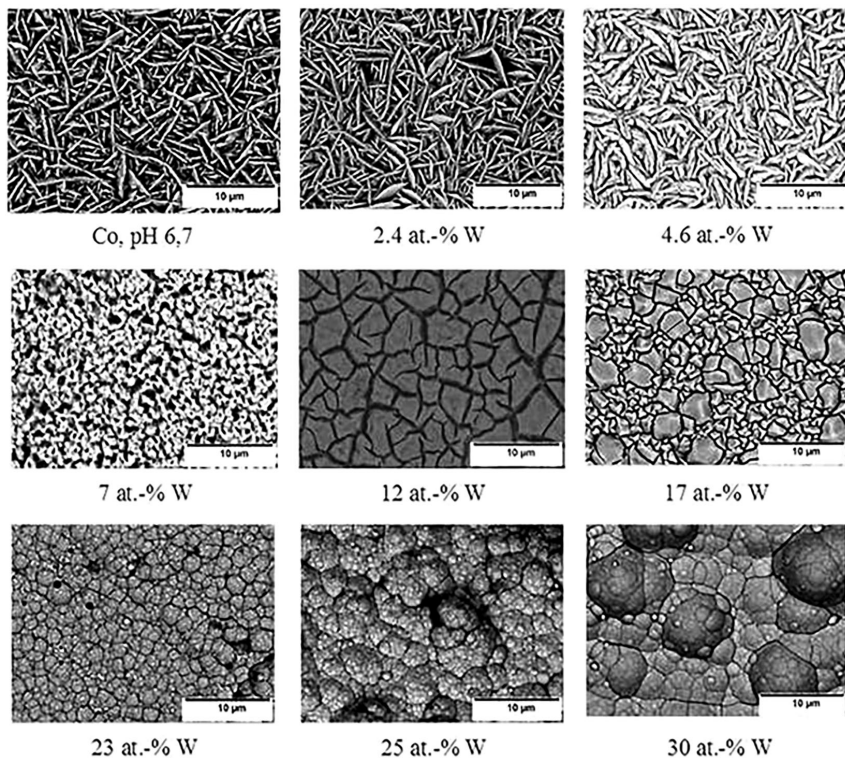
12 Effect of the tungsten content in the alloy on the corrosion resistance of the Co–W coatings, deposited at 60 and 20 °C temperature

coatings having more than 5 at.% W can protect the substrates from corrosion better than the Co deposit.

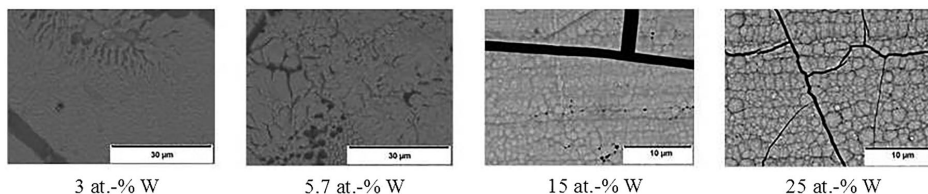
In order to investigate corrosion processes in more depth, the study by nondestructive EIS, was performed at OCP and during anodic polarisation of 0.05 and 0.10 V vs. corresponding OCP. The interpretation of EIS data is built upon a reaction model (or equivalent circuit) consisting of passive elements connected in some order. Regardless of the variety of electrode processes (deposition and corrosion of metals, electroreduction of ions, oxide film formation, adsorption phenomena, etc.) they contain similar stages and comprise similar processes such as formation of double electric layer, the presence of ohmic resistance, charge

transfer resistance of electrochemical reaction or corrosion resistance, adsorbed layers formed by intermediates of complex electrochemical reactions either by protective films, diffusion (transport phenomena) in solutions and in the organic or polymeric films, etc. With the equations of the model it is then possible to calculate the electrochemical impedance as a function of frequency and check conformity of experimental data to the theoretical model. When the electrode reaction involves only simple charge transfer, the electrode resistance is represented by R_{ct} , and the electrochemical impedance is analysed by the Randles circuit,²⁰ (see Fig. 6a). In this case the Nyquist plot contains only a single capacitance arc. Analysis of the ac impedance spectra in the presence of specific adsorption revealed that the complex plane showed formation of deformed semicircles, that might be described by introducing into the equivalent circuit a constant phase element (CPE). When the metal dissolution involves a reaction intermediate, the electrode resistance has the time constant in the dissolution process and is expressed as the frequency-dependent resistance related to a complicated electrode reaction $Me \rightarrow Me(I)_{ad} \rightarrow Me(II)$ such as iron in H_2SO_4 solution.²¹ It was shown that under some kinetic parameters the Faradaic impedance changes sign and an inductive loop appears.²² This inductive loop, appearing at low frequencies, is most probably caused by the relaxation of adsorbed electrochemical species. Some of the characteristics obtained during EIS in Nyquist coordinates and fitting results to corresponding equivalent circuits (shown in Fig. 6) for alloys electrodeposited at 60 °C are presented in Figs. 7–10, that validate the model describing the corrosion processes. Co–W alloys deposited at room temperature were investigated as well but as the adhesion is very poor and no good fitting curves were obtained (see Fig. 11). Thus, EIS reveals that corrosion of Co and Co–W alloys occurs via an intermediate adsorption stage.

The values of corrosion resistance (R_{corr}) for Co–W alloys were extracted from fitting results as a value of R_2 . The EIS analysis indicated that the maximum value of impedance was obtained at 24.8 at.% W in Co–W alloy (see Fig. 12). Based on the XRD data published



13 SEM micrographs of the Co–W alloy, deposited at 60°C temperature, after corrosion test in H₂SO₄ at the polarisation at +0.10 V



14 SEM micrographs revealing the Co–W alloy, deposited at 20°C temperature, structure morphology after corrosion test in H₂SO₄ solution at the polarisation at +0.10 V

and analysed elsewhere,^{3,8,18} for Co–W alloys the deposit has a corrosion resistance maximum corresponding to transition from polycrystalline to nanocrystalline ('amorphous-like') structure.

SEM images were taken after the corrosion test in H₂SO₄ solution at the polarisation at +0.1 V for Co–W alloys electrodeposited at 60°C, and are shown in Fig. 13. When the tungsten content in the alloy is lower than 5 at.-%, the deposit layer does not show significant change in the microstructure and is characterised by sub-micron fibre morphology. When the tungsten content in the alloy is higher, the coatings show visible defects and cracks are formed. It is clearly seen that the propagation of cracks is along the grain boundaries.

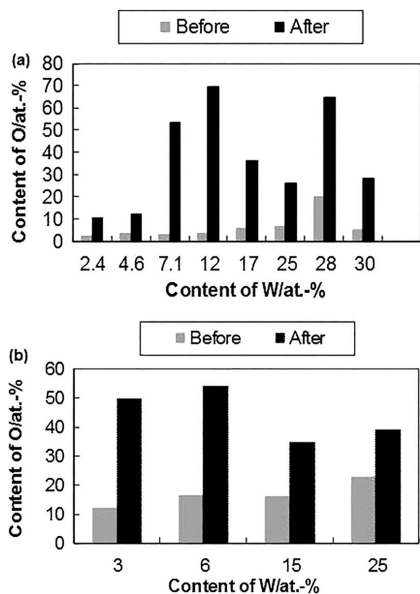
The morphologies of Co–W alloys obtained at room temperature after the corrosion test show dramatic

changes (Fig. 14): the surface becomes rough and full of minor cracks.

Investigations by EDS showed that the oxygen content in the alloy significantly increases after the corrosion experiments (see Fig. 15). This indicates that the electrochemical corrosion process occurs via an intermediate stage of forming oxide-containing compounds on the surface.

As follows from the EIS data, the capacitance of the double electric layer (CPE1) and values of index n close to 1 (see Table 2) allow calculating the thickness of the adsorbed oxide layer. As is seen, the double layer capacitance varies in the wide range, but evidently these values for alloys electrodeposited at 20°C are much higher.

The thickness of the oxide layer and capacitance might be expressed by the equation applied for a planar



15 The relation between the tungsten content in Co–W alloy and the oxygen atomic percentage in the deposits before and after corrosion test in 0.01 M H₂SO₄; Co–W alloys were electrodeposited at 60°C a and at 20°C b

capacitor:

$$C = \epsilon_r \epsilon_0 \frac{S}{d}$$

where d is the thickness of the oxide layer (m), C is the capacitance of the oxide layer (F), S is the surface area (m²), ϵ_0 is the electric constant ($\epsilon_0 \approx 8.854 \times 10^{-12}$ F m⁻¹); ϵ_r is the dielectric constant of Co and W oxides.

Because the dielectric constants of Co and W significantly differ, the total ϵ_r was calculated using the following equation:

$$\epsilon_r = X_{Co} \epsilon_{CoO} + X_W \epsilon_{WO_3}$$

where X_{Co} and X_W are atomic fractions of Co and W in the alloy, respectively.

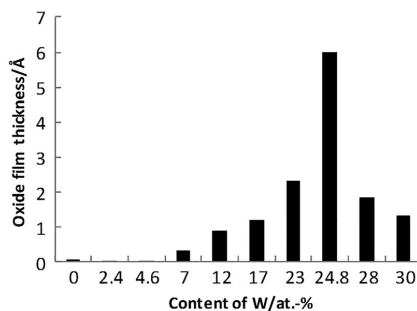
Taking $\epsilon_r = 12.9$ for CoO and $\epsilon_r = 300$ for WO₃ it was estimated that the thickness of oxide layer varies from 0.02 to 6 Å when tungsten content in the alloy increases from 2.4 to 24.8 at.-%, respectively (see Fig. 16). Such values are close to the thickness of the monolayer of oxides. With a further increase of tungsten content in the alloy, the thickness of oxide layer on the Co–W alloy surface decreases. Increasing the tungsten content in the alloy up to ~25 at.-% leads to the formation of thicker oxide layer on the coating.

Conclusions

Nanocrystalline Co–W coatings with 0–30 at.-% W were obtained from citrate–borate electrolyte at pH 5.0, 6.0, 6.7 and 8. Alloys electrodeposited at 60°C become ‘amorphous-like’ when W content exceeds 20 at.-%, whereas when deposited at 20°C they gave lower content of W,

Table 2 Extracts from EIS spectra values of CPE and index n attributed to the capacity of double electric layer for Co, W and Co–W alloys

Coating	CPE1-T/F cm ⁻²	CPE1-P
<i>Electrodeposition at 60°C</i>		
Co–2.4 W, OCP	5.20×10^{-3}	0.728
Co–2.4 W, +0.05 V	3.32×10^{-2}	0.600
Co–2.4, +0.10 V	3.12×10^{-2}	0.633
Co–4.6 W, OCP	9.96×10^{-3}	0.712
Co–4.6 W, +0.05 V	2.67×10^{-2}	0.678
Co–4.6 W, +0.10 V	3.38×10^{-2}	0.604
Co–7 W, OCP	3.15×10^{-4}	0.861
Co–7 W, +0.05 V	6.26×10^{-3}	0.824
Co–7 W, +0.10 V	1.43×10^{-2}	0.943
Co–12 W, OCP	1.58×10^{-4}	0.899
Co–12 W, +0.05 V	4.92×10^{-3}	0.842
Co–12 W, +0.10 V	3.73×10^{-3}	0.7919
Co–17 W, OCP	2.15×10^{-4}	0.738
Co–17 W, +0.05 V	1.23×10^{-3}	0.8534
Co–17 W, +0.10 V	9.00×10^{-4}	0.6854
Co–24.8 W, OCP	2.00×10^{-4}	0.809
Co–24.8 W, +0.05 V	5.73×10^{-5}	0.859
Co–24.8 W, +0.10 V	5.67×10^{-4}	0.912
Co–28 W, OCP	3.69×10^{-4}	0.866
Co–28 W, +0.05 V	4.58×10^{-4}	0.895
Co–28 W, +0.10 V	5.40×10^{-4}	0.922
Co–30 W, OCP	5.19×10^{-4}	0.726
Co–30 W, +0.05 V	7.27×10^{-4}	0.912
Co–30 W, +0.10 V	8.16×10^{-4}	0.923
<i>Electrodeposition at 20°C</i>		
Co–3 W, OCP	3.40×10^{-1}	0.666
Co–3 W, +0.05 V	4.13×10^{-2}	0.557
Co–3 W, +0.10 V	3.89×10^{-2}	0.634
Co–5.7 W, OCP	3.20×10^{-2}	0.655
Co–5.7 W, +0.05 V	5.37×10^{-2}	0.683
Co–5.7 W, +0.10 V	4.99×10^{-2}	0.616
Co–15 W, OCP	6.31×10^{-2}	0.654
Co–15 W, +0.05 V	7.05×10^{-2}	0.554
Co–15 W, +0.10 V	6.98×10^{-2}	0.459
Co–25 W, OCP	4.74×10^{-2}	0.583
Co–25 W, +0.05 V	7.13×10^{-2}	0.678
Co–25 W, +0.10 V	3.74×10^{-3}	0.701



16 Effect of tungsten content in Co–W alloys on oxide layer thickness forming at the polarisation +0.10 V; Co–W alloys were deposited at 60°C

i.e. above 13 at.-%. However, alloys electrodeposited at 20°C show poor resistance to corrosion.

Co–W alloys possessing highest corrosion resistance should be deposited at 60°C and contain 17–24 at.-% of W, i.e. have a structure close to the intermetallic phase Co₃W. The corrosion occurs via an intermediate

adsorbed stage by forming oxygen-containing compounds; the estimated thickness of the adsorbed layer varies in the range 0–1.6 Å.

Acknowledgements

The authors acknowledge funding from HORIZON2020 SELECTA project (642642) and FP7 Oil & Sugar project (295202). Also, partial funding was granted by the Research Council of Lithuania (MIP-031/2014) and Moldavian national projects (15.817.02.05A).

References

1. E. Lassner and W. D. Schubert: 'Tungsten – properties, chemistry, technology of the element, alloys, and chemical compounds', 1999, New York, Springer.
2. N. Eliaz and E. Gileadi: 'Induced codeposition of alloys of tungsten, molybdenum and rhenium with transition Metals', in 'Modern aspects of electrochemistry', Vol. 42, 191–301; 2008, New York, Springer.
3. N. Tsyntsaru, H. Cesiulis, M. Donten, J. Sort, E. Pellicer and E. J. Podlaha-Murphy: *Surf. Eng. Appl. Electrochem.*, 2012, 48, 491–520.
4. N. Sulitanu and F. Brinza: *J. Optoelectron. Adv. Mater.*, 2003, 5, 421–427.
5. N. Sulitanu: *J. Magn. Magn. Mater.*, 2001, 231, 85–93.
6. N. V. Myung, D. Y. Park, B. Y. Yoo and P. T. A. Sumodjo: *J. Magn. Magn. Mater.*, 2003, 265, 189–198.
7. H. H. Yang, N. V. Myung, J. Lee, D. Y. Park, B. Y. Yoo, M. Schwartz, K. Nobe and J. W. Judy: *Sens. Actuators A*, 2002, 97–98, 88–97.
8. N. Tsyntsaru, H. Cesiulis, E. Pellicer, J. P. Celis and J. Sort: *Electrochim. Acta*, 2013, 104, 94–103.
9. O. Bersirova, H. Cesiulis, M. Donten, A. Krolkowski, Z. Stoek and G. Baltrunas: *Physicochem. Mech. Mater.*, 2004, 4, 620–625.
10. V. A. Safonov, L. N. Vykhodtseva, A. A. Edigaryan, A. D. Aliev, E. B. Molodkina, A. I. Danilov, E. N. Lubnin and Y. M. Polukarov: *Russ. J. Electrochem.*, 2001, 37, 127–134.
11. J. Sinkeviciute: 'Corrosion study of electrodeposited W and Mo alloys with iron group metals', PhD Thesis, University of Vilnius, Vilnius, Lithuania, 2009, 112.
12. A. Królikowski, E. Płońska, A. Ostrowski, M. Donten and Z. Stojek: *J. Solid State Electrochem.*, 2009, 13, 263–275.
13. H. Cesiulis, J. Sinkeviciute, O. Bersirova and P. Ponthiaux: 'Tribocorrosion testing of self-passivating molybdenum and tungsten alloys containing cobalt and iron', Proceedings of Int. Conf. BALTRIB' 2009, Kaunas, Lithuania, 2009, 253–258.
14. M. G. Hosseini, M. Abdolmaleki, H. Ebrahimzadesh and S. A. Seyed Sadjadi: *Int. J. Electrochem. Sci.*, 2011, 6, 1189–1205.
15. N. Tsyntsaru, A. Dikusar, H. Cesiulis, J. P. Celis, Z. Bobanova, S. Sidel'nikova, S. Belevskii, Y. Yapontseva, O. Bersirova and V. Kublanovskii: *Powder Metall. Met. Ceram.*, 2009, 48, 419–428.
16. V. Kublanovsky, O. Bersirova, A. Dikusar, Z. Bobanova, H. Cesiulis, J. Sinkeviciute and I. Prosycevas: *Physicochem. Mech. Mater.*, 2008, 7, 308–314.
17. H. Cesiulis and A. Budreika: *Physicochem. Mech. Mater.*, 2010, 8, 808–814.
18. N. Tsyntsaru, H. Cesiulis, A. Budreika, X. Ye, R. Juskenas and J. P. Celis: *Surf. Coat. Technol.*, 2012, 206, 4262–4269.
19. H. Cesiulis and J. Sinkeviciute: *Physicochem. Mech. Mater.*, 2004, 4, 128–132.
20. M. Sluyters-Renbach: *Pure Appl. Chem.*, 1994, 6, 1831–1891.
21. M. Itagaki, M. Tagaki and K. Watanabe: *Electrochim. Acta*, 1996, 41, 1201–1207.
22. M. Itagaki, A. Tava, K. Watanabe and K. Noda: *Anal. Sci.*, 2002, 18, 641–644.
23. M. S. Halper and J. C. Ellenbogen: 'Supercapacitors: a brief overview'; 2006, McLean, Virginia, Mitre.

Article V

**Electrochemical co-deposition of tungsten with cobalt and copper:
peculiarities of binary and ternary alloys coatings formation**

E.Vernickaite, N. Tsyntsaru, H. Cesiulis

Surface & Coatings Technology, 307 (2016) 1341–1349



Electrochemical co-deposition of tungsten with cobalt and copper: Peculiarities of binary and ternary alloys coatings formation



E. Vernickaite^a, N. Tsyntsaru^{a,b,*}, H. Cesiulis^a

^a Vilnius University, Naugarduko str. 24, Vilnius, Lithuania

^b Institute of Applied Physics of ASM, 5 Academy str., Chisinau, Republic of Moldova

ARTICLE INFO

Article history:

Received 31 March 2016

Revised 5 July 2016

Accepted in revised form 8 July 2016

Available online 9 July 2016

Keywords:

Tungsten co-deposition

Copper-tungsten alloys

Potentiostatic mode

Ternary alloys

ABSTRACT

Binary Cu-W, Co-W and ternary Co-Cu-W alloy coatings were electrochemically deposited onto stainless steel substrate from a citrate-borate electrolyte under potentiostatic mode at 20 and 60 °C. The cathodic polarization, current efficiency of co-deposition, chemical composition and structure of the prepared alloys as a function of deposition potential and temperature were studied and compared to those of binary Cu-W and Co-W alloys. All deposits were of uniform thickness, without cracks and well adhered to the substrate. The cathodic current efficiency increases with the bath temperature and cathodic deposition potential increase. The polarization studies revealed that Cu-W alloy deposition starts at more negative potentials than those of Co-W and Co-Cu-W that leads to the lowest current efficiency for Cu-W (20%) in comparison with up to ~90% obtained for Co-Cu-W and Co-W alloys electrodeposition. Also, this results in the low W content in the Cu-W coatings (<6 at.%) that strongly depends on deposition potential and bath temperature. The morphology of deposited coatings depended rather on electrodeposition conditions than on W content in the alloys. X-ray diffraction analysis indicated that Cu-W alloy is a solid solution with typical Cu-type face centered cubic (fcc) lattice. Introduction of Co into this alloy resulted in the formation of additional hexagonal (hcp) Co XRD patterns for ternary Co-Cu-W alloy.

© 2016 Elsevier B.V. All rights reserved.

1. Introduction

Nanocrystalline metal alloys are of special interest in the materials science due to their enhanced strength, superior hardness, magnetic properties and corrosion resistance [1–4]. Such alloys have become an important component in microelectromechanical systems (MEMS) [5], for wear protection of cutting tools and for the reduction of friction in sliding parts [6]. Mechanical alloying, sputtering and vapor deposition have been common methods to produce nanocrystalline materials. However, since the late 1980s electrodeposition has been moved into the commercial production because of its simplicity and low cost in comparison with the other methods [7]. There are large number of pure metals, alloys and composites that can be electrodeposited with grain size below 100 nm: Ni [8], Co [4], Cu–Ni [9], Ni–W [10,11], Co–W [8,11], Fe–W [11], Ni–Co [4], Ni–Fe [8], Co–Cu [12], Ni–Fe–W [11], Co–W–P [8], etc. Among them, tungsten alloys are very promising because of their satisfactory appearance, mechanical, magnetic and anti-corrosion properties [13,14]. In a large number of works, it was shown that the hardness of the nanocrystalline Co–W alloy coatings increases with decreasing grain size and increasing W content in the alloy.

Accordingly, an increase of W content in the alloy significantly improves the corrosion resistance of the nanocrystalline Co–W coatings [15]. Tungsten content in its turn depends on the current density [16–18], the bath pH and temperature [13].

For the first time the phenomenon of co-deposition of tungsten with copper was noted by Vasko [19] and first quantitative data reported in [20]. This Cu–W alloy is the fourth known electrodeposited binary alloy of tungsten with a non-iron-group metal. Cu–W thin films can be very useful for engineering applications because they may provide the combination of good electrical conductivity, ductility, wear resistance, low expansion coefficient and excellent strength [21]. Accordingly, it can be used in manufacture of heavy-duty electrical contacts, resistance welding electrodes, heat sinks, shaped charge liners, vacuum switches, contact tips, etc.

It is known, that the introduction of the third element to a binary system can affect its chemical and structural properties and, thus improve their mechanical properties. It was indicated, that generally W content in the ternary deposits increases with an increase in its content in the bath and with an increase in pH, temperature, and current density [22,23]. The nodular Ni–W–Co alloy surface show a substantial decrease in microcracks compared to those of Co–W deposit. Fe addition into the Ni–W alloy effectively reduces the tensile stress in the electrodeposited layers. Furthermore, the experimental results indicate that Fe–Ni–W alloy deposits have higher wear resistance under dry sliding condition than hard chromium deposits [24]. The Ni–Fe–W coating having

* Corresponding author at: Vilnius University, Naugarduko str. 24, Vilnius, Lithuania.
E-mail address: tintaru@phys.asm.md (N. Tsyntsaru).

Table 1

Composition of the baths used for electrodeposition of Cu-W, Co-W and Co-Cu-W alloys.

Reagents	Concentration, mol·l ⁻¹		
	Cu-W alloy	Co-W alloy	Co-Cu-W alloy
CuSO ₄ ·5H ₂ O	0.05	–	0.05
CoSO ₄ ·7H ₂ O	–	0.2	0.2
Na ₂ WO ₄ ·2H ₂ O	0.2	0.2	0.2
C ₆ H ₈ O ₇ (citric acid)	0.04	0.04	0.04
H ₃ BO ₃	0.65	0.65	0.65
Na ₃ C ₆ H ₅ O ₇ ·2H ₂ O (tri-sodium citrate dihydrate)	0.25	0.25	0.25

20 at.% of W shows improved mechanical properties [25]. Meanwhile the values of resistance to corrosion for ternary alloy coatings were lower compared to those of the Ni–W alloy coatings due to preferential dissolution of iron from the matrix [11]. Meanwhile the hardness of the Co–Fe–W alloys containing 30 wt.% of Fe was close to that of electrodeposited chromium and its corrosion resistance was much better [26]. Besides, it was showed that Co–Fe–W alloys are potential materials for applications in magnetic devices such as read/write heads and hard disks [27].

Therefore, we can anticipate that merging the properties of Co-W and Cu-W alloys in one alloy via the electrodeposition of Co-Cu-W ternary alloy can create a new material to be considered. The main objectives of this research was to electrodeposit Cu-W, Co-W and Co-Cu-W alloy coatings onto stainless steel substrates from non-toxic citrate bath and to study the influence of deposition parameters on cathodic polarization, cathodic current efficiency, composition and structure of the alloys. Non-volatile citrate electrolytes are attractive for long-term electrodeposition at higher temperatures [28], therefore they were chosen for W co-deposition with Cu and Co.

2. Material and methods

Co-W, Cu-W and Co-Cu-W deposits were electrodeposited onto stainless steel (type 304) substrates having low roughness (mean value $R_a = 12$ nm) from citrate-borate electrolytes under potentiostatic mode. The compositions of the plating baths are given in Table 1. Pure Co and Cu were also electrodeposited from the similar electrolyte without sodium tungstate for the comparison with the alloys electrodeposition. CuSO₄·5H₂SO₄, CoSO₄·7H₂SO₄ and Na₂WO₄·2H₂SO₄ were used as the sources of copper, cobalt and tungsten, respectively. Non-toxic tri-sodium citrate was used as a complexing agent. In addition, it was chosen because of its brightening and buffering actions. Boric acid

considerably improves the stability of the bath. The pH of the solution was adjusted to 6.7 ± 0.1 by adding concentrated solutions of NaOH or H₂SO₄. This value of pH is convenient for study, because this value is settled exactly after mixing of the components of solution, and was used in previous work [28]. The temperature of electrolyte was maintained at 20 and 60 ± 2 °C by means of a water bath.

Electrodeposition was performed in a standard three-electrode cell. A platinum mesh was used as a counter and saturated Ag/AgCl as reference electrodes, respectively. All potentials in this paper are given with respect to the saturated Ag/AgCl electrode. Before the electrodeposition the stainless steel substrates were washed with detergent and rinsed with water and acetone using ultrasonic to remove any contaminants from the surface. In order to improve the adhesion of alloys to the substrates, a nickel seed layer was electrodeposited from an electrolyte containing 1 M NiCl₂ and 2.2 M HCl, at a cathodic current density of $10 \text{ mA} \cdot \text{cm}^{-2}$ for 1 min.

The thickness of the coatings was calculated based on gravimetric and elemental analysis results, and was $\sim 10 \mu\text{m}$. The cathodic current efficiencies (CE) were determined based on charge passed, the mass and chemical composition of the deposited alloys using Faraday's law.

The morphological structure and adhesion by folding of the coatings were examined by scanning electron microscopes (SEM) using Hitachi TM3000 and high resolution Hitachi SU-70 instruments. The chemical composition of the alloys was determined with an energy dispersive X-ray spectroscopy (EDS) analysis tool attached to the Hitachi SU-70. EDS analysis was taken over the entire field of view sized at $4000 \times$ with an accelerating voltage of 20 kV. The crystallographic structure of the alloys was studied by X-ray diffraction method using Rigaku MiniFlex II diffractometer using Cu K_α radiation ($\lambda = 1.54183 \text{ \AA}$) at a constant scan speed in the range of 2θ from 30° to 100° at a 0.01° step and counting time of 540 s. The values of grain size were calculated based on the broadening of XRD peaks using Sherrer's equation.

3. Results and discussion

3.1. Cathodic polarization curves

Deposition potential is one of the key factors in the electrodeposition process because it influences the changes in alloy composition and quality of the obtained coatings [29]. Accordingly, the suitable cathodic potentials for electrodeposition for Cu-W, Co-W and Co-Cu-W coatings were selected based on the polarization curves. Fig. 1 shows the cathodic polarization curves for individual metals deposition and for the co-deposition of W alloys at 20 °C and 60 °C from their respective plating solutions given in Table 1. Note, the curves indicated as W, in fact

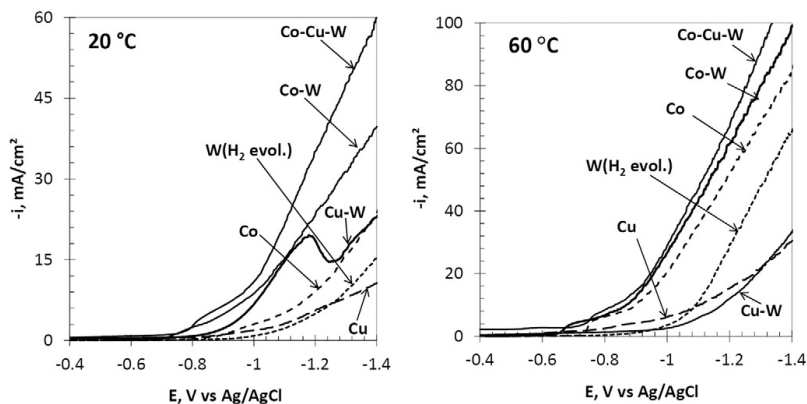


Fig. 1. Cathodic polarization curves for Co, Cu, W (H₂) reduction, and Cu-W, Co-W, Co-Cu-W alloys co-deposition at 20 °C and 60 °C.

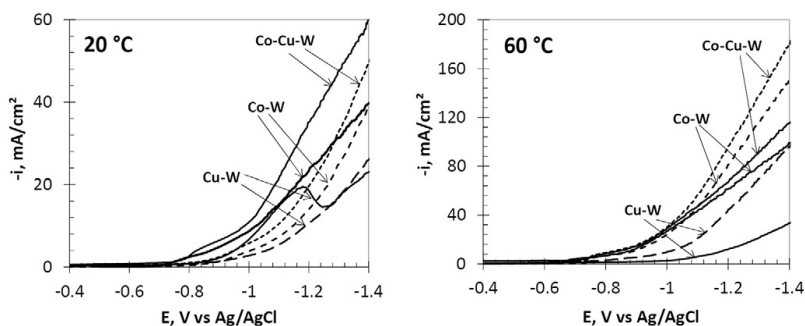


Fig. 2. Calculated (dashed lines) and experimentally obtained (straight lines) cathodic polarization curves for Cu-W, Co-W, Co-Cu-W alloys co-deposition.

represent hydrogen evolution only, because pure W cannot be deposited from aqueous sodium tungstate solutions as well as no tungsten oxides formation was observed. In this case, the current density increases with an increase in cathodic potential mainly due to the reduction reaction of hydrogen ions that result in H₂ evolution. The polarization curves presented in Fig. 1 indicate that Co is electrodepositing as more noble metal than Cu in the present complex system, because the curve for pure Co lies at the more positive potentials than for pure Cu. Thus, it is expected that Cu, being less noble metal in this complex solution, will be deposited preferentially in the ternary Co-Cu-W alloy. It was also found that the polarization curves after introducing of WO_4^{2-} ions into plating solution at 20 °C demonstrates a depolarization effect and the currents at the same potential are higher compared to those of pure metal deposition because of tungsten co-deposition and lower hydrogen overvoltage on the tungsten alloys. All polarization curves obtained at 20 °C have a similar shape, except in the case of Cu-W alloy, at potentials below -1.15 V the current density does not increase the same way as it did for other investigated electrolytes. The obtained maximum of resulting current density might be attributed to the particular sum of partial current densities of Cu, W and H₂ and their influence on each other in the vicinity of the potential -1.15 V. As it can be clearly seen, the bath temperature has a strong effect on the polarization curves and, consequently, on the co-deposition process. The current density shifts to the higher value with increase in the temperature from 20 to 60 °C. During the electrochemical process at elevated temperature, the curves for Co-W and Co-Cu-W alloys co-deposition are almost identical as for pure Co deposition. This observation is in agreement with the data reported in the literature in which the difference between the deposition of the W alloy and the iron-group metals is very small (about 15 mV) [30]. The curves for pure Cu deposition and Cu-W co-deposition also are positioned close to each other. It is clearly seen that the

polarization curves for Cu-W electrodeposition at both temperatures are shifted towards more negative potential values compared to those of Co-W and Co-Cu-W, and thus the fraction of tungsten in Cu-W deposits is expected to be lower than that of Co-W and Co-Cu-W coatings. This shift leads to the increasing of the hydrogen evolution rate during the Cu-W electroplating.

The calculated polarization curves based on the independence of electrode reactions on each other for alloys co-deposition differ greatly from the corresponding experimental polarization curves for individual deposition (Fig. 2). It was depicted that Cu-W, Co-W and Co-Cu-W alloys co-deposition at 20 °C starts at more positive potentials than it is expected based on polarization curves for individual components of the alloys, indicating more pronounced anomalous co-deposition. Meanwhile, the calculated polarization curves for Co-W and Co-Cu-W co-deposition at 60 °C coincide closely with plateaus appearing during the experiments, especially at more positive potentials. In contrast, the electrodeposition of Cu-W at elevated temperature occurs at more negative potentials compared to those of calculated ones.

3.2. Elemental analysis of alloys

The dependence of the tungsten content in the electrodeposited Cu-W, Co-W and Co-Cu-W alloy coatings was investigated as a function of the cathodic potential. As it can be seen from Fig. 3, W content in all deposits obtained at 20 °C, increases gradually with the change of deposition potential from -0.7 to -1.0 V, and tungsten content remains almost constant at more negative cathodic potentials. Though, the tungsten content in the Cu-W deposits obtained at 20 °C in the whole range of cathodic potential was anomalously low, <1 at.% and the precise W amount in the coatings is rather difficult to quantify. Nevertheless, the XRD data (Fig. 11) depict the shift of diffraction peaks for Cu-W alloy

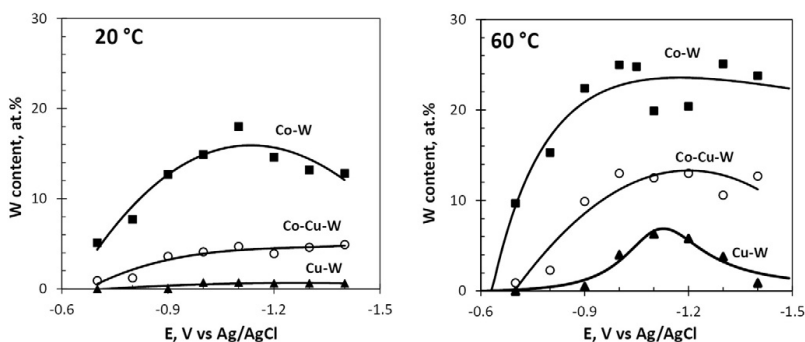


Fig. 3. Compositions of Cu-W, Co-Cu-W and Co-W alloys electrodeposited at 20 °C and 60 °C.

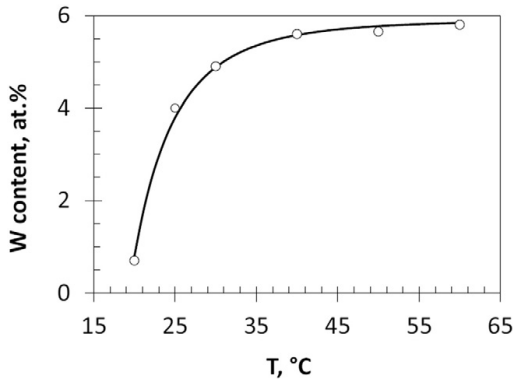


Fig. 4. Effect of bath temperature on tungsten content in the Cu-W alloy coating.

in comparison with pure Cu to lower 2θ that is linked with the presence of W in the alloy, and its incorporation into the Cu lattice.

After introduction of Co into the Cu-W alloy the content of W in the alloys increases (~4 at.%) and does not change with the increase in cathodic potential during the electrodeposition process, while the high content of tungsten even at low temperature was observed during Co-W alloy deposition (up to 18 at.%). It is known, that the bath temperature strongly affects the composition of the deposits. It was reported that the highest W content in the Co-W deposit was achieved at low temperature [18]. In contrary [13], it was found that the percentage of the tungsten in the alloy increases with increasing the bath temperature up to 50 °C. In this study, EDS analysis also exhibited an increase in the W content of Cu-W, Co-W and Co-Cu-W deposits with increase in the temperature of the electrolyte. In the case of Cu-W alloy, W content in the deposit obtained at higher temperature (60 °C) increases from 0.5 to 6 at.% in the cathodic potential range between -0.8 and -1.1 V, and reaches a maximum at -1.1 V, then slowly decreases to 0.9 at.% with increasing the cathodic potential from -1.1 to -1.4 V. Below -0.8 V only pure copper deposit was formed. The effect of the plating bath temperature on the Cu-W alloy electrodeposited at potential -1.1 V (there the highest W amount was observed) is shown in Fig. 4. It is apparent that with increasing the bath temperature from 20 to 40 °C tungsten content in the Cu-W alloy sharply increases from ~0.5 to 6 at.%. With the further increase of temperature the composition of Cu-W coating is almost the same and at 60 °C the W percentage in the deposits does not exceed 6 at.%. On the contrary, during the Co-Cu-W alloy deposition W content in the alloy continuously increases from 4 to 10 at.% in the whole investigated temperature range (Fig. 5). Meanwhile Cu content in the deposit gradually decreased and Co content in the deposit slightly increased with increasing bath temperature from 20 to 55 °C. With the further increase in bath temperature up to 60 °C, this tendency has been changed and Cu content in the ternary alloy increased up to 50 at.% and Co percentage decreased to 40 at.%. The relationship between W content in the Co-Cu-W alloy and applied cathodic potential at elevated temperature is given in Fig. 3. With the decrease in deposition potential from -0.7 to -1.0 V a significant increase in W percentage in the coating was observed and then it becomes almost stable regardless of the applied deposition potential value. It is seen, that a similar correlation between W amount and deposition potential was observed for Co-W alloy coatings obtained at 60 °C. Actually, in this case W content increases even more steeply in the cathodic potential ranged from -0.7 to -1.0 V.

According to the results mentioned above, an increase in cathodic potential leads to a growth in the tungsten content in the deposited coating. On the other hand, under the fixed potential, the content of the element in the alloy is dependent upon the composition of the

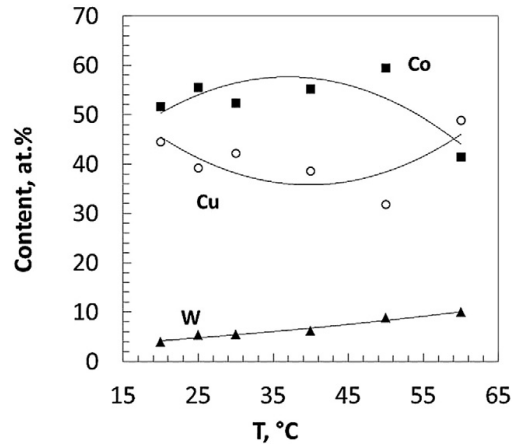


Fig. 5. Relationship between bath temperature and Co, Cu, W content (in at.%) in the Co-Cu-W alloy coatings obtained at -1.2 V.

electrolyte. So those experiments were also conducted at a fixed CoSO_4 and Na_2WO_4 concentrations in the presence of different Cu(II) ion concentrations in the plating solution in order to examine the effect of Cu co-deposition on ternary Co-Cu-W alloy formation at -1.1 V, as at this potential the highest content of W in Cu-W deposit was observed. The influence of Cu(II) at concentrations, ranging from 0.005 to $0.1 \text{ mol}\cdot\text{l}^{-1}$, while the concentrations of the other components maintained constant at $0.2 \text{ mol}\cdot\text{l}^{-1} \text{ CoSO}_4$ and $0.2 \text{ mol}\cdot\text{l}^{-1} \text{ Na}_2\text{WO}_4$ is presented in Fig. 6. It is shown that the Cu content in the deposit gradually increases almost linearly from 10 to ~60 at.% with the Cu(II) ion concentration in the electrolyte, in the range from 0.005 to $0.075 \text{ mol}\cdot\text{l}^{-1}$. The further increase in Cu(II) ion concentration in the solution does not affect the Co-Cu-W alloy composition. The increase of Cu(II) concentration in the electrolyte causes the decreasing of Co and W content in the deposits at a given potential. W content in the Co-Cu-W coatings obtained at 60 °C decreases 4 times with increasing the CuSO_4 concentration in the plating bath from 0 to $0.075 \text{ mol}\cdot\text{l}^{-1}$. Whereas in the same concentration range W percentage in the Co-Cu-W alloys deposited at 20 °C decreases up to 10 times.

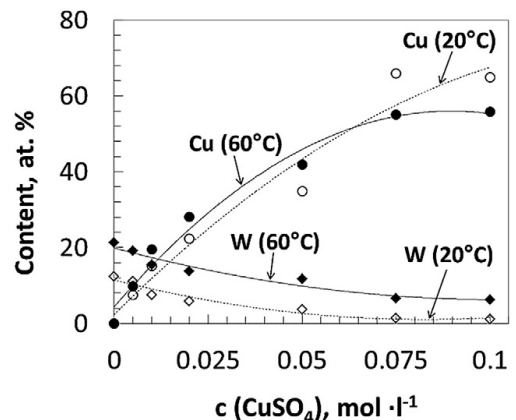


Fig. 6. Effect of CuSO_4 concentration on the tungsten content in the Co-Cu-W alloy coating. The dashed lines illustrate the composition of the coatings obtained at 20 °C and solid lines – at 60 °C.

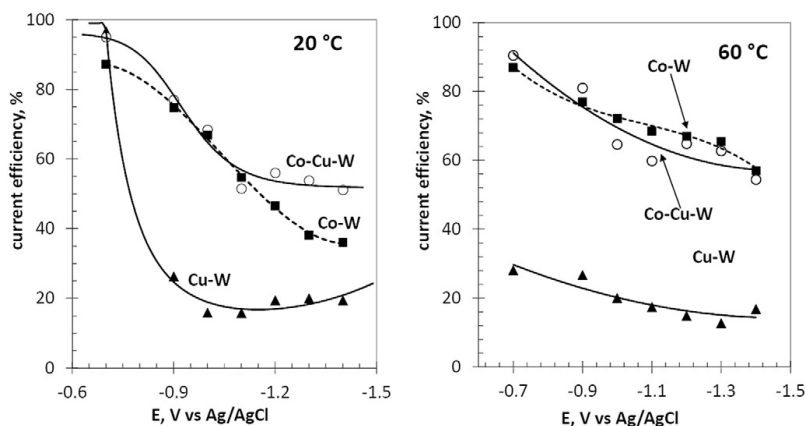


Fig. 7. Current efficiencies for the deposition of Cu-W, Co-Cu-W and Co-W alloys at 20 °C and 60 °C.

Usually, when W content in the Co-W deposits is in the range of 14–20 at.% the current efficiencies are close to 50% [31]. Meanwhile in [17] the maximal cathodic current efficiency as 27.5% was found when the W content in the deposit was 20 at.%. Then the higher W content (~30 at.%) in the alloy causes a lower overvoltage for hydrogen evolution and the current efficiency significantly decreases and in most cases does not exceed 20%. In this study, the results of the calculated cathodic current efficiencies for Cu-W, Co-Cu-W and Co-W alloy coatings electrodeposition at different temperatures are presented in Fig. 7. As it can be seen, that the higher temperature during electrodeposition positively influences the current efficiency of the metallic phase deposition processes. It seems that at elevated temperature the W transport to the cathodic surface is faster due to the higher mobility of the ions and lower viscosity of the plating solution, so that the co-deposition of W films is much easier [32]. Meanwhile in this work the current efficiency depends rather on the alloy composition rather than on the bath temperature. It was indicated, that current efficiency decreases as the cathodic potential increases and higher amount of tungsten in the coatings is deposited (Fig. 8). A similar behavior was observed by Oliveira et al. [33] during electrodeposition of Ni-Fe-W alloys. They reported that increase in W content in the deposit approximately from 29 to 46 at.% results the decrease in cathodic current efficiency from 34% up to 22%.

Meanwhile in the studied systems the current efficiency depends rather on the alloy type and composition rather than on the temperature. In addition, the current efficiency decreases with increase of cathodic potential and higher amount of tungsten in the coatings is codeposited (Fig. 8). A similar behavior was observed by Oliveira et al. [33] during electrodeposition of Ni-Fe-W alloys. They reported that increase in W content in the deposit approximately from 29 to 46 at.% results in the decrease of cathodic current efficiency from 34% up to 22%.

These results correspond with the earlier findings confirming that iron group metal deposition is hindered by tungstate ions [17]. The decrease in cathodic current efficiency with increasing the cathodic potential is attributed to the higher hydrogen overvoltage than overvoltage of co-depositing metals at the given potential. At the higher values of electrode polarizations the exponential grow of partial current density for hydrogen is steeper than that for partial current densities of metals. Therefore, the highest current efficiency (~90% for Co-W and Co-Cu-W alloys) was determined for the coatings consisted practically of pure Co and Cu that were obtained at -0.7 V. The higher W percentage was observed for the Cu-W, Co-W, Co-Cu-W alloy coatings deposited in the potential range from -1.0 to -1.4 V.

With an increase the cathodic potential from -0.7 V to -1.4 V the Faradaic efficiency decreases from ~90 to 60%. Anyway, even this value is relatively higher in comparison to those calculated for Ni-Fe-

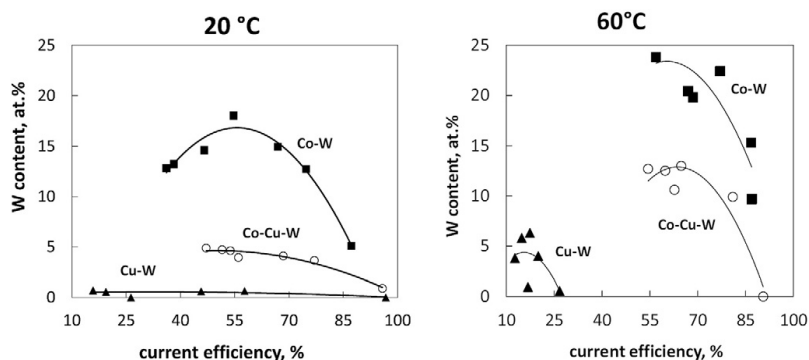


Fig. 8. Effect of tungsten content in the Cu-W, Co-Cu-W and Co-W alloy coatings on current efficiency.

W - 38% in [25] and 46% in [34]. In this study, no significant difference was observed in the current efficiency between Co-W and Co-Cu-W electrodeposition in the entire studied potentials range.

In the case of Cu-W, the electrodeposition of alloy begins at more negative potentials which leads to the lower current efficiency than that for Co-W and Co-Cu-W deposition. The relationships between cathodic current efficiency and applied deposition potential for all investigated systems were similar at temperatures 20 and 60 °C.

3.3. Surface morphology of alloys

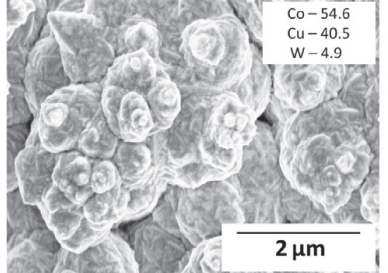
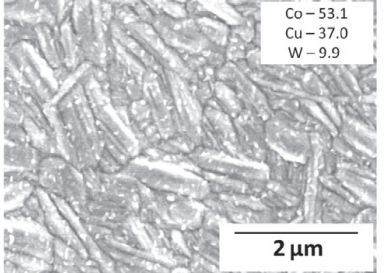
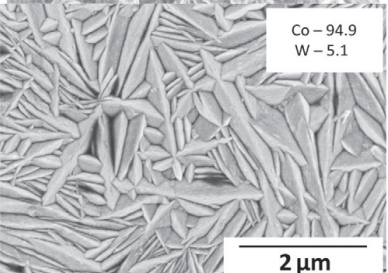
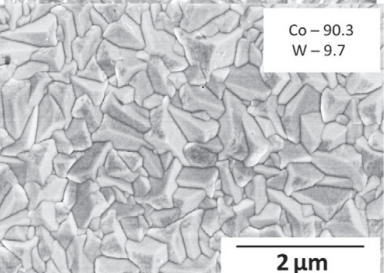
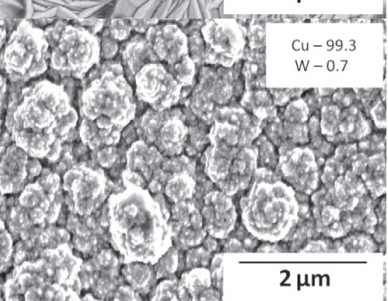
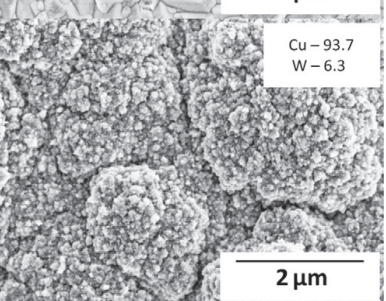
SEM images of the various compositions Cu-W, Co-W and Co-Cu-W alloys deposited at 20 and 60 °C are shown in Table 2. In general, all coatings have uniform thickness. The roughness of coatings was measured by means of AFM and determined that in all cases the values of mean roughness R_a are below 200 nm. Taking into account that the total thickness of the coatings is ~10 µm, so the uniformity of coatings thickness is estimated as no <98%.

The electrodeposited alloys adhere well to substrate. The deposits can be folded without evident peeling. Only some cracks may appear in the folding area. The typical test result is shown in Fig. 9.

The variety in the morphology of the deposits having the similar W content was noticed. When the percentage of W is lower than 5 at.%,

the Cu-W coatings are porous, and rough cauliflower-type nodules are formed that are similar to that of pure copper Fig. 10 (a). Each nodule could contain several smaller elements (fracture-like morphology). Meanwhile, the morphology of the surface changed after the incorporation of Co into the alloy composition. The bigger semi-spherical cauliflower-like clusters are dominant for the dark grey Co-Cu-W coating morphology when W percentage in the alloy is <5 at.%. The cauliflower-type morphology is typical for the relatively low W containing alloys and has been observed also by Della Noce et al. [27] in Co-Fe-W alloys containing 4.5–9 at.% of W, and by Oliveira et al. [33] in Ni-Fe-W deposits containing ~14–20 at.% of W; M. Spasojević et al. reported that Ni-Fe-W coatings with the much lower amount of W (~1 wt.%) had a globular structure containing a large number of craters, mostly located between the globules [35]. The cauliflower-like nodules size can be decreased by increasing the current density and bath temperature, which promotes an increase in microhardness. Whereas the Co-W deposits containing ~5 at.% of W consist of randomly orientated needle-like crystallites resembling that of pure Co coating Fig. 10 (b). When the W content in deposits exceeds 10 at.%, the ternary Co-Cu-W alloy coating is characterized by columnar morphology consisted of irregular size crystallites. At the higher W content needle-like Co-W alloy structure disappeared as well, and the coating is consisted of densely packed tripyramidal grains.

Table 2
SEM images of electrodeposited Cu-W, Co-W and Co-Cu-W alloys at 20 °C and 60 °C.

20 °C			
	Co – 54.6 Cu – 40.5 W – 4.9		Co – 53.1 Cu – 37.0 W – 9.9
	Co – 94.9 W – 5.1		Co – 90.3 W – 9.7
	Cu – 99.3 W – 0.7		Cu – 93.7 W – 6.3

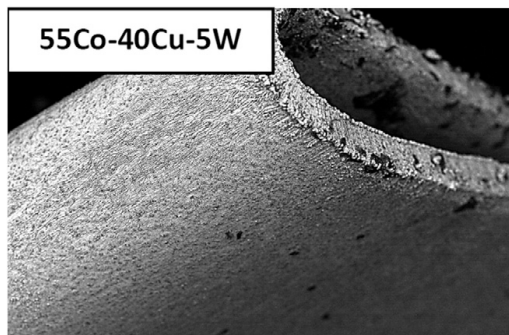


Fig. 9. SEM image of a folded sheet coated by 55Co-40Cu-5W alloy (in at.%) alloy deposited at 20 °C Thickness of deposit – 10 μm.

3.4. Analysis of XRD patterns

The phase composition of Cu-W, Co-Cu-W and Co-W alloys containing various amounts of W as well as that of the pure Co and Cu was investigated using X-ray diffraction method (XRD) (Fig. 11). As can be seen, the pure Co electrodeposit has hexagonal (hcp) lattice with remarkable {110} texture orientation. Diffraction patterns of pure Cu show the peaks characteristic for face-centered cubic (fcc) lattice: Cu {111}, {200}, {220}, and {311} while during co-deposition of W, the Cu-W solid solution with typical Cu-type cubic lattice was formed. According to [20] the Cu-W alloy containing 10 at.% of W consists of the polycrystalline copper with preferred orientation {111} incorporated into amorphous-like phase containing tungsten. The asymmetry of the Cu {111} signal for Cu-W alloy is caused by the appearance of the broad diffraction peak attributed to W {110}. This would confirm the amorphous-like character of the tungsten structure in the layer. However, in our case of electrodeposited Cu-W alloys, no peaks attributed to W phase were found in the XRD patterns. The XRD patterns indicated that Cu-W alloys with low W content (<1 at.%) exhibits dominating of Cu {111} texture, whereas the fractions of Cu {200}, {220} and {311} are smaller. The further increase in W content (up to 6 at.%) caused a decrease in intensity of Cu {111} peak while that of Cu {200}, {200} and {311} peaks remained nearly the same. All peaks were of similar intensity that suggests a less textured structure. Based on the results discussed above, it can be concluded that W atoms are considered as the solutes, expected to be randomly distributed in the (fcc) Cu crystal lattice. In addition, the small shift to lower 2θ values was determined. It is attributed with incorporation of W atoms into Cu lattice that cause the changes of lattice parameter.

While after the incorporation of Co into the Cu-W alloy XRD patterns showed the formation of peaks corresponding to (fcc) Cu phase and

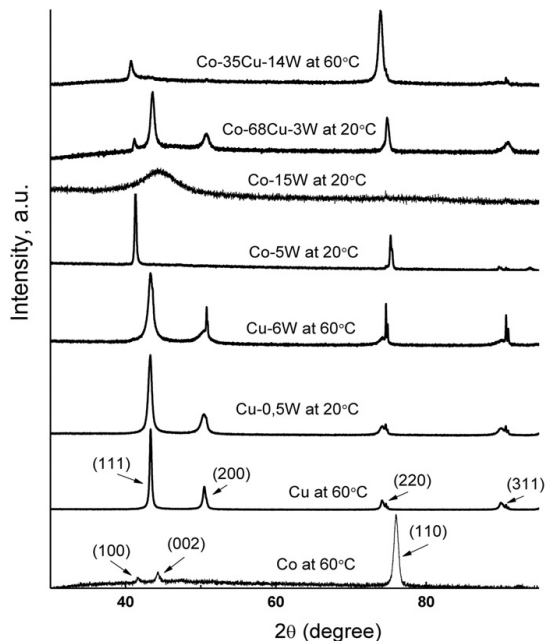


Fig. 11. XRD diffractograms of electrodeposited Co and Cu, and for W alloys having different compositions (in at.%). (1) Co, (2) Cu, (3) Cu-0.5W, (4) Cu-6W, (5) Co-5W, (6) Co-15W, (7) 29Co-68Cu-3W, (8) 51Co-35Cu-14W. Peaks were identified based on JCPDS cards (no. 7440-48-4).

additional lines that can be indexed considering the formation of W solid solution in (hcp) Co, and it is supported by the fact that solubility limit of W in Co is 17.5 at.% [28]. The crystalline structures of the Co-Cu-W alloys depend on the composition of the alloys. According to XRD data the largest amount of the (fcc) Cu phase was formed in the deposit obtained at -0.8 V, i.e. for the coating containing 68 at.% of Cu and 3 at.% of W. In this case the peaks revealed that Co-Cu-W alloy contains the significant amount of (fcc) of Cu {111} and diminutive amounts of Cu {200}, {220} and (hcp) Co {100}. The lines attributed to (fcc) Cu {111} and {200} disappear with increase of tungsten content in Co-Cu-W alloys up to 14 at.%. Additionally, the XRD pattern illustrates a slight shift of Cu {220} and Co {100} peaks position compared to those of 29Co-68Cu-3W deposit probably due to Co incorporation into crystalline lattice of Cu. Both mentioned ternary alloys exhibit crystallographic structure regardless of their composition. On the contrary, the XRD diffractograms of Co-W alloy show the microstructure changes as a

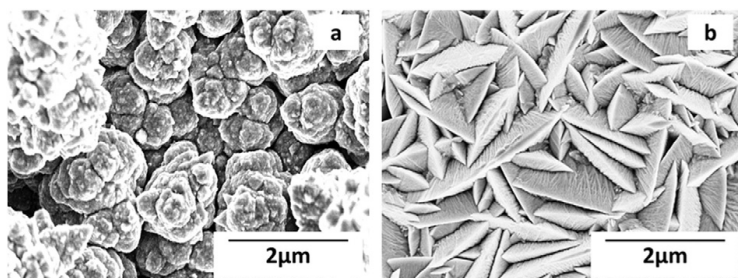


Fig. 10. SEM micrographs of electrodeposited pure (a) copper and (b) cobalt.

function of W content in the deposit: for tungsten content of 14 at.%, the (hpc) Co {100} phase in Co-W alloy is dominating and it is seen in the diffractogram with an increase in W content (> 14 at.%) when only the one broad peak occurs and the microstructure becomes “amorphous-like” (nanocrystalline), as it was reported [27] for W amounts < 20 at.%. With an increase in W content, the Co₃W phase becomes more pronounced, while the hexagonal Co phase diminishes. For a W content of 25 wt.%, the microstructure contains a mixture of Co₃W and Co₇W₆, and no traces of the pure Co phase was seen [18]. It is known that the broadening of XRD peaks is attributed to a decrease in grain size [28]. Interestingly, it was presented that the transformation from crystalline Co-W alloy structure to “amorphous-like” appears at higher W content (> 30 at.%) and a grain size is < 2 nm [18]. In the case of Cu-W the values of grain size decreases from 37 nm (for pure Cu) to 10 nm (for Cu-W containing 6 at.% of W).

4. Conclusions

Uniform and well-adherent Cu-W, Co-W and Co-Cu-W alloy coatings were deposited from citrate-borate electrolyte under potentiostatic mode at 20 and 60 °C. The cathodic polarization, current efficiency of co-deposition, composition and structure of the prepared alloys as a function of deposition potential and temperature were studied. Based on the obtained experimental data the following conclusions can be drawn:

- Deposition of Co-W and Co-Cu-W alloys starts at more positive potentials than that was expected based on the parent metals of the alloys electrodeposition, whereas Cu-W electrodeposition occurs at more negative potential compared to those of Co-W and Co-Cu-W. After increasing, the bath temperature from 20 to 60 °C a depolarization effect was observed and the deposition potential for all investigated W alloys shifted towards the more positive direction.
- In general, W content in the alloys increased with increasing the cathodic deposition potential from −0.7 V to −1.0 V and then remains almost constant regardless of the applied potential. At elevated temperatures the percentage of W in the alloys increases. The highest amount of W that co-deposits with Cu reached 6 at.% and it strongly depends on the deposition potential. After the introduction of Co into Cu-W alloy, the amount of W increased up to 14 at.%. W content in the ternary alloy decreased with increasing Cu(II) concentration in the electrolyte.
- The cathodic current efficiency depends rather on the alloys composition than on the bath temperature. It decreased with increasing the cathodic potential when the higher amount of tungsten in the coatings was detected. The calculated current efficiencies varied from 20% for Cu-W to ~90% for Co-Cu-W alloys.
- When W amount is lower than 5 at.%, Cu-W coatings consisted of granular clusters, that became even larger after the introduction of Co into the Cu-W alloy. The grain size of Cu-W alloy decreased as the W percentage in the composition increased (~6 at.%). After an increase of W percentage in the composition up to 10 at.%, the morphology of Co-Cu-W deposit transformed from nodular to columnar structure having irregular crystallite size.
- XRD analysis indicated that Cu-W alloy is a solid solution with typical Cu-type face centered cubic (fcc) lattice. Introduction of Co into this alloy resulted in the formation of additional hexagonal (hpc) Co patterns that can be identified as W solid solution in hpc Co.

Acknowledgements

The authors acknowledge funding from the Research Council of Lithuania (MIP-031/2014), Moldavian national project 15.817.02.05A and with the support of the Marie Curie Alumni Association.

References

- [1] K.S. Kumar, H. Van Swygenhoven, S. Suresh, Mechanical behavior of nanocrystalline metals and alloys, *Acta Mater.* 51 (2003) 5743–5774.
- [2] M. Dao, L. Lu, R.J. Asaro, J.T.M. De Hosson, E. Ma, Toward a quantitative understanding of mechanical behavior of nanocrystalline metals, *Acta Mater.* 55 (2007) 4041–4065.
- [3] D. Kim, D.Y. Park, B.Y. Yoo, P.T.A. Sumodji, N.V. Myung, Magnetic properties of nanocrystalline iron group thin film alloys electrodeposited from sulfate and chloride baths, *Electrochim. Acta* 48 (2003) 819–830.
- [4] G.D. Hibbard, K.T. Aust, U. Erb, Thermal stability of electrodeposited nanocrystalline Ni–Co alloys, *Mater. Sci. Eng. A* 433 (2006) 195–202.
- [5] J.L. McCrea, G. Palumbo, G.D. Hibbard, U. Erb, Properties and applications for electrodeposited nanocrystalline Fe–Ni alloys, *Rev. Adv. Mater. Sci.* 5 (2003) 252–258.
- [6] C.C. Koch, Structural nanocrystalline materials: an overview, *J. Mater. Sci.* 42 (2007) 1403–1414.
- [7] Z. Fekih, N. Ghellai, S. Sam, N.E. Chabanne-Sari, N. Gabouze, The iron-nickel-molybdenum (Fe–Ni–Mo) electrodeposition alloy on n-type silicon, *Adv. Mater. Sci.* 12 (2012) 17–26.
- [8] U. Klement, M. Da Silva, Thermal stability of electrodeposited nanocrystalline Ni and Co-based materials, *J. Iron Steel Res. Int.* 14 (2007) 173–178.
- [9] I. Baskaran, T.S.N. Sankara Narayanan, A. Stephen, Pulsed electrodeposition of nanocrystalline Cu–Ni alloy films and evaluation of their characteristic properties, *Mater. Lett.* 60 (2006) 1990–1995.
- [10] M. Donten, Z. Stojek, H. Cesiulis, Formation of nanofibers in thin layers of amorphous W alloys with Ni, Co, and Fe obtained by electrodeposition, *J. Electrochem. Soc.* 150 (2) (2003) C95–C98.
- [11] K.R. Sriraman, S.G.S. Raman, S.K. Seshadri, Corrosion behavior of electrodeposited nanocrystalline Ni–W and Ni–Fe–W alloys, *Mater. Sci. Eng. A* 460–461 (2007) 39–45.
- [12] Y. Nakamoto, M. Yuasa, Y. Chen, H. Kusuda, M. Mabuchi, Mechanical properties of a nanocrystalline Co–Cu alloy with a high-density fine nanoscale lamellar structure, *Scr. Mater.* 58 (2008) 731–734.
- [13] Z.A. Hamid, Electrodeposition of cobalt-tungsten alloys from acidic bath containing cationic surfactants, *Mater. Lett.* 57 (2003) 2558–2564.
- [14] M.P.Q. Arganaraz, S.B. Ribotta, M.E. Folquer, L.M. Gassa, G. Benitez, M.E. Vela, R.C. Salvezza, Ni–W coatings electrodeposited on carbon steel: chemical composition, mechanical properties and corrosion resistance, *Electrochim. Acta* 56 (2011) 5898–5903.
- [15] F. Su, C. Liu, P. Huang, Establishing relationships between electrodeposition techniques, microstructure and properties of nanocrystalline Co–W alloy coatings, *J. Alloys Compd.* 557 (2013) 228–238.
- [16] H. Cesiulis, X. Xie, E. Podlaha-Murphy, Electrodeposition of Co–W alloys with P and Ni, *Mater. Sci. (Medziagotyra)* 15 (2009) 115–122.
- [17] A. Subramanian, G.N. Kousalya, V.S. Muralidharan, T. Vasudevan, Cobalt-tungsten alloy electrodeposition and characterization, *Indian J. Chem. Technol.* 9 (2002) 513–518.
- [18] M. Svensson, U. Wahlstrom, G. Holmbom, Compositionally modulated cobalt-tungsten alloys deposited from a single ammoniacal electrolyte, *Surf. Coat. Technol.* 105 (1998) 218–223.
- [19] A.T. Vasko, Electrochemistry of Molybdenum and Tungsten, *Naukova Dumka, Kiev*, 1977.
- [20] P. Bacal, P. Indyka, Z. Stojek, M. Donten, Unusual example of induced codeposition of tungsten. Galvanic formation of Cu–W alloy, *Electrochem. Commun.* 54 (2015) 28–31.
- [21] J.P. Chu, C.J. Liu, C.H. Lin, T.N. Lin, S.F. Wang, Characterizations of super hard Cu films containing insoluble W prepared by sputter deposition, *Mater. Chem. Phys.* 72 (2001) 286–289.
- [22] V.B. Singh, L.C. Singh, K. Tikoo, Studies on electrodeposition of nickel-cobalt-tungsten alloys, *J. Electrochem. Soc.* 127 (1980) 590–596.
- [23] M. Donten, H. Cesiulis, Z. Stojek, Electrodeposition and properties of Ni–W, Fe–W and Fe–Ni–W amorphous alloys. A comparative study, *Electrochim. Acta* 45 (2000) 3389–3396.
- [24] H. Fengjiao, W. Miao, L. Xin, Properties of electrodeposited amorphous Fe–Ni–W alloy deposits, *Trans. Nonferrous Metals Soc. China* 16 (2006) 1289–1294.
- [25] J. Ahmad, K. Asami, A. Takeuchi, D.V. Louzguine, A. Inoue, High strength Ni–Fe–W and Ni–Fe–W–P alloys produced by electrodeposition, *Mater. Trans.* 44 (2003) 1942–1947.
- [26] H. Capel, P.H. Shipway, S.J. Harris, Sliding wear behaviour of electrodeposited cobalt-tungsten-iron alloys, *Wear* 255 (2003) 917–923.
- [27] R. Della Noce, A.V. Benedetti, M. Magnani, E.C. Passamani, H. Kumar, D.R. Cornejo, C.A. Ospina, Structural, morphological and magnetic characterization of electrodeposited Co–Fe–W alloys, *J. Alloys Compd.* 611 (2014) 243–248.
- [28] N. Tsyntaru, H. Cesiulis, A. Budreika, X. Ye, R. Juskenas, J.-P. Celis, The effect of electrodeposition conditions and post-annealing on nanostructure of Co–W coatings, *Surf. Coat. Technol.* 206 (2012) 4262–4269.
- [29] M.M. Abou-Krishna, Influence of Ni²⁺ concentration and deposition potential on the characterization of thin electrodeposited Zn–Ni–Co coatings, *Mater. Chem. Phys.* 125 (2011) 621–627.
- [30] M.A.M. Ibrahim, S.S. Abd el Rehim, S.O. Moussa, Electrodeposition of noncrystalline cobalt-tungsten alloys from citrate electrolytes, *J. Appl. Electrochem.* 33 (2003) 627–633.
- [31] D.P. Weston, S.J. Harris, P.H. Shipway, N.J. Weston, G.N. Yap, Establishing relationships between bath chemistry, electrodeposition and microstructure of Co–W alloy coatings produced from a gluconate bath, *Electrochim. Acta* 55 (2010) 5695–5708.

- [32] R. Alexandre, C. Santana, A.R.N. Campos, E.A. Medeiros, A.L.M. Oliveira, L.M.F. Silva, S. Prasad, Studies on electrodeposition and corrosion behaviour of a Ni–W–Co amorphous alloy, *J. Mater. Sci.* 42 (2007) 9137–9144.
- [33] A.L.M. Oliveira, J.D. Costa, M.B. de Sousa, J. Ja, N. Alves, A.R.N. Campos, R.A.C. Santana, S. Prasad, Studies on electrodeposition and characterization of the Ni–W–Fe alloys coatings, *J. Alloys Compd.* 619 (2015) 697–703.
- [34] V.B. Singh, Studies on the electrodeposition of ternary nickel-iron-tungsten alloys, *Surf. Coat. Technol.* 7 (1978) 443–450.
- [35] M. Spasojević, L. Ribić-Zelenović, A. Maričić, P. Spasojević, Structure and magnetic properties of electrodeposited Ni_{87.3}Fe_{11.3}W_{1.4} alloy, *Powder Technol.* 254 (2014) 439–447.

Article VI

Tribological and corrosion properties of iron-based alloys

E.Vernickaite, Z. Antar, A. Nicolenco, R.Kreivaitis N.Tsyntaru, H. Cesiulis

Proceedings of BALTRIB'2015 edited by prof. J. Padgurskas, 162-169

TRIBOLOGICAL AND CORROSION PROPERTIES OF IRON-BASED ALLOYS

*E. Vernickaite**, *Z. Antar***, *A. Nicolenco* ****, *R. Kreivaitis*****, *N. Tsyntsaru* ****,
H. Cesiulis†*

* Vilnius University, Department of Physical Chemistry, Vilnius, Lithuania

** University of Sfax, Materials Engineering and Environment Laboratory, Tunisia

*** Institute of Applied Physics, Chisinau, Moldova

**** Aleksandras Stulginskis University, Institute of Power and Transport Machinery Engineering,
Kaunas, Lithuania

Abstract: Corrosion is responsible for industrial maintenance and industrial accidents costs. A helpful way to prevent corrosion is to develop advanced materials with highly anti-corrosive properties. The electrodeposition is one of the most attractive methods for obtaining these materials. This work deals with evaluation of the tribological and corrosion behaviour of electrodeposited Fe-W and Fe-W-P alloys. Electrodeposits were obtained from 4 different baths and were characterized by means of scanning electron microscopy; X-ray dispersive energy spectroscopy; X-ray diffraction spectroscopy. The hardness was determined by Micro-indentation carried out at normal forces varying from 98 mN up to 980 mN with a loading rate of 1961 mN/min. A ball-disc tribometer was used to study the tribological properties at 90 °C. A diamond indenter, having a radius of 100 μm, was used to carry the scratch test. Corrosion behaviour was studied using polarization and electrochemical impedance spectroscopy technique. It was investigated that in all cases Fe-W and Fe-W-P alloy coatings exhibit greater micro-hardness than the stainless steel substrate. The amorphous-like ternary Fe-W-P alloy coatings demonstrate higher wear and corrosion resistance and lower friction coefficient compared to binary Fe-W alloy coating.

Keywords: iron-based alloys, electrodeposition, tribology, wear, hardness, corrosion.

1. INTRODUCTION

Electrodeposited nanostructured tungsten alloys with iron-group metals are attractive because of tunable mechanical, chemical and magnetic properties, and can be electrodeposited from a number of solutions using various electrodeposition modes [1]. The electrodeposited Fe–W alloys containing higher amount of tungsten are “amorphous-like” and remain nanocrystalline after annealing up to 800 °C. After heating at 1000 °C, the nanocrystalline structure transforms into a microcrystalline one, and three phases are formed, namely FeWO₄, Fe, and possibly Fe₂W [2].

The Fe–W coatings undergo a high degree of wear resulting from the oxidation of the surface and may be considered as alternative to the chromium coatings, which are formed in the hazardous process based on hexavalent chromium [3, 4]. It should be taken into account that features of a sliding system depend on a variety of interrelated mechanical, chemical, physical, and surface properties of materials and surfaces. Tribological behavior largely depends on the crystal structure. When percent of tungsten in iron-group alloys reaches more than 22 at. % its grain size become less than 10 nm, which leads to enhances the hardness of the coating [5]. It has been shown that the nanohardness of as-plated Fe-W with 29 at. % coatings reaches 13 GPa that is comparable to the hardness of electrodeposited chromium [2]. The study of the tribological and mechanical properties of the multilayer Fe-W/Cu coatings by means of electrodeposition leads to the improvement of the wear characteristics of the coatings even at dry friction and at a sufficiently high load of 10 N. Investigations of wear resistance of Fe-W alloy at dry friction and in presence of oil were performed and described in [6]. The specific feature of Co-W and Fe-W alloys under dry friction consists in the formation of oxide layer that results in a faster wear, especially in the case of Fe-W alloys, nevertheless that the W content is similar

† Author for contacts: Prof. Henrikas Cesiulis
E-mail: henrikas.cesiulis@chf.vu.lt

in Fe-W and Co-W alloys. The presence of oils substantially decreases oxygen's access to the contact areas and reduces wear of such alloys.

An addition of tungsten in the alloys apparently increases the chemical resistance [7]. This and lower overvoltage for anodic oxidation of methanol in sulfuric acid medium opens perspectives to Fe-W alloys to use its in the fuel cells [8]. It was shown that the presence of tungsten in same binary system results in improvement on corrosion resistance. In the case of Ni-Fe-W alloys, the maximal corrosion resistance is obtained for alloys having tungsten up to 9.2 at. %. However, the charge transfer resistance values of ternary alloy coatings were lower compared to those of the binary alloy coatings due to preferential dissolution of iron from the matrix [9]. These results show that same ternary alloys (Fe-W-Co/Ni) are potential materials for applications in magnetic devices [10]. Also, Fe-W alloys have attracted magnetic properties, electrical resistivity, and reduced films stress that allows using it as new material in micro-/nano-electromechanical systems (MEMS/NEMS) [11].

Recent researches show that the presence of phosphorus in iron alloys influences on tribological properties and its corrosion resistance [12]. The amorphous Ni-W-P alloy with high strength properties was obtained [13, 14]. Introduction of phosphorous into the alloys, for example Co-W, eliminates the cracks even at higher current densities applied for electrodeposition [15].

The aim of this work is to obtain Fe-W and Fe-W-P coatings from different electrolytes and to evaluate their tribological properties and corrosion behaviour.

2. EXPERIMENTAL

The solutions were prepared by dissolving appropriate amounts of chemicals in distilled water and the pH 8.5 was adjusted by additions of concentrated H₂SO₄. Electrodeposition of thin films was performed at 70 °C temperature in a typical three-electrode cell under direct current mode at 30 mA/cm². A graphite and Ag/AgCl electrode were used as a counter electrode and a reference electrode, respectively. All potential values are expressed versus the Ag/AgCl electrode. The electrodeposition of Fe, Fe-W and Fe-W-P layers were carried out on the stainless steel (Type 304) substrate. Before the experiments the working electrode was rinsed with acetone and 0.1 M H₂SO₄ solution under ultrasound irritation. The thickness of the electrodeposits was calculated from gravimetric and elemental analysis data.

The phase composition and microstructure of the deposited alloys were identified by X-ray diffractometer (XRD, Rigaku MiniFlex II) and scanning electron microscope (SEM, Hitachi TM-3000), supplied with an Oxford EDS analyzer.

Hardness was determined by Micro-indentation (Micro Combi Tester, CSM Instruments) carried out at normal forces varying from 98 mN up to 980 mN with a loading rate of 1961.4 mN/min. The indenter was a Vickers shaped tip with a centreline-to-face angle of 68°. A ball-disc tribometer (TRM 500, WAZAU) was used to study the tribological properties at 90 °C. The ball, designed with 100Cr6 steel, have 6 mm diameter. The normal load applied on the contact was about 5 N and average linear velocity was estimated by 0.125 m/s. A diamond Rockwell indenter, having a radius of 100 µm, was used to carry on the scratch test. The wear path was characterized by optical microscopy (Eclipse MA100, Nikon).

Electrochemical corrosion measurements of obtained coatings were performed in the mixture 0.012 M Na₂SO₄ and 0.027 M NaCl (pH 5) at 90 °C. The solution was open to air. The exposed area of the sample was 1 cm². The corrosion tests were performed by means of voltammetry and electrochemical impedance spectroscopy (EIS), recorded at open circuit potential (OCP). The investigations were carried out using AUTOLAB system and GPES and FRA 4.9 software. The registration of EIS and voltammetric data was started after stabilization of the open circuit potential within 15 minutes in the test solution. The amplitude of the modulation potential for the EIS measurements was 5 mV, and the frequency range was 10 kHz-0.01 Hz.

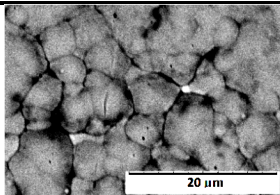
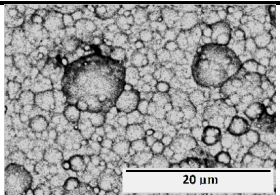
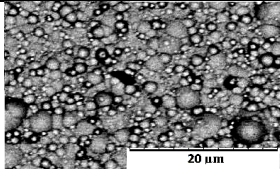
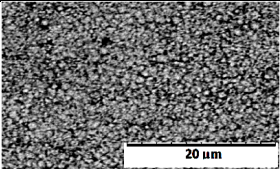
3. RESULTS AND DISCUSSION

Composition and morphology of Fe-alloys. Fe, Fe-W and Fe-W-P thin films were electrodeposited from citrate-containing baths, which compositions are given in Table 1. The SEM images of electrodeposited Fe-W, Fe-W-P alloys and their compositions are shown in Table 2. As it can be seen, the coatings possess micro-granular structure, and Fe-W contains ~25 at. % of W whereas the W content in electrodeposited Fe-W-P alloys contains ~26 at. % of W. Also it was indicated, that wetting and brightening agents presenting in the bath (Bath 4) slightly increases the phosphorous percentage in the deposit. Fe-W and Fe-W-P alloy coatings are uniform and free of cracks. It is clearly seen that even a small amount of phosphorous in the composition (1-1.6 at. %) leads to refining the structure and the deposits become tight, compact and dense.

Table 1. Composition of the baths used for the electrodeposition of Fe-W (Bath 1, 2) and Fe-W-P (Bath 3, 4).

Electrolyte content	Bath 1	Bath 2	Bath 3	Bath 4
Na ₂ WO ₄ ·2H ₂ O (sodium tungstate), M	0.2	0.4	0.4	0.4
FeSO ₄ ·7H ₂ O (iron sulfate), M	0.02	0.2	0.2	0.2
Na ₃ C ₆ H ₅ O ₇ ·2H ₂ O (tri-sodium citrate), M	0.2	0.33	0.33	0.33
C ₆ H ₈ O ₇ ·H ₂ O (citric acid), M	-	0.17	0.17	-
H ₃ BO ₃ (boric acid), M	0.16	-	-	-
H ₂ NaO ₂ P·H ₂ O (sodium hypophosphite), M	-	-	0.02	0.02
H ₃ PO ₄ (phosphoric acid), g/L	7.69	-	-	-
C ₄ H ₁₀ O ₂ (butindiol 1,4), μg/l	-	-	-	50
Wetting agent Rokafenol N-10, μg/l	-	-	-	100

Table 2. The micrographs of as-deposited Fe-W and Fe-W-P alloy coatings.

Composition, in at. %	SEM image	Composition, in at. %	SEM image
Fe-72.7 W-24.3		Fe-74.7 W-25.3	
	Bath 1		Bath 2
Fe-72.1 W-26.8 P-1.11		Fe-72.7 W-25.6 P-1.56	
	Bath 3		Bath 4

Mechanical and tribological properties. Micro-indentation test shows an increase of micro-hardness for all coated sample compared to 304-type stainless steel substrate. The hardest coating was obtained from Bath 2 and had a micro-hardness of 725 HV (Figure 1). Figure 2 shows the evolution of friction coefficient with sliding distance for all prepared coatings. The lowest friction coefficient was recorded for the Fe-P-W sample obtained from Bath 4 (containing wetting and brightening agents) and most of the electrochemically prepared samples presented lower friction coefficients than the 304-type stainless steel substrate.

The scratch test profiles were taken for all deposited samples too. It was noticed that coatings prepared using Bath 1 were the most brittle and cracks spread quickly causing damages on the surface. Samples prepared from Bath 3 and 4 were more stable and the density of cracks is lower (Figure 3). It seems

that phosphorous leads to the formation of more wear resistant coating and enhance the adhesion to the substrate.

Corrosion behaviour. The aim of these experiments was to study the corrosion parameters of pure Fe, Fe-W and Fe-W-P alloy coatings and compare the results to those of 304-type stainless steel. According to the results discussed above, Bath 4 was selected for pure Fe deposition (electrolyte without $\text{Na}_2\text{WO}_4 \cdot 2\text{H}_2\text{O}$ and $\text{H}_2\text{NaO}_2 \cdot \text{H}_2\text{O}$), Fe-W (electrolyte without $\text{H}_2\text{NaO}_2 \cdot \text{H}_2\text{O}$) and Fe-W-P electrodeposition. Electrochemical corrosion measurements of obtained coatings were performed in 0,012 M Na_2SO_4 and 0,027 M NaCl solution (pH 5) at 90 °C. Table 3 presents the SEM micrographs of as deposited Fe, Fe-W and Fe-W-P coatings and morphology of specimens after the corrosion test.

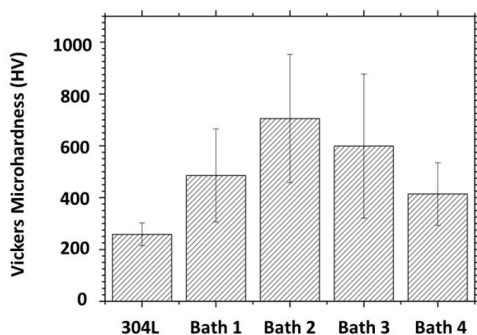


Figure 1. The micro-hardness of as-deposited coatings.

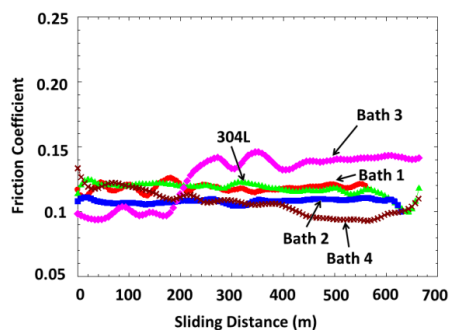


Figure 2. Friction coefficient evolution with sliding distance.

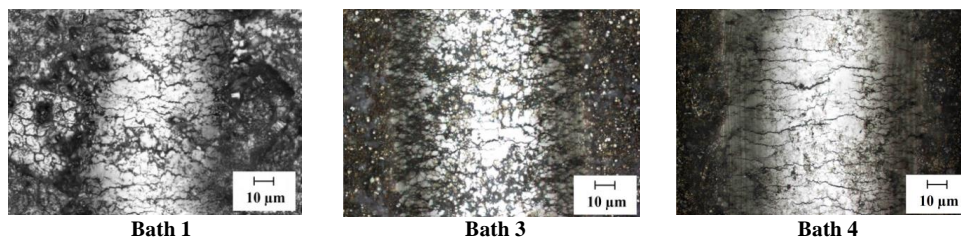


Figure 3. Multi-focus images of the scratch test profiles after exceeding the critical load.

It is seen, that the surface structure after the corrosion experiments in aggressive media significantly changed: granular structure was destroyed and the dense cracks are visible. Investigations also showed that oxygen content in the alloy significantly increases after corrosion experiments.

XRD patterns of as-deposited pure Fe, Fe-W and Fe-W-P alloy coatings are shown in Figure 3. Results indicate that the pure Fe coating exhibit texture with preferred orientation of {211} crystallographic plane. The high content of tungsten in the alloy after electrodeposition causes a significant decrease of grain size and formation of an XRD amorphous-like phase.

Table 3. The micrographs of as-deposited Fe, Fe-W and Fe-W-P alloy coatings. Composition is given in at. %.

<i>As-deposited</i>		<i>After corrosion test</i>	
Composition	SEM image	Composition	SEM image
Fe – 100		Fe – 100	
O - 5.62 Fe - 94.4		O - 22.6 Fe - 77.4	
W - 33.1 Fe - 66.9		W - 46.9 Fe - 53.1	
O - 26.6 W - 41.8 Fe - 31.5		O - 71.1 W - 13.2 Fe - 15.7	
W - 34.5 Fe - 63.9 P - 1.60		W - 33.7 Fe - 60.5 P - 5.81	
O - 23.2 W - 26.4 Fe - 49.2 P - 1.200		O - 68.8 W - 10.2 Fe - 19.5 P - 1.55	

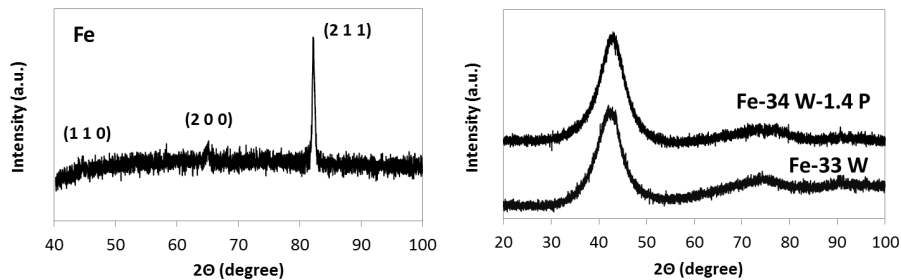


Figure 3. XRD diffraction pattern for pure Fe, Fe-W and Fe-W-P alloy coatings. Composition is given in at. %.

Polarization curves of the specimens tested in 0.012 M Na₂SO₄ and 0.027 M NaCl solution (pH 5) at 90 °C are shown in Figure 4.

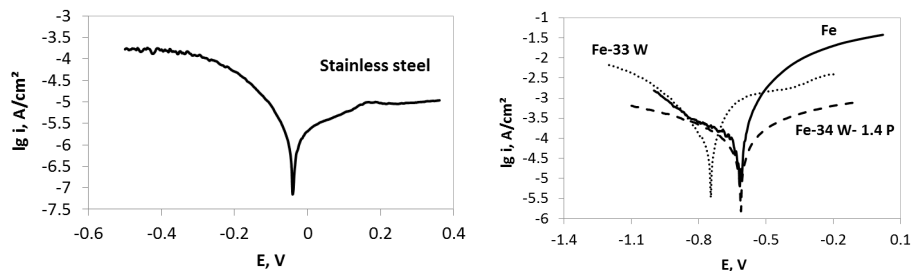


Figure 4. E vs log i plots for 304-type stainless steel, pure Fe, Fe-W and Fe-W-P coatings. Composition is given in at. %.

The polarization curves can be summarised in terms of E_{corr} and i_{corr} , which were calculated using Tafel fit and Allen-Hickling equation, and obtained data is summarized in Table 4. It has been found that adding phosphorous into alloys, and electrodeposited ternary Fe-W-P alloy surface shows nobler E_{corr} and the lowest i_{corr} and thus potentially better corrosion resistance in the tested media.

Table 4. Extracted corrosion parameters from E vs. log i plots in Figure 4.

Coating	E_{corr} , V	j_{corr} , A/cm ²	R_{corr} , Ω -cm ²
Stainless steel	-0.039	$9.09 \cdot 10^{-7}$	6567
Fe	-0.616	$3.9 \cdot 10^{-5}$	335.9
Fe-33 W	-0.746	$4.32 \cdot 10^{-5}$	380.7
Fe-34 W-1.4 P	-0.613	$1.81 \cdot 10^{-5}$	388.9

Electrochemical impedance spectroscopy (EIS) data have been obtained in order to investigate the performance of electrodeposited thin films in media containing Cl⁻ and SO₄²⁻. Nyquist plots for stainless steel, electrodeposited pure Fe, Fe-W and Fe-W-P coatings are shown in Figure 5. The dots indicated measured data while lines present best-fit data based on electric circuits shown in Figure 6. Impedance data were fitted using different electrical equivalent circuit models to interpret the corrosion resistance processes.

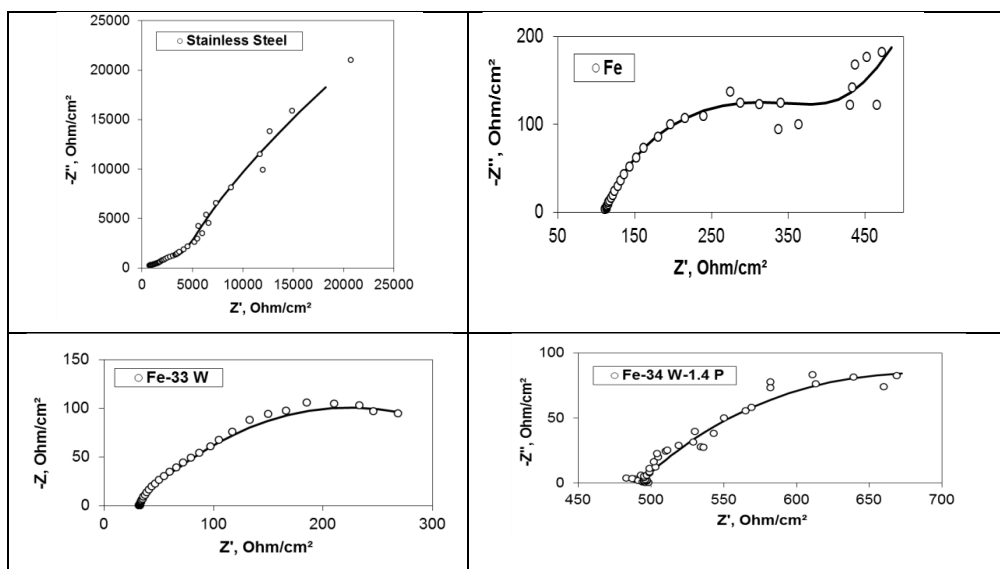


Figure 5. EIS Nyquist plots for stainless steel, pure Co and Fe-W, Fe-W-P alloy coatings in 0.012 M Na₂SO₄ + 0.027 M NaCl (pH 5) solution at OCP. Composition is given in at. %. Equivalent circuit model for stainless steel and Fe-W electrodeposit is given in Figure 6 c; for pure Co – in Figure 6 b; for Fe-W-P – in Figure 6 a.

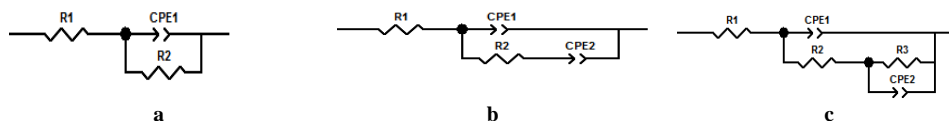


Figure 6. Equivalent circuits of the cell for impedance measurements. R1 - solution resistance; CPE1 - a constant phase element; R2 - charge transfer resistance; CPE2 – the absorption-related constant phase element; R3 – the absorption-related resistance.

R_{corr} values extracted from Nyquist's plots are shown in Table 4. The diameter of medium-frequency capacitive loops is considered as R_{corr} . The ternary Fe-W-P alloy coating demonstrated the higher corrosion resistance than pure Fe and Fe-W electrodeposit. The highest R_{corr} value was obtained for stainless steel substrate. The used equivalent circuit for fitting of EIS data suppose the complicated

mechanism of alloy corrosion involving intermediate stages probably containing adsorbed oxygen compounds; that can explain an increase in oxygen content in the alloys and some changes in tungsten content obtained after corrosion tests.

3. CONCLUSIONS

1. Homogenous and compact Fe-W and Fe-W-P alloy cracks-free coatings containing the high amount of tungsten (24-25 at. %) were deposited from four different plating baths (Table 1). It was indicated that wetting and brightening agents presenting in the plating bath slightly increase the phosphorous percentage in the Fe-W-P deposit. Even a small amount of phosphorous in the composition (1-1.6 at. %) leads to refining the structure.
2. It was found that the hardest Fe-W coating was obtained from Bath 2 and had a micro-hardness of 725 HV. Meanwhile, the lowest friction coefficient was recorded for Fe-W-P sample deposited from Bath 4.
3. Three coatings of pure Fe, Fe-W and Fe-W-P were chosen to evaluate the corrosion behaviour and the results were compared with those of stainless steel. It was found that the Fe-W-P alloy possesses the highest corrosion resistance among pure Fe, and amorphous-like Fe-W. However, cast stainless steel of Type 304 possesses less corrosion current and higher corrosion resistance than deposited Fe-W and Fe-P-W alloys.

ACKNOWLEDGMENT

The authors acknowledge funding from HORIZON2020 SELECTA project (642642) and FP7 Oil&Sugar project (295202). Also, partial funding was granted by the Research Council of Lithuania (MIP-031/2014) and Moldavian national projects (14.02.121A), (14.819.02.16F).

REFERENCES

- [1] N. Tsyntaru, H. Cesiulis, M. Donten, J. Sort, E. Pellicer, E. J. Podlaha-Murphy, *Modern Trends in Tungsten Alloys Electrodeposition with Iron Group Metals, Surface Engineering and Applied Electrochemistry*, 48(6), 2012, p. 491-520.
- [2] N. Tsyntaru, J. Bobanova, X. Ye, H. Cesiulis, A. Dikumar, I. Prosycevas, J.-P. Celis, *Iron-tungsten alloys electrodeposited under direct current from citrate-ammonia plating baths, Surface and Coatings Technology*, 203, 2009, p. 3136-3141.
- [3] E.W. Brooman, *Wear behavior of environmentally acceptable alternatives to chromium coatings: nickel-based candidates, Metal Finishing*, 102(9), 2004, 75-82.
- [4] Zh.I. Bobanova, A.I. Dikumar, H. Cesiulis, J.-P. Celis, N.I. Tsyntaru, I. Prosycevas, *Micromechanical and Tribological Properties of Nanocrystalline Coatings of Iron-Tungsten Alloys Electrodeposited from Citrate-Ammonia Solutions, Russian Journal of Electrochemistry*, 45(8), 2009, p. 895-901.
- [5] C. A. Schuh, T. G. Nieh, H. Iwasaki, *The Effect of Solid Solution W Additions on the Mechanical Properties of Nanocrystalline Ni, Acta Materialia*, 51, 2003, p. 431-443.
- [6] N. I. Tsyntaru, Zh. I. Bobanova, D. M. Kroitoru, V. F. Cheban, G. I. Poshtaru, A.I. Dikumar, *Effect of a multilayer structure and lubrication on the tribological properties of coatings of Fe-W alloys, Surface Engineering and Applied Electrochemistry*, 46(6), 2010, p. 538-546.
- [7] M. Donten, Z. Stojek, J.G. Osteryoung, *Voltammetric, Optical, and Spectroscopic Examination of Anodically Forced Passivation of Cobalt-Tungsten Amorphous Alloys, Journal of the Electrochemical Society*, 140(12), 1993, p. 3417-3424.
- [8] C.N. Tharamani, B. Barthasarathi, V. Jayaram, N.S. Begum, S.M. Mayanna, *Studies on electrodeposition of Fe-W alloy for fuel cell application, Applied surface science*, 253, 2006, p. 2031-2037.
- [9] K.R. Sriraman, S. Ganesh S. Raman, S.K. Seshadri, *Corrosion behaviour of electrodeposited nanocrystalline Ni-W and Ni-Fe-W alloys, Materials Science and Engineering A460-461*, 2007, p. 39-45.
- [10] D. Noce, A.V. Benedetti, M. Magnani, E.C. Passamani, H. Kumar, D.R. Cornejo, C.A. Ospina, *Structural, morphological and magnetic characterization of electrodeposited Co-Fe-W alloys, Journal of Alloys and Compounds*, 611, 2014, p. 243-248.
- [11] W. Ehrfeld, V. Hessel, H. Luwe, Ch. Schulz, L. Weber, *Microsystem Technologies*, 5(3), 1999, p. 105-112.
- [12] J. Nowacki, *Phosphorus in iron alloys surface engineering, Journal of Achievements in Materials and*

Manufacturing Engineering, 24(1), 2007, p. 57-67.

[13] J. Ahmad, K. Asami, A. Takeuchi, D.V. Louzguine and A. Inoue, High Strength Ni-Fe-W and Ni-Fe-W-P Alloys Produced by Electrodeposition, Materials Transactions, 44(10), 2003, p. 1942-1947.

[14] E.Valova, S. Armeanov, A. Franquet, K. Petrov, D. Kovacheva, J. Dille, Comparison of the Structure and Chemical Composition of Crystalline and Amorphous Electroless Ni-W-P Coatings, Journal of The Electrochemical Society, 151(6), 2004, C385-C391.

[15] H. Cesiulis, X. Xie, E. Podlaha-Murphy, Electrodeposition of Co-W Alloys with P and Ni, Materials Science, 15(2), 2009, p. 1392-1320.

Article VII

A Hybrid approach to W alloy and Au nanoparticles

E. Vernickaite, U. Bubnienė, H. Cesiulis, A. Ramanavičius, E. J. Podlaha

Journal of The Electrochemical Society, 163(7) (2016) D344-D348



A Hybrid Approach to Fabricated Nanowire-Nanoparticle Composites of a Co-W Alloy and Au Nanoparticles

E. Vernickaite,^a U. Bubniene,^a H. Cesiulis,^a A. Ramanavicius,^{a,b} and E. J. Podlaha^{c,*}

^aDepartment of Physical Chemistry, Vilnius University, Vilnius LT-03225, Lithuania

^bLaboratory of BioNanoTechnology, State Research Institute Center for Physical Sciences and Technology, LT-01108 Vilnius, Lithuania

^cDepartment of Chemical Engineering, Northeastern University, Boston, Massachusetts 02115, USA

Co-W nanowires were fabricated by pulsed electrodeposition from a citrate-glycine electrolyte onto rotating cylinder electrodes and into nanoporous polycarbonate membranes. The characterization of the electrodeposition conditions and alloy composition of electrodeposited Co-W alloy thin films were determined and used to guide conditions to electrodeposit the nanowires. Gold nanoparticles of 50 nm size were also added to the electrolyte and deposited during electrodeposition of the Co-W alloy nanowires, embedded within, and attached to the nanowire tip, introducing a novel procedure to attached nanoparticles onto nanowires.

© The Author(s) 2016. Published by ECS. This is an open access article distributed under the terms of the Creative Commons Attribution Non-Commercial No Derivatives 4.0 License (CC BY-NC-ND, <http://creativecommons.org/licenses/by-nc-nd/4.0/>), which permits non-commercial reuse, distribution, and reproduction in any medium, provided the original work is not changed in any way and is properly cited. For permission for commercial reuse, please email: oa@electrochem.org. [DOI: 10.1149/2.1401607jes] All rights reserved.

Manuscript submitted March 10, 2016; revised manuscript received April 22, 2016. Published May 7, 2016.

Nano-electrodes can be used for various sensing applications, and they can be easily integrated in micro- and nano-scale devices.¹ The sensitivity of nano-electrodes depends on the diameter of electrode tip, and the highest sensitivity is observed by most electrochemical methods if the diameter of the working electrode tip is on the same order of the molecular species being detected. To this end, nano-gaping technology has been applied for the fabrication of nano-electrodes that are based on FIB and E-beam lithographic approaches,^{2,3} including electrodeposition and/or chemical etching techniques.⁴

Gold-based 1D nanostructures (e.g., nanowires, gold nanoparticles) have been recognized as unique materials for electrical and optical sensing applications.⁵ Gold nanowires can provide high current densities, high signal to noise ratio and low double layer capacitance,⁶ while surface plasmon resonance, often exploited with nanoparticles, can uniquely probe interactions of molecules at chemical surfaces and provide label-free bio detection.⁵⁻⁸

Gold nanoparticles (AuNPs) are excellent materials for functionalizing electrode surfaces.^{9,10} Functionalization can be achieved via the use of bi-functional chemical linking agents, mixing with the components of composite electrodes, covalent binding and others. Notably, gold nanoparticles alone have limited applications in sensing unless surface modification is performed. Careful selection and design of ligands strongly influence the sensitivity and selectivity of a sensor.^{5,11} Gold nanoparticles can be synthesized by a citrate reduction method pioneered by Turkevich¹² and later advanced by Frens,¹³ with a variety of modification's methods.^{6,14-18} The nanoparticle morphology is dependent upon chemical nanoparticle synthesis methods.

Linking agents are typically applied in order to bind gold nanoparticles to surfaces of various substrates.^{7,14,19-23} Surface chemical modification and functionalization using linkers both are attractive methodologies because of highly active and selective layer formation, strong electrode intersectional binding, and changeable physical properties. However, there are a few important disadvantages if linkers are applied in order to design nano-electrodes: additional materials affect surface conductivity and can reduce it or lead to poor electrical contact, and they can shorten an electrode's applicable potential window by interfering with electrochemical processes.²⁴ Direct attachment of AuNPs on the nano-electrode without using any linkers may overcome these disadvantages and even improve the electrochemical performance of the electrode due to uninterrupted conductivity throughout the electrode material. Electrodeposition is one of the most versatile, simple, and cost effective fabrication methods of electrochemical formation

of structures and it provides a systematic control of the size and morphology of formed structures.

Hence, this research presents a novel approach for the creation of nanometric electrodes with nanoparticles deposited within and on the top of nanowires. This approach combines two processes: synthesis of nanoparticles, then co-deposition of them in an electrodeposited metal matrix. In order to expand the functionality of the resulting composite nanowire structure, the Co-W alloy was selected as the metal matrix to provide the ability to magnetically move the wire, in contrast to gold. Co-W also offers superior corrosion resistance. As thin films, Co-W alloy has been widely studied for its outstanding tribological properties,²⁵⁻²⁹ mechanical durability and superior hardness,³⁰⁻³³ corrosion resistance,^{34,35} and magnetic properties.³⁶⁻³⁸

The electrodeposition of tungsten alloys can be performed in citrate, pyrophosphate and/or ammonium ions containing electrolytes,³⁹ with the use of citrate being the most widespread particularly for Co-W alloys.^{40,41} A challenge in depositing Co-W alloys arises due to the inherent hydrogen evolution side reaction. In order to improve the efficiency of the electrodeposition process and the structure of the obtained Co-W deposits organic additives, such as saccharin, thiourea, methacrylate, glycine can be used in the electrolyte.⁴² Recently, glycine-based solutions are of interest because it is a non-toxic complexing agent, which stabilizes the pH close to the electrode surface in both alkaline and acidic electrolytes,^{43,44} although the side reaction cannot be completely eliminated. Thus, the management of the hydrogen evolution side reaction can be problematic when translating thin film deposition parameters for Co-W alloys to nanometer architectures via templating methods.

The template-assisted method has been employed for the electrodeposition of nanostructures using a variety of templates, such as polycarbonate membranes,^{45,46} and anodized aluminum oxides (AAO).⁴⁶⁻⁴⁹ Although many investigations have focused on single-element, binary and ternary alloy magnetic nanowires such as Ni, Co, Fe-Co, Co-Ni, Ni-Fe and Fe-Co-Ni,⁵⁰⁻⁵⁶ no reports of electrodeposited Co-W alloy nanowires exists, except those by the coauthors here. In previous work, Co-W and Co-W-P nanowires and nanotubes were fabricated through the use of pulse deposition using nanoporous alumina templates from ammonia-citrate electrolytes⁵⁷ and from ammonia-free electrolytes containing citrate and boric acid.⁵⁸ The pulse mode facilitated deposition by minimizing the accumulation of hydrogen gas bubbles and the generation of a significant pH gradient that can disturb the deposition of Co-W alloys, as evident in thin film deposition.

Here, not only is there a further improvement in past techniques of electrodepositing Co-W alloy nanowires, from both an ammonia-free and boric acid-free electrolyte, but a novel composite

*Electrochemical Society Member.

[†]E-mail: e.podlaha-murphy@neu.edu

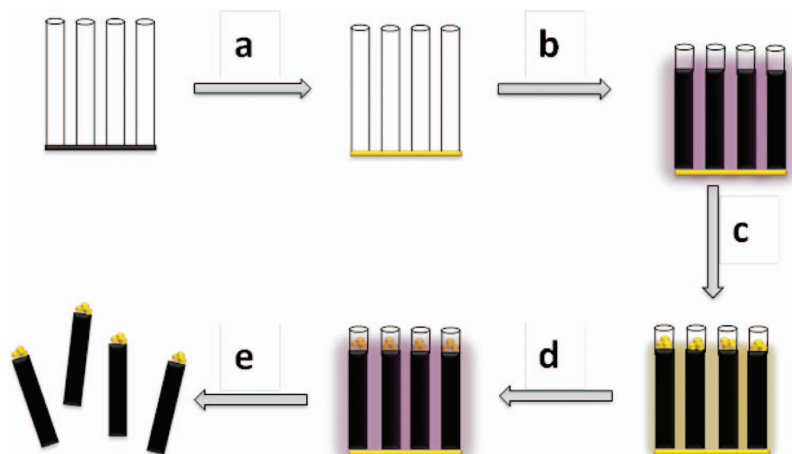


Figure 1. Schematic of the development of nanowire-nanoparticle composites: (a) sputtering a layer of gold; (b) pulsed electrodeposition of Co-W nanowires; (c) adding colloidal gold nanoparticles; (d) pulsed electrodeposition of Co-W alloy; (e) dissolving the membrane.

codeposition approach is presented with nanoparticles deposited on the top of nanowires. The conditions for nanowire deposition were guided by results obtained from polarization curves and galvanostatic, thin film Co-W deposition. In order to avoid mass transport controlled reactions thin, polycarbonate membranes were used as templates compared to previous reports with deeper alumina templates.

Experimental

Co-W thin film alloys and nanowires were fabricated from an electrolyte consisting of: 0.2 M CoSO_4 , 0.2 M Na_2WO_4 , 0.25 M $\text{Na}_3\text{C}_6\text{H}_5\text{O}_7$, 0.2 M $\text{C}_2\text{H}_5\text{NO}_2$ and 0.2 M NaOH , at a pH of 10.

The electrodeposition of Co-W thin films was carried out galvanostatically on rotating cylinder brass electrodes (RCE) at 300 rpm under pulsed (PC) and direct current (DC) mode. A platinum anode and a saturated calomel electrode (SCE) were used as the counter and reference electrode, respectively.

Co-W nanowires were electrodeposited into nanoporous polycarbonate membranes using a pulse current mode. Although, past literature reports of pulse parameters have been reported for meso-scale Co-W nanowires,⁵⁸ these parameters were selected due to the mass transport considerations inherent to alumina templates, and were optimized for a different electrolyte. With a goal to maintain kinetic control and avoiding gas accumulation and concentration gradients within the pores, thinner polycarbonate films are used here, and a relaxation, or off-time, was chosen to be twice as long as the on-time. Nanoporous polycarbonate membranes with 100 nm pore diameter, 6 μm thickness, having an average porosity of 12% were purchased from Whatman International Ltd. (Whatman Inc., MA, USA). The procedure to fabricate the nanowire-nanoparticle materials is sketched in Fig. 1. In order to provide an electric contact to the membrane a layer of gold was sputtered (Hummer model #Hummer 6.2, Anatech Inc.) on the one side of the templates (Fig. 1a). This Au layer served as a cathode substrate. The Co-W nanowires are formed (Fig. 1b) with an applied cathodic pulsed current density of 80 mA/cm^2 with a 5 s on-time and a 10 s off-time current. After the deposition, the electrolyte was flushed with water. Then the nanoparticle solution was added to the membrane with formed nanowire electrodes and vacuum was applied for 1 minute (Fig. 1c). The nanoparticles were fixed on the surface by deposition of an additional Co-W alloy layer while applying 20 pulses in the same pulse mode as described previously (Fig. 1d). The last step (Fig. 1e) is the release of the wires from the polycarbonate membrane by dissolving the membrane in dichloromethane.

Results and Discussion

The conditions for Co-W electrodeposition were characterized using the RCE at 300 rpm at room temperature. Fig. 2 shows the cathodic polarization curves obtained from -0.4 to -1.8 V vs. SCE in the presence and absence of glycine at pH 10. Addition of glycine to the citrate electrolyte causes an increase in polarization. The cathodic deposition is shifted to more negative potentials due to the expected additional complexation of Co^{2+} and the associated reduction of CoOH^+ by the glycine ligand.

Thin film deposition under DC and PC mode was also examined over a range of applied cathodic current densities, 10–80 mA/cm^2 (Fig. 3). The pulse deposition times were: 5 s on-time, t_{on} , and a 10 s off-time, t_{off} . The W content in the alloys electrodeposited under PC mode is slightly higher in comparison with alloys electrodeposited under direct current (DC) mode (Fig. 3a), especially at lower current densities. In both DC and PC modes of deposition the W content is the largest at the low current density and decreases with the applied current density. For DC deposition, there is a limiting amount of the tungsten weight percentage of ~ 3 wt% at high current densities. Simultaneously, with a decrease in tungsten content the current efficiency increases sufficiently in both DC and PC modes (Fig. 3b).

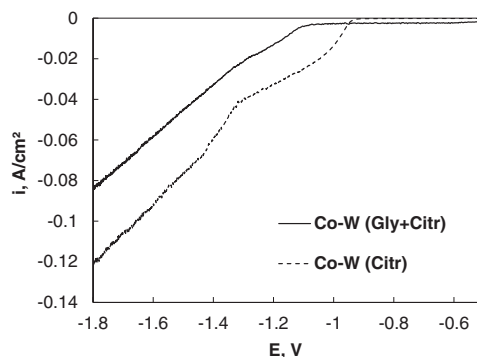


Figure 2. Cathodic polarization curves at 10 mV/s with a RCE at 300 rpm from a citrate bath in the absence and presence of glycine at pH 10, room temperature.

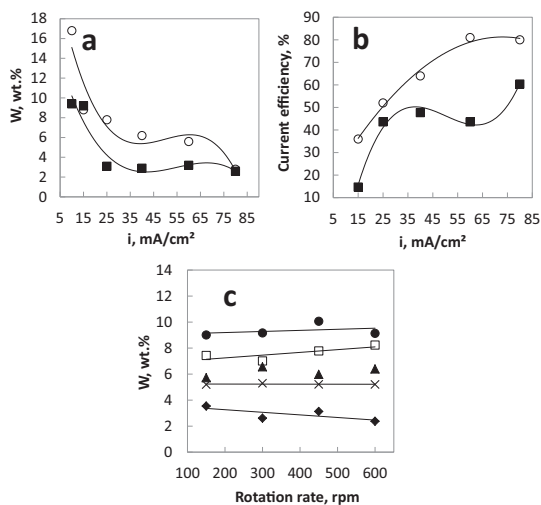


Figure 3. Composition of the Co-W alloys (a) comparing DC (■) and PC (○) deposition; (b) current efficiency; and (c) the influence of the electrode rotation rate under DC plating mode at different current densities: ● 15 mA/cm², □ 25 mA/cm², ▲ 40 mA/cm², × 60 mA/cm², ◆ 80 mA/cm².

Fig. 3c shows the W wt% for deposition under DC for different applied cathodic current densities at different electrode rotation rates. It is expected, under kinetic control, that the composition would be independent of rotation rate as indeed it is for a cathodic current density of 15–80 mA/cm². At higher current densities, a small change in the deposit composition is observed with rotation rate that can signify a mass transport contribution.

The following pulse current conditions were used to form Co-W nanowires within polycarbonate membranes: current density 80 mA/cm², pulse on-time of 5 s, and a 10 s off-time. The potential transient during pulse deposition is presented in Fig. 4. The top and bottom of the resulting potential pulse represents the transient in the open circuit potential (OCP) and the deposition potential. Three transient regions were observed in the OCP region, but it is less distinct in the deposition region. The change of slope in the OCP between regions (1) and (2), in Fig. 4, indicates a significant change in either the alloy composition or the surface concentration. During deposition, the potential response is relatively independent with time, confirming little to no mass transport influence of the metal deposition. Thus the changes in regions (1) and (2) during OCP may be reflecting the change in surface pH or adsorbed hydrogen. The last region, (3)

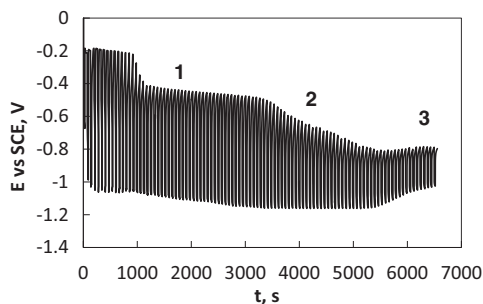


Figure 4. Potential response during PC electrodeposition of Co-W alloy within pores of the membrane.

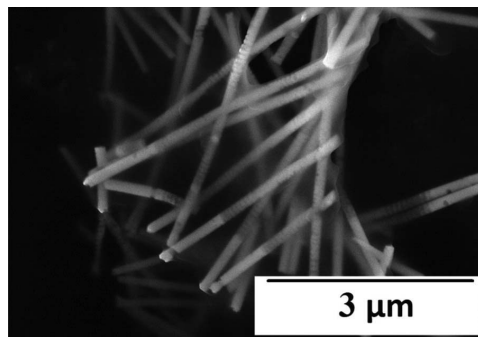


Figure 5. SEM images of electrodeposited Co-W nanowires separated from polycarbonate membranes.

shows the transient response when the nanowires reach the top of the template and commence to grow outside of the pore. The nanowire electrodeposition process was halted at stage (2). After the template was dissolved and the nanowires released SEM (Fig. 5) and TEM images (Fig. 6) confirmed that the long and continuous Co-W nanowires were deposited and their cylindrical shape reflects a complete filling of the nanopores in the radial direction in the template and that they are uniform in diameter. The length of the nanowires matched the expected pore length (6–7 μm). Interestingly, the average diameter of the Co-W nanowires is about 130 nm, which is slightly bigger than the pore size of the PC templates (100 nm).

The composite nanowires, combining the gold nanoparticles with the Co-W matrix, was fabricated using shorter nanowires, (4 μm) created by terminating the deposition process earlier, after 20 min. The Au nanoparticles were placed into the electrolyte, and the deposition process re-commenced to trap them onto the nanowire tip, within the template.

The TEM of the gold nanoparticles (Fig. 7) show that the diameters were fairly uniform having a size of 50 ± 5 nm. Fig. 8 shows that gold nanoparticles were indeed attached to the top of Co-W nanowires. To the best of the authors' knowledge it is the first demonstration of physically attaching nanowires to the end of a metallic nanowire in the form of a composite metal matrix deposit, in contrast to thiol-based chemical attachment.

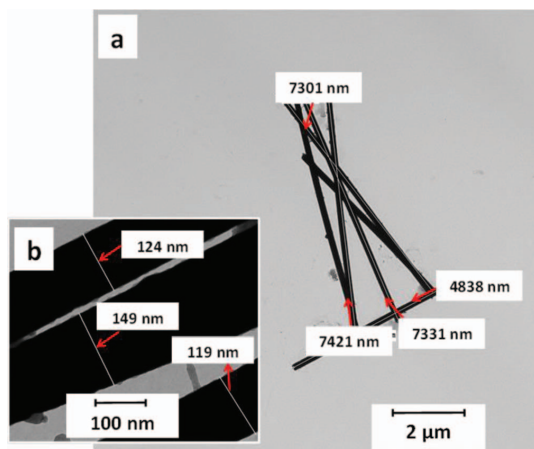


Figure 6. TEM images of Co-W nanowires, (a) low and (b) high magnification with measured wire diameters.

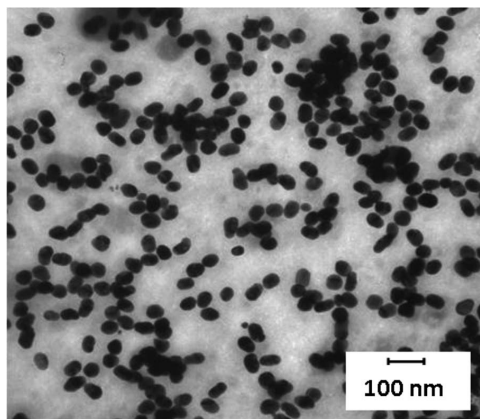


Figure 7. TEM image of 50 nm diameter Au nanoparticles.

Conclusions

Co-W nano-electrodes were fabricated by pulsed electrodeposition from a citrate-glycine electrolyte onto RCEs and into polycarbonate, nanoporous templates having a pore size of 100 nm. Thin film, Co-rich deposits were obtained over a large range of current density, under kinetic control. The addition of gold nanoparticles to the electrolyte enabled the fabrication of unique nano-composite nanowires, composed of Au nanoparticles and a Co-W matrix. The Co-W nanowire and AuNP was chosen as a model system, although the methodology is highly impactful as it could be adapted for other nanowire-nanoparticle complex structures.

Acknowledgments

This work has been funded by the MIP-031/2014 project from the Research Council of Lithuania, European Research Council under European "TEMADEP" (IRSES #05-104-7540), the US National Science Foundation #CHE-0957448, the US National Institutes of Health #1R21hg006278-01. Authors gratefully acknowledged Dr. William

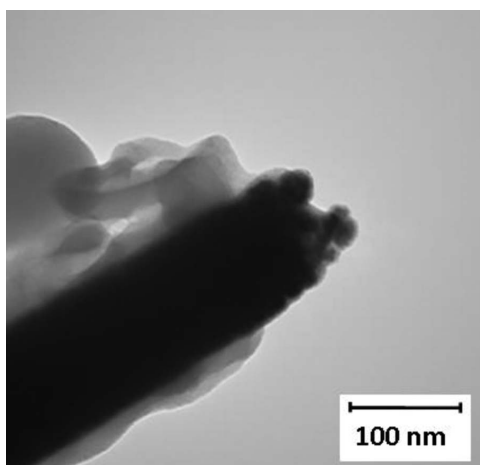


Figure 8. TEM image of Co-W nanowire with Au nanoparticles captured at the nanowire tip.

Fowle from Department of Biology, EM Lab, NU for help with TEM analyses.

References

1. J. I. Yeh and H. Shi, *Interdiscip. Rev. Nanomed. Nanobiotechnol.*, **2**, 176 (2010).
2. T. Li, W. Hu, and D. Zhu, *Adv. Mater.*, **22**, 286 (2010).
3. Y. Kashimura, H. Nakashima, K. Furukawa, and K. Torimitsu, *Thin Solid Films*, **438-439**, 317 (2003).
4. X. Chen, Z. Guo, G. M. Yang, J. Li, M. Q. Li, J. H. Liu, and X. J. Huang, *Mater. Today*, **13**, 28 (2010).
5. Y. Zhang, W. Chu, A. D. Foroushani, Ho. Wang, D. Li, J. Liu, C. J. Barrow, X. Wang, and W. Yang, *Materials*, **7**, 5169 (2014).
6. A. Akbarzadeh, D. Zare, A. Farhangi, M. R. Mehrabi, D. Norouziyan, Sh. Tangestaninejad, M. Moghadam, and N. Bararpour, *Am. J. Applied Sci.*, **6**, 691 (2009).
7. S. T. Sivapalan, B. M. DeVetter, T. K. Yang, M. V. Schulmerich, R. Bhargava, and C. J. Murphy, *J. Phys. Chem. C*, **117**, 10677 (2013).
8. J. Homola, S. S. Yee, and G. Gauglitz, *Sens. Actuators B*, **54**, 3 (1999).
9. F. Li, Y. Feng, P. Dong, and B. Tang, *Biosens. Bioelectron.*, **25**, 2084 (2010).
10. S. Z. Bas, *Mater. Lett.*, **150**, 20 (2015).
11. A. W. Snow and M. G. Ancona, *IEEE Sens. J.*, **14**, 3330 (2014).
12. J. Turkevich, P. C. Stevenson, and J. Hillier, *Discuss. Faraday Soc.*, **11**, 55 (1951).
13. G. Frens, *Nat. Phys. Sci.*, **241**, 20 (1973).
14. U. Bubniene, M. Oćwieja, B. Bugelyte, Z. Adamczyk, M. Naticch-Rak, J. Voronovic, A. Ramanaviciene, and A. Ramanavicius, *Colloids Surf. A*, **441**, 204 (2014).
15. J. T. Au, G. Craig, V. Longo, P. Zanzonico, M. Mason, Y. Fong, and P. J. Allen, *Am. J. Roentgenol.*, **200**, 1347 (2013).
16. C. Li, D. Li, G. Wan, J. Xu, and W. Hou, *Nanoscale Res. Lett.*, **6**, 440 (2011).
17. K. Zabetakis, W. E. Ghann, S. Kumar, and M. Ch. Daniel, *Gold Bull.*, **45**, 203 (2012).
18. M. Sikora, P. Szymczak, D. Thompson, and M. Cieplak, *Nanotechnology*, **22**, 445601 (2011).
19. M. Oyama, A. Orimo, and K. Nouneh, *Electrochim. Acta*, **54**, 5042 (2009).
20. W. Sun, Q. Dai, J. G. Wordena, and Q. Huo, *J. Phys. Chem. B*, **109**, 20854 (2005).
21. F. Patolsky, Y. Weizmann, and I. Willner, *Angew. Chem. Int. Ed.*, **114**, 2429 (2002).
22. M. Urzúa, A. Leiva, F. J. Espinoza-Beltrán, X. Briones, C. Saldías, and M. Pino, *J. Nanosci. Nanotechnol.*, **12**, 8382 (2012).
23. L. Zhang, X. Jiang, E. Wang, and Sh. Dong, *Biosens. Bioelectron.*, **21**, 337 (2005).
24. J. Zhang and M. Oyama, *Anal. Chim. Acta*, **540**, 299 (2005).
25. S. M. Mayanna, L. Ramesh, B. N. Maruthi, and D. Landolt, *J. Mater. Sci. Lett.*, **16**, 1305 (1997).
26. L. Wang, Y. Gao, T. Xu, and Q. Xue, *Mater. Chem. Phys.*, **99**, 96 (2006).
27. P. Weston, P. H. Shipway, S. J. Harris, and M. K. Cheby, *Wear*, **267**, 934 (2009).
28. H. Capel, P. H. Shipway, and S. J. Hartus, *Wear*, **255**, 917 (2003).
29. N. Tsytsaru, S. Belevsky, A. Dikumar, and J. P. Celis, *Trans. Inst. Met. Finish*, **86**, 301 (2008).
30. M. Donten, H. Cesiulis, and Z. Stojek, *Electrochim. Acta*, **45**, 3389 (2000).
31. D. P. Weston, S. J. Harris, H. Capel, N. Ahmed, P. H. Shipway, and J. M. Yellup, *Trans. Inst. Met. Finish*, **88**, 47 (2010).
32. T. Yamasaki, *Mater. Phys. Mech.*, **1**, 127 (2000).
33. K. R. Sriraman, S. G. S. Raman, and S. K. Seshadri, *Mater. Sci. Eng. A*, **418**, 303 (2006).
34. R. A. C. Santana, A. R. N. Campos, E. A. Medeiros, A. L. M. Oliveira, L. M. F. Silva, and Sh. Prasad, *J. Mater. Sci.*, **42**, 9137 (2007).
35. Z. A. Hamid, *Mater. Lett.*, **57**, 2558 (2003).
36. H. Chiriac, A. E. Moga, C. Gherasim, and N. Lupu, *Rev. J. Inform. Sci. Technol.*, **11**, 123 (2008).
37. T. Osaka, M. Takai, K. Hayashi, K. Ohashi, M. Saito, and K. Yamada, *Nature*, **392**, 796 (1998).
38. X. Liu, G. Zangari, and M. Shamsuzzoha, *J. Electrochem. Soc.*, **150**, C159 (2003).
39. N. Tsytsaru, H. Cesiulis, M. Donten, J. Sort, E. Pellicer, and E. J. Podlaha-Murphy, *Surf. Eng. Appl. Electrochem.*, **48**, 491 (2012).
40. Zh. I. Bobanova, V. I. Petrenko, G. F. Volodina, D. Z. Grabko, and A. I. Dikumar, *Surf. Eng. Appl. Electrochem.*, **47**, 493 (2011).
41. N. Tsytsaru, H. Cesiulis, E. Pellicer, J. P. Celis, and J. Sort, *Electrochim. Acta*, **104**, 94 (2013).
42. G. Wei, H. Ge, X. Zhu, Q. Wu, J. Yu, and B. Wang, *Appl. Surf. Sci.*, **253**, 7461 (2007).
43. O. Ergeneman, K. M. Sivaraman, S. Pané, and E. Pellicer, A. Teleki, A. M. Hirt, M. D. Baró, and B. J. Nelson, *Electrochim. Acta*, **56**, 1399 (2011).
44. M. C. Esteves, P. T. A. Sumodjo, and E. J. Podlaha, *Electrochim. Acta*, **56**, 9082 (2011).
45. S. Dubois, J. Colin, J. L. Duvail, and L. Piroux, *Phys. Rev. B*, **61**, 14315 (2000).
46. S. Aravamudan, J. Singleton, P. A. Goddard, and S. Bhansali, *J. Phys. D: Appl. Phys.*, **42**, 115008 (2009).
47. I. Z. Rahman, K. M. Razeem, M. Kamruzzaman, and M. Serantoni, *J. Mater. Process. Technol.*, **153-154**, 811 (2004).
48. A. Saedi and M. Ghorbani, *Mater. Chem. Phys.*, **91**, 417 (2005).
49. Q. Zhan, Z. Chen, D. Xue, F. Li, H. Kunkel, X. Zhou, R. Roshko, and G. Williams, *Phys. Rev. B*, **66**, 134436 (2002).
50. O. Yalçın, G. Kartopu, H. Çetin, A. S. Demiray, and S. Kazan, *J. Magn. Magn. Mater.*, **373**, 207 (2015).
51. B. Hamrakulov, I. S. Kim, M. G. Lee, and B. H. Park, *T. Nonferr. Metal Soc. China*, **19**, s83 (2009).

52. C. Bran, A. P. Espejo, E. M. Palmero, J. Escrig, and M. Vázquez, *J. Magn. Magn. Mater.*, **396**, 327 (2015).
53. A. S. Samardak, F. Nasirpour, M. Nadi, E. V. Sukovatitsina, A. V. Ognev, L. A. Chebotkevich, and S. V. Komogortsev, *J. Magn. Magn. Mater.*, **383**, 94 (2015).
54. S. Aravamudhan, J. Singleton, P. A. Goddard, and S. Bhansali, *J. Phys. D: Appl. Phys.*, **42**, 115008, (2009).
55. S. Samanifar, M. Almasi Kashi, A. Ramazani, and M. Alikhani, *J. Magn. Magn. Mater.*, **378**, 73 (2015).
56. A. Ramazani, M. Almasi Kashi, M. Alikhani, and S. Erfanifam, *Mater. Chem. Phys.*, **112**, 285 (2008).
57. H. Cesiulis, X. G. Xie, and E. Podlaha-Murphy, *Mater. Sci. Medzg.* **15**, 115 (2009).
58. N. Tsyntsaru, S. Silkin, H. Cesiulis, M. Guerrero, E. Pellicer, and J. Sort, *Electrochim. Acta*, **188**, 589 (2016).

Article VIII

Evaluation of corrosion and tribological behavior of electrodeposited tungsten alloys

E.Vernickaite, N.Tsyntsaru, H. Cesiulis

Proceedings of BALTRIB'2017 edited by prof. J. Padgurskas, 207-214

EVALUATION OF CORROSION AND TRIBOLOGICAL BEHAVIOR OF ELECTRODEPOSITED TUNGSTEN ALLOYS

*E. Vernickaite**, *H. Cesiulis*¹*, *N. Tsyntsaru****

* Physical Chemistry Department, Vilnius University, Vilnius, Lithuania

** Institute of Applied Physics of ASM, Chisinau, Moldova

Abstract: Tungsten alloy coatings with iron group metals (Ni, Fe, Co) are considered as advanced materials for various surface engineering applications. Such coatings should be resistant to mechanical and corrosive damage, and to have improved functionality and durability. Accordingly, the objectives of this review consist in a comparative study of available literature on corrosive and wear behavior of electrodeposited tungsten alloys with iron group metals, including our recent results on evaluation of electrodeposited Co-W coatings. The wear and corrosion resistance of Ni-W, Fe-W and Co-W strongly depends on the chosen deposition conditions and subsequently on tungsten content and structure of obtained protective coatings.

Key words: electrodeposition, Fe-W, Ni-W, Co-W, wear rate, corrosion resistance.

INTRODUCTION

It is a great interest to fabricate iron-group based alloy coatings possessing functional properties for various applications in industry. Currently, the hard chromium coatings are used most extensively due to high hardness, excellent wear resistance, low coefficient of friction and excellent protection against corrosion [1–3]. However, because of the environmental and health risks associated with usage of toxic and carcinogenic hexavalent chromium baths during the electroplating, there is an urgent demand in a potential replacement for this coating. Tungsten based alloy coatings have been found to be very promising candidates for such purpose as they provided to have competitive physical and mechanical characteristics, combined with improved ductility, high thermal stability, satisfactory barrier layer capability in microelectronic devices and increased deposition rates compared to those determined for electrodeposited hard chromium [4]. Tungsten can be easily co-deposited from aqueous solutions with an iron group (Fe, Co, Ni) metals forming the corresponding alloys [5]. Thus, comprehensive studies were conducted by a number of researchers, during which different models were proposed to explain the co-deposition mechanism depending on the chosen iron group metal and plating bath composition [4].

Tungsten alloy coatings having various compositions and tailored microstructures can be obtained by varying the plating solution chemistry and deposition parameters. Amorphous and crystalline Fe-W, Ni-W and Co-W electrodeposits have been reported in the literature [6–8]. XRD analysis results indicated that as-deposited Ni-W alloys having tungsten content in their composition higher than 19–23 at.% forms nanocrystalline (“amorphous-like”) structure [9–12]. Meanwhile for electrodeposited Co-W and Fe-W alloy coatings the crystallographic structure is changing from polycrystalline to nanocrystalline at tungsten content above 20 at.% [4, 11]. During the structural transformations the crystallite sizes are reduced from 60 nm to 7 nm for Co-W, from 41 nm to 3–4 nm for Fe-W and Ni-W alloys [13]. From practical point of view, alloys having nanocrystalline or amorphous structures have gained more interest since they usually possess better corrosion resistance and tribological properties (e. g. wear resistance). The later can be related to an increase in tungsten

¹ Author for contacts: prof. Henrikas Cesiulis
E-mail: henrikas.cesiulis@chf.vu.lt

content in the alloy which results in the grain size refinement and consequently in strengthening effect [14, 15].

Evaluation of different tungsten alloy coatings and their properties can be ambiguous, because it is depending on the given iron group metal, elemental composition, structure, grain size, etc. Accordingly, in this paper an attempt has been made to estimate wear and corrosion behavior of tungsten alloy coatings with iron group metals published elsewhere and to compare these results with our study on Co-W and Fe-W alloys.

EXPERIMENTAL

Co-W and Fe-W alloy coatings were obtained by electrodeposition under galvanostatic mode from a citrate electrolyte, which was described in our previous publications [16–19]. The pH was adjusted to 5.0, 6.7 or 8.0 by the addition of concentrated H_2SO_4 or NaOH. The plating temperature for Co-W alloys was kept at 20 and 60 °C to observe the influence of temperature on the properties of coatings. Fe-W electrodeposits were prepared at room temperature. The corrosion behavior of Co-W coatings was studied in 0.01 M H_2SO_4 solution by using electrochemical impedance spectroscopy (EIS) and linear voltammetry methods. Electrochemical corrosion measurements of obtained Fe-W coatings were performed in the mixture of 0.012 M Na_2SO_4 and 0.027 M NaCl (pH 5) at 90 °C. In both cases thicker coatings of ~10 μm have been deposited in order to avoid substrate influence on measurements. During the corrosion studies the registration of EIS and voltammetric data has been started after stabilization of the OCP within 15 min in the tested media. The amplitude of the sinusoidal voltage was 5 mV and the spectrum was obtained in the frequency range: 10 kHz–0.01 Hz. The charge transfer values for tested alloys were extracted from Nyquist's plots since the diameter of medium-frequency capacitive loops is considered as corrosion resistance (R_{corr}). The electrodeposition and corrosion tests were performed in a three-electrode cell with a platinized mesh as a counter electrode and saturated Ag/AgCl electrode as a reference electrode. All potential values are expressed vs. this reference electrode. The surface morphology of the coatings and content of alloys was investigated by scanning electron microscopy (Hitachi TM-3000 equipped with EDS analyser and software Swift ED-3000). Hardness of Fe-W and Co-W coatings was determined from nanoindentation tests (Nano-Hardness Tester, CSM) carried out at normal loads varying from 2 up to 200 mN. Linear loading and unloading speeds between 4 and 400 $mN\ min^{-1}$ were used. A Berkovitch indenter was used and 5 indentations were performed at each normal load, and analyzed statistically.

RESULTS AND DISCUSSION

Tribological properties

Nanocrystalline materials with the grain sizes less than 100 nm, are typically very hard and are commonly produced as protective coatings which can assist in decreasing the wear. The Hall-Petch mechanism predicts that as the grain size decreases the hardness values increases, but it was demonstrated, that this mechanism is not applicable for very small grain sizes [20]. In our previous studies we have shown that the hardness of Co-W alloys increases up to ~917 HV_{20} at increase in the tungsten content from 8 to 25 at.% which is linked to a decrease in the grain size till the critical value. After this critical value of 5 nm the inverse Hall-Petch relation is observed for Co-W alloys [17]. Meanwhile for Fe-W alloy the critical grain size of about 4 nm was determined, while the hardness reaches the maximum value of 1020 HV_{980} when tungsten content in Fe-W deposit increases up to 26 at.% [21]. Overall, Fe-W alloy coatings are characterized by higher hardness than that of Co-W deposits in the range of normal loads of 2–100 mN [18]. The maximum hardness values for Ni-W deposits usually are lower (in the range of $734 \pm 70\ HV_{10}$) than for Co-W and Fe-W alloys [12, 14, 22, 23]. At higher applied loads the hardness of Fe-W and Co-W alloys can decrease, e. g. for Fe-24 at.% W deposits decreases up to 500 HV_{980} [19], and for Co-13 at.% W – up to 600 HV_{980} [24]. Overall, it should be noted that the electrodeposited binary tungsten alloy coatings are harder than those prepared from pure iron group metals [14, 25].

The hardness of tungsten alloy coatings with iron group metals can be improved by applying heat treatment due to partial crystallization, which causes the strengthening effect of the iron metal matrix containing the dissolved tungsten. Annealing also yields reduced internal stresses of the deposit that were related to the hydrogen evolution reaction occurring simultaneously during tungsten alloy co-deposition with iron group metals. For example, the hardness of Co-27 at.% thin film increases up to 1200 HV₂₅₀ after the heat treatment at 600 °C for 2 hours in Ar atmosphere [26]; for Ni-25 at.% the hardness reaches maximum of 1450 HV₂₀₀ at annealing temperature of 600 °C for 24 h in vacuum [12]. Other authors have also reported the maximum hardness for Ni-W alloys with different compositions after annealing at ≤700 °C [27–29]. The hardness of as-deposited Co-12 at.% W sample increased from 450 HV₉₈₀ (as-deposited) to ~700 HV₉₈₀ following heat treatment for 1 h at 600 °C in the air [30]. At the higher temperatures, the hardness decreases due to the increased grain size [12].

Tribological investigation includes the processes of interaction at the interface between two bodies forming a tribo-system and during the evaluation of tribological behavior of materials both surfaces, their properties and testing conditions (load, time, speed, displacement, relative humidity, temperature, etc.) must be taken into consideration. Accordingly, it is difficult to compare the wear rates for tests performed for Ni-W, Co-W and Fe-W systems in different laboratories and under different conditions (Table 1). Nevertheless, Co-W alloy electrodeposits in some works has been characterized by the lower rate of wear due to their relatively high hardness combined with the formation of the stable hexagonal close-packed (hcp) structure that is resistant to the high loads [30]. Meanwhile the fretting of Fe-W alloys at dry friction is accompanied by tribooxidation during which iron oxides are accumulated leading to increased wear loss [13].

Table 1. Wear resistance under dry conditions of the different tungsten alloys coatings.

Alloy, reference	Counter body	Load	Wear loss
Fe-W [18]	Corundum	10 N	Wear track depth ~6 μm
Co-W [26]	Martensitic stainless steel	61 N	Wear track depth 20.9 μm
Ni-W [27]	St52 steel, Ni-W	20 N	$7.14 \times 10^{-6} \text{ mm}^3/\text{mN}$
Co-W [25]	Martensitic stainless steel	15, 30, 61 N	$3 \times 10^{-15} \text{ m}^3/\text{Nm}$
Ni-W [31]	GCr15 stainless steel	5 N	$3.49 \times 10^{-5} \text{ mm}^3/\text{mN}$
Ni-W [32]	Tungsten carbide	5 N	$2.77 \times 10^{-6} \text{ μm}^3$
Ni-W [33]	Tungsten carbide	3 N	$9.8 \times 10^{-6} \text{ mm}^3/\text{Nm}$
Ni-W [34]	Untreated ductile iron	1, 3, 5 N	$5 \times 10^{-5} \text{ mm}^3/\text{m}$
Co-W [35]	Stainless steel	15 N	0.095 mg/h
Ni-W [36]	Hardened steel	1 N	$1.14 \times 10^{-5} \text{ mm}^3/\text{Nm}$

Corrosion resistance

The investigation of the corrosion properties of functional materials is an integral part of modern materials science and crucial in terms of their potential technological applications. However, till now we can only speculate on a systematic investigation of corrosive properties of tungsten with iron group metal alloys. The composition of coatings, their microstructure and morphology strongly depend on alloys' preparation methods and parameters of ones. Thus, the wide variation of corrosion parameters can be observed even for the alloys with similar composition and the overall picture of corrosion behavior of Ni-W, Fe-W and Co-W alloys remains inconclusive.

In our study we presented the mapping of corrosion behavior of various compositions of Co-W alloy deposits (2.4–30 at.% of W) since previous papers reported that Co-W is characterized by the corrosion resistance that is similar to that of the hard-chromium plate [30]. Usually the corrosion behavior of the prepared metal alloy coatings is investigated mainly by means of electrochemical technique, such as open circuit potential (OCP), linear voltammetry and electrochemical impedance spectroscopy (EIS). However, there are some limitations for the correct estimation of corrosion parameters (e. g., charge transfer resistance, corrosion potential, corrosion current density) by using mentioned above electrochemical techniques. The porosity, cracks, smoothness and thickness of the deposits should be evaluated impartially to ensure that the obtained data corresponds particularly to the tested alloys and the substrate below has no influence on the results. But in some papers related to

tungsten alloys electrodeposition the discussion about the coating morphology or structure is suppressed and we can only guess about the accuracy of the summarized anti-corrosive characteristics, which sometimes are presented as more attractive than those determined for electrolytic chromium or metallurgical steel. For example in [37] it was concluded that the anticorrosive protection ability of Co-7 at.% W alloy coating can be 6–14 times better than mild steel and that corrosion resistance varies in the range of 170–375 kOhm cm² depending on to the tested acid (1 M HCl > 1 M H₂SO₄ > 1.0 M HClO₄). Interestingly, our results show that comparable charge transfer resistance values in acidic environment (0.1 M H₂SO₄) can be found only for stainless steel substrate ($R_{corr} = 123.7 \text{ kOhm cm}^{-2}$) (Fig. 1).

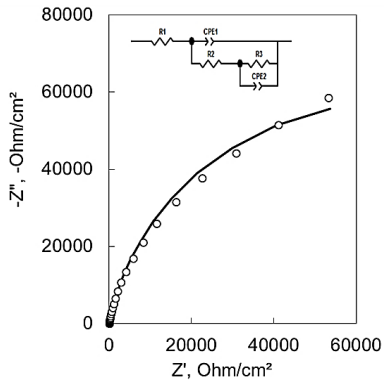


Figure 1. Nyquist plots (dots) for stainless steel substrate (AISI Type 304) and Equivalent circuit used for EIS fitting (continuous line).

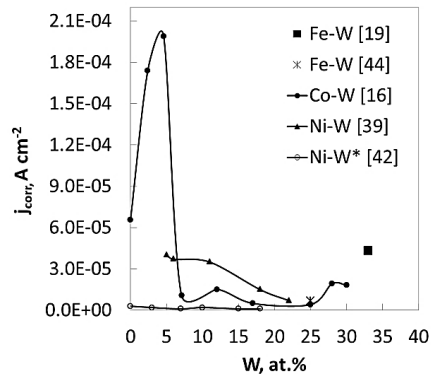


Figure 2. Corrosion current density (j_{corr}) values in acidic media of as-deposited W alloys with iron group metals published in the literature.

Among a number of corrosion parameters, the values of j_{corr} and E_{corr} are often used to compare corrosion behavior of electrodeposited coatings. Notwithstanding the corrosion potential values usually do not show any evident dependence on the composition of alloy thin films and varied independently from the corrosion rate. This is under the assumption that potential values are driven by the rates of cathodic reaction (hydrogen evolution) and anodic reaction (electrolytic dissolution or passivity of the metal) of corresponding system and are strongly affected by the corrosive media, chemical composition of material and its surface state. Thus, the further investigation of the corrosion behavior of tungsten alloy with iron group metal coatings is mainly based on the j_{corr} determined from linear voltammetry analysis results. Noticeably, here can be also found some disagreements between different studies. Hence, for Co-W alloys containing >7 at.% of tungsten the obtained voltammograms are asymmetrical and j_{corr} cannot be determined by applying the regular routine, i.e Tafel extrapolation method. In such case all curves should be transformed into Allen-Hickling coordinates that enable to estimate the corrosion rate using a narrow range of potentials [38].

It is noted that the lowest corrosion currents were obtained for Co-W alloys electrodeposited at 60°C, because those electrodeposited at room temperature were full of cracks and could be easily peeled off mechanically from the stainless steel substrate and exhibited high corrosion rate ($j_{corr} = 2.4 \times 10^{-4} \text{ A cm}^{-2}$) [16]. In mostly works the co-deposition of tungsten with iron group metals is performed at the higher temperature (60–75 °C) which enables not only to improve the quality of the thin film, but also allows increasing the tungsten content in the alloy which leads to ameliorate the corrosion resistance. Thus, our study depicted that by increasing the tungsten content in Co-W thin coatings from 5 at.% up to 25 at.%, crystallite size reduces from ~60 nm to 3–6 nm and the corrosion current density in acidic media decreases from $2 \times 10^{-4} \text{ A cm}^{-2}$ up to $4.2 \times 10^{-6} \text{ A cm}^{-2}$, respectively (Fig. 2) [16]. The highest determined corrosion resistance value at 25 at.%W is most likely related to the formation of thermodynamically stable intermetallic compound Co₃W. Similar trend by other researchers was also observed for Ni-W alloy coatings which showed that the corrosion rate of Ni-W samples in acidic environment decreases with grain size reduction from 63 nm to 5 nm, i. e. when the

tungsten content arises from 5 to 22 at.% [39]. This correlate with results [40] where it was revealed that at high tungsten content a stable intermetallic compound of Ni_4W is formed. Besides, it is claimed that both Ni and W metals undergo passivation state in electrolytes forming non-porous layer of $Ni(OH)_2$, NiO and WO_3 on the top of Ni-W alloy surface [41]. These oxidation products inhibit the corrosion process and reduce the rate of oxidation reaction. Thus, in [42] where observed that all polarization curves for Ni-W samples show an active/passive transition in H_2SO_4 solution. Notable that in the recent study of Ni-W alloys [42] the corrosion current densities do not show any significant variation versus W content in the deposit and varied in the range between $1 \cdot 10^{-6}$ and $3 \cdot 10^{-6}$ A cm^{-2} , however these values were much lower than those measured under similar conditions in other works. This can be influenced by deaerated 1 M H_2SO_4 solution used in this study.

It is claimed that the superior corrosion resistance of Co-W can be related due to the formation of rich film or $Co(OH)_2$ passive films on the surface [43]. In fact, our EDS investigations of Co-W alloys after corrosion test showed significantly increased oxygen content in composition after the corrosion test and this indicates that the electrochemical corrosion process occurs via an intermediate stage of forming oxide-containing compounds on the surface [16]. It is noted that this tendency was less pronounced for alloys containing small amount of tungsten, i. e. which were characterized by higher corrosion rate, and thus it can be summarized that coatings having more than 5 at.% W can protect the substrates from corrosion in acidic media better than the pure Co deposit. However it is hard to distinguish one particular iron group metal which possesses the best anti-corrosive protection in acidic environment after the alloying with tungsten.

For Fe-25 at.% W was found that in 0.5 M H_2SO_4 the surface is covered by iridescent film, which is characteristic for thin oxide films of W and Fe and reveals the passive state of Fe-W, thus the calculated j_{corr} value is comparable to that of Co-W having similar amount of W in composition [44]. Our previous investigation of Fe-W thin coatings revealed an active state and extremely high corrosion rates in acidic environment even when the tungsten content in the alloy reached 33 at.% [19]. Probably this can be explained by different corrosion experiment conditions, since in our case the voltammetry analysis was performed in $Na_2SO_4 + NaCl$ (pH 5) at high temperature of 90 °C. As it can be seen from (Fig. 3), the Ni-W and Co-W alloys in neutral 3.5 wt.% NaCl solutions exhibited a clearly increased corrosion resistance compared to that of the acidic media. Also, in the case of neutral solutions a positive influence of higher tungsten content on corrosion resistance was confirmed [45–47].

According to linear voltammetry results described in different papers, it can be concluded that the tungsten alloy coatings barely have the transition to the passivation state in neutral corrosive solution [11].

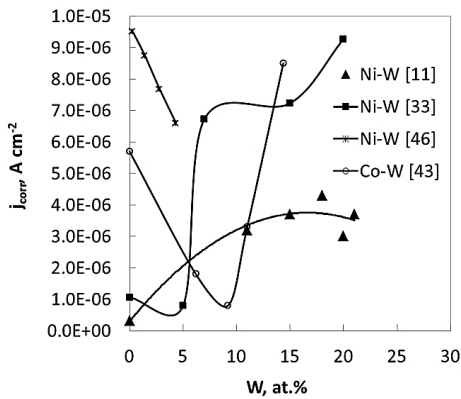


Figure 3. Corrosion current density (j_{corr}) values in neutral NaCl solution of as-deposited W alloys with iron group metals published in literature.

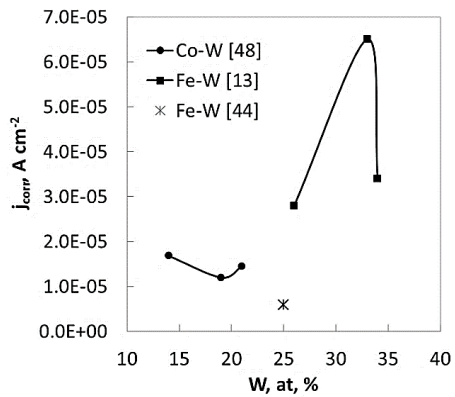


Figure 4. Corrosion current density (j_{corr}) values in neutral Na_2SO_4 or $NaCl + Na_2SO_4$ solution of as-deposited W alloys with iron group metals published in literature.

After adding SO_4^{2-} ions to the neutral corrosive medium containing NaCl, the corrosion resistance of Co-W alloys slightly depends on the coating thickness. Thus, it was depicted that the corrosion current density decreases from $4.6 \cdot 10^{-5}$ (for thin coatings) to $1.4 \cdot 10^{-5}$ A cm^{-2} (for 20 μm), meanwhile the corrosion potential for both samples was similar -0.60 ± 0.05 V [48]. It was not determined a clear correlation between the tungsten content in the deposit and corrosion current density in NaCl + Na_2SO_4 solution neither for Co-W nor Fe-W alloys [13, 48] (Fig. 4). However, for Co-W case the corrosion current density was higher than that in neutral single NaCl solution and this change might be caused by different dissolution mechanism in the presence of Cl^- and SO_4^{2-} ions. An addition of organic additives (saccharin, neonol, OP-10 emulgator, neoinogenic SAS) to the electrolyte prior the electroplating of alloys did not reveal any favourable effect on examined corrosion resistance of Co-W alloys in different neutral solutions, in fact in all cases the prepared coatings demonstrated relatively lower corrosion resistance in neutral NaCl + Na_2SO_4 solution [13, 49]. Significantly poorer anti-corrosive protection was noticed for Co-W alloy coatings in alkaline (6 M KOH) media, when the corrosion current density value increased up to 0.84×10^{-3} A cm^{-2} and corrosion potential decreased up to -1.03 V at 24 at.% of W [49]. However, for nanocrystalline Ni-W alloys having 5–22 at.% of W, j_{corr} values in alkaline solution (pH 10) are lower than those in acidic media (pH 3) [39].

CONCLUSIONS

- The hardness of Ni-W, Fe-W and Co-W alloy coatings increases with increasing W content. The direct Hall-Petch relation is observed up to the minimum values of grain size of 8–15 nm, 4 nm and 5 nm for Ni-W, Fe-W and Co-W deposits, respectively. Among all W alloy coatings, Fe-W deposits possess the highest hardness.
- The evaluation of tribological behavior of the deposits reported in articles is an complex issue due to a large number of variables involved during testing, such as load, speed, time, counterbody material, etc. However wear resistance of Ni-W, Fe-W and Co-W electrodeposits is quite high and comparable to that of electrolytic chromium. Nevertheless, Co-W alloy electrodeposits usually has demonstrated a lower wear rate than in the case of Ni-W and Fe-W.
- The Ni-W and Co-W alloys, in neutral 3.5 wt.% NaCl solutions, exhibited a clearly increased corrosion resistance compared to that of acidic and alkaline media, while this characteristic slightly decreased after SO_4^{2-} ions addition to corrosive solution. The anti-corrosive behaviour of individual Fe-W, Ni-W and Co-W systems depends not only on their elemental composition, but also on deposition conditions and chemistry of electrolyte. Commonly, the corrosion rate decreases with increasing W content in the coating.

REFERENCES

- [1] A. Darbeida, J. von Stebut, M. Barthole, P. Belliard, L. Lelait, G.Zacharie, Comparative tribological study of chromium coatings with different specific hardness, Surface and Coatings Technology, 68–69, 1994, p. 582–590.
- [2] L. Fedrizzi, S. Rossi, F. Bellei, F. Deflorian, Wear–corrosion mechanism of hard chromium coatings, Wear, 253 (11–12), 2002, p. 1173–1181.
- [3] N. Imaz, M. Ostra, M. Vidal, J. A. Díez, M. Sarret, E.García-Lecina, Corrosion behaviour of chromium coatings obtained by direct and reverse pulse plating electrodeposition in NaCl aqueous solution, Corrosion Science, 78, 2014, p 251–259.
- [4] N. Tsyntsaru, H. Cesiulis, M. Donten, J. Sort, E. Pellicer, E. J. Podlaha-Murphy, Modern trends in tungsten alloys electrodeposition with iron group metals, Surface Engineering and Applied Electrochemistry, 48(6), 2012, p. 491–520.
- [5] A. Brenner, Electrodeposition of Alloys: Principles and Practice, Academic Press Inc., New York, 2, 1963, 347–456 p.
- [6] M. Donten, Bulk and surface composition, amorphous structure, and thermocrystallization of electrodeposited alloys of tungsten with iron, nickel, and cobalt, Journal of Solid State Electrochemistry 3, 1999, p. 87–96.
- [7] N. Tsyntsaru, H. Cesiulis, A. Budreika, X. Ye, R. Juskenas, J.-P. Celis, The effect of electrodeposition conditions and post-annealing on nanostructure of Co-W coatings, Surface and Coatings Technology, 206 (19–20), 2012, p. 4262–4269.

- [8] M. Mulukutla, V. K. Kommineni, S. P. Harimkar, Pulsed electrodeposition of Co-W amorphous and crystalline coatings, *Applied Surface Science*, 258(7), 2012, p. 2886–2893.
- [9] P. Indyka, E. Beltowska-Lehman, L. Tarkowski, A. Bigos, E. García-Lecina, Structure characterization of nanocrystalline Ni–W alloys obtained by electrodeposition, *Journal of Alloys and Compounds*, 590, 2014, p. 75–79.
- [10] K. H. Hou, Y. F. Chang, S.M. Chang, C.H. Chang, The heat treatment effect on the structure and mechanical properties of electrodeposited nano grain size Ni-W alloy coatings, *Thin Solid Films* 518, 2010, p. 7335–7540.
- [11] A. Królikowski, E. Płońska, A. Ostrowski, M. Donten, Z. Stojek, Effects of compositional and structural features on corrosion behavior of nickel–tungsten alloys, *Journal of Solid State Electrochemistry*, 13, 2009, p. 263–275.
- [12] T. Yamasaki, P. Schloßmacher, K. Ehrlich, Y. Ogino, Formation of amorphous electrodeposited Ni-W alloys and their nanocrystallization, *Nanostructured Materials*, 10(3), 1998, p. 375–388.
- [13] N. Tsyntaru, A. Dikumar, H. Cesiulis, J.-P. Celis, Zh. Bobanova, S. Sidelnikova, S. Belevskii, Yu. Yapontseva, O. Bersirova, V. Kublanovskii, Tribological and corrosive characteristics of electrochemical coatings based on cobalt and iron superalloys, *Powder Metallurgy and Metal Ceramics*, 48, 2009, p. 419.
- [14] C. A. Schuh, T. G. Nieh, H. Iwasaki, The effect of solid solution W additions on the mechanical properties of nanocrystalline Ni, *Acta Materialia*, 51, 2003, p. 431.
- [15] K. R. Sriraman, S. Ganesh Sundara Raman, S. K. Seshadri, Synthesis and evaluation of hardness and sliding wear resistance of electrodeposited nanocrystalline Ni–W alloys, *Materials Science and Engineering A*, 418, 2006, p. 303–311.
- [16] E. Vernickaite, N. Tsyntaru, H. Cesiulis, Electrodeposition and corrosion behaviour of nanostructured cobalt–tungsten alloys coatings, *Transactions of the IMF*, 94(6), 2016, p. 313–321.
- [17] N. Tsyntaru, H. Cesiulis, E. Pellicer, J.-P. Celis, J. Sort, Structural, magnetic, and mechanical properties of electrodeposited cobalt–tungsten alloys: Intrinsic and extrinsic interdependencies, *Electrochimica Acta*, 104, 2013, p. 94–103.
- [18] N. I. Tsyntaru, Zh. I. Bobanova, D. M. Kroitoru, V. F. Cheban, G. I. Poshtaru, A. I. Dikumar, Effect of a Multilayer Structure and Lubrication on the Tribological Properties of Coatings of Fe-W Alloys, *Surface Engineering and Applied Electrochemistry*, 46(6), 2010, p. 538–546.
- [19] E. Vernickaite, Z. Antar, A. Nicolenco, R. Kreivaitis, N. Tsyntaru, H. Cesiulis, TRIBOLOGICAL AND CORROSION PROPERTIES OF IRON-BASED ALLOYS, The 8th International Conference BALTRIB'2015 Aleksandras Stulginskis University 26–27 November 2015, Kaunas, Lithuania.
- [20] D. Wolf, V. Yamakov, S. R. Phillpot, A. K. Mukherjee, Deformation mechanism and inverse Hall–Petch behavior in nanocrystalline materials, *Zeitschrift für Metallkunde*, 94(10), 2003, p. 1091–1097.
- [21] N. Tsyntaru, J. Bobanova, X. Ye, H. Cesiulis, A. Dikumar, I. Prosycevas, J.-P. Celis, Iron–tungsten alloys electrodeposited under direct current from citrate–ammonia plating baths, *Surface & Coatings Technology*, 203, 2009, p. 3136–3141.
- [22] C. N. Panagopoulos, E. P. Georgiou, D.A. Lagaris, V. Antonakaki, The effect of nanocrystalline Ni-W coating on the tensile properties of copper, *AIMS Materials Science*, 3(2), 2016, 324–338.
- [23] A. Giga, Y. Kimoto, Y. Takigawa, K. Higashi, Demonstration of an inverse Hall–Petch relationship in electrodeposited nanocrystalline Ni-W alloys through tensile testing, *Scripta Materialia* 55, 2006, p. 143–146.
- [24] Z. Abdel Hamid, Electrodeposition of cobalt–tungsten alloys from acidic bath containing cationic surfactants, *Materials Letters*, 57, 2003, p. 2558–2564.
- [25] D. P. Weston, P. H. Shipway, S. J. Harris, M. K. Cheng, Friction and sliding wear behaviour of electrodeposited cobalt and cobalt–tungsten alloy coatings for replacement of electrodeposited chromium, *Wear*, 267, 2009, p. 934–943.
- [26] H. Capel, P. H. Shipway, S. J. Harris, Sliding wear behaviour of electrodeposited cobalt–tungsten and cobalt–tungsten–iron alloys, *Wear*, 255, 2003, p. 917–923.
- [27] J. Auerswald, H. J. Fecht, Nanocrystalline Ni-W for Wear-Resistant Coatings and Electroforming, *Journal of The Electrochemical Society*, 157(4), 2010, D199–D205.
- [28] S. Hayata, S. Oue, H. Nakano, T. Takahashi, Effect of Annealing on the Structure and Hardness of Electrodeposited Ni–W Alloys, *ISIJ International*, 55(5), 2015, p. 1083–1090.
- [29] N. Sunwang, P. Wangyao, Y. Boonyongmaneerat, The effects of heat treatments on hardness and wear resistance in Ni-W alloy coatings, *Surface & Coatings Technology*, 206, 2011, p. 1096–1101.
- [30] S. Eskin, O. Berkh, G. Rogalsky, J. Zahavi, Co-W Alloys for Replacement of Conventional Hard Chromium, *Plating Surf. Finishing*, 85, 1988, p. 79–84.

- [31] L. Xu, H. Guan, D. Li, L. Wang, Tribological properties of electroplated crack Ni-W alloy coatings, *Proceedings of the Institution of Mechanical Engineers Part J: J Engineering Tribology* 229 (11), 2015, p. 1372–1378.
- [32] T. J. Rupert, C. A. Schuh, Sliding wear of nanocrystalline Ni-W: Structural evolution and the apparent breakdown of Archard scaling, *Acta Materialia*, 58, 2010, p. 4137–4148.
- [33] J. Druga, M. Kašiarová, E. Dobročka, M. Zemanová, Corrosion and tribological properties of nanocrystalline pulse electrodeposited Ni-W alloy coatings, *Transactions of the IMF*, 95(1), 2007, p. 39–45.
- [34] A. Ayday, H. Skulev, tudy of the Nickel-Tungsten and Nickel-Cobalt Coatings Plated on Ductile Iron, 5th International Science Congress & Exhibition APMAS2015, Lykia, Oludeniz, April 16–19, 2015.
- [35] N. Dadvand, G. Jarjoura, G. J. Kipouros, Electrodeposition of cobalt-tungsten alloys from alkaline citrate containing bath as alternative for chromium hexavalent replacement, *Canadian Metallurgical Quarterly*, 52(4), 2013, p. 391–397.
- [36] A. S. M. A. Haseeb, U. Albers, K. Bade, Friction and wear characteristics of electrodeposited nanocrystalline nickel-tungsten alloy films, *Wear*, 264, 2008, p. 106–112.
- [37] A. Subramanian, G. N. Kousalya, V. S. Muralidharan, T. Vasudevan, Cobalt tungsten alloy-electrodeposition and characterization, *Indian Journal of Chemical Technology*, (9), 2002, p. 513–518.
- [38] H. Cesiulis and J. Sinkeviciute: *Physicochem. Mech. Mater.*, 4, 2004, p. 128–132.
- [39] A. Chianpairot, G. Lothongkum, C. A. Schuh, Y. Boonyongmaneerat, Corrosion of nanocrystalline Ni-W alloys in alkaline and acidic 3.5 wt.% NaCl solutions, *Corrosion Science*, 53, 2011, p. 1066–1071.
- [40] M. Obradovic, J. Stevanovic, A. Despic, R. Stevanovic, J. Stoch, Characterization and corrosion properties of electrodeposited Ni-W alloys, *Journal of the Serbian Chemical Society*, 66(11–12), 2001, p. 899–912.
- [41] H. B. Lee, Synergy Between Corrosion and Wear of Electrodeposited Ni-W Coating, *Tribology letters*, 50, 2013, p. 407–419.
- [42] N. Shakibi Nia, J. Creus, X. Feaugas, C. Savall, Influence of metallurgical parameters on the electrochemical behavior of electrodeposited Ni and Ni-W nanocrystalline alloys, *Applied Surface Science*, Accepted Manuscript, 2016.
- [43] A. Bodaghi, J. Hosseini, Corrosion Behavior of Electrodeposited Cobalt-Tungsten Alloy Coatings in NaCl Aqueous Solution, *International Journal of Electrochemical Science*, 7, 2012, p. 2584–2595.
- [44] V. Kublanovsky, O. Bersirova, A. Dikuser, Z. Bobanova, H. Cesiulis, J. Sinkeviciute, I. Prosycevas, Electrodeposition and Corrosion Properties of Nanocrystalline Fe-W alloys, *Problems of corrosion and corrosion protection of materials, Physico Chemical Mechanics of Materials, special issue No. 7, Lviv*, 2008.
- [45] M. Zemanova, V. Jorik, M. Krivosudska, M. Chovancova, Pulse current electrodeposition and corrosion properties of Ni-W alloy coatings, *The Journal of Applied Electrochemistry*, 41, 2011, p. 1077–1085.
- [46] L. Elias, A. Chitharanjan Hegde, Electrodeposition of laminar coatings of Ni-W alloy and their corrosion behavior, *Surface & Coatings Technology*, 283, 2015, p. 61–69.
- [47] A. Bodaghi, J. Hosseini, Corrosion resistance and electrocatalytic properties of Co-W alloy coatings, *Surface Engineering*, 28(8), 2012, p. 632–635.
- [48] N. I. Tsyntsaru, S. S. Belevskii, G. F. Volodina, O. L. Bersirova, Yu. S. Yapontseva, V. S. Kublanovskii, A. I. Dikuser, Composition, Structure, and Corrosion Properties of Coatings of Co-W Alloys Electrodeposited under Direct Current, *Surface Engineering and Applied Electrochemistry*, 43(5), 2007, p. 312–317.
- [49] Yu. S. Yapontseva, A. I. Dikuser, V. S. Kyblanovskii, Study of the Composition, Corrosion, and Catalytic Properties of Co-W Alloys Electrodeposited from a Citrate Pyrophosphate Electrolyte, *Surface Engineering and Applied Electrochemistry*, 50(4), 2014, p. 330–336.

NOTES

Vilniaus universiteto leidykla
Universiteto g. 1, LT-01513 Vilnius
El. p. info@leidykla.vu.lt,
www.leidykla.vu.lt
Tiražas 16 egz.